Czech Technical University in Prague
Faculty of Electrical Engineering
Department of Telecommunication Engineering

Self-Optimizing Mobile Networks with UAVs

Ph.D. Dissertation

BSc. Mohammadsaleh Nikooroo, MPhil

Supervisor: Doc. Ing. Zdeněk Bečvář, Ph.D.

DS programme: P2612 Electrical Engineering and Information Technology
Field of study: 2601V013 Telecommunication Engineering

Prague, October 2022

Thesis Supervisor:
Doc. Ing. Zdeněk Bečvář, Ph.D.
Department of Telecommunication Engineering
Faculty of Electrical Engineering
Czech Technical University in Prague
Technická 2
166 27 Prague 6
Czech Republic

Honour statement

I declare that I have written my dissertation thesis independently and consistently quoted the sources in the submitted work.

Specification of the author‘s share:

For the reference [C4], the author has participated in the technical presentation/writing of the problem formulation and the proposed solution.

For the reference [J1], the author has provided the analytical solution to the formulated problem and also has conducted simulations for the results section.

For the other included articles, the author has taken over the following major roles: i) Initiation of the writing of the entire sections within each article, ii) formulation of the problem followed by proposing and developing solutions, iii) implementation of simulations and presentation/investigation of results.

In Prague, October 2022

.....
BSc. Mohammadsaleh Nikooroo, MPhil

To Salo, The Unchangeable...

Abstract

Unmanned aerial vehicles (UAVs) have received an extensive attention in wireless communications in the recent years. Due to a high flexibility and adaptability to the environment, UAVs can be regarded as flying base stations (FlyBSs) that potentially bring a significant enhancement in the performance of mobile networks. Such potential enhancements, however, are essentially subject to an effective management of available resources. In particular, several challenges are required to be addressed to efficiently integrate FlyBSs into mobile networks, including positioning, power consumption, association of users to the FlyBSs, and allocation of transmission power and channel bandwidth to the users.

Power allocation/consumption is a critical aspect that could directly manifest in those mentioned challenges. In particular, due to transmission power limitations, the FlyBS would require to relocate in order to avoid unwanted loss in the system's performance. Furthermore, a relocation might also be required either to reduce the distance between the FlyBS and the user, or to access better FlyBS-to-user channel conditions. Such displacements of the FlyBS would basically incur a propulsion energy consumption. Thus, there is a potential trade-off between the transmission and propulsion power consumptions. From the perspective of power consumption, saving the propulsion energy could be more crucial due to limitations on the FlyBS's battery. Nevertheless, from the perspective of user's connectivity, the transmission power allocation is the key aspect.

In the view of the significance of energy on the communication's performance, this dissertation is dedicated to investigating the deployment of FlyBSs in mobile networks from various major aspects while with a consideration of power in one way or another. Such aspects include transmission/propulsion/total power consumption, user coverage duration, sum capacity maximization, and minimum user's capacity maximization. Several practical constraints are considered, such as the FlyBS's maximum transmission/propulsion power limit, speed, acceleration, available battery, and altitude. Other constraints related to the network's metrics include individual user's capacity, network's sum capacity, and backhaul link capacity. A variety of system models and assumptions also play key roles in the network, including i) communication mode, i.e., orthogonal and non-orthogonal multiple access (OMA and NOMA, respectively) together with related aspects such as NOMA user clustering and determination of user decoding order in the successive-interference-cancellation (SIC), and ii) multi-hop connection between the FlyBSs and the ground base station (GBS) via relaying FlyBSs on the backhaul link. In an attempt to provide comprehensive research in the area of FlyBS communications, several works are carried out separately in the framework of this PhD dissertation. Novel solutions are proposed, and benchmarks against the state-of-the-art are provided. The results demonstrate the potential of FlyBSs and encourage a more tactful utilization of resources.

Keywords: Unmanned aerial vehicle, flying base station, transmission power, propulsion power, mobile networks, sum capacity, non-orthogonal multiple access, relay, backhaul.

Abstrakt

Bezpilotním letadlům (UAV) se v posledních letech věnuje velká pozornost v oblasti bezdrátové komunikace. Díky vysoké flexibilitě a přizpůsobivosti prostředí lze bezpilotní letadla využívat jako létající základnové stanice (FlyBS), které potenciálně mohou významně zlepšit výkonnost mobilních sítí. Takové potenciální zlepšení však vyžaduje efektivní správu dostupných zdrojů. Pro efektivní integraci FlyBS do mobilních sítí je třeba vyřešit zejména několik problémů, včetně určení polohy, spotřeby energie, přiřazení uživatelů k FlyBS a přidělení přenosového výkonu a šířky pásma kanálu uživatelům.

Alokace/spotřeba energie je v sítích FlyBS kritickým aspektem, který by se mohl projevit ve všech uvedených výzvách. Zejména kvůli omezení přenosového výkonu, je nutné FlyBS změnit polohu, aby nedošlo k nežádoucí ztrátě výkonu systému. Přemístění by navíc mohlo být zapotřebí buď ke snížení vzdálenosti mezi FlyBS a uživatelem, nebo k zajištění lepšího kanálu mezi FlyBS a uživatelem. Takové posunutí FlyBS by znamenalo spotřebu pohonné energie. Existuje tedy potenciální kompromis mezi přenosovou a pohonnou energií. Proto by z hlediska spotřeby energie mohla být úspora pohonné energie výhodnější vzhledem k omezením baterie FlyBS. Nicméně z hlediska konektivity uživatele přidělení přenosového výkonu je klíčovým aspektem.

Cílem této disertační práce je prozkoumat nasazení FlyBS v mobilních sítích z různých pohledů s ohledem na význam energie na výkon komunikace. Mezi naše zkoumané problémy patří přenosová/pohonná/celková spotřeba energie, délka pokrytí uživatele, maximalizace součtové kapacity a maximalizace minimální kapacity uživatele. Zvažuje se řada praktických omezení, jako je maximální limit přenosového/pohonného výkonu FlyBS, rychlost, zrychlení, dostupná baterie a nadmořská výška. Další omezení související s metrikami sítě zahrnují kapacitu jednotlivých uživatelů, součtovou kapacitu sítě a kapacitu zpětného spoje. Klíčovou roli hrají také různé modely a předpoklady systému, ke kterým patří i) ortogonální a neortogonální vícenásobný přístup (OMA, resp. NOMA) spolu se souvisejícími aspekty, jako je seskupování uživatelů NOMA a určení pořadí dekódování uživatelů při postupném rušení (SIC), a ii) vícenásobné spojení mezi FlyBS a pozemní základnovou stanicí (GBS) prostřednictvím relačních FlyBS na zpětném spoji. Ve snaze poskytnout komplexní výzkum v oblasti komunikace s pomocí FlyBS je v rámci této disertační práce zpracováno několik samostatných prací. Jsou navržena nová řešení a poskytnuta srovnání s nejnovějšími technologiemi. Výsledky ukazují potenciální účinnost FlyBS a podporují šetrnější využití zdrojů v síti.

Klíčová slova: Bezpilotní letoun, létající základnové stanice, vysílací výkon, výkon pohonu, mobilní sítě, součet kapacity kanálu, neortogonální vícenásobný přístup, relé, Páteřní připojení.

Acknowledgements

I would like to sincerely thank my supervisor, Prof. Zdeněk Bečvář, for his guidance and encouragement throughout my studies. I sure am grateful for his precious support and for what is achieved under his motivating supervision.
To my dear family in Iran who never did/will stop believing in me. My mom, dad, and brothers, I am endlessly thankful for every moment that I am blessed having you all in this world.
To dear Anesa, sag moon žučo, the sparking whisper of hope in a dark and deep dream. . . , no kidding.
To my valued friend, Dr. Mostafa Kishani, for his genial companionship over many years. Sure have I been enlightened in personal and in professional life by his inspiring thoughts.
I would like to also thank my esteemed friends/colleagues, Ms. Aida Madelkhanova and Dr. Pavel Mach and Dr. Omid Esrafilian who I had the chance to work together with and to gain knowledge and professional insight from during my studies.

Contents

Chapter 1

Introduction

The 6G mobile networks introduce many challenges in line with inevitably growing demands in the future of mobile networks. Regardless of whether such demands prompt the emerging technology or vice versa, the *urge for communication* stays at the frontier of human needs and hence it deserves prevalent attention to be aptly nourished. An increasing density in data traffic, not only necessitates a smart design of more advanced equipment as well as resources, but also calls for a wise utilization of the existing. Conventional ground base stations, as one of the pillars of communication setups in mobile networks, cannot always adapt fully to the user's demands in their conventional static form. This is mainly due to a changing topology of network and environment as well as constraints on hardware supplies incorporated with limited available radio resources. Such obstacles are alleviated by a notable degree once the base stations are enabled to change their position over time. Unmanned aerial vehicles (UAVs) can offer such a feature and play the role of flying base stations (FlyBSs) [1]-[5].

Along with the UAV's mobility comes the advantage of allocating the users channels containing less (or ideally, no) intercepting obstacles leading to even higher quality of communication [6], [7]. Thanks to providing a more reliable communication, FlyBSs have caught an abundance of interest in many wireless applications. Much as every advantage offered by FlyBSs with respect to static BSs, the adverse impacts inherent to those advantages should also be dealt with; a (fast) relocation of the FlyBS requires consumption of energy, which is commonly referred to as propulsion energy [8], and a more dense connectivity accompanies a more intense interference in the network [9]. Consequently, many aspects already studied in scenarios with static BSs need to be revisited to address the concerns raised by the FlyBSs. For instance, the problem of power optimization for static BSs only targets the transmission power allocation/optimization, whereas a similar problem for FlyBSs requires also a dealing with the aspect of propulsion power consumption. That being said, the transmission power, despite its relatively lower magnitude with

respect to propulsion power [10], still remains a crucial factor from the perspective of user quality of service. Hence, there is a trade-off between the transmission and propulsion power consumptions in many scenarios.

To carry out a fair research on such trade-offs in FlyBS-assisted networks, this dissertation targets to study the network performance from different perspectives. Each perspective is essentially evoked in a set of specific applications, and it highlights particular objectives together with certain metrics that are tailored to evaluate the system's performance. For each studied objective we focus on the main challenges and we propose novel solutions that pioneer existing works in one way or another.

The main contributions of this dissertation is summarized as follows

- From the perspective of power consumption, the problem of minimizing the total power consumption of the FlyBSs is studied. In order to not underestimate the transmission power solely based on its magnitude comparing to propulsion power, we emphasize its importance by imposing a minimum individual capacity required by each user. Such cases are present in many emerging time-critical applications, such as autonomous driving, where the users are delay-sensitive, and a guarantee of instantaneous capacity is necessary. We investigate a minimization of the total power consumption via FlyBS's positioning and allocation of bandwidth and transmission power to the users. The problem is solved under constraints for the FlyBS's speed and altitude. Solutions are proposed for single-point and multi-point cases where the FlyBS's positions are optimized over one and multiple time steps, respectively.

- Next, in order to stress the importance of transmission power even more, we target the aspect of the user coverage in the network. More specifically, the user coverage is conditioned by whether all the users are provided with their required capacity. Accordingly, the duration of user coverage is considered as the metric. Non-orthogonal multiple access (NOMA) is adopted as the transmission mode in order to efficiently utilize the available radio resources. This aspect necessitates to also address NOMA user clustering and SIC user decoding. Since the operational duration of the FlyBS could also limit the coverage duration, a constraint on the FlyBS's battery is also included. From this point of view, the transmission power consumption shows a high importance while the FlyBS's battery's remaining energy is relatively high. In contrast, the significance of propulsion power consumption increases as the remaining battery's energy decreases over time. Analytical solutions are developed for the FlyBS's positioning, transmission power allocation, and NOMA user clustering. The problem is solved under constraints for NOMA cluster size as well as the FlyBS's

transmission power, propulsion power, battery's capacity, speed, and acceleration. Compared to existing works, our proposed solution considers all the mentioned aspects together. Furthermore, the proposed solution also allows for having clusters of different sizes leading to a lower transmission power consumption and, hence, prolonging the coverage duration.

- Next, the problem of NOMA clustering and transmission power allocation is investigated to maximize the minimum capacity achieved among all the users. This metric indicates the fairness of service among users when they actually do not demand for a certain amount of capacity due to any specific applications, however, the provided service would still affect their satisfaction. The problem is solved under constraints for the FlyBS's altitude, speed, and maximum transmission power. A novel analytical solution is provided to show the relevance between the main objective, i.e., the optimization of minimum capacity, and the minimization of transmission power. Then, a low-complexity solution for optimal user clustering is proposed. In particular, a geometrical solution based on a selection of convex polygons is developed to find the optimal clustering. The solution allows for clusters with different sizes.

- Then, from the perspective of QoS in terms of total communication capacity of the users, we investigate the power consumption of airship-based FlyBSs aiming to maintain the network's instantaneous total capacity above an expected threshold. In particular, in order to avoid redundant movements of the FlyBSs leading to a (excessive) propulsion power consumption, we try to keep the FlyBSs as much inert as possible while a minimum sum capacity is always guaranteed in the network. Constraints on the FlyBS's altitude and speed are considered in the optimization problem. A low-complexity novel solution is proposed based on a successive selection of the FlyBS with the smallest required propulsion energy to contribute a certain increment in the sum capacity. Importantly, it is shown that, by allowing only slight (few percent) decreases in the sum capacity of the network with respect to the maximum achievable sum capacity, a considerable amount of propulsion energy could be saved.

- Next, we study the problem of transmission power allocation and FlyBS's positioning to maximize the sum capacity in delay-sensitive applications where a minimum user's capacity is always guaranteed. The problem is solved under practical constraints for the FlyBS's speed, transmission power, and altitude. In addition, a constraint for the maximum propulsion power consumption is also included so that the FlyBS's displacements would not incur an excessive consumption of power leading to a relatively fast termination of the FlyBS's operation. Due to non-convexity

of the objective, an analytical solution based on an alternating optimization of the transmission power allocation and FlyBS's positioning is proposed. For the problem of positioning, a novel solution based on radial approximations of sum capacity is proposed. The heuristic solution shows a significant enhancement in the achieved sum capacity with respect to existing works.

- After developing solutions for different objectives in FlyBS networks, we then take another step forward and target to exploit the advantages of a multi-FlyBS network even more effectively by extending the adopted model. More specifically, a backhaul link is included so that the FlyBSs communicate with a ground base station (GBS). In addition to serving the users in such extended model, the FlyBSs also assist each other to establish a connection with the GBS. Such model, referred to as multi-hop FlyBS communication in our work, is very useful in scenarios where some FlyBSs move too far away from the GBS to be able to communicate with the GBS given their limited transmission power. Complications regarding this model include additional constraints that ensure the capacity of the backhaul link for every FlyBS would not be smaller than the capacity of the fronthaul link. The problem of sum capacity maximization is investigated via a user association and positioning of the FlyBSs. Due to non-tractability of the problem caused by non-convexity of the objective as well as discreteness of user association, we develop a novel heuristic solution based on an alternating optimization of user association and positioning of FlyBSs. The results demonstrate a significant increase in the sum capacity of the network with respect to the state-of-the-art solutions.

Chapter 2

Dissertation Objectives

In this Chapter, we outline the objectives investigated throughout the dissertation. Every objective highlights the network's performance from a different perspective as follows

- Minimization of the total power consumption via optimization of the transmission power allocation and FlyBS's positioning while a minimum instantaneous capacity is always guaranteed to each individual user.
- Maximization of the duration of user coverage provided by FlyBSs in NOMA networks via FlyBS's positioning, transmission power allocation, and user clustering for NOMA such that a minimum capacity is guaranteed to the users all the time.
- Maximization of minimum instantaneous capacity among users via transmission power allocation, FlyBS's positioning, and NOMA user clustering.
- Optimization of the FlyBSs' positioning to minimize the propulsion energy consumption in airship-based FlyBS networks such that the sum capacity provided to the mobile users would not fall below a given minimum threshold at any time.
- Maximization of sum capacity in mobile networks via an optimization of the FlyBS's positioning and transmission power allocation to the users while a minimum instantaneous capacity is always guaranteed to the users.
- Optimization of the FlyBSs' positioning and user association in multi-hop relaying networks with backhaul to maximize sum capacity in mobile networks.

The rest of the dissertation is organized as follows. In Chapter 3, we present our studied works within the scope of the dissertation and corresponding to the mentioned perspectives and objectives as listed above. Each section is structured to first introduce briefly the targeted objective. Then, the discussion of the section is followed by our written articles in line with the targeted objective. Within each attached article, we elaborate

a review of the literature followed by list of own contributions. Then, the formulated problem and the proposed solution is provided in details. The proposed solutions are then benchmarked against existing works to show their effectiveness. Last, we summarize the contribution of this dissertation in Chapter 4 and we point out to the future topics of research in line with the conducted research work.

Chapter 3

Results

In this chapter, different objectives (as mentioned in the previous chapter) are investigated in FlyBS-assisted mobile networks. Each objective is presented in a separate section followed by the associated article where a review of existing related works is presented as well.

3.1 Minimization of FlyBS total power with user QoS constraint

In this section, we focus on FlyBSs in mobile networks from a perspective of total power consumption which consists of the transmission and propulsion power consumptions. The transmission power is associated with providing the user's required minimum capacity at all time. A guarantee of such minimum capacity also depends on the relative positions of the FlyBS and the users. Thus, a positioning of the FlyBS over time might be required, otherwise, a guarantee of the user's required capacity might lead to an excessive consumption of transmission power which is not always the option due to limitations on the FlyBS's transmitter and battery. Hence, a minimization of the total power consumption is done via a dynamic allocation of transmission power to the users as well as a positioning of the FlyBS.

The following papers, which are references [C5] and [J2], respectively, present our work regarding the problem of total power optimization.

Optimizing Transmission and Propulsion Powers for Flying Base Stations

Mohammadsaleh Nikooroo, Zdenek Becvar
Department of Telecommunication Engineering, Faculty of Electrical Engineering
Czech Technical University in Prague
Prague, Czech Republic
nikoomoh@fel.cvut.cz, zdenek.becvar@fel.cvut.cz

***Abstract*—Unmanned aerial vehicles acting as flying base stations (FlyBSs) have been considered as an efficient tool to enhance capacity of mobile networks and to facilitate communication in emergency cases. The enhancement provided by such network necessitates a dynamic positioning of the FlyBSs with respect to the users. Despite that, the power consumption of the FlyBS remains an important issue to be addressed due to limitations on the capacity of FlyBS's batteries. In this paper, we propose a novel solution combining a transmission power control and the positioning of the FlyBS in order to ensure quality of service to the users while minimizing total consumed power of the FlyBS. We derive a closed-form solution for joint transmission and propulsion power optimization in a single future step. Moreover, we also provide a numerical method to solve the joint propulsion and transmission power optimization problem when a realistic (i.e. inaccurate) prediction of the users' movement is available. According to the simulations, the proposed scheme brings up to 26% of total FlyBS's power saving compared to existing solutions.**

***Index Terms*—Flying base station, transmission power, propulsion power, prediction, mobile users, mobile networks, 6G**

I. Introduction

Deployment of Flying Base Stations (FlyBSs) is a promising technique to address multiple concerns in wireless networks. In contrast to the conventional static base stations, the FlyBSs feature exclusive advantages due their high-mobility, which enables to adapt the network topology to an environment and actual user requirements on communication. This makes FlyBSs a suitable solution for various applications including surveillance in an area [1], offloading traffic from static base stations (BSs) [2], emergency operations [3], extending coverage [4]-[7], collection of data from IoT devices [8],[9], or improving quality of service for users [10]-[12]. In [13], several key challenges regarding the FlyBS's services to the users are listed. These challenges include, among others, positioning of the FlyBSs to provide coverage for as many users as possible, controlling the FlyBSs' power consumption to enhance their serving duration, or maximizing the quality of service (e.g., throughput). The problem of maximizing the coverage for networks with single FlyBS is studied in [4] and [6]. The authors in [7] investigate optimization of the number of required FlyBSs to guarantee the service quality to all ground users in a given area. The authors in [14] adopt evolutionary-based algorithms to maximize the users' satisfaction in terms of experienced data rates. In [10], the authors study the problem of the uplink throughput maximization in a scenario with multiple-antenna FlyBS. However, in all these papers, the power consumption is not addressed at all.

The problem of power consumption in a network with a fixed-wing FlyBS along with the ground users is investigated in [15]. The objective is to identify the trajectory of the FlyBS along several ground users and collect/deliver information from/to these users while minimizing the total power spent by the FlyBSs for flying and communication. Then, in [16], the same problem for rotary-wing FlyBS is studied. In [17], a reinforcement-learning (RL) framework is proposed to control the power consumption in the mobile networks with multiple FlyBSs. However, in [15], [16], and [17], the impact of transmission power is ignored and only the propulsion power spent for the movement of the FlyBS is considered. The efficient 3D placement of the FlyBSs with the consideration of transmission power minimization is studied in several works with a variety of goals including maximization of the number of covered users [18], maximization of the downlink coverage [5], maximization of network throughput [19], maximization of the users' quality-of-experience (QoE) [20], etc. These works are focused on reducing the FlyBSs' transmission power, but the power consumption due to the movement of the FlyBS is not considered. The energy consumption caused by the FlyBS's movement as well as by transmission of data is considered in [21]. However, the work is focused on a scenario in which the FlyBS tracks a mobile target. In such scenario, the constraint on quality of communication towards the users is ignored.

In our previous work [22], the combination of both the FlyBS's transmission power and propulsion power is considered for a single-point optimization. The single-point optimization is understood as adjustment of the FlyBS position and transmission power between each two time steps of the FlyBS

This work was supported by Grant No. P102-18-27023S funded by Czech Science Foundation and by the grant of Czech Technical University in Prague No. SGS17/184/OHK3/3T/13

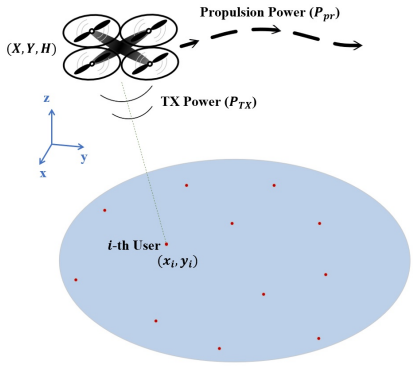

Fig. 1. System model with multiple mobile users deployed within coverage area of the FlyBS.

operation disregarding potential (even inaccurate) estimation of future movement of the users that could further reduce the total power consumption. Moreover, the model proposed in [22] assumes the propulsion power as a linear function of the FlyBS's velocity, which might not be realistic for rotary-wing FlyBSs as shown in [16].

In this paper, we analytically express the total power consumption as a function of the users' relative location with respect to the FlyBS and users requirements on the downlink capacity. Then a closed-form solution is provided for the case of single-point optimization, where, similar to [22], the total power is minimized between two consecutive time steps, although here we adopt a realistic non-linear model for the propulsion power consumption of the rotary-wing FlyBSs, which makes the solution significantly more complicated. Furthermore, a numerical solution is proposed to reduce the total power consumption over multiple time steps (multi-point optimization), as the idea of single-point optimization does not show a good performance in scenarios where the movement velocity of the ground users is very high. We show the performance of the proposed solution and compare it to the existing approaches. Our proposed method shows up to 26% improvement in the total power consumption compared with state-of-the-art methods.

The rest of the paper is organized as follow. In section II, we present the system model. The problem of the power optimization via determination of the FlyBS position and transmission power is presented in Section III. In section IV, we provide simulation results and compare performance with existing solutions. Last section concludes the paper and outlines potential directions to the future research.

II. System Model and Formulations

We consider a mobile network cell with a rotary-wing FlyBS that serves n mobile users in an area as shown in Fig. 1. All n users in the area communicate directly with the FlyBS.

Let $\{X(t), Y(t), H(t)\}$ denote the location of the FlyBS at the time t. By adopting the model from [15], we assume that the FlyBS operates at a fixed altitude H. Hence, the FlyBS can either hover or flight horizontally over the area. Let $\{x_i(t), y_i(t)\}$ denote the coordinates of the i-th ground user at the time t. Then, $d_i(t)$ denotes Euclidian distance of the i-th user to the FlyBS at time t.

We adopt orthogonal downlink channel allocation for all users as considered in a conventional mobile network. Thus, we assume no interference among channels of different users. With that, the channel capacity of the i-th user is calculated from the Shannon–Hartley theorem as:

$$C_i(t) = B_i \log_2(1 + \frac{p_i^R(t)}{N_i}), \tag{1}$$

where B_i denotes the bandwidth of the i-th user's channel, N_i denotes the noise power at the channel of the i-th user, and $p_i^R(t)$ is the received power by the i-th user at time t.

According to the Friis transmission equation, the transmission power of the FlyBS to the i-th user (p_i^T) is given as:

$$\begin{aligned} p_i^T &= Q_i d_i^2, \\ Q_i &= \frac{p_i^R (4\pi f_c)^2}{G_i^T G_i^R c^2}, \end{aligned} \tag{2}$$

where G_i^T is the gain of the FlyBS's antenna, G_i^R is the gain of the user's antenna, f_c is the communication frequency, and $c = 3 \times 10^8$m/s is the speed of light. Note that the coefficient $\frac{p_i^R (4\pi f_c)^2}{G_i^T G_i^R c^2}$ is denoted by Q_i for the ease of presentation in later discussions. Note that we assume the antennas of all users with the same gain. From (2), we can conclude that the power consumed by the FlyBS due to transmission power P_{TX} is expressed as a function of the coordinates of the users and the FlyBS as follow:

$$P_{TX}(X, Y, H, t_k) = \sum_{i=1}^{n} Q_i d_i^2 = \tag{3}$$

$$\sum_{i=1}^{n} Q_i ((X(k) - x_i(k))^2 + (Y(k) - y_i(k))^2 + H^2).$$

Following (3), the average transmission power (denoted as P_{TX}^{avg}) over the time span of $\{t_1, \ldots, t_T\}$ can be written as:

$$P_{TX}^{avg}(t_1, \ldots, t_T) = \frac{1}{T} \sum_{k=1}^{T} \sum_{i=1}^{n} Q_i d_i^2 =$$

$$\frac{1}{T} \sum_{k=1}^{T} \sum_{i=1}^{n} Q_i ((X(k) - x_i(k))^2 + (Y(k) - y_i(k))^2 + H^2). \tag{4}$$

As in many related works, we assume that the current positions of the users are known to the FlyBS (see, e.g. [4], [23], [24]). Also, the FlyBS can determine its own position as the knowledge of the FlyBS's position is needed for a common flying and navigation of the FlyBSs ([25]).

In order to formulate the power spent for the FlyBS's movement (propulsion power), we refer to the model provided in [16] for rotary-wing FlyBSs. In particular, the propulsion power is written as a function of the FlyBS's average velocity (denoted by V) in the following way:

$$P_{pr}(V) = L_0 (1 + \frac{3V^2}{U_{\text{tip}}^2}) + L_i (\sqrt{1 + \frac{V^4}{4v_{0,h}^4}} - \frac{V^2}{2v_{0,h}^2})^{\frac{1}{2}} + \frac{1}{2} d_0 \rho s_r A V^3. \tag{5}$$

where L_0 and L_i are the blade profile and induced powers in hovering status, respectively, U_{tip} denotes the tip speed of the rotor blade, $v_{0,h}$ denotes the mean rotor induced velocity during hovering, d_0 is the fuselage drag ratio, s_r is the rotor solidity, ρ is the air density, and A is the rotor disc area, see [16] for more details about the model.

Note that the FlyBS's average velocity can be calculated by dividing the distance moved between two points with the duration of the movement. In particular, if the FlyBS moves from $\{X(k), Y(k), H\}$ to the new location $\{X(k+1), Y(k+1), H\}$, the average velocity is rewritten as:

$$V(k, k+1) = \frac{1}{\Delta t_k}\sqrt{((X(k+1) - X(k))^2 + (Y(k+1) - Y(k))^2)}, \tag{6}$$

where $\Delta t_k = t_{k+1} - t_k$.

Let us define the initial position of the FlyBS as $(X(0), Y(0), H)$, the average propulsion power over the time period of $\{t_0, \ldots, t_T\}$ is written as:

$$P_{pr}^{avg} = \frac{1}{T}\sum_{k=0}^{T-1} P_{pr}(V(k, k+1)). \tag{7}$$

In order to formulate the total power consumption, we jointly optimize both the communication power and the propulsion power. We consider also the power consumption of on-board circuits at the FlyBS (denoted by $P_{circuit}$). Hence, the average overall power consumption P_{tot}^{avg} is written as:

$$P_{tot}^{avg}(X, Y, H, t_1, \ldots, t_T) = P_{circuit}^{avg} + P_{TX}^{avg} + P_{pr}^{avg} \tag{8}$$

According (3), (4), and (7)), we rewrite P_{tot}^{avg} as:

$$P_{tot}^{avg} = P_{circuit}^{avg} + \frac{1}{T}\sum_{k=1}^{T}\sum_{i=1}^{n} Q_i((X(k) - x_i(k))^2 + (Y(k) - y_i(k))^2 + H^2) + \frac{1}{T}\sum_{k=0}^{T-1} P_{pr}(V(k, k+1)). \tag{9}$$

Equation (9) can be further expanded by using (5) and (6), but we do not show the expanded form to avoid cluttering. Note that $P_{circuit}$ in (8) depends on the FlyBS's computational (processing) and communication chipsets and it can be regarded as a constant [16].

In [26], it is shown that, in order to achieve the optimal network's capacity while neglecting the propulsion power of FlyBS, the optimal coordinates $X_{opt}(k)$ and $Y_{opt}(k)$ of the FlyBS correspond to the center of gravity of the users' positions:

$$\begin{aligned} X_{opt}(k) &= \frac{\sum_{i=1}^{n} Q_i x_i(k)}{\sum_{i=1}^{n} Q_i}, \\ Y_{opt}(k) &= \frac{\sum_{i=1}^{n} Q_i y_i(k)}{\sum_{i=1}^{n} Q_i}. \end{aligned} \tag{10}$$

With a similar logic, in case that the users' capacities are not degraded, (8) indicates the position of the FlyBS that achieves the minimum transmission power. Note that the received power by the users is already incorporated in Q_i $(1 \leq i \leq n)$ according to (2), and so in case the users have different throughputs, the coefficients Q_i are not necessarily equal for different users.

III. Power Optimization and FlyBS Positioning

In this section, we first define the optimization problem. Then, we derive a closed-form solution to the defined problem for case $T = 1$, which is the single-point optimization as in [22], however, with non-linear power consumption model based on [16], which completely changes the solution. Next, we provide a numerical solution for the multi-point optimization problem ($T > 1$), as deriving a closed-form solution for this case is too difficult if not impossible.

A. Problem formulation

We formulate the problem of the total power consumption minimization over the time period T as follow:

$$\begin{aligned} &\underset{X(k), Y(k), H(k)}{\operatorname{argmin}} \; P_{tot}^{avg}, (1 \leq k \leq T) \\ &s.t. \quad C_j(t) \geq {C_j}^{min}, j \in \{1, ..., n\}, \forall t. \end{aligned} \tag{11}$$

The constraint in (11) guarantees that every user within the coverage area receives the minimum required capacity (denoted by $C_j^{min}, j \in 1, \ldots, n$) at all time. In our case, we define C_j^{min} as the capacity that would be experienced by the j-th user over the duration of $\{t_1, \ldots, t_T\}$ if a static BS was deployed. We remark that the transmission power (and so the total power consumption) is increasing with the received capacity according to (1) and (2). Thus, the minimum total power consumption in (11) occurs when every user receives exactly the minimum required capacity, hence, the constraint can be rewritten as $C_j(t) = C_j^{min} (\forall j \in \{1, \ldots, n\}, \forall t)$. From (1), it is concluded that for a constant capacity, the received power is also constant, which implies that the coefficients Q_i are constants. Hence, the transmission power for each user changes only when there is a relative displacement between the FlyBS and the users (e.g., due to users' movement). Here we note that the optimization problem in (11) is repeated every T time steps to calculate the optimum locations of the FlyBS over time.

B. Closed-form solution for single-point optimization

In this subsection, we derive closed-form solution to the optimization problem when $T = 1$. First, we find the critical points at which the partial derivatives of P_{tot}^{avg} are equal to zero. However, due to the complicated expression of $P_{pr}(V)$ in (5), calculation of the exact closed-form solution is not feasible. More specifically, we find that solving $\frac{\partial P_{tot}^{avg}}{\partial X} = 0$ and $\frac{\partial P_{tot}^{avg}}{\partial Y} = 0$ together leads to calculating the roots of polynomials of degree fourteen, which cannot be provided with algebraic solution. Instead, we find an approximation of $P_{pr}(V)$ using polynomial fitting and then solve $\frac{\partial P_{tot}^{avg}}{\partial X} = 0$ and $\frac{\partial P_{tot}^{avg}}{\partial Y} = 0$ by referring to the approximated expression. More specifically, it is observed that the propulsion power in (5) can be well approximated by a polynomial of degree five with respect to V. Fig. 2 shows the actual and the approximated curves for the FlyBS with physical specifications of the FlyBS provided in [27] for " DJI Spreading Wings S900" (see Table I in [27]). Since the error is negligible, we use the approximated propulsion power (denoted by $P_{pr}^{apx}(V)$) that is expressed as:

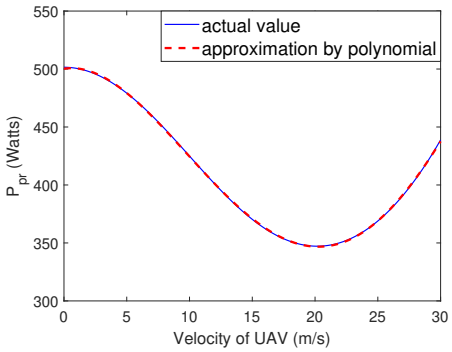

Fig. 2. Actual propulsion power and polynomial approximation vs. velocity of rotary-wing FlyBS.

$$P_{pr}^{apx}(V) = \sum_{j=0}^{5} c_j V^j, \tag{12}$$

$$c_0 = 500.2700, c_1 = 1.6360, c_2 = -1.4103, c_3 = 0.0479,$$
$$c_4 = 2.3521 \times 10^{-4}, c_5 = -1.3452 \times 10^{-5}.$$

The coefficients in (12) are calculated using MATLAB to fit the polynomial to the actual curve with the minimized mean-square-error (MSE).

Now by using P_{pr}^{apx} in (12) and rewriting the equations $\frac{\partial P_{tot}^{avg}}{\partial X} = 0$ and $\frac{\partial P_{tot}^{avg}}{\partial Y} = 0$ for the period of $\{t_0, t_1\}$ we get:

$$\sum_{i=1}^{n} 2Q_i(X(1) - x_i(1)) =$$
$$-\left(\frac{X(1) - X(0)}{\sqrt{(X(1) - X(0))^2 + (Y(1) - Y(0))^2}}\right) \cdot \frac{dP_{pr}^{apx}}{dV}|_{V=V(0,1)}$$

$$\sum_{i=1}^{n} 2Q_i(Y(1) - y_i(1)) =$$
$$-\left(\frac{Y(1) - Y(0)}{\sqrt{(X(1) - X(0))^2 + (Y(1) - Y(0))^2}}\right) \cdot \frac{dP_{pr}^{apx}}{dV}|_{V=V(0,1)} \tag{13}$$

From (13) we derive a new equation as follows

$$\frac{\sum_{i=1}^{n} 2Q_i(X(1) - x_i(1))}{\sum_{i=1}^{n} 2Q_i(Y(1) - y_i(1))} = \frac{X(1) - X(0)}{Y(1) - Y(0)}. \tag{14}$$

Equation (14) can be further rewritten as

$$\frac{(\sum_{i=1}^{n} 2Q_i)X(1) - (\sum_{i=1}^{n} 2Q_i x_i(1))}{(\sum_{i=1}^{n} 2Q_i)Y(1) - (\sum_{i=1}^{n} 2Q_i y_i(1))} = \frac{X(1) - X(0)}{Y(1) - Y(0)}. \tag{15}$$

From (15), it is concluded that (intermediate steps leading to (16) are not presented here):

$$(Y(1) - Y(0)) =$$
$$\frac{(\sum_{i=1}^{n} 2Q_i)Y(0) - (\sum_{i=1}^{n} 2Q_i y_i(1))}{(\sum_{i=1}^{n} 2Q_i)X(0) - (\sum_{i=1}^{n} 2Q_i x_i(1))}(X(1) - X(0)). \tag{16}$$

With (16), we can simplify the expression for V in (6) to

$$V = M|X(1) - X(0)|,$$
$$M = \frac{1}{\Delta t_k}\left(1 + \frac{(\sum_{i=1}^{n} 2Q_i)Y(0) - (\sum_{i=1}^{n} 2Q_i y_i(1))}{(\sum_{i=1}^{n} 2Q_i)X(0) - (\sum_{i=1}^{n} 2Q_i x_i(1))}\right)^{\frac{1}{2}}. \tag{17}$$

Now by expanding the first equation in (13) using (12) and (17) we get:

$$(\sum_{i=1}^{n} 2Q_i)X(1) - (\sum_{i=1}^{n} 2Q_i x_i(1)) = \tag{18}$$
$$-\left(\frac{X(1) - X(0)}{M|X(1) - X(0)|}\right)(5c_5V^4 + 4c_4V^3 + 3c_3V^2 + 2c_2V + c_1) =$$
$$-\left(\frac{X(1) - X(0)}{M|X(1) - X(0)|}\right)(5c_5M^4|X(1) - X(0)|^4 +$$
$$4c_4M^3|X(1) - X(0)|^3 + 3c_3M^2|X(1) - X(0)|^2 +$$
$$2c_2M|X(1) - X(0)| + c_1).$$

Equation (18) can be solved by considering two different possibilities: a) $X(1) > X_0$ (equivalently, $|X(1) - X(0)| = (X(1) - X(0))$ or b) $X(1) < X_0$ (equivalently, $|X(1) - X(0)| = -(X(1) - X(0))$. Presuming a) or b), (18) is rewritten as a quartic function with respect to $X(1)$ that can be provided with a closed-form solution as elaborated below. For $X(1) > X(0)$, (18) is rewritten as:

$$a_4X^4(1) + a_3X^3(1) + a_2X^2(1) + a_1X(1) + a_0 = 0,$$
$$a_4 = 5c_5M^3, \quad a_3 = -20c_5M^3X(0) + 4c_4M^2,$$
$$a_2 = 30c_5M^3X^2(0) - 12c_4M^2X(0) + 3c_3M,$$
$$a_1 = \sum_{i=1}^{n} 2Q_i - 20c_5M^3X^3(0) + 12c_4M^2X^2(0) - 6c_3MX(0) + 2c_2,$$
$$a_0 = 5c_5M^3X^4(0) - 4c_4M^2X^3(0) + 3c_3MX^2(0) - 2c_2X(0) +$$
$$\frac{c_1}{M} - (\sum_{i=1}^{n} 2Q_i x_i(1)). \tag{19}$$

There are four solutions to (19) that are given by:

$$\frac{-a_3}{4a_4} - S \pm \frac{1}{2}\sqrt{-4S^2 - 2p + \frac{q}{S}},$$
$$\frac{-a_3}{4a_4} + S \pm \frac{1}{2}\sqrt{-4S^2 - 2p - \frac{q}{S}}, \tag{20}$$

where

$$p = \frac{8a_4a_2 - 3a_3^2}{8a_4^2}, \quad q = \frac{a_3^3 - 4a_4a_3a_2 + 8a_4^2a_1}{8a_4^3},$$
$$S = \frac{1}{2}\sqrt{\frac{-2}{3}p + \frac{1}{3a_4}(G + \frac{\Delta_0}{G})}, \quad G = \sqrt[3]{\frac{\Delta_1 + \sqrt{\Delta_1^2 - 4\Delta_0^3}}{2}},$$
$$\Delta_0 = a_2^2 - 3a_3a_1 + 12a_4a_0,$$
$$\Delta_1 = 2a_2^3 - 9a_3a_2a_1 + 27a_3^2a_0 + 27a_4a_1^2 - 72a_4a_2a_0. \tag{21}$$

For $X(1) < X_0$, (18) is rewritten as:

$$b_4X^4(1) + b_3X^3(1) + b_2X^2(1) + b_1X(1) + b_0 = 0,$$
$$b_4 = 5c_5M^3, \quad b_3 = -20c_5M^3X(0) - 4c_4M^2,$$
$$b_2 = 30c_5M^3X^2(0) - 12c_4M^2X(0) + 3c_3M,$$
$$b_1 = -\sum_{i=1}^{n} 2Q_i - 20c_5M^3X^3(0) - 12c_4M^2X^2(0) - 6c_3MX(0) - 2c_2,$$
$$b_0 = 5c_5M^3X^4(0) + 4c_4M^2X^3(0) +$$
$$3c_3MX^2(0) + 2c_2X(0) + \frac{c_1}{M} + (\sum_{i=1}^{n} 2Q_i x_i(1)). \tag{22}$$

Similar to (19), there are four solutions to (22) that can be derived by using the coefficients $b_4, ..., b_0$ instead of $a_4, ..., a_0$, respectively. Of course, only the real roots of the quartic functions in (19) and (22) are considered. Furthermore, the solutions to (19) and (22) must meet their presumptive conditions $X(1) > X(0)$ and $X(1) < X(0)$, respectively.

For each of the candidates for $X(1)$, the corresponding value of $Y(1)$ is calculated from (18). In addition to the derived solutions, we also note that $(X(1), Y(1)) = (X(0), Y(0))$ is another critical point of P_{tot}^{avg} (of type 2). By collecting all the (real-valued) critical points, the optimal location of the FlyBS at t_1 (i.e.,$(X(1), Y(1), H)$) can be decided by evaluating P_{tot}^{avg} over $\{t_0, t_1\}$ for all those candidate points for $X(1)$. Next, the optimization is performed over $\{t_1, t_2\}$ to find $(X(2), Y(2), H)$, and so on.

C. Numerical solution for FlyBS power optimization $(T > 1)$

Note that solving the problem (11) requires determination of $2T$ unknown variables in (10), namely $X(k)$ and $Y(k)$ for $1 \leq k \leq T$, and so it is very difficult if not impossible to derive a closed-form expression in general. Instead, we try to optimize P_{tot}^{avg} in (11) by providing a numerical solution. There are several known methods that are commonly used to perform function optimization, such as descent algorithms (Newton's method, Broyden's method, etc.), evolutionary algorithms (genetic algorithms, simulated annealing, etc.), and pattern search methods (Simplex, multidirectional search, etc). The descent algorithms are typically fast in convergence, however, compared to other numerical solvers, they are more likely to get stuck in local optima or even in minimax points. In contrast, the pattern search methods are more reliable to find the global optima of the objective function. Hence, in this paper, we adopt pattern search methods to solve our defined problem. More specifically, we exploit Downhill Simplex Algorithm (also known as Nelder-Mead Algorithm [28]) to find the minimum value of the objective function f (namely, P_{tot}^{avg} in our formulation). This method is based on direct search in multidimensional space (with dimension m) and function comparison using simplex, which is a polytope of $m+1$ vertices in m dimensions. In our setup, each vertex is an m-dimensional point with $m = 2T$ which is corresponding to the (X, Y) sequence of the FlyBS over T time steps. The simplex is updated during following steps:

1. We start from $m+1$ points $P_1, P_2, \ldots, P_{m+1}$. Without loss of generality, we rearrange their indices to satisfy the following order (here we use the general notation of f as the objective function for the sake of simplicity of presentation):

$$f(P_1) \leq f(P_2) \leq \ldots \leq f(P_{m+1}). \tag{23}$$

2. Compute the centroid of all points except P_{m+1}, and let P_0 denote it.

3. Compute the reflected point with reflection coefficient α as:

$$P_r = P_0 + \alpha(P_0 - P_{m+1}). \tag{24}$$

4. If $f(P_1) \leq f(P_r) \leq f(P_m)$, then the simplex is updated by replacing P_{m+1} with P_r, and then we go back to step 1.

5. If $f(P_r) \leq f(P_1)$, the expanded point with expansion coefficient β is calculated as:

$$P_e = P_0 + \beta(P_r - P_0). \tag{25}$$

6. If $f(P_e) \leq f(P_r)$, then the simplex is updated by replacing P_{m+1} with P_e, and going to step 1. Otherwise, we replace P_{m+1} with P_r and then go to step 1.

7. Compute the contracted point with contraction coefficient γ as:

$$P_c = P_0 + \gamma(P_{m+1} - P_0). \tag{26}$$

8. If $f(P_c) \leq f(P_{m+1})$, then we replace P_{m+1} with P_c and go back to step 1. Otherwise, we compute the following shrunk points with shrinkage coefficient δ:

$$P_i = P_1 + \delta(P_i - P_1), 1 \leq i \leq m+1, \tag{27}$$

and then go to step 1.

The termination in this method occurs when the standard deviation of the function values at the simplex vertices falls below a given threshold. It is notable that the performance of Simplex method in terms of precision and termination time relies significantly on the parameters specified in the algorithm, such as the starting point (initial simplex), reflection, expansion, contraction and shrinkage coefficients that should be tuned according to the objective function. We derive the appropriate values of such parameters via experiments. For the initial simplex, we choose the values in the vicinity of the optimal solution. To do this, we use the points derived from the closed-form solution for single-point optimization as elaborated in the previous subsection. We also remark that during the calculation of the initial simplex from the closed form solution, the predicted location of the users are adopted as the reference. The details about the prediction of the users' locations as well as the specifications of Simplex method are elaborated in the next section.

IV. Simulation Results

In this section, we provide details of simulations and models adopted to evaluate the performance of the proposed power control for minimizing the total power consumed by the FlyBS. We also demonstrate the advantages of the proposed scheme over the existing non-optimal scheme.

TABLE I
Parameter Configurations

System Parameter	Numerical value
Number of users in the coverage area, n	180
Antenna gains, G_i^T,G_i^R	0 dBi [33]
Noise power spectral density, N_i	-174 dBm/Hz
Minimum capacity for the j-th user, C_j^{min}	1 Mbps
Communication frequency, f_c	2.6 GHz
System bandwidth	10 MHz [22]
Simulation step, Δt_j	1 second
Altitude of FlyBS, H	100 meters
Velocity of users, v_i	{2,5,10,12,15,20,25,30}m/s
On-board circuit consumption power, $P_{circuit}$	22 dBm [22]
Simulation Duration	320 seconds
Number of simulation drops	100

A. Simulation scenario and models

The simulations are performed using MATLAB. We consider a scenario where the FlyBS serves users represented by vehicles and/or users in vehicles, for example, during a traffic jam at a road or highway. In such situation, the conventional

network is usually overloaded as plenty of active users are located at a small area with limited network coverage. FlyBS can help to improve communication performance in such a scenario ([26], [29]). More specifically, the users are assumed to move on a 3-lane highway in the positive direction of y-axis. A wide range of velocities of the vehicles is considered ($\{2, 5, 10, 12, 15, 20, 25, 30\}$m/s) to cover different traffic situations. As mentioned in section II, the current positions of the users are assumed to be known to the FlyBS. However, the location of the users at the future time slots are unknown in general. There are many solutions for prediction of the user's movement, see, e.g., [30]-[32]. As each of the users-movement predictions reaches different performance depending on scenario and availability of additional information, the evaluation of our proposal for any specific prediction would lead to validity of the results only for such specific scenario and conditions of the predictor. Thus, we generalize the evaluation across the different predictive models for the position of each user via modeling a general prediction error as follows.

The next position of the users is extrapolated from their last two previous positions and this predicted position is further influenced by an addition of a random error. More specifically, we calculate the expected positions of the users by adding the prediction error to the actual positions of the users as follow:

$$\begin{aligned} x_i(s) &= x_i(0) + e_i^x(s), \\ y_i(s) &= y_i(0) + v_{i,0}^y(s) \times s + e_i^y(s), \end{aligned} \tag{28}$$

where $e_i^x(s)$ and $e_i^y(s)$ denote the added error to the x and y coordinates of the user i at the time s, respectively, and $v_{i,0}^y(s)$ denotes the velocity of the user i in the direction of y-axis at the time s. In our scenario, we consider the following model for $e_i^x(s)$ and $e_i^y(s)$:

$$\begin{aligned} |e_i^x(s)| &\leq W_H, \\ |e_i^y(s)| &\leq \frac{1}{2} v_i^y(s) \times s, \end{aligned} \tag{29}$$

where W_H denotes the highway's width.

Table I shows the values of the system parameters that we adopt in the simulations provided later in this section. For the wireless channel, we assume Free-Space Path Loss (FSPL) model, and omnidirectional antennas with a gain of 0 dBi as considered e.g., in [33]. We set spectral density of noise to be -174 dBm/Hz. The radio frequency $f_c = 2.6$ GHz and a bandwidth of 10 MHz [22] are selected. Following [16], the FlyBS's flight altitude is set to $H = 100$ m. Each simulation is of 320 s duration with a step of 1 s and the results are averaged out over 100 simulation drops (simulation runs).

We investigate four different schemes: i) proposed *multi-point optimization scheme (MPS)* with the location of FlyBS determined by numerical optimization of P_{tot}^{avg} as elaborated in section III; ii) *Single-point optimization scheme (SPS)* as in [22] where the locations of the FlyBS is determined by minimizing P_{tot}^{avg} for $T = 1$, although here we adopt the nonlinear model for propulsion power as in (5); iii) *Minimal TX scheme (MTX)* as studied in [26], where only the transmission power is minimized, and the propulsion power is ignored; iv) *Stationary FlyBS* scheme in which the FlyBS does not move, and so there is no propulsion power consumption.

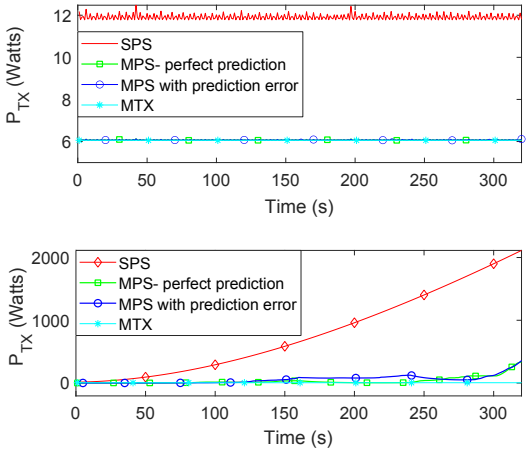

Fig. 3. P_{TX} for different optimization schemes and for $v_i = 5$ m/s (top figure) and 25 m/s (bottom figure).

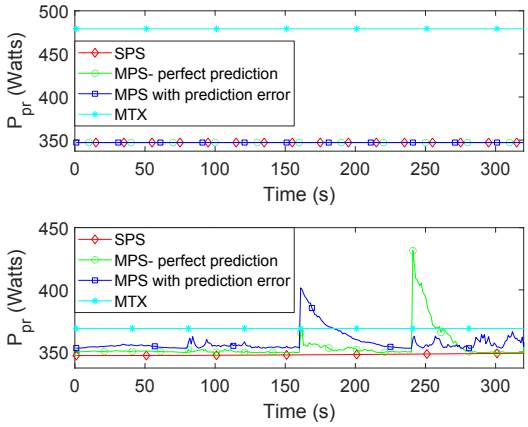

Fig. 4. P_{pr} for different optimization schemes and for $v_i = 5$ m/s (top figure) and 25 m/s (bottom figure).

For the Simplex method we derived the coefficient values for reflection (α), expansion (β), contraction (γ), and shrinkage (δ) factors through experiments as:

$$\alpha = 0.85, \beta = 1.75, \gamma = 0.4, \delta = 0.45. \tag{30}$$

The parameters' values in (30) are selected with respect to the accuracy and the termination time of the method.

B. Simulation results and discussion

First, we compare the average total power between multi-point and single-point optimization schemes.

Figures 3, 4, and 5 illustrate the transmission, propulsion, and total power consumption, respectively, over time for different methods. The figures show the average results for $v_i = 5$ m/s and $v_i = 25$ m/s. For MPS scheme, the duration of optimization period is $T = 80$.

It is observed that at a low velocity of the users, there is no significant change in transmission and propulsion power for

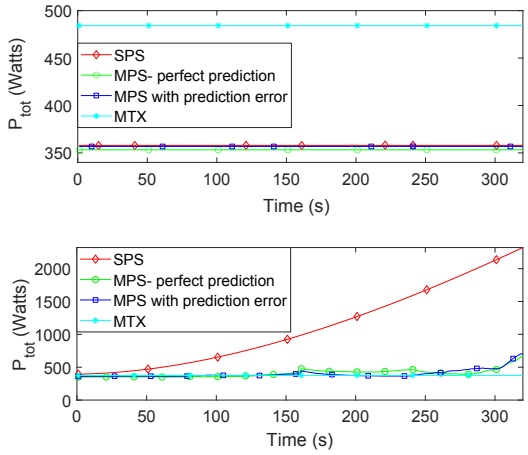

Fig. 5. P_{tot} for different optimization schemes and for $v_i = 5$ m/s (top figure) and 25 m/s (bottom figure).

both MPS and SPS schemes. This is because the propulsion power is a decreasing function at low velocities according to Fig. 2, and this impels the FlyBS to reduce P_{pr} by moving at higher speed than the users. Roughly speaking, at the early steps of movement, this strategy seems to make the FlyBS overtake the center of gravity of the users' locations, which causes an increase in the transmission power. In order to tackle this issue, the FlyBS moves back to the center of gravity after a few steps with almost the same velocity as before (to keep P_{pr} low as well). This strategy is selected by both MPS and SPS, and so there is no significant difference between the performance of the two methods at low users' velocities. It is notable that for high users' velocities, this strategy does not work, as choosing to fly at a lower speed (to reduce P_{pr}) at the beginning steps causes the FlyBS to fall behind the center of gravity, and so it may require the FlyBS to speed up towards the same direction, which introduces more propulsion power. This explains the degradation in SPS scheme's performance at high users' velocities.

According to Fig. 5, the MPS scheme provides a significantly more control over the total power consumption over time, by increasing the FlyBS's speed during some steps to avoid significant increase in transmission power. Note that For Stationary FlyBS scheme (scheme iv as indicated in the previous subsection), the average transmission powers (and so the average total powers) for $v_i = 5$ m/s and 25 m/s are 700 Watts and 18000 Watts, respectively, which is very larger than the average total power consumption in other schemes.

Next, we investigate an impact of the duration of the optimization period on the average power consumption of the FlyBS. Figures 6, 7, and 8 illustrate the average transmission, propulsion, and total power consumptions, respectively, versus the velocity of the vehicles. The results are shown for the optimization periods of $T = \{20, 50, 80\}$. According to all these figures, the power consumption decreases by performing optimization over larger optimization period for all velocities.

According to Fig. 6, there is negligible difference between

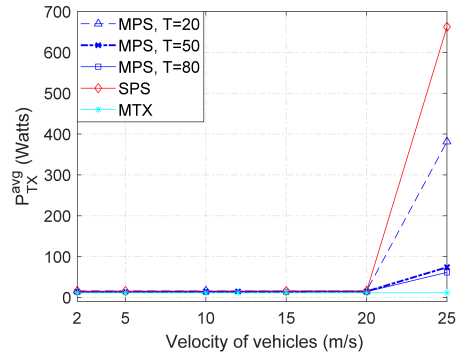

Fig. 6. P_{TX}^{avg} vs. user's velocity for different optimization schemes.

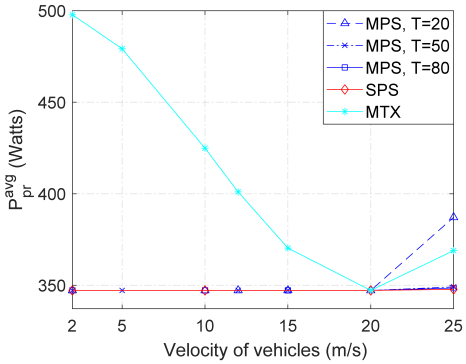

Fig. 7. P_{pr}^{avg} vs. user's velocity for different optimization schemes.

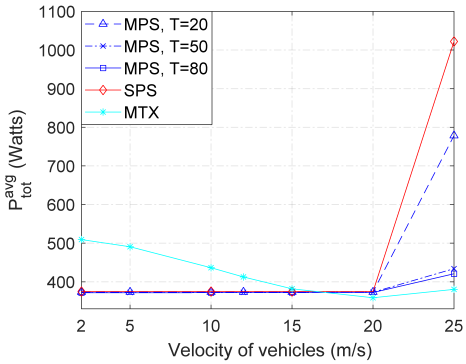

Fig. 8. P_{tot}^{avg} vs. user's velocity for different optimization schemes.

the transmission powers in MPS and SPS schemes for low velocities of the users. As discussed earlier in this section, at low speeds of the users, the FlyBS is basically able to reduce both the transmission and propulsion powers by increasing its speed, and staying close to the center of gravity of the users' locations at the same time. We also explained the reason for significantly increasing behavior of transmission and propulsion powers at high users' speeds. It is observed that the performance gap between MPS and SPS schemes in terms of both propulsion and transmission power is also increasing with respect to velocity, as higher speeds can be interpreted as higher FlyBS's displacements from the center of gravity of the

users, which makes the FlyBS increase either the transmission power or the propulsion power (or both) depending on the values of those powers.

As mentioned before, MTX scheme always ignores the impact of propulsion power. Such strategy causes more propulsion power (and hence more total power) at both high and low speeds where the propulsion cost is higher compared with medium speeds where the propulsion cost is relatively low (which is around the speed of 20 m/s according to Fig. 2). It is also notable that MTX slightly outperforms MPS at very high speeds, although the performance gap is negligible.

Figure 8 shows the advantage of MPS over both SPS and MTX schemes at different speeds. More specifically, the proposed MPS scheme can bring up to 26% improvement in the total power savings compared with MTX in the low-velocity regime, and up to 60% improvement in the total power savings compared with SPS in high-velocity regime.

V. Conclusions

In this paper, we have studied the problem of power optimization in future wireless networks with the FlyBSs. Contrary to existing papers, we optimize the total power consumed by the FlyBS including both the transmission power of the FlyBS and the propulsion power spent for movement of the FlyBS. We first provide closed-form solution determining the position of transmitting power of FlyBS for a realistic non-linear power consumption model in the case of single-point optimization. Then, we develop a numerical solution for the optimal location of the FlyBS and the transmission power of the FlyBS to minimize the total power consumed by the FlyBS over any arbitrary duration (multi-point optimization). We show that the proposed joint transmission power control and FlyBS's movement allows a significant reduction in the total power consumed by the FlyBS while the required capacity of the moving users is always satisfied. In the future, the multiple FlyBS scenario should be studied. In this scenario, association of the users to individual FlyBSs should also be considered.

References

[1] A. Puri, "A survey of unmanned aerial vehicles (UAV) for traffic surveillance," Department of computer science and engineering, University of South Florida, 2005.

[2] J. Lyu, Y. Zeng, and R. Zhang, "UAV-aided offloading for cellular hotspot," *IEEE Trans. Wireless Commun.*, Vol. 17, No. 6, 2018.

[3] K. P. Valavanis and G. J. Vachtsevanos, "Handbook of unmanned aerial vehicles," Springer Publishing Company, Incorporated, 2014.

[4] A. Al-Hourani, S. Kandeepan, and S. Lardner, "Optimal LAP altitude for maximum coverage," *IEEE Commun. Lett.*, Vol. 3, No. 6, 2014.

[5] M. Mozaffari et al., "Efficient deployment of multiple unmanned aerial vehicles for optimal wireless coverage," *IEEE Commun. Lett.*, Vol. 20, No. 8, 2016.

[6] I. Bor-Yaliniz and H. Yanikomeroglu, "The new frontier in ran heterogeneity: Multi-tier drone-cells," *IEEE Communications Magazine*, Vol. 54, No. 11, 2016.

[7] E. Kalantari, H. Yanikomeroglu, and A. Yongacoglu, "On the number and 3D placement of drone base stations in wireless cellular networks," *IEEE VTC Fall*, 2016.

[8] J. Chakareski, "Aerial UAV-IoT sensing for ubiquitous immersive communication and virtual human teleportation," *IEEE INFOCOM Workshops*, 2017.

[9] H. Kim, and J. Ben-Othman, "A collision-free surveillance system using smart UAVs in multi-domain IoT," *IEEE Commun. Lett.*, Vol. 22, No. 12, 2018.

[10] F. Jiang, and A. L. Swindlehurst, "Optimization of UAV heading for the ground-to-air uplink," *IEEE J. Sel. Areas Commun.*, Vol. 30, No. 5, 2012.

[11] V.Sharma, and M. Bennis, "UAV-assisted heterogeneous networks for capacity enhancement," *IEEE Commun. Lett.*, 2016.

[12] L. Wang, "Multiple access mmwave design for UAV-aided 5g communications," *IEEE Wireless Communications*, Vol. 26, 2019.

[13] M. Mozaffari et al., "A tutorial on UAVs for wireless networks: Applications, challenges, and open problems", *IEEE Commun. Surveys Tuts.*, 2019.

[14] J. Plachy et al., "Joint Positioning of Flying Base Stations and Association of Users: Evolutionary-Based Approach," *IEEE Access*, Vol. 7, 2019.

[15] Y. Zeng, and R. Zhang, "Energy-Efficient UAV Communication With Trajectory Optimization," *IEEE Trans. Wireless Commun.*, Vol. 16, No. 6, 2017.

[16] Y. Zeng, J. Xu, and R. Zhang, "Energy Minimization for Wireless Communication With Rotary-Wing UAV," *IEEE Trans. Wireless Commun.*, Vol. 18, No. 4, 2019.

[17] C. Liu et al., "Energy-Efficient UAV Control for Effective and Fair Communication Coverage: A Deep Reinforcement Learning Approach," *IEEE J. Sel. Areas Commun.*, Vol. 36, No. 9, 2018.

[18] H. Shakhatreh et al., "Efficient 3D placement of a UAV using particle swarm optimization," *Proc. IEEE ICICS*, 2017.

[19] Z. Becvar et al., "Positioning of Flying Base Stations to Optimize Throughput and Energy Consumption of Mobile Devices," *IEEE VTC Spring*, 2019.

[20] M. Chen et al., "Caching in the sky: Proactive deployment of cache-enabled unmanned aerial vehicles for optimized quality-of-experience," *IEEE J. Sel. Areas Commun.*, Vol. 35 , No. 5, 2017.

[21] M. Elloumi et al., "Designing an energy efficient UAV tracking algorithm," *IEEE IWCMC*, 2017.

[22] M. Nikooroo, and Z. Becvar, "Joint Positioning of UAV and Power Control for Flying Base Stations in Mobile Networks," *IEEE WiMOB*, 2019.

[23] E. Koyuncu et al., "Deployment and Trajectory Optimization for UAVs: A Quantization Theory Approach," *IEEE WCNC*, 2018.

[24] I. Bor-Yaliniz, A. El-Keyi, and H. Yanikomeroglu, "Efficient 3-D placement of an aerial base station in next generation cellular networks," *IEEE ICC*, 2016.

[25] B. Lee, J. Morrison, and R. Sharma, "Multi-UAV Control Testbed for Persistent UAV Presence: ROS GPS Waypoint Tracking Package and Centralized Task Allocation Capability," *ICUAS*, 2017.

[26] Z. Becvar et al., "Performance of Mobile Networks with UAVs: Can Flying Base Stations Substitute Ultra-Dense Small Cells?," *European Wireless*, 2017.

[27] A. Fotouhi et al., "Survey on UAV Cellular Communications: Practical Aspects, Standardization Advancements, Regulation, and Security Challenges," *IEEE Commun. Surveys Tuts.*, 2019.

[28] J.A. Nelder, and R. Mead, "A simplex method for function minimization," *The Computer Journal*, Vol. 7, No. 4, 1965.

[29] P. Yang et al., "Proactive Drone-Cell Deployment: Overload Relief for a Cellular Network Under Flash Crowd Traffic," *IEEE Trans. Intell. Transp. Syst.*, 2017.

[30] B. Prabhala, and T. La Porta,"Next place predictions based on user mobility traces," *IEEE INFOCOM Workshops*, 2015.

[31] Z. Zhao et al., "A demonstration of mobility prediction as a service in cloudified LTE networks," *IEEE CloudNet*, 2015.

[32] N. Kuruvatti, W. Zhou, and H. Schotten, "Mobility Prediction of Diurnal Users for Enabling Context Aware Resource Allocation," *IEEE VTC Spring*, 2016.

[33] 3GPP Technical Report 36.777, "Technical specification group radio access network; Study on enhanced LTE support for aerial vehicles (Release 15)," 2017.

[34] M. Xiong et al., "A Crowd Simulation Based UAV Control Architecture for Industrial Disaster Evacuation," *IEEE VTC Spring*, 2016.

Optimization of Total Power Consumed by Flying Base Station Serving Mobile Users

Mohammadsaleh Nikooroo, *Member, IEEE,* Zdenek Becvar, *Senior Member, IEEE*

***Abstract*—The unmanned aerial vehicles (UAVs) acting as flying base stations (FlyBSs) are considered as an efficient way to enhance the capacity of mobile networks. The enhancement provided by such network requires a dynamic positioning of the FlyBSs with respect to the users demands on communication. However, the power consumption of the FlyBS is a challenge due to a limited capacity of the FlyBS's power supply. In this paper, we reduce a total power consumption of the FlyBS while a required communication capacity is guaranteed to the mobile users in every time instant of their movement. To this end, we derive a closed-form solution for an optimization of the FlyBS's total power consumption in every single time step. Then, we provide a numerical solution for the total power optimization problem over a long period of the users' movement. Via the simulations, we show that the proposed scheme reduces the overall power consumed by the FlyBS significantly (by up to 91%) comparing to existing solutions.**

***Index Terms*—Flying base station, transmission power, propulsion power, mobile users, mobile networks, 6G.**

I. Introduction

Deployment of unmanned aerial vehicles (UAVs) acting as flying base stations (FlyBSs) is a promising way to address multiple concerns in wireless networks. Compared to the conventional static base stations, the FlyBSs present exclusive advantages due to their high mobility that enables to adapt the network topology to an environment as well as to actual user requirements on communication. Such features make the FlyBSs an efficient solution for various applications including surveillance [1], offloading traffic from static base stations (BSs) [2], emergency operations [3], extension of the network coverage [4]-[8], collection of data from IoT devices [9], [10], or improvement in quality of service [11]-[13].

Key challenges regarding the FlyBS's integration and deployment in mobile networks include [14]: positioning of the FlyBSs to maximize coverage, controlling the FlyBSs' power consumption to enhance their operational time [5], or maximizing the quality of service. The problem of the coverage maximization for the networks with a single FlyBS is studied, e.g., in [4] and [7]. Then, in [8], the authors investigate an optimization of the number of required FlyBSs to guarantee the quality of service to the users. In [15], an evolutionary-based algorithm is adopted to maximize the satisfaction of the users with the experienced data rates. In [11], the authors study the uplink throughput maximization in a scenario with multiple-antenna FlyBS. A throughput enhancement and a communication delay reduction by a dynamic control of the FlyBSs' trajectories is addressed in [16]. Furthermore, in [17], the authors minimize a delay for communication between the FlyBSs via planning the FlyBSs' trajectories. Then, the authors in [18] address the problem of FlyBS's positioning and user association for the FlyBSs acting as transparent relays to maximize sum capacity of users. However, in all these papers, the power consumption is not taken into account at all.

In [19], the problem of transmission power allocation is tackled to maximize an energy efficiency. However, the FlyBSs' positioning is not considered and the FlyBSs only hover at fixed points all the time. An efficient positioning of the FlyBSs considering the transmission power consumption is a scope of several works with a variety of goals including maximization of the network throughput [20]-[24], maximization of the difference between the profit in terms of the user capacity and the transmission cost [25], maximization of the number of covered users [26], minimization of the outage probability [27], or maximization of the users' quality-of-experience (QoE) [28]. However, the propulsion power consumption due to the movement of the FlyBS is not considered in any of [19]-[28].

Many works also address the problem of the FlyBS's trajectory planning in a scenario with static users. In [29], the authors minimize the total power consumption in the networks with a fixed-wing FlyBS collecting/delivering data from/to one static user. This work is then extended towards multiple static users in [30]-[32]. Furthermore, the authors in [33] and [34] maximize the minimum data rate of the users served by FlyBSs, However, in [29]-[34], the problem is defined as a planning of the trajectories among the static users and an allocation of the time for a sequential communication with each user and hovering in order to minimize the overall energy consumed by the FlyBS. The problem addressed in these papers is an analogy of the traveling salesman problem with a planning of the FlyBS trajectory among fixed and a priory known positions of the static users. The authors assume the users communicate sequentially in a non-real time manner. Hence, these works are suitable for delay-tolerant services and scenarios with static users (e.g., collection of data from sensors or power meters), however, an extension towards mobile users requiring real-time services is not straightforward, if not impossible.

In addition to [29]-[34], several other related works, e.g., [35]- [41], are also focused on the power consumption of the FlyBSs in different scenarios, where the users are static with coordinates known in advance. Unfortunately, the solutions proposed for the static users rely on a priori known and not

This work has been supported by the grant No. P102-18-27023S funded by Czech Science Foundation and by the grant of Czech Technical University in Prague No. SGS20/169/OHK3/3T/13.

M. Nikooroo and Z. Becvar are with the Department of Telecommunication Engineering, Faculty of Electrical Engineering, Czech Technical University in Prague, 166 27 Prague, Czech Republic (e-mail: nikoomoh@fel.cvut.cz, zdenek.becvar@fel.cvut.cz).

changing positions of the users. Thus, these solutions cannot be applied to a dynamic scenario with moving users.

The problem of the propulsion and transmission power consumption in mobile networks is considered in [42], where the FlyBS tracks a single moving target. However, the quality of communication channel is not taken into account. Up to our best knowledge, the problem of the power optimization for the FlyBSs serving mobile users with a constraint on the quality of service guarantee to the users has not been investigated in the literature.

In this paper, we focus on the minimization of the total power consumed by the rotary-wing FlyBS for the movement and for the communication while the minimum required communication capacity is continuously guaranteed to each mobile user in a real-time over the whole period of the FlyBS's operation. We propose a power saving scheme adjusting the FlyBS's position and the transmission power over a sequence of time steps to serve the mobile users. Even if we are aware of the fact that the transmission power consumption is usually lower than the propulsion power consumption for the FlyBSs, we still investigate both the transmission and propulsion powers jointly, as neglecting the transmission power would lead to a sub-optimal solution in some cases. We provide a generic solution applicable to any case disregarding whether the transmission power is negligible or not.

The major contributions of this paper are summarized as follows:

- The total power consumption is analytically expressed for rotary-wing FlyBS as a function of the system parameters including locations of the users and the FlyBS and the minimum capacity required by the users.
- Then, we propose a single-point optimization scheme (denoted as SPS) to minimize the total power consumed by the FlyBS between two consecutive time steps. At each time step, the bandwidth allocation and the position of the FlyBS for the next time step is determined. For this case, we derive a closed-form solution expressing the next position of the FlyBS for arbitrary allocation of the bandwidth.
- We extend the SPS towards a multi-point optimization scheme (referred to as MPS), as the SPS does not guarantee the optimum over a long time period. For the MPS, we provide a numerical solution based on Nelder-Mead Simplex algorithm considering a constraint on the FlyBS's speed.
- Furthermore, we extend the idea of the MPS towards an enhanced MPS (EMPS) to further reduce the propulsion power consumption. The extension combines the aspects of both SPS and MPS via a sliding window to continuously adjust the future positions of the FlyBS.
- As the above-mentioned solutions might lead to an excessive transmission power of the FlyBS to fulfill the constraints on the users' required capacity, we further enhance the proposed solution towards a more practical case with the transmission power of the FlyBS considered. Then, we reformulate such a constrained problem to be solvable numerically.
- By simulations, we show that our proposed solution leads to a significant (up to 91%) improvement in the total power consumption comparing to the state-of-the-art methods.

Note that this paper is an extension of our prior works [43], [44], where we have provided an initial analysis of the total power optimization.

The rest of the paper is organized as follow. In Section II, we present the system model. In Section III, the problem of the power optimization via a determination of the FlyBS's position and the transmission power for the moving users is formulated for a scenario with an unconstrained transmission power to show a theoretical maximum performance. Besides, we propose novel solutions for this problem in Section IV. In Section V, we formulate the problem and we provide solution for a practical power optimization in the scenario with a constrained transmission power. Then, in Section VI, we explain the simulation scenario and models, in section VII we present results and compare these with the performance of existing solutions. Last section concludes the paper and outlines potential directions to the future research.

II. System model

We consider a rural scenario with n mobile users (e.g., vehicles) moving on a road or a highway as illustrated in Fig. 1. In such scenario, the FlyBSs are a suitable solution to provide temporary connectivity in case of a traffic jam or an accident [45], [46], when the users search for information about the traffic situation and, hence, move rather slower than in a common traffic situation. All n users in the area communicate directly with the FlyBS, as the communication capacity of the conventional static base stations in the rural areas is usually not sufficient to serve many users in the traffic jam.

Let $\boldsymbol{r}(t) = [X(t), Y(t), H(t)]$ denotes the location of the FlyBS at the time t and $[x_i(t), y_i(t)]$ denotes the coordinates of the i-th user at the time t. Then, $d_i(t)$ denotes Euclidean distance of the i-th user to the FlyBS at the time t.

The channel capacity of the i-th user is calculated from the Shannon–Hartley theorem as:

$$C_i(t) = B_i(t)\log_2(1 + \frac{p_i^R(t)}{N_i}), \tag{1}$$

where $B_i(t)$ denotes the bandwidth of the i-th user's channel, N_i denotes the noise power at the channel of the i-th user, and $p_i^R(t)$ is the power received by the i-th user at the time t. In case of additional interference at the receiver, the superimposed interference can be assumed to be of Gaussian distribution and, thus, its power can be incorporated into (and treated as) the noise power [29], [48].

The transmission power of the FlyBS to the i-th user (p_i^T) is calculated according to the Friis' transmission equation as:

$$p_i^T = Q_i d_i^{\gamma_i} = \frac{p_i^R (4\pi f_c)^{\gamma_i} d_i^{\gamma_i}}{G_i^T G_i^R c^{\gamma_i} (\frac{M}{M+1}\overline{h}_i + \frac{1}{M+1}\tilde{h}_i)}, \tag{2}$$

where γ_i is the path-loss exponent between the FlyBS and the i-th user, G_i^T and G_i^R are the gains of the FlyBS's

Table I: Summary of Parameters

Parameter	Description
$[X(t), Y(t), H(t)]$	Coordinates of FlyBS
H_{min}, H_{max}	FlyBS's minimum and maximum allowed flying altitudes
$[x_i(t), y_i(t)]$	Coordinates of user i
$d_i(t)$	Distance between FlyBS and user i
$C_i(t), C_i^{min}(t)$	Instantaneous capacity and minimum required capacity of user i
$p_i^R(t)$	Received power by user i
$p_i^T(t)$	FlyBS's transmission power to user i
$B_i(t)$	Bandwidth of user i
N_i	Noise power at the channel of user i
G_i^R, G_i^T	Antenna gain of user i and FlyBS
f_c	Communication frequency
c	Speed of light
$P_{TX}(t)$	FlyBS's instantaneous transmission power
P_{TX}^{avg}	FlyBS's average transmission power
P_{TX}^{max}	maximum transmission power of FlyBS
$P_{pr}(t)$	FlyBS's instantaneous propulsion power
P_{pr}^{avg}	FlyBS's average propulsion power
$V(t)$	FlyBS's speed
V_{max}	Maximum FlyBS's speed
$P^{circuit}$	FlyBS circuits' power consumption
L_0, L_i	FlyBS hovering blade profile and induced power
U_{tip}, A	Blade speed and disk area of FlyBS rotor
$v_{0,h}$	Rotor induced speed for hovering FlyBS
d_0	FlyBS's fuselage drag ratio
s_r	FlyBS's rotor solidity
ρ	Air density
T	Number of time steps in multi-point optimization
T_Δ	Number of time steps in EMPS's output
W_H	Highway's width
η	Error factor in prediction
$\{e_i^{M,x}, e_i^{M,y}\}$	Real-time measurement error in $\{x, y\}$-coordinates of user i
$\{e_i^{Pr,x}, e_i^{Pr,y}\}$	Prediction error in $\{x, y\}$-coordinates of user i
$\{v_i^x(t), v_i^y(t)\}$	Velocity of user i in directions of $\{x, y\}$-axes
$\alpha, \beta, \nu, \delta$	Reflection, expansion contraction, and shrinkage factors in Simplex

and user's antennas, respectively, f_c is the communication frequency, $c = 3 \times 10^8$m/s is the speed of light, M is the Rician fading factor, $\overline{h}_i$ is the line-of-sight (LoS) component satisfying $|\overline{h}_i| = 1$, and $\tilde{h}_i$ denotes the non-line-of-sight (NLoS) component satisfying $\tilde{h}_i \sim CN(0,1)$ Note that the coefficient $\frac{p_i^R(4\pi f_c)^{\gamma_i}}{G_i^T G_i^R c^{\gamma_i}(\frac{M}{M+1}\overline{h}_i + \frac{1}{M+1}\tilde{h}_i)}$ is substituted with Q_i for the ease of presentation in later discussions. Furthermore, despite high velocities of the users, an impact of Doppler shift is still marginal and can be ignored, as the ratio of the relative speed between the FlyBS and the users to the speed of light is very small.

From (2), we observe that the transmission power P_{TX} consumed by the FlyBS is expressed as a function of the

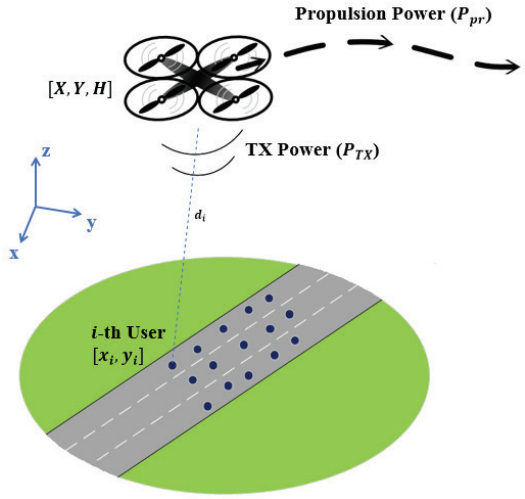

Fig. 1. System model with multiple mobile users deployed within coverage area of the FlyBS.

coordinates of the users and the FlyBS, i.e.,:

$$P_{TX}(X, Y, H, t_k) = \sum_{i=1}^{n} Q_i d_i^{\gamma_i} = \quad (3)$$

$$\sum_{i=1}^{n} Q_i \big((X(t_k) - x_i(t_k))^2 + (Y(t_k) - y_i(t_k))^2 + H^2(t_k)\big)^{\frac{\gamma_i}{2}}.$$

Following (3), the average transmission power, denoted as P_{TX}^{avg}, over the time span of $\{t_1, \ldots, t_T\}$ is written as:

$$P_{TX}^{avg}(t_1, \ldots, t_T) = \frac{1}{T}\sum_{k=1}^{T}\sum_{i=1}^{n} Q_i d_i^{\gamma_i} = \frac{1}{T}\sum_{k=1}^{T}\sum_{i=1}^{n} Q_i \big($$

$$(X(t_k) - x_i(t_k))^2 + (Y(t_k) - y_i(t_k))^2 + H^2(t_k)\big)^{\frac{\gamma_i}{2}}. \quad (4)$$

As in many related works, we assume that the current positions of the users are known to the FlyBS (see, e.g., [4], [29], [31], [49], [50]). However, in any realistic case, the positioning information is inaccurate and contains a positioning error. Thus, the user's position known to the FlyBS is given as:

$$x_i(t) = x_i^{exact}(t) + e_i^{M,x}(t),$$
$$y_i(t) = y_i^{exact}(t) + e_i^{M,y}(t), \quad (5)$$

where $x_i^{exact}(t)$ and $y_i^{exact}(t)$ are the exact x and y coordinates of the i-th user at the time t, respectively, and $e_i^{M,x}(t)$ and $e_i^{M,y}(t)$ are the positioning errors in x and y coordinates at the time t, respectively. We further assume that the FlyBS can determine its own position, as the knowledge of the FlyBS's position is needed for a common flying and navigation of the FlyBSs [51].

In order to formulate the power spent for the FlyBS's movement (propulsion power), we refer to the model provided in [31] for rotary-wing FlyBSs. In particular, the propulsion power is a function of the FlyBS's average velocity V in the

following way:

$$P_{pr}(V) = L_0(1 + \frac{3V^2}{U_{\text{tip}}^2}) + L_i(\sqrt{1 + \frac{V^4}{4v_{0,h}^4}} - \frac{V^2}{2v_{0,h}^2})^{\frac{1}{2}} + \frac{1}{2}d_0\rho s_r A V^3, \quad (6)$$

where L_0 and L_i are the blade profile and induced powers in hovering status, respectively, U_{tip} denotes the tip speed of the rotor blade, $v_{0,h}$ represents the mean rotor induced velocity during hovering, d_0 is the fuselage drag ratio, s_r is the rotor solidity, ρ is the air density, and A denotes the rotor disc area. Interested readers can find more details about the model in [31]. Note that we consider the setting of parameters of the propulsion power model in line with the FlyBS with physical specifications provided in [52] for "DJI Spreading Wings S900" (see Table I in [31] and Table I in [52]).

Note that the FlyBS's average velocity is calculated by dividing the distance moved between two points with the duration of the movement. In particular, if the FlyBS moves from the position $\boldsymbol{r}(t_k)$ to the new position $\boldsymbol{r}(t_{k+1})$, the average speed is determined as:

$$V(t_k, t_{k+1}) = \frac{1}{\Delta t_k}||\boldsymbol{r}(t_{k+1}) - \boldsymbol{r}(t_k)||, \quad (7)$$

where $\Delta t_k = t_{k+1} - t_k$.

Let us define the initial position of the FlyBS as $[X(t_0), Y(t_0), H(t_0)]$. Thus, the average propulsion power over the time period of $\{t_0, \ldots, t_T\}$ is written as:

$$P_{pr}^{avg} = \frac{1}{T}\sum_{k=0}^{T-1} P_{pr}\big(V(t_k, t_{k+1})\big). \quad (8)$$

We jointly optimize both the transmission power and the propulsion power as these are main parts of the total power consumption of the FlyBS. Nevertheless, we also consider a power consumption of on-board circuits of the FlyBS (denoted by $P_{circuit}$). Hence, the average overall power consumption P_{tot}^{avg} is written as:

$$P_{tot}^{avg}(\boldsymbol{r}, t_0, t_1, \ldots, t_T) = P_{circuit}^{avg} + P_{TX}^{avg} + P_{pr}^{avg}. \quad (9)$$

Note that $P_{circuit}$ in (9) depends on the FlyBS's computational (processing) and communication chipsets, and can be regarded as a constant [31].

Inserting (4) and (8) into (9), we rewrite P_{tot}^{avg} as:

$$P_{tot}^{avg} = P_{circuit}^{avg} + \frac{1}{T}\sum_{k=0}^{T-1} P_{pr}(V(t_k, t_{k+1})) + \frac{1}{T}\sum_{k=1}^{T}\sum_{i=1}^{n} Q_i \times \big((X(t_k) - x_i(t_k))^2 + (Y(t_k) - y_i(t_k))^2 + H^2(t_k)\big)^{\frac{\gamma_i}{2}}. \quad (10)$$

Equation (10) can be further expanded by simply plugging (7) into (6), however, we do not show the expanded form to avoid cluttering.

III. Problem formulation for unconstrained transmission power

We formulate the problem of the total power consumption minimization over the period of T time steps as:

$$\min_{\boldsymbol{r}(t_k), \boldsymbol{B}(t_k)} P_{tot}^{avg}, (1 \le k \le T) \quad (11)$$
$$s.t. \quad C_i(t_k) \ge {C_i}^{min}, \forall i \in \{1, ..., n\}, \forall k, \quad (a)$$
$$H_{min}(X(t_k), Y(t_k)) \le H(t_k) \le H_{max}(X(t_k), Y(t_k)), \quad (b)$$
$$||\boldsymbol{r}(t_{k+1}) - \boldsymbol{r}(t_k)|| \le V_{max}(t_{k+1} - t_k). \quad (c),$$
$$\sum_{i=1}^{n} B_i \le B_{tot} \quad (d),$$

where V_{max} is the FlyBS's maximum speed and B_{tot} is the total available bandwidth that can be allocated by the FlyBS. The constraint (a) in (11) guarantees that every user within the coverage area receives the minimum required capacity $C_i^{min}, \forall i \in \{1, \ldots, n\})$ at all time as the users move. Furthermore, the constraint (b) in (11) bounds the FlyBS's movement to the allowed altitude range of $[H_{min}(X, Y), H_{max}(X, Y)]$ at every time step. The values of $H_{min}(X, Y)$ and $H_{max}(X, Y)$ are determined based on the environment's topology (e.g., obstacles, buildings, etc.) and/or flight regulations given by local authorities in every country at each $[X, Y]$ position of the FlyBS. Furthermore, the constraint (c) guarantees that the FlyBS's movement does not incur a speed larger than the maximum limit of V_{max}, and the constraint (d) ensures that the total allocated bandwidth does not exceed the maximum available bandwidth B_{tot}.

For further elaboration and solution of the problem defined in (15), we simplify the constraint on the minimum capacity via the following proposition.

Proposition 1. *The minimum transmission power in (11) is achieved for $C_i(t) = {C_i}^{min}, \forall i \in \{1, ..., n\}, \forall t$.*

Proof. From (1), the received power p_i^R is rewritten as:

$$p_i^R(t) = N_i(2^{\frac{C_i(t)}{B_i}} - 1), \quad (12)$$

and, hence, the transmission power is formulated as:

$$p_i^T = Q_i d_i^{\gamma_i} = \frac{N_i(2^{\frac{C_i(t)}{B_i}} - 1)(4\pi f_c)^{\gamma_i}}{G_i^T G_i^R c^{\gamma_i}(\frac{M}{M+1}\overline{h}_i + \frac{1}{M+1}\tilde{h}_i)} d_i^{\gamma_i}. \quad (13)$$

From (13), we see that p_i^T is increasing with C_i for $i = 1, ..., n$. Thus, the minimum transmission power is obtained when $C_i(t) = C_i^{min}$ $(\forall i \in \{1, \ldots, n\}, \forall t)$. □

Proposition 1 implies that, in order to achieve the minimum transmission power, the constraint (a) in (11) should be rewritten as $C_i(t) = C_i^{min}$ $(\forall i \in \{1, \ldots, n\}, \forall t)$.

IV. Optimization of Power and FlyBS Positioning and Bandwidth Allocation

In this section, we introduce the proposed approach to solve (11) via a successive optimization of the bandwidth allocation and the FlyBS's positioning. Then, we explain solution to the subproblem of the bandwidth allocation at the given position of the FlyBS. Afterwards, for the problem of the FlyBS's

positioning, we provide a high-level overview of the proposed solutions for the FlyBS positioning. Next, we derive a closed-form solution of the problem for the first proposed solution represented by the single-point optimization scheme SPS, (i.e., for $T = 1$). Next, we provide a numerical solution for the multi-point optimization scheme MPS ($T > 1$), as deriving a closed-form solution for this case is extremely difficult if not impossible. Furthermore, we enhance the MPS towards EMPS via a multi-point optimization with a sliding window to eliminate a problem with the power consumption discovered at the end of the optimization period of T time steps.

A. Successive optimization of the bandwidth and the FlyBS's positioning

A joint optimization of the FlyBS's position and bandwidth to solve (11) is difficult, as the total power consumption is a non-convex problem with respect to the FlyBS's position. To tackle this issue, we propose a solution based on a successive optimization of the bandwidth $\boldsymbol{B}$ and the FlyBS's position. In other words, we optimize the bandwidth allocation for a given position of the FlyBS. Afterwards, a new position of the FlyBS is found and we solve again the problem of bandwidth optimization at the updated position of the FlyBS. This process is repeated until the changes in the derived $\boldsymbol{r}(t_k)$ and $\boldsymbol{B}(t_k)$ falls below a given threshold, or until the maximum number of iterations is reached in the proposed sequential optimization of $\boldsymbol{r}(t_k)$ and $\boldsymbol{B}(t_k)$.

B. Optimization of the bandwidth allocation

To optimize bandwidth, let us note that the problem in (11) is convex with respect to $\boldsymbol{B}$ at any fixed position of the FlyBS. Hence, at the given position of the FlyBS (i.e., $\boldsymbol{r}(t_k)$), the convex subproblem of the bandwidth optimization is formulated as:

$$\min_{\boldsymbol{B}(t_k)} P_{tot}^{avg}, (1 \leq k \leq T) \tag{14}$$
$$s.t. \quad C_i(t_k) = {C_i}^{min}, \forall i \in \{1, ..., n\}, \forall k, \quad (a)$$
$$\sum_{i=1}^{n} B_i \leq B_{tot}, \quad (b)$$

Using Shannon's formula, the constraint (a) in (14) is rewritten as $B_i(t_k) \geq \frac{C_i^{min}}{\log_2(1+\frac{p_i^R}{N_i})}$. Thus, the problem in (14) is convex with respect to $\boldsymbol{B}$ and we solve it using CVX which is an efficient optimization tool for convex problems [53].

C. Optimization of the FlyBS's positioning

Next, for the optimal bandwidth allocation derived by CVX, we reformulate the subproblem of the FlyBS's positioning to:

$$\min_{\boldsymbol{r}(t_k)} P_{tot}^{avg}, (1 \leq k \leq T) \tag{15}$$
$$s.t. \quad C_i(t_k) = {C_i}^{min}, \forall i \in \{1, ..., n\}, \forall k, \quad (a)$$
$$H_{min}\big(X(t_k), Y(t_k)\big) \leq H(t_k) \leq H_{max}\big(X(t_k), Y(t_k)\big), \quad (b)$$
$$||\boldsymbol{r}(t_{k+1}) - \boldsymbol{r}(t_k)|| \leq V_{max}(t_{k+1} - t_k). \quad (c)$$

The solution to (15), i.e. finding the FlyBS position, is outlined in next subsections.

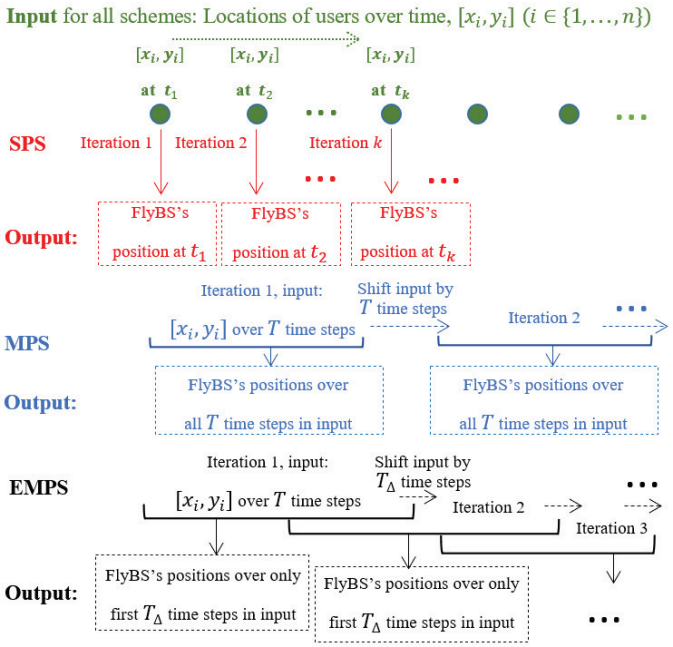

Fig. 2. Illustration of a high-level principle of all three proposed schemes for single-point, multi-point, and enhanced multi-point optimizations of the total power consumed by FlyBS.

D. Overview of the proposed solutions to the FlyBS's positioning

Before going into details of individual proposed solutions, we first provide a high-level illustration of all three proposed schemes to outline key differences among them. Note that the bandwidth allocation problem is solved in a similar way for all the proposed solution as explained in the subsection IV.A.

According to Fig. 2, at each iteration of the optimization, the proposed SPS calculates the FlyBS's position only for a given single time step, while the MPS and the EMPS determine multiple future positions of the FlyBS in several time steps. In the MPS as well as in the EMPS, for each input including a set of the expected locations of the users over next T time steps, the future T positions of the FlyBS are determined. While the MPS navigates the FlyBS over all these determined positions during the whole period of T and new positions are determined again after T, the EMPS continuously updates all future positions exploiting new updated inputs.

Details of individual proposed solutions are presented in the following subsections.

E. Single-point optimization of the total power consumption ($T = 1$)

In this subsection, we derive closed-form solution to the problem defined in (15) for $T = 1$. Note that the solution is derived for the FlyBS's movement with no constraint on the speed and at a fixed altitude. The motivation to consider a fixed altitude is that, the available propulsion power consumption model for rotary-wing FlyBSs (provided by [31]) considers only a horizontal flight at a fixed altitude. However, we further

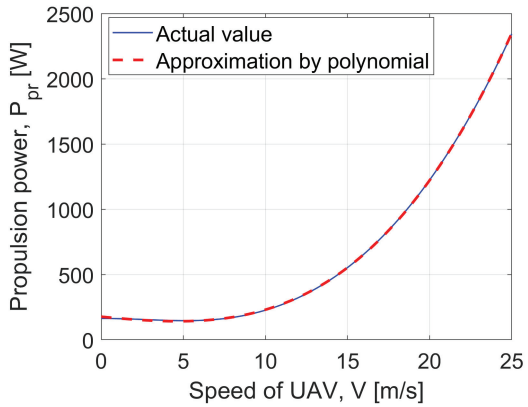

Fig. 3. Actual propulsion power and polynomial approximation vs. velocity of rotary-wing FlyBS.

enhance the solution to variable altitude in subsection IV.F for multi-point optimization. We also adopt $\gamma_i = 2$ (see (13)) in this subsection for simplicity of formulations and expressions, nevertheless, the solution can be easily extended to any value of γ_i and we generalize γ_i also in subsection IV.F.

To solve (15), first, we find the critical points at which the partial derivatives of P_{tot}^{avg} are equal to zero. A calculation of the exact closed-form solution for $P_{pr}(V)$ defined in (6) is extremely complicated, as solving $\frac{\partial P_{tot}^{avg}}{\partial X} = 0$ and $\frac{\partial P_{tot}^{avg}}{\partial Y} = 0$ together leads to calculating the roots of polynomials of degree fourteen. Thus, we first find an approximation of $P_{pr}(V)$ using polynomial fitting and then solve $\frac{\partial P_{tot}^{avg}}{\partial X} = 0$ and $\frac{\partial P_{tot}^{avg}}{\partial Y} = 0$ by referring to the approximated expression. To this end, we approximate the propulsion power in (6) by a polynomial of degree five with respect to V as:

$$P_{pr}^{apx}(V) = \sum_{j=0}^{5} c_j V^j, \tag{16}$$

$$c_0 = 215.6755, c_1 = 3.0695, c_2 = -2.5831, c_3 = 0.3497,$$
$$c_4 = -0.0064, c_5 = 7.5336 \times 10^{-5}.$$

The propulsion power approximation coefficients c_j in (16) are calculated via the minimum mean-square-error (MSE). The actual and approximated curves are shown in Fig. 3 to demonstrate sufficient fitting of the approximated propulsion power consumption model.

Using the approximation in (16), we calculate the critical points of P_{tot}^{avg}. The following Theorem 1 determines the optimum position of the FlyBS in closed-form via a derivation of the critical points for P_{tot}^{avg} and an evaluation of P_{tot}^{avg} in these critical points.

Theorem 1. *The FlyBS's optimum position at the time t_1 is derived as:*

$$[X(t_1), Y(t_1)] = \underset{[X,Y],\, X \in X^c}{\operatorname{argmin}} \; P_{tot}^{avg} \tag{17}$$

where $X^c = \{X_1^c, ..., X_5^c\}$ is the set of the x-coordinates of the critical points for P_{tot}^{avg} given by:

$$X_1^c = X(t_0),$$
$$\{X_2^c, X_3^c\} = \frac{-A_3}{4A_4} - S \pm \frac{1}{2}\sqrt{-4S^2 - 2p + \frac{q}{S}}, \tag{18}$$
$$\{X_4^c, X_5^c\} = \frac{-A_3}{4A_4} + S \pm \frac{1}{2}\sqrt{-4S^2 - 2p - \frac{q}{S}},$$

and $Y(t_1)$ is determined as:

$$(Y(t_1) - Y(t_0)) = \frac{(\sum_{i=1}^{n} 2Q_i)Y(t_0) - \big(\sum_{i=1}^{n} 2Q_i y_i(t_1)\big)}{(\sum_{i=1}^{n} 2Q_i)X(t_0) - \big(\sum_{i=1}^{n} 2Q_i x_i(t_1)\big)}\big(X(t_1) - X(t_0)\big), \tag{19}$$

with the following substitutions adopted:

$$p = \frac{8A_4A_2 - 3A_3^2}{8A_4^2}, q = \frac{A_3^3 - 4A_4A_3A_2 + 8A_4^2A_1}{8A_4^3},$$
$$S = \frac{1}{2}\sqrt{\frac{-2}{3}p + \frac{1}{3A_4}(G + \frac{\Delta_0}{G})}, G = \sqrt[3]{\frac{\Delta_1 + \sqrt{\Delta_1^2 - 4\Delta_0^3}}{2}},$$

$$\Delta_0 = A_2^2 - 3A_3A_1 + 12A_4A_0,$$
$$\Delta_1 = 2A_2^3 - 9A_3A_2A_1 + 27A_3^2A_0 + 27A_1^2A_4 - 72A_4A_2A_0,$$
$$A_4 = 5c_5M^3, \quad A_3 = -20c_5M^3X(t_0) + (-1)^{I_g}(4c_4M^2),$$
$$A_2 = 30c_5M^3X^2(t_0) - 12c_4M^2X(t_0) + 3c_3M,$$
$$A_1 = -20c_5M^3X^3(t_0) + (-1)^{I_g}\big(12c_4M^2X^2(t_0)\big) -$$
$$6c_3MX(t_0) + (-1)^{I_g}(\sum_{i=1}^{n} 2Q_i + 2c_2),$$
$$A_0 = 5c_5M^3X^4(t_0) - (-1)^{I_g}\big(4c_4M^2X^3(t_0)\big) + 3c_3MX^2(t_0)$$
$$-(-1)^{I_g}(2c_2X(t_0)) + \frac{c_1}{M} - (-1)^{I_g}\big(\sum_{i=1}^{n} 2Q_i x_i(t_1)\big),$$
$$M = \frac{1}{\Delta t_k}\Big(1 + \frac{(\sum_{i=1}^{n} 2Q_i)Y(t_0) - \big(\sum_{i=1}^{n} 2Q_i y_i(t_1)\big)}{(\sum_{i=1}^{n} 2Q_i)X(t_0) - \big(\sum_{i=1}^{n} 2Q_i x_i(t_1)\big)}\Big)^{\frac{1}{2}},$$
$$I_g = \mathbb{1}_{\{X(t_1) < X(t_0)\}}. \tag{20}$$

Proof. See Appendix A.

After the FlyBS moves to the new position derived via Theorem 1, the optimization is performed over $\{t_1, t_2\}$ to find $[X(t_2), Y(t_2), H]$, and so on and so forth.

F. Multi-point optimization of the total power consumption ($T > 1$)

The single-point optimization in the previous subsection minimizes the total power consumption over a duration of one time step. Hence, the positioning of the FlyBS might be sub-optimal in terms of the power consumption from the perspective of a longer operation of the FlyBSs. To tackle this problem we provide an extended solution by optimizing the total power consumption over multiple time steps ($T > 1$).

Solving the FlyBS positioning, i.e., the problem defined in (15), for multi-point optimization requires a determination of $3T$ unknown variables in (10), namely $X(t_k)$, $Y(t_k)$, and

$H(t_k)$ for $1 \leq k \leq T$, and so it is extremely difficult, if not impossible, to derive a closed-form expression in general. Hence, we optimize P_{tot}^{avg} in (15) by providing a numerical solution.

There are several known methods that are commonly used to perform function optimization, such as descent algorithms (Newton's method, Broyden's method, etc.), evolutionary algorithms (genetic algorithms, simulated annealing, etc.), or pattern search methods (Simplex, multidirectional search, etc). The descent algorithms are typically fast in convergence, however, compared to other numerical methods, they are more likely to get stuck in local optima or even in minimax points. In contrast, the pattern search methods are more reliable and find the global optima of the objective function. Hence, in this paper, we adopt the pattern search methods to solve our defined problem. More specifically, we exploit Downhill Simplex Algorithm (also known as Nelder-Mead Simplex Algorithm) [54] to find the minimum value of P_{tot}^{avg} according to the objective formulated in (15). This algorithm is based on a direct search in a multidimensional space with m dimensions and a function comparison using simplex, which is a polytope of $m+1$ vertices among m dimensions. The simplex is updated based on the values obtained from reflection, expansion, contraction, and shrinkage operations on the vertex at which the function reaches the largest value, and the centroid of the remaining vertices.

The Nelder-Mead Simplex algorithm requires all the unknown variables in the objective function to be unconstrained. However, the constraints (b) and (c) in (15) explicitly bound the coordinates of the FlyBS. To resolve this issue, we provide a change of variables to guarantee that the constraints (b) and (c) in (15) are automatically fulfilled and, hence, the constraints can be removed from the problem in (15). To always guarantee the constraints (b) and (c), we define the new variables ϱ_k, ς_k, and τ_k so that:

$$\begin{aligned} X(t_{k+1}) &= X(t_k) + V_{max}(t_{k+1}-t_k)cos(\varrho_{k+1})cos(\varsigma_{k+1}),\\ Y(t_{k+1}) &= Y(t_k) + V_{max}(t_{k+1}-t_k)cos(\varrho_{k+1})sin(\varsigma_{k+1}),\\ H(t_{k+1}) &= min\{H_{min}\big(X(t_{k+1}),Y(t_{k+1})\big)+ \\ &\Big(H_{max}\big(X(t_{k+1}),Y(t_{k+1})\big) - H_{min}\big(X(t_{k+1}),Y(t_{k+1})\big)\Big)\\ &\times sin^2(\tau_{k+1}), max\{H(t_k)+V_{max}(t_{k+1}-t_k)sin(\varrho_{k+1}),\\ &H_{min}\big(X(t_{k+1}),Y(t_{k+1})\big)\}\}, \end{aligned} \tag{21}$$

With the new defined variables ϱ_k, ς_k, and τ_k and knowing that $0 \leq sin^2(\tau_k) \leq 1$ all the time, it is concluded that:

$$\begin{aligned} &H_{min}\big(X(t_{k+1}),Y(t_{k+1})\big) \leq H(t_{k+1}) \leq \\ &H_{min}\big(X(t_{k+1}),Y(t_{k+1})\big) + (H_{max}\big(X(t_{k+1}),Y(t_{k+1})\big) - \\ &H_{min}(X(t_{k+1}),Y(t_{k+1})))sin^2(\tau_{k+1}) \leq \\ &H_{min}\big(X(t_{k+1}),Y(t_{k+1})\big) + \Big(H_{max}\big(X(t_{k+1}),Y(t_{k+1})\big) - \\ &H_{min}\big(X(t_{k+1}),Y(t_{k+1})\big)\Big) = H_{max}\big(X(t_{k+1}),Y(t_{k+1})\big). \end{aligned} \tag{22}$$

Thus, with the parameterization proposed in (21), the constraint (b) on the FlyBS's altitude is fulfilled. Furthermore, from (21), we also have

$$\begin{aligned} ||\boldsymbol{r}\,(t_{k+1}) - \boldsymbol{r}\,(t_k)\,|| \leq ||V_{max}(t_{k+1}-t_k)\times \\ [cos(\varrho_{k+1})cos(\varsigma_{k+1}), cos(\varrho_{k+1})sin(\varsigma_{k+1}), sin(\varrho_{k+1})]|| = \\ V_{max}(t_{k+1}-t_k). \end{aligned} \tag{23}$$

Hence, the constraint (c) in (15) is also fulfilled, and the optimization problem in (15) can be reformulated as

$$\begin{aligned} &\min_{\varrho_k,\varsigma_k,\tau_k} P_{tot}^{avg}, (1 \leq k \leq T) \\ &s.t. \quad C_i(t) = {C_i}^{min}, \forall i \in \{1,...,n\}, \forall t. \end{aligned} \tag{24}$$

where the constraint in (24) is presented considering Proposition 1. Now we explain details of the proposed algorithm, which is also summarized in Algorithm 1. In our setup, each vertex of the simplex (denoted by $S_i, 1 \leq i \leq m$) is an m-dimensional point with $m = 3T$ corresponding to the sequence of ϱ_k, ς_k, and τ_k for $1 \leq k \leq T$, i.e., $\{\varrho_1, \varsigma_1, \tau_1, ..., \varrho_T, \varsigma_T, \tau_T\}$. The $3T+1$ vertices of the simplex are selected by guessing an initial point as one of the vertices (denoted as S_{m+1}) and, then, generating each of the other $3T$ vertices by changing the value at one dimension of the initial point. More specifically, for $1 \leq i \leq m$,

$$S_i = \begin{cases} S_{m+1} + \kappa_i S_{m+1,i}\mathbf{e_i} & S_{m+1,i} \neq 0, \\ S_{m+1} + \epsilon_i \mathbf{e_i} & \text{otherwise}, \end{cases} \tag{25}$$

where $S_{m+1,i}$ denotes the i-th element of S_{m+1}, and $\mathbf{e_i}$ is the m-dimensional unit vector with zero elements at all dimensions except the i-th dimension, and ϵ_i and κ_i are real coefficients that adjusts the convergence of the algorithm. The values for ϵ_i and κ_i create the initial simplex, and choosing a larger ϵ_i and κ_i leads to a larger search space for the optimization and, hence, to a prolongation of the optimization process. Thus, we start with the setting $\epsilon_i = 0$ and $\kappa_i = 0$ and, then, we gradually increase these values and run the algorithm repeatedly until the found the solution does not change anymore. This indicates that the optimum point is already enclosed by the initial simplex and, thus, a further increase in ϵ_i and κ_i is not necessary [55].

From the definition of the simplex's vertices, it is inferred that the values of the vertices should be selected carefully to achieve an efficient numerical optimization in terms of an accuracy as well as a convergence time. The algorithm is terminated when the standard deviation of the corresponding values of P_{tot}^{avg} at the updated simplex's vertices fall below a given threshold. In other words, when the vertices are close enough to each other, the algorithm stops to save time. In our setup, the value of threshold is set by trial and error considering the convergence time.

Also, the internal parameters specified in the algorithm, such as reflection, expansion, contraction, and shrinkage coefficients are tuned through trial and error and by considering both precision and convergence time, as there is no deterministic approach to select the optimal values for these coefficients. An option to determine the parameter's values is to exploit

evolutionary algorithms, such as genetic algorithms. However, these algorithms require a relatively long time to find suitable values of parameters, and there is still no guarantee that the derived values would be optimal [56].

Another common approach, adopted also in our paper, is to find the parameters' values empirically and by testing the performance of the algorithm for different values, as suggested in [57], where the authors provide an experimental testbench for the choice of the parameters, and analyze the performance of the Simplex. In line with [57], we find the values of the parameters in the Simplex algorithm via an evaluation of the algorithm's performance for a variety of the parameters' values exploiting a knowledge of the Simplex's principle. Thus, we start from the default values proposed in the original Nelder-Mead algorithm, i.e., 1.00, 2.00, 0.50, and 0.5 for the reflection, expansion, contraction, and shrinkage parameters, respectively. Then, at each time, we change one of those parameters by a specified increment/decrement value, and check the corresponding performance of the Simplex. According to the results presented in [57] and [58], the performance of the Simplex starts degrading if the values of those parameters become too large or too small. Hence, we do not need to check every possible combination of different values of these parameters and we choose an increment/decrement value of ± 0.05 for all Simplex's parameters. We find the minimum total power consumption of the FlyBS for the values of 0.87, 1.75, 0.46, and 0.45 of the reflection, expansion, contraction, and shrinkage parameters, respectively.

We note that, after the Simplex algorithm is applied to find ϱ_k, ς_k, and τ_k for $1 \leq k \leq T$, we repeat the algorithm to find ϱ_k, ς_k, and τ_k for $T+1 \leq k \leq 2T$, and so on for the entire operational time.

G. Enhanced multi-point optimization of transmission power and position

From (11), it is inferred that the obtained positions of the FlyBS at time steps $t_1, \ldots, t_T$ guarantee the minimal power consumption over the period of T time steps only, and if the operational time of the FlyBS is longer than T time steps, such solution might not be suitable due to the problem of having a transition edge between two optimization periods. More specifically, the location of the FlyBS at t_T is considered as the end position of one optimization period $\{t_1, \ldots, t_T\}$ and also as the initial position of the FlyBS for the next period $\{t_{T+1}, \ldots, t_{2T}\}$. Since (11) is solved for each time period disregarding the next period, the transition among the optimization periods at t_T can potentially increase the propulsion power consumption over $\{t_{T+1}, \ldots, t_{2T}\}$. This can be solved by setting a long-enough T. However, performing the optimization over a larger T may not be useful in realistic scenarios with erroneous prediction of the users movement, as increasing T introduces a higher prediction error in general.

In order to tackle this issue, we enhance the previous multi-point optimization scheme by a sliding window optimization over multiple time points. To this end, we solve (11) over $\{t_1, \ldots, t_T\}$, however, only the derived locations of the FlyBS for the first T_Δ time steps (i.e., $t_1, \ldots, t_{T_\Delta}$, where $T_\Delta < T$) are actually used and the rest is adjusted in the next steps. Next, we solve (11) over $\{t_{T_\Delta+1}, \ldots, t_{T_\Delta+T}\}$ with the initial position of the FlyBS as at t_{T_Δ}. Then, this optimization is repeated when the FlyBS reaches $t_{T_\Delta+1}$, thus, only the derived locations of the FlyBS at time steps $\{t_{T_\Delta+1}, \ldots, t_{2T_\Delta}\}$ are used. This process is repeated for the rest of the entire operational time.

Algorithm 1 3-dimensional optimal positioning of the FlyBS

Input: $[x_i(t_k), y_i(t_k)]$, $(1 \leq i \leq n,\ 1 \leq k \leq T)$,
Output: FlyBS's position at $t_k = \text{argmin}_{\varrho_k, \varsigma_k, \tau_k} P_{tot}^{avg}, (1 \leq k \leq T)$
$\sigma(A)$: standard deviation of elements in set A
σ_0: standard deviation threshold for termination
S_{m+1}: random initial guess for $\varrho_k, \varsigma_k, \tau_k$
S_i $(1 \leq j \leq m)$: other simplex's vertices calculated from (25)
$f(S_i)$: P_{tot}^{avg} at the FlyBS's positions given by S_i.

Sort and rearrange simplex's vertices as $f(S_1) \leq f(S_2) \leq \ldots \leq f(S_{m+1})$.
while $\sigma\big(f(S_1), f(S_2), \ldots, f(S_{m+1})\big) > \sigma_0$ **do**
  $S_0 = \text{centroid}\{S_1, ..., S_m\}$
  if $f(S_1) \leq f(S_r) \leq f(S_m)$ **then** $S_{m+1} \leftarrow S_r$
  else $S_e = S_0 + \beta(S_r - S_0)$
  end if
  if $f(S_e) \leq f(S_r)$ **then** $S_{m+1} \leftarrow S_e$ and go to step 13
  else $S_{m+1} \leftarrow S_r$ and go to step 13
  end if
  $S_c = S_0 + \nu(S_{m+1} - S_0)$.
  if $f(S_c) \leq f(S_{m+1})$ **then** $S_{m+1} \leftarrow S_c$ and go to step 13
  else $S_i = S_1 + \delta(S_i - S_1)$ for $1 \leq i \leq m+1$ and go to step 13
  end if
  Sort points so that $f(S_1) \leq f(S_2) \leq \ldots \leq f(S_{m+1})$.
end while
Calculate $H(t_k)$ from the updated τ_k in S_{m+1} and (21)

H. Summary of all three proposed solutions

The basic principle of all three proposed schemes (SPS, MPS, EMPS) is summarized in Fig. 4. For all proposed schemes, the user's coordinates represent the inputs to the algorithm. The outputs are in a form of the FlyBS's coordinates and the transmission power setting.

The SPS determines the FlyBS's positioning and the transmission power allocation to each user at every time step t_k in a single-time-step-input to single-time-step-output manner, while the MPS and the EMPS provide positions and transmission power allocations for a whole period of $T > 1$ time steps on a basis of multiple-time-step-input to multiple-time-step-output optimization. Furthermore, the MPS does not update the calculated positions of the FlyBS in the previous optimization iteration, while the EMPS constantly adjusts later FlyBS's positions and transmission powers calculated in the previous iterations.

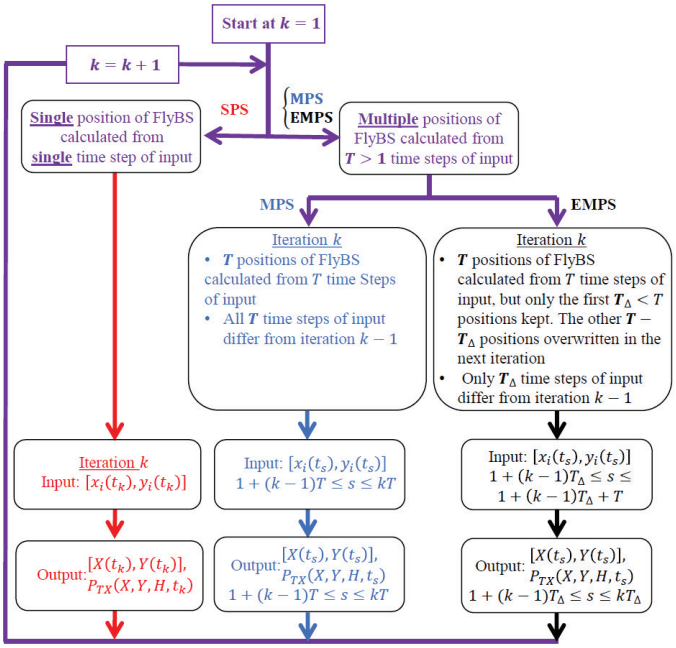

Fig. 4. Detailed principle of all three proposed schemes based on single-point optimization, multi-point optimization, and enhanced multi-point optimization.

V. Power Optimization with Transmission Power Constraints

The presented solutions in the previous section show a theoretical achievable performance in the communication system with unbounded transmission power. In real networks, however, the transmission power is limited by regulations or simply by capabilities of the physical equipment. Thus, in this section, we focus on a realistic case with the limited transmission power of the FlyBS.

In case the transmission power is limited, the power optimization problem is enhanced with a new constraint as:

$$\min_{\boldsymbol{r}(t_k)} P_{tot}^{avg}, (1 \le k \le T) \tag{26}$$
$$s.t. \quad C_i(t_k) = {C_i}^{min}, \forall i \in \{1, ..., n\}, \forall k, \quad (a)$$
$$H_{min}(X(t_k), Y(t_k)) \le H(t_k) \le H_{max}(X(t_k), Y(t_k)), \quad (b)$$
$$||\boldsymbol{r}(t_{k+1}) - \boldsymbol{r}(t_k)|| \le V_{max}(t_{k+1} - t_k). \quad (c)$$
$$P_{TX}(X, Y, H, t_k) \le P_{TX}^{max}, \forall k \in \{1, ..., T\} \quad (d)$$

where the equality in the constraint (a) corresponds to the Proposition 1. To fulfill the constraint (d) in (26), global parameters of the mobile network should be set properly in the same way as expected in any existing research work dealing with a resource allocation and management in the mobile networks (not limited to FlyBSs). If the system is not globally set up properly (e.g., when a too narrow band is available, user's are guaranteed with too high capacity, etc.), the constraint (d) in (26) might not hold even for the optimum X_{opt} and Y_{opt} at some time step(s). Thus, to solve the practical problem with the transmission power constraint, we assume that the system level parameters including available bandwidth (B_i) and antennas' gains (G_i^T, G_i^R) are pre-set with respect to the environment so that the following condition is fulfilled:

$$\min_{\boldsymbol{r}(t_k)} \sum_{i=1}^{n} \frac{N_i(2^{\frac{C_i^{min}}{B_i}} - 1)(4\pi f_c)^{\gamma_i}}{G_i^T G_i^R c^{\gamma_i} (\frac{M}{M+1}\bar{h}_i + \frac{1}{M+1}\tilde{h}_i)} d_i^{\gamma_i} \le P_{TX}^{max} \tag{27}$$

The solution adopted for MPS and EMPS (sections IV.F and IV.G) is based on Simplex algorithm. However, the Simplex algorithm is not able to solve optimization problems with constraints on the optimization variables in the objective function. In other words, we cannot apply the same solution directly to (26), as if we expand the constraint (d) in (26) using (3), the constraint contains unknown positions of the FlyBS in the following way:

$$\sum_{i=1}^{n} Q_i \big((X(t_k) - x_i(t_k))^2 + (Y(t_k) - y_i(t_k))^2 + H^2(t_k)\big)^{\frac{\gamma_i}{2}} \le$$
$$P_{TX}^{max}, \forall k \in \{1, ..., T\}. \tag{28}$$

Furthermore, the constraint (b) in (26) also limits the FlyBS's altitude. Thus the Simplex algorithm cannot be immediately applied to the current optimization setting in (26). In order to address this issue, we propose a solution based on the change of variables $X(t_k)$, $Y(t_k)$, and $H(t_k)$ $(1 \le k \le T)$ to eliminate the constraints (b), (c), and (d) in (26) as follow. We first consider the constraint (b) in (26). Suppose that $H_{max}(X(t_k), Y(t_k)) \le H_M$. Then, by rewriting the transmission power in terms of the system parameters, the constraint (b) is fulfilled if:

$$\sum_{i=1}^{n} Q_i \big((X(t_k) - x_i(t_k))^2 + (Y(t_k) - y_i(t_k))^2 + H_M^2(t_k)\big)^{\frac{\gamma_i}{2}} \le P_{TX}^{max} \tag{29}$$

Using the first-order Taylor approximation for $\Big((X(t_k) - x_i(t_k))^2 + (Y(t_k) - y_i(t_k))^2\Big)$, the left-hand side in (29) is rewritten as:

$$\sum_{i=1}^{n} Q_i \big((X(t_k) - x_i(t_k))^2 + (Y(t_k) - y_i(t_k))^2 + H_M^2(t_k)\big)^{\frac{\gamma_i}{2}} \cong$$
$$A_0 + (\sum_{i=1}^{n} Q_i)\big((X(t_k) - X_*)^2 + (Y(t_k) - Y_*)^2\big) \tag{30}$$

where

$$A_0 = \sum_{i=1}^{n} Q_i \big((H_M^2 + \Lambda_i H_M^2 \Omega)^{\frac{\gamma_i}{2}} - \frac{\gamma_i}{2}\Lambda_i H_M^2 \Omega \times$$
$$(H_M^2 + \Lambda_i H_M^2 \Omega)^{\frac{\gamma_i}{2}-1}\big) + \frac{\gamma_i}{2}(H_M^2 + \Lambda_i H_M^2 \Omega)^{\frac{\gamma_i}{2}-1}(x_i^2 + y_i^2) -$$
$$\Big(\frac{\sum_{i=1}^{n} \Upsilon_i x_i}{\sum_{i=1}^{n} \Upsilon_i}\Big)^2 - \Big(\frac{\sum_{i=1}^{n} \Upsilon_i y_i}{\sum_{i=1}^{n} \Upsilon_i}\Big)^2,$$
$$X_* = \frac{\sum_{i=1}^{n} \Upsilon_i x_i}{\sum_{i=1}^{n} \Upsilon_i}, Y_* = \frac{\sum_{i=1}^{n} \Upsilon_i y_i}{\sum_{i=1}^{n} \Upsilon_i},$$

$$\Upsilon_i = Q_i(H_M^2 + \Lambda_i H_M^2 \Omega)^{\frac{\gamma_i}{2}-1},$$
$$\Lambda_i = \left\lfloor \frac{\big(X(t_k) - x_i(t_k)\big)^2 + \big(Y(t_k) - y_i(t_k)\big)^2}{H_M^2 \Omega} \right\rfloor. \quad (31)$$

Note that the value Ω is an approximation parameter and choosing a smaller Ω results in a smaller error in the approximation in (30). Using the approximation in (31), the inequality in (29) is rewritten as:

$$\big(X(t_k) - X_*\big)^2 + \big(Y(t_k) - Y_*\big)^2 \leq \zeta^2, \quad (32)$$

where $\zeta = (\frac{P_{TX}^{max} - A_0}{\sum_{i=1}^{n} Q_i})^{\frac{1}{2}}$. Next, with a consideration of (32) and to also fulfill the constraints (c) and (d) in (26), we take a similar approach as in the solution to (15) and we define ϕ_k, ψ_k, χ_k, ω_k, and ξ_k so that the following equations hold:

$$\begin{aligned} X(t_{k+1}) = min\{&X(t_k) + V_{max}(t_{k+1} - t_k)cos(\omega_k)cos(\xi_k), \\ &X_*(t_{k+1}) + \zeta sin(\phi_{k+1})cos(\psi_{k+1})\} \\ Y(t_{k+1}) = min\{&Y(t_k) + V_{max}(t_{k+1} - t_k)cos(\omega_k)sin(\xi_k), \\ &Y_*(t_{k+1}) + \zeta sin(\phi_{k+1})sin(\psi_{k+1})\} \\ H(t_{k+1}) = min\{&H_{min}\big(X(t_{k+1}), Y(t_{k+1})\big) + \\ &\Big(H_{max}\big(X(t_{k+1}), Y(t_{k+1})\big) - H_{min}\big(X(t_{k+1}), Y(t_{k+1})\big)\Big) \times \\ &sin^2(\chi_{k+1}), max\{H(t_k) + V_{max}(t_{k+1} - t_k) \times sin(\omega_{k+1}), \\ &H_{min}\big(X(t_{k+1}), Y(t_{k+1})\big)\}\}. \end{aligned} \quad (33)$$

With the defined ϕ_k, ψ_k, χ_k, ω_k, and ξ_k the constraints (b)-(d) in (26) fulfill automatically and, thus, the problem of the total power minimization is rewritten as:

$$\begin{aligned} &\min_{\phi_k, \psi_k, \chi_k, \omega_k, \xi_k} P_{tot}^{avg}, (1 \leq k \leq T) \\ &s.t. \quad C_i(t) = {C_i}^{min}, \forall i \in \{1, ..., n\}, \forall t. \end{aligned} \quad (34)$$

Similar to (15), the solution to optimization problem in (34) is based on the Simplex method as elaborated in Section IV.F.

In general, an analysis of the computational complexity is not possible for the Nelder-Mead Simplex, as it highly depends on the objective function [65]. Nevertheless, we can still derive the order of the computational complexity by counting the total number of clock cycles taken for fixed-point operations performed during the optimization. To this end, we assume each multiplication of two numbers takes 3 clock cycles and each addition takes 1 clock cycle [66]. Then, by simulating the scenario for different number of time steps T in the optimization and counting the total number of clock cycles, it is observed that the computational complexity of the proposed solution scales as $O\left(T^{3.2}\right)$. Furthermore, an evaluation of the total power consumption in (10) is of a linear complexity with respect to the number of users (n). Hence, the overall complexity of the proposed solution is $O\left(nT^{3.2}\right)$.

VI. Simulation Scenario and Models

In this section, we provide details of simulations and models adopted to evaluate the performance of the proposed solution minimizing the total power consumed by the FlyBS serving mobile users. We also define competitive algorithms considered in simulations.

We consider a scenario with the FlyBS serving users represented by vehicles, for example, during a busy traffic or a traffic jam at a road or a highway. In such situation, the conventional network is usually overloaded as plenty of active users are located in a small rural area with a limited network coverage. In such scenario, the FlyBS is a suitable solution to improve the performance, see [45], [46]. The users are assumed to move on a 3-lane highway in the positive direction of y-axis. A wide range of velocities of the vehicles is considered ($\{2, 5, 10, 12, 15, 20, 25\}$ m/s) to cover different traffic situations corresponding to a traffic jam and/or a busy traffic. Note that for higher speeds than 25 m/s, the typical FlyBS is not efficient and cannot follow the vehicles' movement, as common rotary-wing UAVs can fly typically with a maximum speed of about 25 m/s [52]. We assume that a length of the crowd of vehicles served by the FlyBS in the traffic jam is 600 meters (i.e., the length of the line of the vehicles is 600 m).

As mentioned in Section II, the current positions of the users are assumed to be known to the FlyBS. However, the known positions contain a randomly distributed error of $e_i^{M,x} \in [-10, 10]$ m and $e_i^{M,y} \in [-10, 10]$ m, see (5). Furthermore, the location of the users in future time slots are fully unknown in general. There are many solutions for a prediction of the user's movement, see, e.g., [59], [60], [61]. As individual prediction schemes reach different performances depending on a scenario and an availability of additional information, the evaluation of our proposal for any specific prediction would lead to a validity of the results only for such specific scenario and conditions of the predictor. Thus, we generalize the evaluation across different predictive models in the following way: The next position of the users is extrapolated from the last two previous positions of the user and this predicted position is further influenced by an additional random error so that:

$$\begin{aligned} x_i(t) &= x_i(0) + v_i^x(t)t + e_i^{Pr,x}(t), \\ y_i(t) &= y_i(0) + e_i^{Pr,y}(t), \end{aligned} \quad (35)$$

where $e_i^{Pr,x}(t)$ and $e_i^{Pr,y}(t)$ denote the added error to the x and y coordinates of the user i at the time t, respectively, and $v_i^x(t)$ denotes the velocity of the user i in the direction of x-axis at the time t. In our scenario, we consider the following model for $e_i^{Pr,x}(t)$ and $e_i^{Pr,y}(t)$

$$\begin{aligned} |e_i^{Pr,x}(t)| &\leq \eta v_i^x(t)t, \\ |e_i^{Pr,y}(t)| &\leq W_H, \end{aligned} \quad (36)$$

where W_H denotes the highway's width, and η is the error factor that indicates the extent of error incurred by the prediction. Note that, although our proposed solution for the positioning of the FlyBS is designed for 3D movement of the FlyBS, the only suitable propulsion power consumption model of the rotary-wing FlyBSs, see [31], only applies to a fixed altitude. Thus, for the simulations, the FlyBS's altitude is set to $H = 100$ m, and the optimization problems in (11) and (26) are solved only for x and y coordinates of the FlyBS.

Table II shows the values of the system parameters adopted in the simulations. For the wireless channel, we assume free space path loss (FSPL) model, as the communication link between the FlyBS and the users (vehicles) on a road is typically without any obstacles and the FSPL is a commonly adopted model in such cases [23], [29], [38]. Omni-directional antennas with gains of 7 dBi and 0 dBi for the FlyBS and the users are considered, respectively, [62], [67]. We set spectral density of noise to -174 dBm/Hz. The radio frequency $f_c = 2.6$ GHz and a bandwidth of 100 MHz are selected. We consider the same minimum required capacity for all users, i.e., ${C_i}^{min} = C^{min}, \forall i \in \{1, ..., n\}$ and the simulations are performed for $C^{min} = 5$ Mbps and $C^{min} = 10$ Mbps.

To suppress randomness in the models, each simulation is of 15 minutes duration with a step of 1 s and the results are averaged out over 100 simulation drops.

To solve the problems by Simplex algorithm, we set $\kappa_i = 0.05$ and $\epsilon_i = 0.00025$ to create the initial simplex from (25). These values are selected with respect to the accuracy and the termination time of the algorithm, as explained in Section IV.F.

For the initial simplex, we choose the points derived from the closed-form solution for the single-point optimization as elaborated in Section IV.F. The input used for this single-point optimization is the predicted location of the users calculated from (35).

We investigate five different schemes:

i) Proposed multi-point optimization scheme (MPS) with the location of FlyBS determined by the numerical optimization of P_{tot}^{avg} as elaborated in subsection IV.F;

ii) Enhanced MPS (EMPS) as elaborated in subsection IV.G, with $T = 2$ and $T_\Delta = 1$, i.e., the optimization is done over 2 time steps, and it is iterated after each time step. Note that the values for T and T_Δ are selected experimentally;

iii) Single-point optimization scheme (SPS), where the locations of the FlyBS is determined by minimizing P_{tot}^{avg} for T =1, as explained in subsection IV.E;

iv) Minimal TX power scheme (MTX), as outlined in [45] and further exploited and elaborated in [68], [34], targeting the transmission power minimization while the propulsion power is ignored;

In addition to the above mentioned schemes, we also evaluate the performance for the scenario with conventional static base station (i.e., with no propulsion power consumption) to investigate benefits of the FlyBSs. However, based on the simulation results, the conventional static base station leads to the average transmission powers of 900 and 16 000 Watts for $v_i = 10$ m/s and 25 m/s, respectively even for $C_j^{min} = 5$ Mbps. These values are multiple times larger than the average total power consumption of all other schemes. Thus, for the clarity of presentation of the results, we do not show this scheme in the figures.

Note that up to our best knowledge, there is no other existing solution that targets the minimization of transmission and/or propulsion power while the minimum capacity is guaranteed to the moving users.

Table II: Parameter for simulations

System Parameter	**Numerical value**
Number of users, n	90
FlyBS's antenna gain, G_i^T	7 dBi [62]
Ground users' antenna gain,G_i^R	0 dBi [67]
Noise power spectral density, N_i	-174 dBm/Hz
Minimum capacity for the i-th user, C_i^{min}	{5,10} Mbps
Communication frequency, f_c	2.6 GHz
System bandwidth	100 MHz
Simulation step, Δt_j	1 second
Range of FlyBS altitude, $[H_{min}, H_{max}]$	[100,300] meters
Velocity of users, v_i	{2,5,10,12,15,20,25} m/s
FlyBS's circuit power, $P_{circuit}$	0.15 Watts
Maximum transmission power, p_{max}^T	2 Watts
Simulation Duration	15 minutes
Number of simulation drops	100

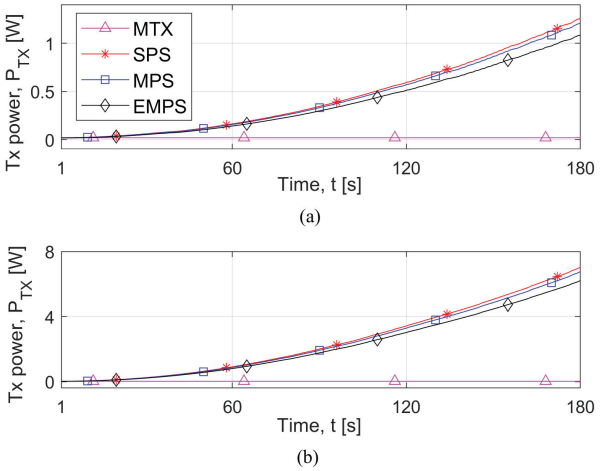

Fig. 5. Evolution of transmission power P_{TX} over a sample of time for a) $v_i = 10$ m/s and b) $v_i = 25$ m/s. $\eta = 0.5$ is assumed for MPS and EMPS.

VII. Performance Evaluation

In this section, we discuss simulation results. First, we illustrate an evolution of the transmission, propulsion, and total power consumption over time for the proposed algorithms. Then, we compare the performance of the proposed scheme with existing state-of-the-art solutions in terms of the average power consumption and we analyze an impact of an error in prediction of the vehicles' movement.

A. Evolution of power consumption over time

Figures 5, 6, and 7 represent a sample of the transmission, propulsion, and total power consumption, respectively, over a sample interval with a duration of 180 s. These figures show a mutual cooperation of the transmission power control and the selection of the position of the FlyBS. The figures show the results for $v_i = 10$ m/s (subplot (a)) and $v_i = 25$ m/s

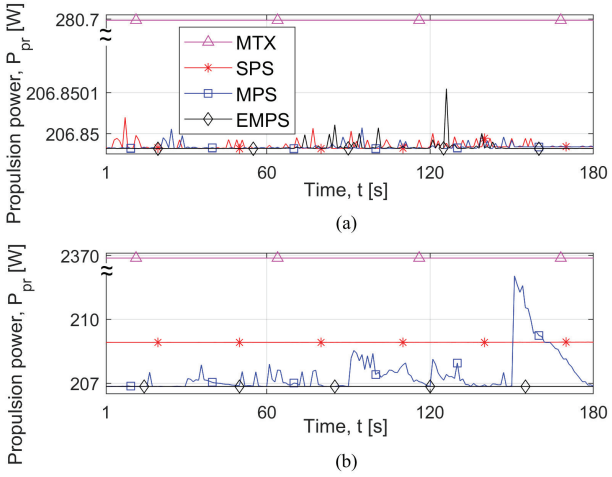

Fig. 6. Evolution of propulsion power P_{pr} over a sample of time for a) $v_i = 10$ m/s and b) $v_i = 25$ m/s. $\eta = 0.5$ is assumed for MPS and EMPS.

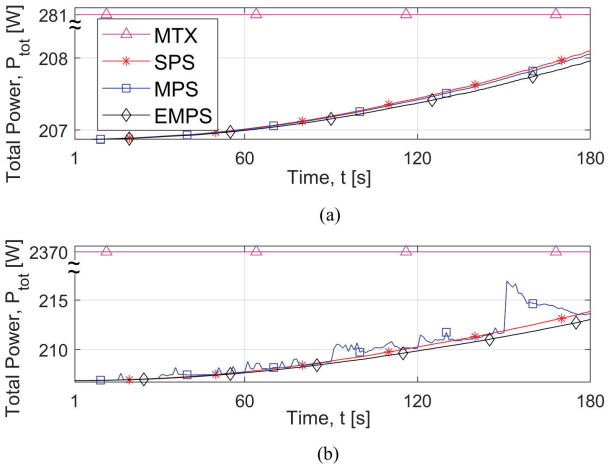

Fig. 7. Evolution of total power P_{tot} over a sample of time for a) v_i =10 m/s and b) 25 m/s. $\eta = 0.5$ is assumed for MPS and EMPS.

(subplot (b)). For the proposed MPS, the number of time steps in the optimization is set to $T = 30$, and ${C_j}^{min}$ =10 Mbps is assumed for all schemes. Note that we break (collapse) the y-axis in Figs. 6 and 7 to increase a separation of the plots for all three proposed solutions (SPS, MPS, and EMPS) and to demonstrate clearly the performance of individual solutions.

According to Fig. 5, the transmission power increases over time for all the proposed solutions. This behavior is justified by evaluating the changes in transmission and propulsion powers with respect to the change in the FlyBS's speed. More specifically, assume that increasing the FlyBS's speed by some $\delta V > 0$ causes an increase and a decrease in the propulsion and transmission powers by δP_{pr} and δP_{TX}, respectively. According to (4), δP_{TX} is directly proportional to C^{min} as well as to the relative distances between the FlyBS and the users (d_i), whereas δP_{pr} is independent of the C^{min} and d_i. Now, let us have $\delta P_{pr} > \delta P_{TX}$ for the considered δV. Then, as a result, the FlyBS endeavors not to increase its speed by more than or equal to δV in the proposed solutions. Consequently, the distance between the FlyBS's position and the center of gravity of the users might increase over time and, this imposes an increase in the transmission power. If the distance between the FlyBS and the users becomes large enough so that $\delta P_{pr} < \delta P_{TX}$, then the FlyBS would start increasing its speed by more than δV to reduce the transmission power.

Furthermore, the increase in the transmission power over time is higher when the difference between the FlyBS's and the users' velocities is larger, as illustrated in Fig. 5 (bottom subplot in Fig. 5 shows about 6-times higher increase in P_{TX} comparing to the top subplot). In contrast, the MTX scheme keeps the FlyBS's position at the center of gravity of the users disregarding the incurred propulsion power. Hence, the MTX results in a significant increase in the propulsion power consumption (see Fig. 6) and, consequently, also in the total consumed power (Fig. 7). As shown in Fig. 6 (subplot (a)), all three propose schemes (SPS, MPS, EMPS) reach similar propulsion power for a low speed of vehicles. However, for higher speeds of vehicles (subplot (b)), the differences among SPS, MPS, and EMPS become more significant, as the propulsion power for MPS undergoes rapid peaks at some time steps. The reason for such peaks is that the MPS optimizes the total power consumption over T time steps by deriving the T locations of the FlyBS. These locations are, however, not necessarily the optimal over a longer period of operation. Therefore, after the T time steps, the FlyBS can be in a suboptimal position and should fly a relatively long distance to reach the long-term optimum in order to reduce the power for the next T time steps. In contrast, the EMPS does not suffer from such sudden jumps in the propulsion power, as it iterates the optimization and adjusts the FlyBS's position and transmission power after each time step while still considering long-term optimization perspective. Fig. 7 confirms that the EMPS always outperforms both SPS and MPS in terms of the total power consumption.

B. Impact of user's velocity

In this subsection, we investigate the impact of the users' velocity on the average power consumption of the FlyBS over a longer period of the operational time of the FlyBS. Figs. 8, 9, and 10 show the average transmission, propulsion, and total power consumption, respectively. The results are shown for the case with no limitation of the transmission power (left subplots) as well as for the case with the transmission power limited to 2 W (right subplots). The figures show the results for $C^{min} = 5$ Mbps as well as $C^{min} = 10$ Mbps. The proposed MPS is investigated for the number of time steps in the optimization T set to 10, 20, and 30.

First, we explain the results for the case with no transmission power limit. According to Fig. 8, the average transmission power increases with the users' velocity. As discussed in the description of Fig. 5, this is caused by the fact that for

higher velocities of users, the distance between the FlyBS and the center of gravity of the users' locations is higher on average, as the FlyBS tends to fly approximately with the speed corresponding to the minimum propulsion power for all the proposed solutions. The FlyBS increases its speed time-to-time in order to reduce the transmission power if the transmission power would be too high with respect to the propulsion power. Clearly, for higher velocities of the users, the FlyBS increases its speed more often and, hence, the average propulsion power increases with the velocity of the users, as illustrated in Fig. 9. In addition, Fig. 9 shows the advantage of the EMPS over the SPS and the MPS in controlling the propulsion power via a continuous adjustment of the FlyBS's positions over time. Contrary to the proposed solutions, the MTX leads to the situation when the FlyBS flies with the speed equal to the users' velocity to keep the transmission power at the lowest level. This causes a relatively high propulsion power, especially for a high velocity of the users. More specifically, at the velocity of 25 m/s, the proposed EMPS, MPS, and SPS reduce the propulsion power by up to about 91%, 90%, and 90%, respectively, comparing to the MTX. Note that roughly the same gains are observed for both $C^{min} = 5$ Mbps and $C^{min} = 10$ Mbps.

Similar behavior and trends in the transmission and propulsion powers are observed also for the case with the transmission power constraint in Figs. 8 and 9 (right subplots). More specifically, before the transmission power reaches the maximum allowed value, the FlyBS keeps the propulsion power low while the transmission power is increasing. However, when the transmission power reaches the maximum, the FlyBS is forced to increase the speed in order to avoid getting too far from the center of gravity of the users. Consequently, the propulsion power is increased to find a position in which the capacity C^{min} is guaranteed to all users. The left subplot in Fig. 9 shows this increase in the average propulsion power compared with the right subplot, especially for high speeds of the users and a high guaranteed C^{min}. For higher users' required capacity, the transmission power becomes comparable to the propulsion power, and hence, the FlyBS increases its velocity to avoid a large increase in the transmission power.

Note that the transmission power limit does not change the results for MTX with respect to the case without the transmission power limit, as the MTX always achieves the minimum transmission power, which should be lower than P_{TX}^{max}, otherwise the problem in (26) would have no solution. According to Fig. 9, the proposed EMPS, MPS, and SPS reduce the propulsion power comparing to the MTX by 91%, 91%, and 89%, respectively, at the velocity of 25 m/s and for $C^{min} = 5$ Mbps. If $C^{min} = 10$ Mbps, the respective gains of EMPS, MPS, and SPS comparing to the MTX are about 36%, 34%, and 33%.

The average total power consumption is investigated in Fig. 10. The average total power consumed by the proposed MPS for $T = 30$ is lower than for $T = 10$ and $T = 20$. Note that we have tested also the performance for larger values of T, but it has lead to no significant improvement in the performance of MPS. Hence, the results for $T > 30$ are not included to keep the figures clear. The reason that increasing T does not always

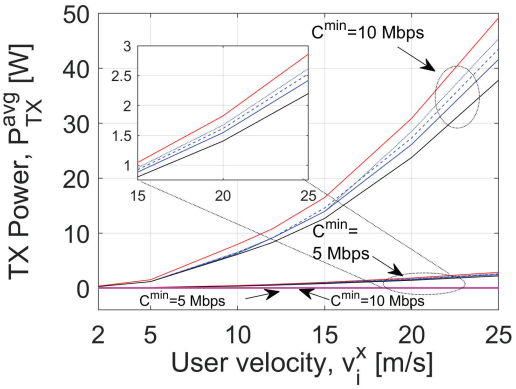

(a) unconstrained transmission power

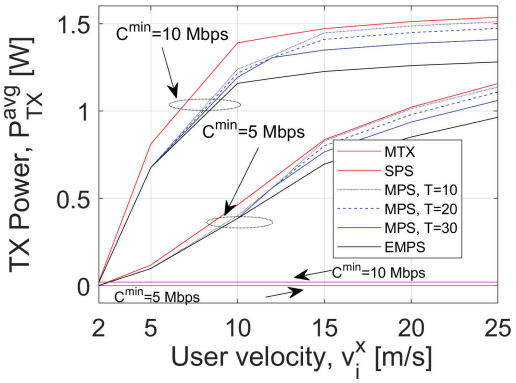

(b) constrained transmission power

Fig. 8. P_{TX}^{avg} vs. user's velocity for a) unconstrained transmission power and b) constrained transmission power with $P_{TX}^{max} = 2$ W. $\eta = 0.5$ is assumed for MPS and EMPS.

improve the performance is because a larger T also entails the prediction over a longer period, thus, a higher prediction error is incurred. Furthermore, increasing T can potentially increase the magnitude of sudden peaks in the propulsion power. Fig. 10 shows that the lowest power consumption is achieved by the EMPS. Comparing to the MPS, the EMPS allows a more frequent adjustment of the future positions of the FlyBS so that the sudden peaks in the propulsion power are suppressed. In the case of limited transmission power, the difference among the proposed solutions becomes more obvious for a higher required users' capacity C^{min} because of a higher gap between the users' and FlyBS's speeds, which allows the FlyBS to leverage an increase in the transmission power for the benefit of a saving in the propulsion power.

Fig. 10 further demonstrates that all proposed solutions outperform the MTX for all velocities. For the case of unconstrained transmission power at the velocity of 25 m/s, the proposed EMPS, MPS, and SPS reduce the total power comparing to the MTX by 91%, 90%, and 89%, respectively, if C^{min} is set to 5 Mbps, and by 90%, 89%, and 87%, respectively, if C^{min} is set to 10 Mbps. For the case of constrained transmission power at the velocity of 25 m/s, the proposed EMPS, MPS, and SPS lead to a reduction in the total power consumption of about 90%, 89%, and 88%, respectively, with respect to the MTX if C^{min} is set to 5 Mbps,

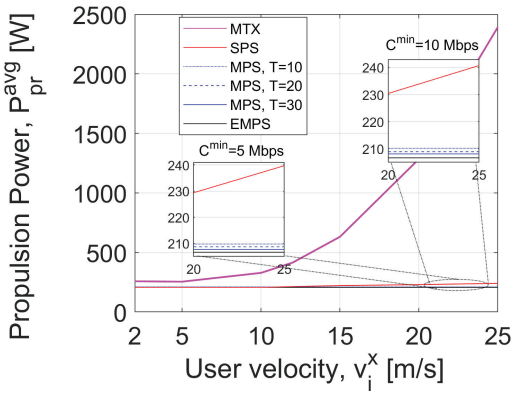

(a) unconstrained transmission power

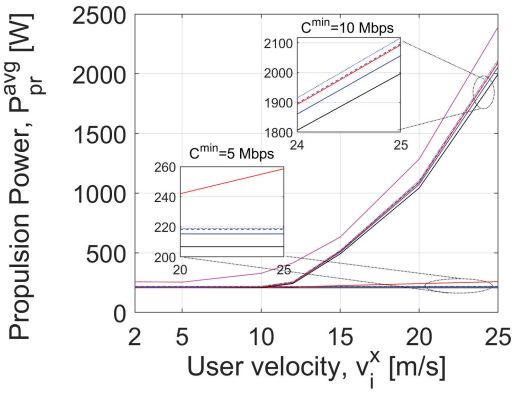

(b) constrained transmission power

Fig. 9. P_{pr}^{avg} vs. user's velocity for a) unconstrained transmission power and b) constrained transmission power with $P_{TX}^{max} = 2$ W. $\eta = 0.5$ is assumed for MPS and EMPS.

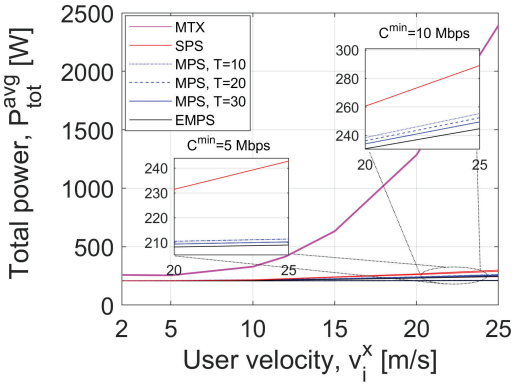

(a) unconstrained transmission power

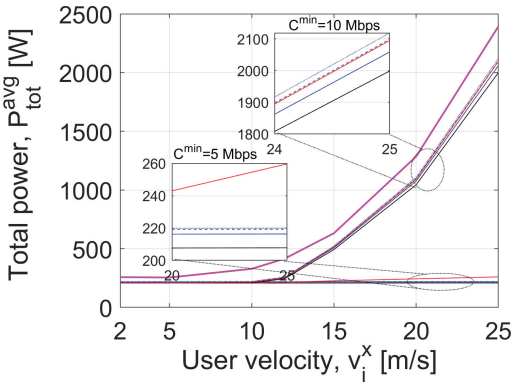

(b) constrained transmission power

Fig. 10. P_{pr}^{avg} vs. user's velocity for a) unconstrained transmission power and b) constrained transmission power with $P_{TX}^{max} = 2$ W. $\eta = 0.5$ is assumed for MPS and EMPS.

and about 16%, 13%, and 12%, respectively, if C^{min} is set to 10 Mbps.

Next, Fig. 11 depicts the trajectory of the FlyBS for the cases with and without constraint on the FlyBS's transmission power. For the constrained transmission power, the FlyBS's displacements are relatively larger compared to the unconstrained transmission power, as the FlyBS has to keep the transmission power below the maximum limit by moving to a favorable point even if such a movement would incur a larger propulsion power.

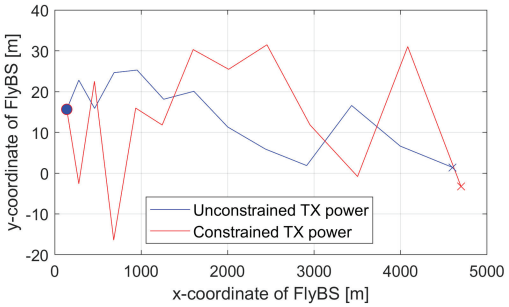

Fig. 11. FlyBS's trajectory. The start and end points of the movement are marked by "•" and "×".

C. Impact of prediction error

Last, we investigate the impact of the error due to a prediction of the vehicles' movement (according to (35)) on the total power consumption of the FlyBS in Fig. 12. The average total power consumption increases for both MPS and EMPS with the prediction error, because having more inaccurate parameters in a function leads to a calculation of more inaccurate optimal values in general. We further see that, for any value of the error factor η (see (36)), the average total power consumption for MPS increases with T as the prediction error increases with T as well. Furthermore, the EMPS shows a stable behavior and robustness against the prediction error comparing to the MPS, as the optimization is adjusted over time to suppress the negative impact of the prediction error.

VIII. Conclusions

In this paper, we have studied the problem of power optimization in future wireless networks with the FlyBSs. Contrary to existing papers, we optimize the total power consumed by the FlyBS while guaranteeing the minimum communication capacity to all users during their movement. We first provide the closed-form solution determining the position and the transmission power of the FlyBS for a realistic

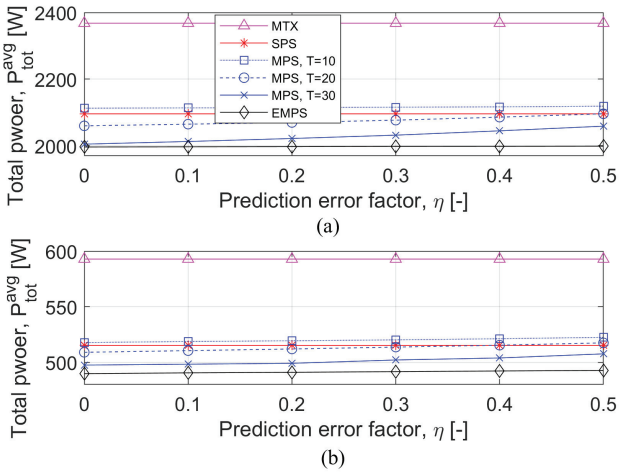

Fig. 12. P_{tot}^{avg} vs. the prediction error's factor (η) for different schemes and for a) $v_i^x = 25$ m/s and b) $v_i^x = 15$ m/s. $C^{min} = 10$ Mbps is assumed.

non-linear power consumption model in the case of single-point optimization. Then, we develop a numerical solution for the optimal positioning of the FlyBS and setting of the FlyBS's transmission power to minimize the total power consumed by the FlyBS over a period with an arbitrary duration (multi-point optimization). We show that the proposed joint transmission power control and FlyBS's movement allows a significant reduction (up to 91%) in the total power consumed by the FlyBS while the required capacity of the moving users is always satisfied.

In the future, the scenario with multiple FlyBSs should be studied. Regarding this, two key aspects that should be addressed jointly are: i) association of the users to the FlyBSs and ii) management of interference among the FlyBSs.

Appendix A
Proof to Theorem 1

Proof. To find the FlyBS's position that minimizes P_{tot}^{avg}, we start by finding the critical points for P_{tot}^{avg}. First, it is noted that $[X(t_1), Y(t_1)] = [X(t_0), Y(t_0)]$ is one the critical points for P_{tot}^{avg}. Now we find the critical points where $[X(t_1), Y(t_1)] \neq [X(t_0), Y(t_0)]$. by using P_{pr}^{apx} in (16) and rewriting $\frac{\partial P_{tot}^{avg}}{\partial X} = 0$ and $\frac{\partial P_{tot}^{avg}}{\partial Y} = 0$ for the period of $\{t_0, t_1\}$ we get:

$$\sum_{i=1}^{n} 2Q_i(X(t_1) - x_i(t_1)) = -\Big(\frac{X(t_1) - X(t_0)}{\sqrt{(X(t_1) - X(t_0))^2 + (Y(t_1) - Y(t_0))^2)}} \cdot \frac{dP_{pr}^{apx}}{dV}|_{V=V(t_0,t_1)},$$

$$\sum_{i=1}^{n} 2Q_i(Y(t_1) - y_i(t_1)) = -\Big(\frac{Y(t_1) - Y(t_0)}{\sqrt{(X(t_1) - X(t_0))^2 + (Y(t_1) - Y(t_0))^2)}} \cdot \frac{dP_{pr}^{apx}}{dV}|_{V=V(t_0,t_1)}. \tag{37}$$

We derive an auxiliary equation from (37) that does not include the complicated term of $\frac{dP_{pr}^{apx}}{dV}$ and helps to derive an explicit relation between $X(t_1)$ and $Y(t_1)$ as:

$$\frac{\sum_{i=1}^{n} 2Q_i(X(t_1) - x_i(t_1))}{\sum_{i=1}^{n} 2Q_i(Y(t_1) - y_i(t_1))} = \frac{X(t_1) - X(t_0)}{Y(t_1) - Y(t_0)}. \tag{38}$$

Equation (38) is further rewritten as:

$$\frac{(\sum_{i=1}^{n} 2Q_i)X(t_1) - (\sum_{i=1}^{n} 2Q_i x_i(t_1))}{(\sum_{i=1}^{n} 2Q_i)Y(t_1) - (\sum_{i=1}^{n} 2Q_i y_i(t_1))} = \frac{X(t_1) - X(t_0)}{Y(t_1) - Y(t_0)}. \tag{39}$$

Then, from (39), it is concluded that:

$$(Y(t_1) - Y(t_0)) = \frac{(\sum_{i=1}^{n} 2Q_i)Y(t_0) - (\sum_{i=1}^{n} 2Q_i y_i(t_1))}{(\sum_{i=1}^{n} 2Q_i)X(t_0) - (\sum_{i=1}^{n} 2Q_i x_i(t_1))}(X(t_1) - X(t_0)). \tag{40}$$

With (40), we can simplify the expression for V in (7) to:

$$V = M|X(t_1) - X(t_0)|,$$
$$M = \frac{1}{\Delta t_k}\Big(1 + \frac{(\sum_{i=1}^{n} 2Q_i)Y(t_0) - (\sum_{i=1}^{n} 2Q_i y_i(t_1))}{(\sum_{i=1}^{n} 2Q_i)X(t_0) - (\sum_{i=1}^{n} 2Q_i x_i(t_1))}\Big)^{\frac{1}{2}}. \tag{41}$$

Now, by expanding the first equation in (37) using (16) and (41), we get:

$$(\sum_{i=1}^{n} 2Q_i)X(t_1) - \big(\sum_{i=1}^{n} 2Q_i x_i(t_1)\big) = \tag{42}$$
$$-\Big(\frac{X(t_1) - X(t_0)}{M|X(t_1) - X(t_0)|}\Big)(5c_5V^4 + 4c_4V^3 + 3c_3V^2 + 2c_2V + c_1)$$
$$= -\Big(\frac{X(t_1) - X(t_0)}{M|X(t_1) - X(t_0)|}\Big)(5c_5M^4|X(t_1) - X(t_0)|^4 + 4c_4M^3|X(t_1) - X(t_0)|^3 + 3c_3M^2|X(t_1) - X(t_0)|^2 + 2c_2M|X(t_1) - X(t_0)| + c_1).$$

Equation (42) can be solved by considering two different possibilities:
a) $X(t_1) > X(t_0)$ (equivalently, $|X(t_1) - X(t_0)| = (X(t_1) - X(t_0))$: with this presumption (42) is rewritten as a quartic equation with respect to $X(t_1)$ as follow

$$a_4X^4(t_1) + a_3X^3(t_1) + a_2X^2(t_1) + a_1X(t_1) + a_0 = 0, \tag{43}$$

where

$$a_4 = 5c_5M^3, \quad a_3 = -20c_5M^3X(t_0) + 4c_4M^2,$$
$$a_2 = 30c_5M^3X^2(t_0) - 12c_4M^2X(t_0) + 3c_3M, a_1 = \sum_{i=1}^{n} 2Q_i - 20c_5M^3X^3(t_0) + 12c_4M^2X^2(t_0) - 6c_3MX(t_0) + 2c_2,$$
$$a_0 = 5c_5M^3X^4(t_0) - 4c_4M^2X^3(t_0) + 3c_3MX^2(t_0) - 2c_2X(t_0) + \frac{c_1}{M} - (\sum_{i=1}^{n} 2Q_i x_i(t_1)). \tag{44}$$

There are four solutions to (43) that are given by:

$$\frac{-a_3}{4a_4} - S \pm \frac{1}{2}\sqrt{-4S^2 - 2p + \frac{q}{S}},$$
$$\frac{-a_3}{4a_4} + S \pm \frac{1}{2}\sqrt{-4S^2 - 2p - \frac{q}{S}}, \quad (45)$$

where

$$p = \frac{8a_4a_2 - 3a_3^2}{8a_4^2}, q = \frac{a_3^3 - 4a_4a_3a_2 + 8a_4^2a_1}{8a_4^3},$$
$$S = \frac{1}{2}\sqrt{\frac{-2}{3}p + \frac{1}{3a_4}(G + \frac{\Delta_0}{G})}, G = \sqrt[3]{\frac{\Delta_1 + \sqrt{\Delta_1^2 - 4\Delta_0^3}}{2}},$$
$$\Delta_0 = a_2^2 - 3a_3a_1 + 12a_4a_0,$$
$$\Delta_1 = 2a_2^3 - 9a_3a_2a_1 + 27a_3^2a_0 + 27a_1^2a_4 - 72a_4a_2a_0. \quad (46)$$

b) $X(t_1) < X(t_0)$: with this presumption, (42) is rewritten as:

$$b_4X^4(t_1) + b_3X^3(t_1) + b_2X^2(t_1) + b_1X(t_1) + b_0 = 0, \quad (47)$$

where

$$b_4 = 5c_5M^3, b_3 = -20c_5M^3X(t_0) - 4c_4M^2,$$
$$b_2 = 30c_5M^3X^2(t_0) - 12c_4M^2X(t_0) + 3c_3M,$$
$$b_1 = -\sum_{i=1}^{n} 2Q_i - 20c_5M^3X^3(t_0) - 12c_4M^2X^2(t_0) -$$
$$6c_3MX(0) - 2c_2, b_0 = 5c_5M^3X^4(t_0) + 4c_4M^2X^3(t_0) +$$
$$3c_3MX^2(t_0) + 2c_2X(t_0) + \frac{c_1}{M} + (\sum_{i=1}^{n} 2Q_ix_i(t_1)). \quad (48)$$

Similar to (43), there are four solutions to (47) that can be derived by using the coefficients $b_0, ..., b_4$ instead of $a_0, ..., a_4$, respectively.

Note that only the real roots of the quartic functions in (43) and (47) are considered. Furthermore, the solutions to (43) and (47) should meet their presumptive conditions $X(t_1) > X(t_0)$ and $X(t_1) < X(t_0)$, respectively. For each of the candidates for $X(t_1)$, the corresponding value of $Y(t_1)$ is calculated from (40).

□

REFERENCES

[1] A. Puri, "A survey of unmanned aerial vehicles (UAV) for traffic surveillance," Department of computer science and engineering, University of South Florida, 2005.

[2] J. Lyu, Y. Zeng, and R. Zhang, "UAV-aided offloading for cellular hotspot," *IEEE Transactions on Wireless Communications*, vol. 17, no. 6, pp. 3988–4001, June 2018.

[3] K. P. Valavanis and G. J. Vachtsevanos, "Handbook of unmanned aerial vehicles," Springer Publishing Company, Incorporated, 2014.

[4] A. Al-Hourani, S. Kandeepan, and S. Lardner, "Optimal LAP altitude for maximum coverage," *IEEE communications letters*, vol. 3, no. 6, December 2014.

[5] Q. Wu, L. Liu and R. Zhang, "Fundamental Trade-offs in Communication and Trajectory Design for UAV-Enabled Wireless Network," in *IEEE Wireless Communications*, vol. 26, no. 1, February 2019.

[6] M. Mozaffari, W. Saad, M. Bennis, and M. Debbah, "Efficient deployment of multiple unmanned aerial vehicles for optimal wireless coverage," *IEEE Communications Letters*, vol. 20, no. 8, pp. 1647–1650, Aug. 2016.

[7] I. Bor-Yaliniz and H. Yanikomeroglu, "The new frontier in RAN heterogeneity: Multi-tier drone-cells," *IEEE Communications Magazine*, vol. 54, no. 11, pp. 48–55, 2016.

[8] E. Kalantari, H. Yanikomeroglu, and A. Yongacoglu, "On the number and 3D placement of drone base stations in wireless cellular networks," *IEEE Vehicular Technology Conference*, September 2016.

[9] J. Chakareski, "Aerial UAV-IoT sensing for ubiquitous immersive communication and virtual human teleportation," *IEEE Conference on Computer Communications Workshops*, May 2017.

[10] H. Kim and J. Ben-Othman, "A collision-free surveillance system using smart UAVs in multi-domain IoT," *IEEE Communications Letters*, vol. 22, no. 12, December 2018.

[11] F. Jiang and A. L. Swindlehurst, "Optimization of UAV heading for the ground-to-air uplink," *IEEE Journal on Selected Areas in Communications*, vol. 30, no. 5, pp. 993–1005, June 2012.

[12] V.Sharma, M. Bennis, "UAV-assisted heterogeneous networks for capacity enhancement," *IEEE Communications Letters*, April 2016.

[13] L. Wang, "Multiple access mmwave design for UAV-aided 5g communications," *IEEE Wireless Communications*, vol. 26, pp. 64-71, Feb 2019.

[14] M. Mozaffari, W. Saad, M. Bennis, Y. Nam, and M. Debbah, "A tutorial on UAVs for wireless networks: Applications, challenges, and open problems", *IEEE Communications Surveys & Tutorials*, 2019.

[15] J. Plachy, Z. Becvar, P. Mach, R. Marik, M. Vondra, "Joint Positioning of Flying Base Stations and Association of Users: Evolutionary-Based Approach," *IEEE Access*, vol. 7, pp. 11454-11463, 2019.

[16] Z. M. Fadlullah, D. Takaishi, H. Nishiyama, N. Kato and R. Miura, "A dynamic trajectory control algorithm for improving the communication throughput and delay in UAV-aided networks," in *IEEE Network*, vol. 30, no. 1, pp. 100-105, January-February 2016.

[17] H. Wang, J. Wang, G. Ding, J. Chen, F. Gao and Z. Han, "Completion Time Minimization With Path Planning for Fixed-Wing UAV Communications," in *IEEE Transactions on Wireless Communications*, vol. 18, no. 7, pp. 3485-3499, July 2019.

[18] M. Najla, Z. Becvar, P. Mach, D. Gesbert, "Positioning and Association Rules for Transparent Flying Relay Stations", *IEEE Wireless Communications Letters*, 2021.

[19] Y. Shi, E. Alsusa and M. W. Baidas, "Energy-Efficient Decoupled Access Scheme for Cellular-Enabled UAV Communication Systems," *IEEE Systems Journal*, 2020.

[20] Z. Becvar, P. Mach, J. Plachy, M.F.P. de Tuleda, "Positioning of Flying Base Stations to Optimize Throughput and Energy Consumption of Mobile Devices," *IEEE Vehicular Technology Conference*, pp. 1-7, 2019.

[21] W. Guo, et al, "Joint Attitude and Power Optimization for UAV-Aided Downlink Communications," in *IEEE Transactions on Vehicular Technology*, vol. 68, no. 12, Dec. 2019.

[22] A. H. Gazestani, S. A. Ghorashi, Z. Yang and M. Shikh-Bahaei, "Joint Optimization of Power and Location in Full-Duplex UAV Enabled Systems," *IEEE Systems Journal*, 2020.

[23] X. Liu, B. Lai, L. Gou, C. Lin and M. Zhou, "Joint Resource Optimization for UAV-Enabled Multichannel Internet of Things Based on Intelligent Fog Computing," *IEEE Transactions on Network Science and Engineering*, 2020.

[24] M. Hua, et al., "3D UAV Trajectory and Communication Design for Simultaneous Uplink and Downlink Transmission," *IEEE Transactions on Communications*, 2020.

[25] N. Zhao, Z. Liu and Y. Cheng, "Multi-Agent Deep Reinforcement Learning for Trajectory Design and Power Allocation in Multi-UAV Networks," *IEEE Access*, vol. 8, 2020.

[26] H. Shakhatreh, et al, "Efficient 3D placement of a UAV using particle swarm optimization," in *Proc. IEEE ICICS*, April 2017.

[27] S. Zhang, H. Zhang, Q. He, K. Bian and L. Song, "Joint Trajectory and Power Optimization for UAV Relay Networks," in *IEEE Communications Letters*, vol. 22, no. 1, pp. 161-164, Jan. 2018.

[28] M. Chen, M. Mozaffari, W. Saad, C. Yin, M. Debbah, and C. S. Hong, "Caching in the sky: Proactive deployment of cache-enabled unmanned aerial vehicles for optimized quality-of-experience," *IEEE Journal on Selected Areas in Communications*, vol. 35, no. 5, May 2017.

[29] Y. Zeng and R. Zhang, "Energy-Efficient UAV Communication With Trajectory Optimization," *IEEE Transactions on Wireless Communications*, vol. 16, no. 6, June 2017.

[30] S. Ahmed, M. Z. Chowdhury and Y. M. Jang, "Energy-Efficient UAV-to-User Scheduling to Maximize Throughput in Wireless Networks," *IEEE Access*, vol. 8, pp. 21215-21225, 2020.

[31] Y. Zeng, J. Xu, and R. Zhang, "Energy Minimization for Wireless Communication With Rotary-Wing UAV," *IEEE Transactions on Wireless Communications*, vol. 18, no. 4, April 2019.

[32] F. Zeng, et al., "Resource Allocation and Trajectory Optimization for QoE Provisioning in Energy-efficient UAV-enabled Wireless Networks," in *IEEE Transactions on Vehicular Technology*.

[33] Q. Wu, Y. Zeng and R. Zhang, "Joint Trajectory and Communication Design for Multi-UAV Enabled Wireless Networks," in *IEEE Transactions on Wireless Communications*, vol. 17, no. 3, March 2018.

[34] B. Khamidehi and E. S. Sousa, "Trajectory Design for the Aerial Base Stations to Improve Cellular Network Performance," in IEEE Transactions on Vehicular Technology, 2021.

[35] X. Zhang and L. Duan, "Energy-Saving Deployment Algorithms of UAV Swarm for Sustainable Wireless Coverage," *IEEE Transactions on Vehicular Technology*, vol. 69, no. 9, pp. 10320-10335, Sept. 2020.

[36] X. Liu, H. Song and A. Liu, "Intelligent UAVs Trajectory Optimization from Space-Time for Data Collection in Social Networks," *IEEE Transactions on Network Science and Engineering*, 2020.

[37] J. Gu, et al, "Energy-Constrained Completion Time Minimization in UAV-Enabled Internet of Things," *IEEE Internet of Things Journal*, vol. 7, no. 6, pp. 5491-5503, June 2020.

[38] L. Li, X. Wen, Z. Lu, W. Jing and H. Zhang, "Energy-Efficient Multi-UAVs Deployment and Movement for Emergency Response," *IEEE Communications Letters*, 2021.

[39] Y. Liu, K. Liu, J. Han, L. Zhu, Z. Xiao and X. -G. Xia, "Resource Allocation and 3-D Placement for UAV-Enabled Energy-Efficient IoT Communications," *IEEE Internet of Things Journal*, vol. 8, no. 3, pp. 1322-1333, 1 Feb.1, 2021.

[40] C. Qiu, Z. Wei, Z. Feng and P. Zhang, "Backhaul-Aware Trajectory Optimization of Fixed-Wing UAV-Mounted Base Station for Continuous Available Wireless Service," in *IEEE Access*, vol. 8, 2020.

[41] C. Liu, Z. Chen, J. Tang, J. Xu, C. Piao, "Energy-Efficient UAV Control for Effective and Fair Communication Coverage: A Deep Reinforcement Learning Approach," *IEEE Journal of Selected Areas in Communications*, vol. 36, no. 9, September 2018.

[42] M. Elloumi, et al, "Designing an energy efficient UAV tracking algorithm," *IEEE IWCMC*, June 2017.

[43] M. Nikooroo, and Z. Becvar, "Joint Positioning of UAV and Power Control for Flying Base Stations in Mobile Networks," *IEEE WiMOB*, October 2019.

[44] M. Nikooroo, and Z. Becvar, "Optimizing Transmission and Propulsion Powers for Flying Base Stations", *IEEE WCNC, 2020*.

[45] Z. Becvar, M. Vondra, P. Mach, J. Plachy, D. Gesbert, "Performance of Mobile Networks with UAVs: Can Flying Base Stations Substitute Ultra-Dense Small Cells?," *European Wireless*, May 2017.

[46] P. Yang, et al, "Proactive Drone-Cell Deployment: Overload Relief for a Cellular Network Under Flash Crowd Traffic," *IEEE Transactions on Intelligent Transportation Systems*, 2017.

[47] J. Lyu, et al, "Placement Optimization of UAV-Mounted Mobile Base Stations," *IEEE Communications Letters,* vol. 21, no. 3, March 2017.

[48] C. Chapman, et al, "A Decentralized Receiver in Gaussian Interference," *Entropy*, vol. 20, no. 4, April 2018.

[49] E. Koyuncu, R. Khodabakhsh, N. Surya, and H. Seferoglu, "Deployment and Trajectory Optimization for UAVs: A Quantization Theory Approach," *IEEE WCNC*, April 2018.

[50] I. Bor-Yaliniz, A. El-Keyi, and H. Yanikomeroglu, "Efficient 3-D placement of an aerial base station in next generation cellular networks," *IEEE International Conference on Communications*, May 2016.

[51] B. Lee, J. Morrison, and R. Sharma, "Multi-UAV Control Testbed for Persistent UAV Presence: ROS GPS Waypoint Tracking Package and Centralized Task Allocation Capability," *International Conference on Unmanned Aircraft Systems (ICUAS)*, June 2017.

[52] A. Fotouhi, et al, "Survey on UAV Cellular Communications: Practical Aspects, Standardization Advancements, Regulation, and Security Challenges," *IEEE Communications Surveys & Tutorials*, March 2019.

[53] Grant M, Boyd S, Ye Y. cvx users' guide. online: http://www. stanford. edu/ boyd/software. html. 2009 Jun 4.

[54] J.A. Nelder, and R. Mead, "A simplex method for function minimization," *The Computer Journal*, vol. 7, no. 4, 1965.

[55] John James Tomick. 1995. "On convergence of the nelder-mead simplex algorithm for unconstrained stochastic optimization," Ph.D. Dissertation. The Pennsylvania State University. Advisor(s) Steven F. Arnold and Russell R. Barton. Order Number: AAI9532037.

[56] Yee Leung, Yong Gao and Zong-Ben Xu, "Degree of population diversity - a perspective on premature convergence in genetic algorithms and its Markov chain analysis," in *IEEE Transactions on Neural Networks*, vol. 8, no. 5, pp. 1165-1176, Sept. 1997.

[57] Shu-Kai S. Fan, Erwie Zahara, "A hybrid simplex search and particle swarm optimization for unconstrained optimization," European Journal of Operational Research, vol. 181, no. 2, 2007, pp 527-548.

[58] Peter C. Wang, Terry E. Shoup, "Parameter sensitivity study of the Nelder–Mead Simplex Method," *Advances in Engineering Software*, vol. 42, no. 7, 2011, pp 529-533.

[59] B. Prabhala and T. La Porta,"Next place predictions based on user mobility traces," *IEEE INFOCOM Workshops*, May 2015.

[60] Z. Zhao, et al, "A demonstration of mobility prediction as a service in cloudified LTE networks," *IEEE International Conference on Cloud Networking*, October 2015.

[61] N. Kuruvatti, W. Zhou, and H. Schotten, "Mobility Prediction of Diurnal Users for Enabling Context Aware Resource Allocation," *IEEE Vehicular Technology Conference*, May 2016.

[62] M. Bekhti, M. Abdennebi, N. Achir, K. Boussetta. "Path Planning of Unmanned Aerial Vehicles With Terrestrial Wireless Network Tracking," *Wireless days*, March 2016.

[63] S. Mao, et al, "Joint UAV Position Optimization and Resource Scheduling in Space-Air-Ground Integrated Networks With Mixed Cloud-Edge Computing," IEEE Systems Journal, vol. 15, no. 3, Sept. 2021.

[64] A. J. Muhammed, et al, "Energy-Efficient Resource Allocation for NOMA Based Small Cell Networks With Wireless Backhauls," IEEE Transactions on Communications, vol. 68, no. 6, June 2020.

[65] S. Singer and S. Singer, "Complexity Analysis of Nelder-Mead Search Iterations", Proceedings of the 1. Conference on Applied Mathematics and Computation, 1999.

[66] E. Matthews and L. Shannon, "TAIGA: A new RISC-V soft-processor framework enabling high performance CPU architectural features," International Conference on Field Programmable Logic and Applications (FPL), 2017, pp. 1-4.

[67] M. Xiong, D. Zeng, H. Yao, Y. Li, "A Crowd Simulation Based UAV Control Architecture for Industrial Disaster Evacuation," *IEEE Vehicular Technology Conference*, May 2016.

[68] A. Bera, S. Misra and C. Chatterjee, "QoE Analysis in Cache-Enabled Multi-UAV Networks," in *IEEE Transactions on Vehicular Technology*, vol. 69, no. 6, pp. 6680-6687, June 2020.

3.2 Maximization of FlyBS coverage duration with user QoS constraint

The optimization of total power consumption of the FlyBS, despite its importance from the aspect of FlyBS's battery capacity, considers the transmission and propulsion power consumptions from the same point of view: a decrease of, e.g., 1 Watt in the transmission power is only as efficient/costly as decreasing 1 Watt in the propulsion power. However, the transmission power could be regarded as a more significant parameter than the propulsion power as long as the user's connectivity is concerned. In particular, it is the transmission power that guarantees the user's required capacity. In case that the required transmission power exceeds the FlyBS's maximum transmitting power, the users could not be provided with their required capacity. This would limit the use of FlyBSs in applications with real-time users. The works presented in this section, which include the reference paper [C3] followed by [J3], are dedicated to highlighting the difference between propulsion and transmission powers from the perspective of user's coverage and with respect to the FlyBS's battery limits. NOMA is adopted as the communication mode to efficiently exploit the available radio resources in the network. Along with the assumption of NOMA, the problem of NOMA user clustering is also targeted, and a low-complexity solution is proposed accordingly.

Optimization of Transmission Power for NOMA in Networks with Flying Base Stations

Mohammadsaleh Nikooroo, Zdenek Becvar
Department of Telecommunication Engineering, Faculty of Electrical Engineering
Czech Technical University in Prague
Prague, Czech Republic
nikoomoh@fel.cvut.cz, zdenek.becvar@fel.cvut.cz

***Abstract*—Deployment of unmanned aerial vehicles (UAVs) as flying base stations (FlyBSs) is considered as an efficient tool to enhance capacity of mobile networks and to facilitate communication in emergency cases. The improvement provided by such network requires a dynamic positioning of the FlyBSs with respect to the mobile users. In this paper, we focus on an optimization of transmission power of the FlyBS in networks with non-orthogonal multiple access (NOMA). We propose a solution jointly positioning the FlyBS and selecting the optimal grouping of users for NOMA in order to minimize the FlyBS's transmission power under the constraint on guaranteeing a minimum required capacity for the mobile users. Moreover, we derive the grouping of users corresponding to the optimal transmission power in a low-degree polynomial time, which makes it suitable for real-time applications. According to the simulations, the proposed method brings up to 31% of FlyBS's transmission power saving compared to existing solutions.**

***Index Terms*—Flying base station, Non-orthogonal multiple access, user grouping, transmission power, mobile users, mobile networks, 6G.**

I. Introduction

Unmanned aerial vehicles (UAVs) acting as flying base stations (FlyBSs) provide a promising way to address various concerns in mobile networks. Due to their high mobility, the FlyBSs present exclusive features, such as adaptability to the network topology and to the actual users' requirements, in comparison to conventional static base stations. These advantages make the FlyBSs an efficient solution for multiple practical applications including surveillance and monitoring [1], data traffic management [2], emergency missions [3], network coverage enhancement [4], data gathering of IoT devices [5], or improvement in users' quality of service [6].

In our previous works ([7], [8]), we study the problem of power optimization for the FlyBS serving moving users and we provide a joint power control and FlyBS's positioning for orthogonal multiple access (OMA) in the mobile networks. In this paper, we focus on the FlyBS's positioning and transmission power consumption for non-orthogonal multiple access (NOMA).

Non-orthogonal multiple access (NOMA) is considered as a promising and suitable technique for future mobile networks. NOMA provides a high spectral efficiency by including superposition coding at the transmitter and successive interference cancellation (SIC) decoding at the receivers [9]. Thus, unlike OMA, NOMA enables to group multiple users into clusters and serve the users in the same cluster at the same time-frequency resources with a separation in a power domain ([10], [11], [12]). Consequently, NOMA increases throughput and spectral efficiency with respect to OMA [6].

Key challenges related to NOMA include fairness control [13], throughput improvement [14], resource allocation [11], network coverage [15], and user pairing or grouping [11], [12]. These key challenges are even emphasized and extended when NOMA is integrated to the networks with FlyBSs. For example, the grouping schemes provided for the networks with static base stations consider instantaneous gains of the users' channels as a criteria to find the user grouping [11], [12]. However, these methods are not suitable for the networks with FlyBS, as the next position of FlyBS is determined based on the current pairing/grouping, while the selected grouping is based on the current position of the FlyBS.

A full exploitation of NOMA together with the FlyBSs' characteristics requires a precise positioning of the FlyBSs, advanced resource allocation, interference control, and grouping of the users for NOMA and SIC in order to efficiently deal with the challenges mentioned above.

In [16], the authors study the coverage in the network with two static ground users served by the FlyBS. Adopting a fading channel model, the authors provide a combination of NOMA and OMA transmission modes to reduce an outage probability of the ground users. However, the positioning of the FlyBS (trajectory) is not optimized. Then, in [15], the authors determine an altitude of the FlyBS serving also only two static ground users in the network with NOMA to maximize Jain's fairness index. The paper [15] is extended in [14] by a power allocation and a determination of the FlyBS's

This work has been supported by Grant No. P102- 18-27023S funded by Czech Science Foundation and by the grant of Czech Technical University in Prague No. SGS20/169/OHK3/3T/13.

altitude to maximize the sum capacity of two static ground users. Nevertheless, the x and y coordinates of the FlyBS are fixed. Thus, the flexibility in a spatial deployment offered by the FlyBSs is not fully exploited. Furthermore, in [17], the authors provide a resource allocation algorithm for NOMA with one FlyBS acting as a relay to maximize the throughput in a scenario with, again, only two static ground users. We note that, since there is only one pair of users in the system model, the problem of user pairing/grouping is not inclusively studied by any of the works in [14]-[17], and none of these works provide a concrete paring/grouping for multiple users.

In [10], a heuristic solution for a joint user grouping and positioning of the FlyBS is proposed to improve the sum capacity. The grouping of users for NOMA is limited to only two users (i.e., pairing of users) and its generalization to the grouping of more than two users is not straightforward. Moreover, the provided solution is sub-optimal and loses performance as the number of users increases.

To the best of our knowledge, a study of the transmission power consumption and an analysis of the user grouping for NOMA in networks with FlyBSs is not investigated in the literature. However, the transmission power consumption affects the coverage and, hence, should not be ignored. This is supported by many works focused on the transmission power consumption of the FlyBSs for a variety of OMA scenarios ([6]-[8]). Moreover, due to limitations on a maximum transmission power of the FlyBSs, the FlyBS might fail to satisfy the minimum required capacity for the users. Thus, a solution reducing the transmission power is necessary to enhance the users' coverage reliability. In NOMA, the transmission power becomes even more critical aspect, as adopting an inefficient grouping scheme can lead to a very high transmission powers beyond the limit of the FlyBS.

In this paper, we focus on the problem of the FlyBS's transmission power optimization in NOMA networks. We formulate the problem of the transmission power minimization with a constraint on a minimum guaranteed capacity for all mobile users. We analytically provide an optimum strategy for the grouping of users for NOMA and we determine related optimum position of the FlyBS to minimize the transmission power. The proposed solution is of a very low complexity (low degree polynomial) and, thus, can be applied in real networks. We show that our proposed solution reduces the transmission power consumption by up to 31% compared to existing solutions.

The rest of the paper is organized as follow. In Section II, we present the system model and formulate the problem of transmission power optimization via the grouping of users for NOMA and FlyBS's positioning. The proposed solution for the transmission power optimization is introduced and thoroughly described in Section III. The performance of the proposed solution and comparison with the performance of existing solutions is discussed in Section IV. Last section concludes the paper and outlines future research directions.

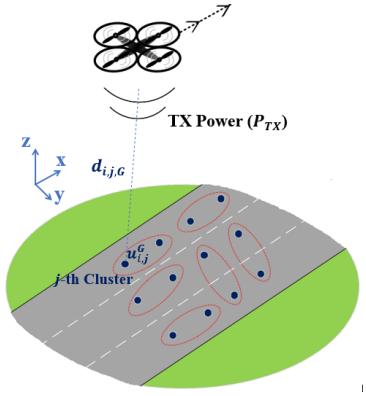

Fig. 1: System model with multiple mobile users (blue dots) deployed within coverage area of the FlyBS and grouped into clusters (red circles) for NOMA purposes.

II. System Model and Problem Formulation

In this section we first define the system model by explaining users grouping in non-orthogonal transmission model, and SIC decoding in the network with FlyBS, and we also provide details about the transmission power modeling. Then, we formulate the transmission power optimization problem.

A. System Model

We consider one FlyBS serving N_u mobile users $U = \{u_1, u_2, \ldots, u_{N_u}\}$ in an area as shown in Fig. 1. The users are moving along the same direction similar to, e.g., vehicles on a road or a highway. Without a loss of generality, we assume the movements are aligned with the x-axis to simplify notations and explanation of the idea. All N_u users in the area communicate directly with the FlyBS.

Let $\{X(t), Y(t), H(t)\}$ denote the location of the FlyBS at the time t. We assume that the altitude of the FlyBS is fixed at $H(t) = H$ as in many previous related works (e.g., [8], [10], [17], [18]). Furthermore, let $\{x^G_{i,j}(t), y^G_{i,j}(t)\}$ denote the coordinates of the i-th user at the time t. Note that we consider mobile users, and so the coordinates of the users as well as of the FlyBS change over time. As commonly expected in related works, we also assume that the current positions of the users are known to the FlyBS (see, e.g., [14], [18]). Also, the FlyBS can determine its own position as the knowledge of the FlyBS's position is needed for a common flying and navigation of the FlyBSs ([17]).

In non-orthogonal transmission, the users are grouped into clusters such that all users in each cluster share the same bandwidth at the same time. Thus, the data transmission to the users in the same cluster imposes an interference (referred to as intra-cluster interference). However, there is no interference among different clusters.

Let $\mathbb{G}$ denote the space of all possible functions that group the users into N_{cl} clusters with N_{cu} users in each cluster, (hence, $N_u = N_{cl} \times N_{cu}$). Each function $G \in \mathbb{G}$ is defined as a bijective mapping G: $\langle 1, N\rangle \rightarrow \langle 1, N_{cl}\rangle \times \langle 1, N_{cu}\rangle$. More

specifically, the function G assigns the user u_n as the n_{cu}-th user in the n_{cl}-th cluster if $G(n) = (n_{cl}, n_{cu})$ for the given n. We refer to n_{cu} and n_{cl} as the index of the user in the cluster and the index of the cluster, respectively. Let $u^G_{1,j}, u^G_{2,j}, \ldots, u^G_{N_{cu},j}$ denote the clustered users in the j-th cluster $(1 \leq j \leq N_{cl})$ that is determined by the grouping function G.

For SIC in non-orthogonal transmission, canceling the strong interferences in each cluster is a more efficient approach than canceling the weak interferences, in the sense that the total transmission power to satisfy the minimum required capacity of all users is lower in the first approach [12]. In the following we define model for the SIC regardless of the different signals' strengths, and only based on the users' indices within each cluster. This assumption helps to solve the problem in a simpler way and without loss of generality, as we find the minimum transmission power among all possible grouping options.

Suppose that, by applying SIC, the user $u^G_{i,j}$ in the j-th cluster $(1 \leq i \leq N_{cu}-1)$ cancels the interfering signals from the user i' in the same cluster (i.e., $u^G_{i',j}$) for $i+1 \leq i' \leq N_{cu}$ to extract its own signal. As a result of this, the achievable SINR $\gamma^G_{i,j}, (1 \leq i \leq N_{cu})$ for the user $u^G_{i,j}$ is expressed as:

$$\begin{aligned} \gamma^G_{1,j} &= \frac{p^{G,R}_{1,j}}{\sigma^2}, \\ \gamma^G_{i,j} &= \frac{p^{G,R}_{i,j}}{\sigma^2 + \sum_{l=1}^{i-1} p^{G,R}_{i,l,j}}, \\ &(2 \leq i \leq N_{cu}) \end{aligned} \tag{1}$$

where $p^{G,R}_{i,l,j}$ denotes the interference power imposed to the user $u^G_{i,j}$ by the signal transmitted to the user $u^G_{l,j}$ in the same cluster j, and σ^2 denotes the noise's power. Now let $C^G_{i,j}$ denote the channel capacity of the user $u^G_{i,j}$. According to the Shannon–Hartley theorem, the channel capacity $C^G_{i,j}$ is defined as:

$$C^G_{i,j} = B\log_2(1 + \gamma^G_{i,j}), \tag{2}$$

where B is the bandwidth assigned to each user and each cluster. Following [11], the channel's bandwidth as well as the noise's power are assumed to be equal for all clusters. The total transmission power of the FlyBS at the time t_k is expressed as:

$$P_{TX}(X, Y, H, t_k, G) = \sum_{j=1}^{N_{cl}} \sum_{i=1}^{N_{cu}} p^{G,T}_{i,j}, \tag{3}$$

where $p^{G,T}_{i,j}$ is the transmission power of the FlyBS to the $u^G_{i,j}$. According to the Friis' transmission equation, $p^{G,T}_{i,j}$ is determined as:

$$\begin{aligned} p^{G,T}_{i,j} &= \frac{(4\pi f)^2}{D^{G,T}_{i,j} D^{G,R}_{i,j} c^2} p^{G,R}_{i,j} {d^G_{i,j}}^2, \\ &1 \leq i \leq N_{cu}, 1 \leq j \leq N_{cl}, \end{aligned} \tag{4}$$

where $p^{G,R}_{i,j}$ is the received signal power by the user $u^G_{i,j}$, $D^{G,T}_{i,j}$ is the gain of the FlyBS's antenna, $D^{G,R}_{i,j}$ is the gain of the user's antenna, $d^G_{i,j}$ is the distance between the FlyBS and the user $u^G_{i,j}$, f is the communication frequency, and $c = 3 \times 10^8$ m/s is the speed of light. The coefficient $\frac{(4\pi f)^2}{D^{G,T}_{i,j} D^{G,R}_{i,j} c^2}$ is substituted by Q in the rest of the paper for clarity and simplicity of the discussions. Using (4), the total transmission power of the FlyBS is rewritten as:

$$P_{TX}(X, Y, H, t_k, G) = \sum_{j=1}^{N_{cl}} \sum_{i=1}^{N_{cu}} Q p^{G,R}_{i,j} {d^G_{i,j}}^2, \tag{5}$$

By expanding (5) with the coordinates of the users and the FlyBS, we get:

$$\begin{aligned} &P_{TX}(X, Y, H, t_k, G) = \\ &\sum_{j=1}^{N_{cl}} \sum_{i=1}^{N_{cu}} Q p^{G,R}_{i,j} ((X(t_k) - x^G_{i,j}(t_k))^2 + (Y(t_k) - y^G_{i,j}(t_k))^2 + H(t_k)^2). \end{aligned} \tag{6}$$

B. Problem Formulation

Our goal is to find the position of the FlyBS jointly with the clustering of the users for NOMA purposes to minimize the transmission power of the FlyBS while guaranteeing a minimum capacity for the users. We formulate the joint problem of the transmission power minimization and users' clustering as:

$$\begin{aligned} &[G_{opt}, [X_{opt}(t_k), Y_{opt}(t_k)]] = \underset{[G,[X(t_k),Y(t_k)]]}{\operatorname{argmin}} P_{TX}, \forall k \\ &s.t. \quad C^G_{i,j}(t_k) \geq C_{min}, \forall j \in \langle 1, N_{cl} \rangle, \forall i \in \langle 1, N_{cu} \rangle, \forall k, \end{aligned} \tag{7}$$

where the constraint guarantees that every user receives at least the minimum required capacity C_{min} all the time. In line with [11], the minimum capacity is assumed to be the same for all the users. We note that, similar to many works (e.g., [14]-[17]) we do not consider the power consumption due to the FlyBS's movement (known as propulsion power). The problem of power optimization including the propulsion power is left for future work due to page limit of this paper.

III. Proposed optimal grouping of users for NOMA and positioning of FlyBS

In this section, we provide a novel method to solve (7) by finding the optimal grouping function G_{opt} as well as the optimal FlyBS's positions $[X_{opt}(t_k), Y_{opt}(t_k)]$ over time. From the definition of grouping, there are $\frac{N_u!}{N_{cl}!}$ different grouping options (grouping options that are obtained by switching the label (index) of clusters are considered the same). Thus, the number of options becomes extremely large for realistic values of N_u (it is about 17.2 million options even for only 14 users). This motivates us to find an analytical solution to grouping.

We start by deriving the conditions that yield the minimum transmission power, and then we find the position of FlyBS corresponding to the minimum transmission power. From the constraint in (7) and using (2), it is inferred that:

$$\gamma_{i,j}^{G} \geq \gamma_{min}, \tag{8}$$

where $\gamma_{min} = (2^{C_{min}/B} - 1)$ is a positive constant. Then, from (1), we rewrite (8) as:

$$\frac{p_{1,j}^{G,R}}{\sigma^2} \geq \gamma_{min}, \frac{p_{i,j}^{G,R}}{\sigma^2 + \sum_{l=1}^{i-1} p_{i,l,j}^{G,R}} \geq \gamma_{min}, \quad (2 \leq i \leq N_{cu}, 1 \leq j \leq N_{cl}). \tag{9}$$

Using (9), we find the conditions to reach the minimum transmission power as follows. Equation (9) is rewritten using (4) as:

$$\frac{\frac{p_{1,j}^{G,T}}{Qd_{i,j}^{G\ 2}}}{\sigma^2} \geq \gamma_{min}, \frac{\frac{p_{i,j}^{G,T}}{Qd_{i,j}^{G\ 2}}}{\sigma^2 + \frac{\sum_{l=1}^{i-1} p_{l,j}^{G,T}}{Qd_{i,j}^{G\ 2}}} \geq \gamma_{min}, \quad (2 \leq i \leq N_{cu}, 1 \leq j \leq N_{cl}). \tag{10}$$

After several simple math operations, (10) is transformed to (assuming $\sum_{1}^{0}$ is equal to 0):

$$\gamma_{min} \sum_{l=1}^{i-1} p_{l,j}^{G,T} + \gamma_{min} Q d_{i,j}^{G\ 2} \sigma^2 \leq p_{i,j}^{G,T}, \quad (1 \leq i \leq N_{cu}, 1 \leq j \leq N_{cl}). \tag{11}$$

Therefore, by writing down (11) for every $j \in \langle 1, N_{cl} \rangle$ and for all $i \in \langle 1, N_{cu} \rangle$, we get

$$\sum_{j=1}^{N_{cl}} \sum_{i=1}^{N_{cu}} p_{i,j}^{G,T} \geq \gamma_{min} Q \sigma^2 \sum_{j=1}^{N_{cl}} \sum_{i=1}^{N_{cu}} ((1+\gamma_{min})^{N_{cu}-i}) d_{i,j}^{G\ 2}. \tag{12}$$

The minimum in (12) is achieved when the equality in (11) holds for $1 \leq i \leq N_{cu}$, and $1 \leq j \leq N_{cl}$, that is, if:

$$\gamma_{min} \sum_{l=1}^{i-1} p_{l,j}^{G,T} + \gamma_{min} Q d_{i,j}^{G\ 2} \sigma^2 = p_{i,j}^{G,T}, \quad (1 \leq i \leq N_{cu}, 1 \leq j \leq N_{cl}). \tag{13}$$

Hence, from (13), we derive $P_{TX}(X, Y, H, t_k, G)$ as:

$$P_{TX}(X,Y,H,t_k,G) = \gamma_{min} Q \sigma^2 \sum_{j=1}^{N_{cl}} \sum_{i=1}^{N_{cu}} ((1+\gamma_{min})^{N_{cu}-i}) d_{i,j}^{G\ 2} = \sum_{j=1}^{N_{cl}} \sum_{i=1}^{N_{cu}} ((1+\gamma_{min})^{N_{cu}-i})((X(t_k) - x_{i,j}^{G}(t_k))^2 + (Y(t_k) - y_{i,j}^{G}(t_k))^2 + H(t_k)^2). \tag{14}$$

From (14), the FlyBS's position to achieve the minimum transmission power is derived for each grouping function G by evaluating the transmission power at its critical point(s). Thus, by solving equations $\frac{\partial P_{TX}}{\partial X} = 0$ and $\frac{\partial P_{TX}}{\partial Y} = 0$ with P_{TX} defined in (14), we get the following critical point:

$$X_{opt}^{G} = \frac{\sum_{j=1}^{N_{cl}} \sum_{i=1}^{N_{cu}} ((1+\gamma_{min})^{N_{cu}-i} x_{i,j}^{G})}{\sum_{j=1}^{N_{cl}} \sum_{i=1}^{N_{cu}} ((1+\gamma_{min})^{N_{cu}-i})}, \quad Y_{opt}^{G} = \frac{\sum_{j=1}^{N_{cl}} \sum_{i=1}^{N_{cu}} ((1+\gamma_{min})^{N_{cu}-i} y_{i,j}^{G})}{\sum_{j=1}^{N_{cl}} \sum_{i=1}^{N_{cu}} ((1+\gamma_{min})^{N_{cu}-i})}. \tag{15}$$

Knowing the coordinates X_{opt}^{G} and Y_{opt}^{G} and considering the definition of the total transmission power in (14), the corresponding minimum transmission power is determined by plugging (15) into (14). After a few simple math operations, the minimum transmission power corresponding to the grouping function G is rewritten as:

$$P_{TX}^{min}(G) = P_{TX}(X_{opt}^{G}, Y_{opt}^{G}, H, t_k, G) = \gamma_{min} Q \sigma^2 N_u H^2 + \gamma_{min} Q \sigma^2 (\delta_x^G + \delta_y^G), \tag{16}$$

where

$$\delta_x^G = -\frac{(\sum_{j=1}^{N_{cl}} \sum_{i=1}^{N_{cu}} ((1+\gamma_{min})^{N_{cu}-i} x_{i,j}^{G})^2}{\sum_{j=1}^{N_{cl}} \sum_{i=1}^{N_{cu}} ((1+\gamma_{min})^{N_{cu}-i})} + \sum_{j=1}^{N_{cl}} \sum_{i=1}^{N_{cu}} ((1+\gamma_{min})^{N_{cu}-i} x^{2\,G}_{i,j}),$$

$$\delta_y^G = -\frac{(\sum_{j=1}^{N_{cl}} \sum_{i=1}^{N_{cu}} ((1+\gamma_{min})^{N_{cu}-i} y_{i,j}^{G})^2}{\sum_{j=1}^{N_{cl}} \sum_{i=1}^{N_{cu}} ((1+\gamma_{min})^{N_{cu}-i})} + \sum_{j=1}^{N_{cl}} \sum_{i=1}^{N_{cu}} ((1+\gamma_{min})^{N_{cu}-i} y^{2\,G}_{i,j}). \tag{17}$$

We note that for the movement in line with the system model, i.e., a crowd of users (e.g., vehicles) moving along the street in the direction of x-axis, the value of δ_x^G is significantly larger than δ_y^G in a system of vehicles at a road or a highway. This is mainly because δ_x^G and δ_y^G can be interpreted as a weighted sample variance of the x and y coordinates of the users' locations, respectively, and the range of x-coordinates corresponding to the vehicles is much larger than the range of y-coordinates (we do not show further details due to page limit). Therefore, we find the optimal grouping function by minimizing δ_x^G.

To minimize δ_x^G, we first derive an optimal grouping function G_{opt} via Theorem 1, that provides a necessary condition for G_{opt}.

Theorem 1. *Suppose that before grouping of users into clusters, the x-coordinates of the users are sorted as $X_{sorted} = \{x_{l_1}, \ldots, x_{l_{N_u}}\}$, such that $x_{l_1} < \ldots < x_{l_{N_u}}$. Then, for the grouping function that minimizes δ_x^G (i.e., the optimal grouping), the set of first users of all clusters (i.e., the users $x_{1,1}^{G_{opt}}, x_{1,2}^{G_{opt}}, \ldots, x_{1,N_{cl}}^{G_{opt}}$) should be N_{cl} consecutive users in the sorted sequence X_{sorted}, i.e., $\{x_{1,1}^{G_{opt}}, x_{1,2}^{G_{opt}}, \ldots, x_{1,N_{cl}}^{G_{opt}}\} = \{x_{l_r}, x_{l_{r+1}}, ..., x_{l_{r+N_{cl}-1}}\}$ for some $r \in \langle 1, N_u - N_{cl} + 1 \rangle$. Furthermore, the set of second users of all clusters (i.e., $x_{2,1}^{G_{opt}}, x_{2,2}^{G_{opt}}, \ldots, x_{2,N_{cl}}^{G_{opt}}$) should be N_{cl} consecutive users in the sorted sequence $X_{sorted} \backslash \{x_{1,1}^{G_{opt}}, x_{1,2}^{G_{opt}}, \ldots, x_{1,N_{cl}}^{G_{opt}}\}$, and so on and so forth for the rest of the users of all groups.*

Proof. We prove Theorem 1 using mathematical contradiction as follow: Suppose that $\{x_{1,1}^{G_{opt}}, x_{1,2}^{G_{opt}}, \ldots, x_{1,N_{cl}}^{G_{opt}}\} = \{x_{i_1}, ..., x_{i_{N_{cl}}}\}$ with $x_{i_1} < ... < x_{i_{N_{cl}}}$. Then, by contradiction, we assume that the users in $\{x_{i_1}, ..., x_{i_{N_{cl}}}\}$ are not consecutive in X_{sorted} and there exists x_j such that $x_{i_1} < x_j < x_{i_{N_{cl}}}$ and $x_j \notin \{x_{i_1}, ..., x_{i_{N_{cl}}}\}$ Also, we assume that, for G_{opt} , x_j is the s-th user in some cluster ($s > 1$).

Let G_1 denote the grouping function that is obtained by swapping x_{i_1} and x_j in G_{opt}. Similarly, G_2 denotes the grouping obtained by swapping $x_{i_{N_{cl}}}$ and x_j in G_{opt}. From the optimality of G_{opt} it is inferred that:

$$\begin{aligned} \delta_x^{G_{opt}} - \delta_x^{G_1} < 0, \\ \delta_x^{G_{opt}} - \delta_x^{G_2} < 0. \end{aligned} \tag{18}$$

Now, we rewrite the left-hand side terms in (18) in terms of the system parameters as follow:

$$\begin{aligned} \delta_x^{G_{opt}} - \delta_x^{G_1} = (x_{i_1}^2 - x_j^2)((1+\gamma_{min})^{N_{cu}-1} - (1+\gamma_{min})^{N_{cu}-s}) - \alpha\beta, \\ \alpha = \frac{(x_{i_1} - x_j)((1+\gamma_{min})^{N_{cu}-1} - (1+\gamma_{min})^{N_{cu}-s})}{\sum_{j=1}^{N_{cl}}\sum_{i=1}^{N_{cu}}((1+\gamma_{min})^{N_{cu}-i}}, \\ \beta = 2\sum_{j=1}^{N_{cl}}\sum_{i=1}^{N_{cu}}((1+\gamma_{min})^{N_{cu}-i}x_{i,j}^G) - (1+\gamma_{min})^{N_{cu}-1}x_{i_1} - \\ (1+\gamma_{min})^{N_{cu}-1}x_j - (1+\gamma_{min})^{N_{cu}-s}x_{i_1} - (1+\gamma_{min})^{N_{cu}-s}x_j. \end{aligned} \tag{19}$$

Using the first inequality in (18) and using the fact that $x_{i_1} < x_j$, it follows from (19) that:

$$(\sum_{j=1}^{N_{cl}}\sum_{i=1}^{N_{cu}}(1+\gamma_{min})^{N_{cu}-i})(x_{i_1} + x_j) - \beta > 0. \tag{20}$$

A similar inequality to (20) can be derived from the second inequality in (18) (details omitted due to page limit). Then, by summing the respective sides in (20) and in the other derived inequality, it is concluded that:

$$\begin{aligned} \sum_{j=1}^{N_{cl}}\sum_{i=1}^{N_{cu}}(1+\gamma_{min})^{N_{cu}-i} - \\ ((1+\gamma_{min})^{N_{cu}-1} + (1+\gamma_{min})^{N_{cu}-s}) < 0, \end{aligned} \tag{21}$$

which is not correct, since the left-hand side in (21) consists of a summation of positive terms (after excluding $(1+\gamma_{min})^{N_{cu}-1}$ and $(1+\gamma_{min})^{N_{cu}-s}$ from $\sum_{j=1}^{N_{cl}}\sum_{i=1}^{N_{cu}}(1+\gamma_{min})^{N_{cu}-i}$), and so this contradicts the initial assumption that the users in $\{x_{i_1}, ..., x_{i_{N_{cl}}}\}$ are not consecutive. Therefore, $\{x_{i_1}, ..., x_{i_{N_{cl}}}\}$ consists of consecutive users in X_{sorted}. By a similar procedure as above, we verify that the second users of all clusters should be consecutive values in $X_{sorted} \backslash \{x_{1,1}^{G_{opt}}, x_{1,2}^{G_{opt}}, \ldots, x_{1,N_{cl}}^{G_{opt}}\}$, and so on for the next users of all clusters. This completes the proof to Theorem 1.

□

Theorem 1 provides a solution to choosing the optimal grouping function as follows: First, we sort the x-coordinates of users as $x_{l_1} < ... < x_{l_{N_u}}$, and list all possible sequences of length N_{cl} that consist of consecutive values in $X_{sorted} = \{x_{l_1}, \ldots, x_{l_{N_u}}\}$. There are $(N_u - N_{cl} + 1)$ of such sequences. According to Theorem 1, the set of first users of all clusters in the optimal grouping is one of those sequences in the list. Therefore, instead of considering all $\binom{N_u}{N_{cl}}$ of such possible subsets, we only have $(N_u - N_{cl} + 1)$ candidates. Of course, the optimal sequence cannot be determined until all of the N_u users are assigned to groups. Therefore, for each of the sequences in the first step, we list all sequences of N_{cl} consecutive users in the remaining set of users in X_{sorted}. Again, according to theorem 1, the set of second users of all clusters in the optimal grouping is one of these sequences. We repeat the procedure until there is no users left, that is, all the groups are completed. Next, we use (14) to evaluate the transmission power corresponding to every grouping completed in the procedure, and then choose the one that yields the minimum transmission power.

The size of the search space in the provided method is

$$\prod_{k=1}^{N_{cu}}(N_u - kN_{cl} + 1). \tag{22}$$

The search space is polynomial with N_u and N_{cl} and its size is significantly reduced with respect to search space of the exhaustive search, which is $\frac{N_u!}{N_{cl}!}$.

IV. Simulations and results

In this section, we provide details of models and simulations adopted for evaluation of the performance of the proposed optimization of the transmission power consumed by the FlyBS serving mobile users. We also demonstrate the advantages of the proposed scheme over existing state of the art schemes.

A. Simulation scenario and models

We consider a scenario where the FlyBS serves users represented by vehicles and/or users in vehicles during a busy traffic or a traffic jam at a road or a highway in a rural area. In such situation, the FlyBS is a suitable solution to improve the performance, since the conventional network is usually overloaded as plenty of active users are located in a small area with a limited network coverage (see, e.g., [20]).

The users are assumed to move on a 3-lane highway in the positive direction of x-axis. The users are distributed uniformly among all three lanes. Within one lane, the velocities of all users are the same so that the minimum regulated distance between the vehicles is kept all the time. More specifically, we set the two-second rule, that is, the minimum distance between two vehicles is equal to the distance moved by the vehicles within two seconds. The velocities are selected uniformly over interval {19-24} m/s, {17-19} m/s, and {14-16} m/s for the first, second, and third lanes, respectively. A common rotary-wing UAVs is considered to serve the users. Such UAV can fly typically with a maximum speed of about 25m/s [21], thus, the typical FlyBS is not efficient for higher speeds than 25 m/s as the FlyBS cannot follow the vehicles' movement.

We assume free space path loss (FSPL) model for the wireless channel, as the communication link between the FlyBS and the vehicles on the road is typically without any obstacles and the FSPL is a commonly adopted model in such cases ([8], [10], [18]). Omni-directional antennas with gains of 7 dBi and 0 dBi for the FlyBS and the users are considered, respectively, in line with [22]. The radio frequency $f = 2.6$ GHz and a bandwidth of 100 MHz are selected. Spectral density of noise is set to –174 dBm/Hz. Following [18], the

TABLE I: Parameter Configurations

System Parameter	Numerical value
Number of users in the coverage area, N_u	{30,60,90}
FlyBS's antenna gain, $D_{i,G}^{j,T}$	7 dBi
User's antenna gain, $D_{i,G}^{j,R}$	0 dBi
Noise power spectral density, N_i	–174 dBm/Hz
Minimum guaranteed capacity to each user C_{min}	15 Mbps
RF frequency, f	2.6 GHz
System bandwidth	100 MHz
Altitude of FlyBS, H	100 meters
Simulation Duration	600 s
Number of simulation drops	100

FlyBS's altitude is fixed at $H = 100$ m. The simulations are performed for the capacity required by each user $C_{min} = 15$ Mbps. Each simulation is of 600 seconds duration with the optimal grouping and transmission power calculated every second. The results are averaged out over 100 simulation drops. The system parameters are summarized in Table I.

Our proposal, which minimizes the FlyBS's transmission power consumption together with the FlyBS's positioning and determination of the optimal grouping of users for NOMA purposes (as elaborated in Section III) is compared with four most-related state of the art schemes: i) the algorithm introduced in [10] that provides a joint NOMA pairing and FlyBS's positioning for sum rate maximization (referred to as SRM in the later discussions in this paper), ii) an enhanced version of SRM in [10] (referred to as ESRM) that adopts the pairing scheme as in [10], but the position of FlyBS is enhanced by our proposed positioning according to (15) in order to achieve the minimum transmission power, as the solution in [10] targets a maximization of sum rate, iii) the algorithm developed in [12] that adopts the optimal grouping corresponding to the minimum transmission power in NOMA with static base station (referred to as SBS), and hence, does not provide any solution to the FlyBS's positioning, iv) an enhanced version of SBS (referred to as ESBS) that adopts the grouping scheme according to [12], but the positioning of the FlyBS is enhanced by our proposed positioning according to (15) to achieve the minimum transmission power consumption.

B. Simulation results

In this subsection, we present and discuss simulation results. First, we focus on an evolution of the transmission power consumption of the FlyBS over time to demonstrate the advantage of our proposed method over the existing solutions in terms of an efficient power management and consequent enhancement of coverage. Then, we compare the performance of the proposed scheme with existing solutions in terms of complexity and average power consumption.

Fig. 2 illustrates the transmission power of the FlyBS over time for $C_{min} = 15$ Mbps guaranteed to each user and for $N_u = 90$ (top subplot) and $N_u = 30$ (bottom subplot). In this figure, we assume NOMA is set so that users are paired ($N_{cu} = 2$), thus, two users share the same time-frequency

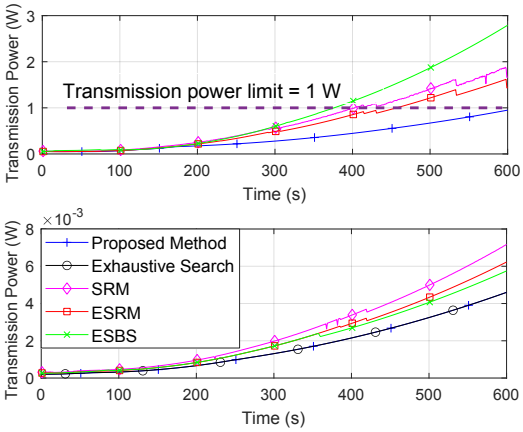

Fig. 2: Transmission power vs. operation time of the FlyBS for $N_u = 90$ (top subplot) and $N_u = 30$ (bottom subplot).

resources. The transmission power consumption is increasing in general over time, for all solutions. This is due to a general increase in the relative distance between the first and the last vehicles in the scenario over time caused by diverse velocities of vehicles on different lanes causing a gradual expansion of the area demarcated by users covered by the FlyBS.

Fig. 2 further shows that the transmission powers corresponding to SRM, ESRM, and ESBS grow notably faster than for our proposed solution and the power is reduced roughly by 33%, 50%, and 66% with respect to SRM, ESRM, and ESBS, respectively for $N_u = 90$. We depict also the optimum power consumption determined via the exhaustive search. As the complexity of the exhaustive search does not allow to determine results for $N_u = 90$, we show it only for $N_u = 30$. The results confirm that the proposed solution reaches almost the optimum performance with totally negligible difference.

The efficiency of the proposed method is explained also in terms of the coverage as, in practice, the transmission power of the FlyBS is limited. Thus, the FlyBS may fail to guarantee C_{min} to all the users if the power limit is reached. In such case, a higher number of FlyBSs is required and the users should be associated to other FlyBSs to ensure a continuous coverage. In this sense, our proposed solution provides a higher coverage radius and less FlyBSs are needed to cover a specific area.

For example, if the transmission power of the FlyBS is limited to 1 Watt, Fig. 2 shows that the FlyBS is not able to guarantee C_{min} to all users after 10 s, 380 s, 400 s, 450 s, and 600 s, for SBS, ESBS, SRM, ESRM, and the proposal, respectively. More specifically, compared with SBS, ESBS, SRM, and ESRM, the maximum covered area provided by the proposal is 155%, 36%, 26%, and 17% larger, respectively. Note that the transmission power reached by SBS (scheme iii, see previous subsection) is in the order of hundreds of watts, since the relative distance between the base station and the users increases notably due to immobility of the base station. Hence, the results of SBS are omitted in the rest of the paper.

Next, we investigate an impact of the number of users on the

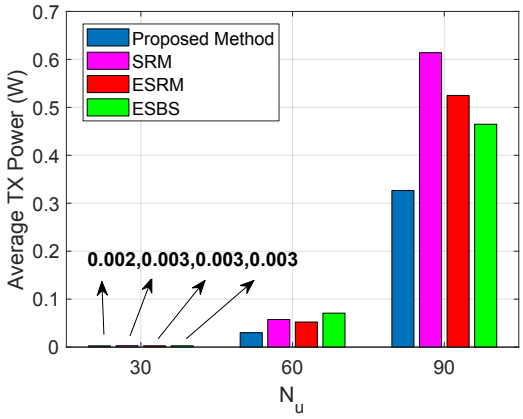

Fig. 3: Average transmission power achieved by individual schemes for various numbers of users N_u.

transmission power in Fig. 3 (with $N_{cu} = 2$ for all schemes). It is observed that the average transmission power increases with the number of users, as a larger N_u results in less bandwidth available for each cluster of users, and so a higher transmission power is required to satisfy $C_{min} = 15$ Mbps. Our proposed solution reaches the lowest transmission power of the FlyBS disregarding the number of served users N_u. For $N_u = 90$, the transmission power is reduced by 48%, 38%, and 31% comparing to SRM, ESRM, and ESBS, respectively.

We also show the complexity of the proposed and state of the art solutions for joint users' pairing and the FlyBS's positions in Table II for $N_u = 90$. The complexity is defined as the number of calculations (math operations) performed by each solution. The results are shown for $N_{cu} = 2$, since ESRM is designed for $N_{cu} = 2$ and its extension to $N_{cu} > 2$ is not straightforward. Note that we do not include the complexity of SRM and ESBS, as the complexity of these is not easy to calculate, because the SRM and ESBS solutions are based on bisection search [10] and convex optimization, respectively. Table II confirms that the proposed optimization reduces the complexity significantly with respect to exhaustive search (2.7×10^{80} times) as well as with respect to ESRM (twice).

TABLE II: Complexity of power optimization represented as the number of math operations required to obtain results.

Method	**Complexity**
Proposed transmission power optimization	46
ESRM	90
Exhaustive search	1.24×10^{82}

V. Conclusions

In this paper, we have studied the problem of joint FlyBS's positioning and transmission power minimization in future mobile networks based on NOMA. We formulate the transmission power minimization problem in terms of the grouping of users for NOMA purposes and determination of the FlyBS's positions over time as the users move. Then, we provided a solution to find the optimum grouping and the FlyBS's positions that yield the minimum transmission power while guaranteeing a minimum required capacity for all users. Furthermore, we show that the proposed solution reduces the transmission power consumed by the FlyBS by tens of percent while the required capacity of the moving users is always satisfied. Due to the efficient transmission power consumption in the proposed method, the coverage area of the FlyBS is significantly expanded.

In the future work, a scenario with multiple FlyBS should be studied. This scenario implies another dimension of the problem related to the user association to individual FlyBSs. Furthermore, the problem of power optimization with inclusion of propulsion power consumption should be considered.

References

[1] A. Chriki, et al, "UAV-GCS Centralized Data-Oriented Communication Architecture for Crowd Surveillance Applications," IWCMC, 2019.

[2] X. Hu, et al, "Joint Optimization of Traffic and Computation Offloading in UAV-Assisted Wireless Networks," *IEEE MASS*, 2018,.

[3] X. Cheng, et al., "Architecture Design of Communication and Backhaul for UAVs in Power Emergency Communication," *ICCCBDA*, 2019.

[4] X. Li, et al, "A Near-Optimal UAV-Aided Radio Coverage Strategy for Dense Urban Areas," *IEEE Trans. Veh. Technol.*, vol. 68, no. 9, 2019.

[5] M. Samir, et al, "UAV Trajectory Planning for Data Collection from Time-Constrained IoT Devices," *IEEE Trans. Wireless Commun.*, 2020.

[6] B. Li, Z. Fei, and Y. Zhang, "UAV Communications for 5G and Beyond: Recent Advances and Future Trends," *IEEE Internet Things J.*, 2019.

[7] M. Nikooroo, and Z. Becvar, "Joint Positioning of UAV and Power Control for Flying Base Stations in Mobile Networks," *IEEE WiMOB*, 2019.

[8] M. Nikooroo, and Z. Becvar, "Optimizing Transmission and Propulsion Powers for Flying Base Stations", *IEEE WCNC, 2020*.

[9] L. Dai, et al, "Non-orthogonal multiple access for 5G: solutions, challenges, opportunities, and future research trends," IEEE Communications Magazine, vol. 53, no. 9, 2015.

[10] M. T. Nguyen and L. B. Le, "NOMA User Pairing and UAV Placement in UAV-Based Wireless Networks," *IEEE ICC* 2019.

[11] J. Kang and I. Kim, "Optimal User Grouping for Downlink NOMA," *IEEE Commun. Lett.*, vol. 7, no. 5, 2018.

[12] L. Lei, et al, "On Power Minimization for Non-orthogonal Multiple Access (NOMA)," *IEEE Commun. Lett.*, vol. 20, no. 12, 2016.

[13] B. Kim, J. Heo, and D. Hong, "Partial Non-Orthogonal Multiple Access (P-NOMA) with Respect to User Fairness," *IEEE VTC*, 2019.

[14] M. F. Sohail, et al, "Non-Orthogonal Multiple Access for Unmanned Aerial Vehicle Assisted Communication," *IEEE Access*, vol. 6, 2018.

[15] M. F. Sohail, and C. Y. Leow, "Maximized fairness for NOMA based drone communication system," *MICC*, 2017.

[16] P. K. Sharma and D. I. Kim, "UAV-Enabled Downlink Wireless System with Non-Orthogonal Multiple Access," *GC Wkshps* 2017.

[17] J. Baek, S. I. Han, and Y. Han, "Optimal Resource Allocation for Non-Orthogonal Transmission in UAV Relay Systems," *IEEE Commun. Lett.*, vol. 7, no. 3, 2018.

[18] Y. Zeng, and R. Zhang, "Energy-Efficient UAV Communication With Trajectory Optimization," *IEEE Trans. Wireless Commun.*, 2017.

[19] L.Zhu, et al, "Optimal User Pairing for Downlink Non-Orthogonal Multiple Access (NOMA)" *IEEE Commun. Lett.*, Vol. 8, No. 2, 2019.

[20] P. Yang, et al, "Proactive Drone-Cell Deployment: Overload Relief for a Cellular Network Under Flash Crowd Traffic," *IEEE Trans. Intell. Transp. Syst.*, 2017.

[21] A. Fotouhi, et al, "Survey on UAV Cellular Communications: Practical Aspects, Standardization Advancements, Regulation, and Security Challenges," *IEEE Commun. Surveys Tuts.*, 2019.

[22] M. Bekhti, et al, "Path Planning of Unmanned Aerial Vehicles With Terrestrial Wireless Network Tracking," *Wireless days*, March 2016.

Optimal Positioning of Flying Base Stations and Transmission Power Allocation in NOMA Networks

Mohammadsaleh Nikooroo, *Member, IEEE,* Zdenek Becvar, *Senior Member, IEEE*

***Abstract*—Unmanned aerial vehicles (UAVs) acting as flying base stations (FlyBSs) are considered as an efficient tool to enhance the capacity of future mobile networks and to facilitate the communication in emergency cases. These benefits are, however, conditioned by an efficient control of the FlyBSs and management of radio resources. In this paper, we propose a novel solution jointly selecting the optimal clusters of an arbitrary number of the users served at the same time-frequency resources by means of non-orthogonal multiple access (NOMA), allocating the optimal transmission power to each user, and determining the position of the FlyBS. This joint problem is constrained with the FlyBS's propulsion power consumed for flying and with a continuous guarantee of a minimum required capacity to each mobile user. The goal is to enhance the duration of a communication coverage in NOMA defined as the time interval within which the FlyBS always provides the minimum required capacity to all users. The proposed solution clusters the users and allocates the transmission power of the FlyBS to the users efficiently so that the communication coverage provided by the FlyBSs is extended by 67%–270% comparing to existing solutions while the propulsion power is not increased.**

***Index Terms*—Flying base station, non-orthogonal multiple access, user clustering, transmission power, mobile users, mobile networks, 6G.**

I. Introduction

Unmanned aerial vehicles (UAVs) acting as flying base stations (FlyBSs) provide a promising way to address various concerns and challenges in the future mobile networks. Due to a high mobility, the FlyBSs present exclusive features, such as adaptability to the network topology and to the actual users' requirements, in comparison to conventional static base stations [1]. These advantages make the FlyBSs an efficient solution for multiple practical applications including surveillance and monitoring [2], [3], data traffic management [4], emergency missions [5], network coverage enhancement [6], [7], data gathering from IoT devices [8], or improving users' quality of service [1], [9], [10].

A critical and limiting aspect in the networks with FlyBSs is a power consumption. In [11], an efficient positioning of the FlyBSs is proposed to maximize the number of covered users while reducing the transmission power in orthogonal multiple access (OMA) network. However, the power consumption due to movement of the FlyBS (denoted as propulsion power) is not considered. Furthermore, the problem of a throughput improvement in the OMA-based mobile networks with FlyBSs is addressed in [12]. Then, in [13], the authors maximize the throughput via a positioning of the FlyBS in the mobile networks with OMA. However, neither the transmission nor the propulsion power consumption is considered in [12] and [13]. In [14] and [15], the power consumption of the FlyBS serving moving users is optimized and a joint power control and FlyBS's positioning is provided for the networks with OMA.

Non-orthogonal multiple access (NOMA) is considered as a promising technique in future mobile networks [16]. NOMA provides a high spectral efficiency by including a superposition coding at a transmitter and a successive-interference-cancellation (SIC) decoding at a receiver [17]. Thus, NOMA enables to group users into clusters and serve all users in one cluster at the same time-frequency resources with a separation in a power domain [18]. Consequently, NOMA potentially increases throughput and spectral efficiency comparing to OMA [1], [17], [19], [20].

Key challenges related to NOMA include fairness control [21], [22], throughput improvement [23], resource allocation [24], [25], [26], [27], [28], network coverage [29], and pairing (or clustering) of the users served at the same time-frequency resources [24], [30]. These key challenges are even emphasized and extended when NOMA is integrated to the networks with FlyBSs [16]. For example, the clustering schemes developed for the networks with the static base stations consider instantaneous gains of the users' channels as a criteria to find the users' clustering in [24], [30]. However, such approach is not suitable for the networks with the FlyBS, as the next position of the FlyBS is determined based on the current pairing/clustering, while the selected clustering of the users is based on the current position of the FlyBS. Hence, the solutions designed for the static base stations are not suitable for the FlyBSs.

In [31], the problem of optimizing the FlyBS's altitude, antenna beamwidth, and transmission power allocation is investigated to maximize the sum capacity in a multiuser NOMA network. However, the problem of the user's pairing/clustering is not investigated, as the authors assume the users are already (beforehand) paired into fixed clusters.

Furthermore, in [32], the authors investigate the coverage

Mohammadsaleh Nikooroo and Zdenek Becvar are with Department of Telecommunication Engineering, Faculty of Electrical Engineering, Czech Technical University in Prague, Czech Republic, e-mail: (nikoomoh@fel.cvut.cz, and zdenek.becvar@fel.cvut.cz).

This work has been supported by Grant No. P102-18-27023S funded by Czech Science Foundation and by the grant of Czech Technical University in Prague No. SGS20/169/OHK3/3T/13.

in a network with two static users served by the FlyBS. The authors provide a combination of NOMA and OMA transmission to reduce an outage probability of the users. However, the positioning (trajectory) of the FlyBS is not optimized. Then, in [29], the authors determine the altitude of the FlyBS serving also only two static users in the network with NOMA to maximize Jain's fairness index. The paper [29] is extended in [23] by a power allocation and a determination of the FlyBS's altitude to maximize the sum capacity of two static users. Nevertheless, the x and y coordinates of the FlyBS are fixed. Thus, the flexibility in a spatial deployment offered by the FlyBSs is not fully exploited. In [33], the authors provide a resource allocation for NOMA with the FlyBS to maximize the throughput in a scenario with, again, only two static users. Then, in [34], the authors focus on a problem of the sum capacity maximization via the transmission power allocation and the FlyBS's trajectory optimization in a hybrid network consisting of the FlyBS serving users via OMA and a static base station serving the users via NOMA so that all users served by the static base station are in one cluster. In [35], a joint FlyBS positioning and the transmission power allocation is targeted to improve the sum capacity of the users that are all grouped into just one cluster. Since there is only one cluster of the users considered in [23], [29], [32], [33], [34], [35], the problem of the users' pairing/clustering is not addressed by any of these works.

In [18], a heuristic solution for a joint user clustering and positioning of the FlyBS is proposed to increase the sum capacity. The user clustering for NOMA is limited to only two users (i.e., a pairing of the users) and its generalization to the clustering of more than two users is not straightforward. Moreover, the FlyBS's power consumption is not considered and the provided solution is sub-optimal and loses performance as the number of users increases.

In [36], the authors target to guarantee a secure transmission for static users served by the FlyBS in NOMA considering also a simultaneous wireless information and power transfer (SWIPT). Then, in [37] the authors provide a joint power allocation, beamspace precoding, and FlyBS positioning to maximize an energy efficiency in NOMA with the static users. However, the problem of the propulsion power consumption is addressed in neither [36] nor [37], as the FlyBS is assumed to hover at a fixed position during the entire operation in these papers.

To the best of our knowledge, the transmission power optimization and the optimal clustering of an arbitrary number of users for NOMA in the networks with FlyBSs is not investigated in the literature. However, the problem of the transmission power allocation should not be ignored, as it directly affects the communication coverage in NOMA provided by the FlyBSs. Due to the maximum transmission power limit of any transmitter in real world application, including the FlyBSs, the FlyBS might fail to satisfy the minimum capacity required by the users if the transmission power in NOMA is not managed and allocated to the users properly. The guarantee of the minimum capacity is mandatory in many real-time applications, such as assisted or autonomous driving, or in emergency situations. Many works focus on the transmission power optimization of the FlyBSs for a variety of OMA scenarios, see e.g., [1], [9], [14]. However, in NOMA, the transmission power becomes an even more critical aspect, as adopting an inefficient clustering of the users and power allocation can lead to a requirement on a very high transmission power beyond the maximum allowed transmission power of the FlyBS and to an inability to guarantee the users' required capacity.

In this paper, we propose a joint clustering of the users for NOMA, optimal allocation of the transmission power for NOMA, and optimal FlyBS's positioning to enhance a duration of the communication coverage in NOMA networks. Moreover, we consider practical constraints on the FlyBS's speed, acceleration, and propulsion power consumption, while continuously guaranteeing a minimum communication capacity to each mobile user. The detailed contribution and novelty presented in our paper are as follow:

- We express analytically the transmission power consumption as a function of i) the user clustering for NOMA, ii) the users' minimum required downlink capacity, and iii) the users' relative locations with respect to the FlyBS. Then, the minimum achievable transmission power is expressed in terms of these parameters.
- As a major contribution, we derive a low-complexity analytical solution determining the optimum user clustering for NOMA with an arbitrary number of users in every cluster, and we determine the corresponding position of the FlyBS to optimize the transmission power allocation. This enables to increase the communication coverage provided by the FlyBS while continuously guaranteeing the minimum capacity required by the mobile user.
- We also take the propulsion power consumption into account to make the proposed solution efficient in terms of a total power consumption and we propose a method to control the propulsion power considering the speed and acceleration limits of the FlyBSs.
- By simulations, we show that our proposed clustering of the users for NOMA, transmission power allocation to the users in the same NOMA cluster, and FlyBS's positioning significantly enhances the communication coverage in NOMA provided by the FlyBS and we show that our proposal is applicable also to a scenario with multiple FlyBSs.

Note that this paper is an extension of our prior work [38], where we outline a general idea of the transmission power optimization for the FlyBS with NOMA and we provide initial results.

The rest of the paper is organized as follow. In Section II, we present the system model and formulate the problem of joint NOMA clustering, transmission power allocation, and FlyBS's positioning. The proposed solution is introduced

and thoroughly described in Section III. The performance of the proposed solution and a comparison with state-of-the-art solutions are discussed in Section IV. Last, Section V concludes the paper and outlines future research directions.

II. System Model and Problem Formulation

In this section we first explain the model for the user clustering and SIC decoding in the networks with NOMA and with FlyBS, and we provide details about transmission power modeling. Furthermore, we formulate the problem of user clustering, power allocation, and FlyBS's positioning.

A. System Model

We consider one FlyBS serving N_u mobile users $U = \{u_1, u_2, \ldots, u_{N_u}\}$ in an area as shown in Fig. 1. The users are moving in the same direction similar to, e.g., movement of vehicles on a sub-urban/rural road or a highway. The deployment of the FlyBS is a suitable solution in busy traffic or traffic jam situations to improve the network performance, as the conventional network is usually overloaded by many active users located in a relatively small area with a limited network coverage, (see, e.g., [39], [40]). Without loss of generality, we assume the movement of the users is aligned with the x-axis to simplify the notations and explanation of the idea. All N_u users in the area communicate directly with the FlyBS. The FlyBS and the users use single antenna, since the principle of our proposed solution is independent of the number of antennas. The proposed solution can be easily enhanced towards MIMO, as the interference between different clusters in MIMO is canceled by allocating orthogonal resources to different clusters [41]. After the interference cancellation, our solution can be directly applied to MIMO.

Let $\{X(t), Y(t), H(t)\}$ denote the location of the FlyBS at the time t. We assume that the altitude of the FlyBS is fixed at $H(t) = H$ as in many related works, see e.g., [15], [18], [33], [36]. Note that we adopt this assumption, as the height optimization does not change the principle of the proposed solution, however, it makes the mathematical derivations and explanations clearer and easier to follow. In our model, we consider mobile users and, thus, the coordinates of the users as well as of the FlyBS change over time. As commonly expected in the related works, we assume that the current positions of the users are known to the FlyBS (see, e.g., [18], [23], [42]). However, we assume a realistic case, where the positioning information is inaccurate and contains a positioning error. Thus, the known user's position is given as:

$$\begin{aligned} x^G_{i,j}(t) &= x^{exact,G}_{i,j}(t) + e^x_{i,j}(t), \\ y^G_{i,j}(t) &= y^{exact,G}_{i,j}(t) + e^y_{i,j}(t), \end{aligned} \tag{1}$$

where $x^{exact,G}_{i,j}(t)$ and $y^{exact,G}_{i,j}(t)$ are the exact x and y coordinates of the user $u^G_{i,j}$ at the time t, respectively, and $e^x_{i,j}(t)$ and $e^y_{i,j}(t)$ are the positioning errors in x and y coordinates at the time t, respectively. The FlyBS is able to determine its own position as this information is anyway mandatory for a common flying and navigation of the FlyBSs [33].

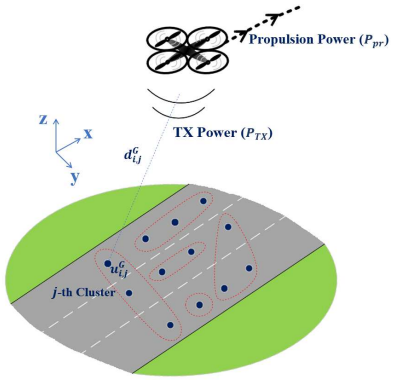

Fig. 1: System model with multiple mobile users (blue dots) deployed within coverage area of the FlyBS and grouped into clusters (red circles) for NOMA purposes.

In NOMA, the users are grouped into clusters such that all users in each cluster share the same frequency at the same time. Thus, the data transmission to the users in the same cluster imposes an interference (referred to as intra-cluster interference). However, there is no interference among different clusters. Let $\mathbb{G}$ denote the space of all possible functions that group the users into N_{cl} clusters such that the number of users in each cluster is larger than or equal to 1 and does not exceed N^{max}_{cu}. For $N_{cl} = 1$, the user in the given cluster is served at orthogonal resources by means of OMA. Furthermore, the maximum cluster size N^{max}_{cu} can be set to an arbitrary value and is practically related to an incurred complexity in SIC decoder. Thus, the maximum cluster size N^{max}_{cu} is typically much lower than the number of users ($N^{max}_{cu} \ll N_u$). Let $N_{cu,j}$ denote the size of the j-th cluster, hence, $N_u = \sum_{j=1}^{N_{cl}} N_{cu,j}$ with $N_{cu,j} \leq N^{max}_{cu}$. Each function $G \in \mathbb{G}$ is defined as a bijective mapping G: $\langle 1, N_u \rangle \rightarrow \langle 1, N_{cl} \rangle \times \langle 1, N^{max}_{cu} \rangle$ and the function G assigns the user u_n as the n_{cu}-th user in the n_{cl}-th cluster if $G(n) = (n_{cl}, n_{cu})$ for the given n. We refer to n_{cu} and n_{cl} as the index of the user in the cluster and the index of the cluster, respectively. Let $u^G_{1,j}, u^G_{2,j}, \ldots, u^G_{N_{cu,j},j}$ denote the users assigned by the clustering function G to the j-th cluster ($1 \leq j \leq N_{cl}$). Then, $\{x^G_{i,j}(t), y^G_{i,j}(t)\}$ represent the coordinates of the user $u^G_{i,j}$ at the time t.

Now we focus on SIC as a common interference cancellation method in NOMA. Suppose that in SIC, the user $u^G_{i,j}$ in the j-th cluster ($1 \leq i \leq N_{cu,j} - 1$) cancels the interfering signals from the user i' in the same cluster (i.e., $u^G_{i',j}$) for $i + 1 \leq i' \leq N_{cu}$ to extract its own signal. As a result of this, the achievable SINR $\gamma^G_{i,j}, (1 \leq i \leq N_{cu,j})$ for the user $u^G_{i,j}$ is expressed as:

$$\gamma^G_{i,j} = \frac{p^{G,R}_{i,j}(t)}{\sigma^2 + \sum_{l=1}^{i-1} p^{G,R}_{i,l,j}(t)}, (1 \leq i \leq N_{cu,j}), \tag{2}$$

where $p_{i,j}^{G,R}(t)$ represents the received signal power by the user $u_{i,j}^G$, $p_{i,l,j}^{G,R}(t)$ denotes the interference power imposed to the user $u_{i,j}^G$ by the signal transmitted to the user $u_{l,j}^G$ in the same cluster j, and σ^2 is the noise power. Furthermore, let $C_{i,j}^G(t)$ denotes the channel capacity of the user $u_{i,j}^G$. According to the Shannon–Hartley theorem, the channel capacity $C_{i,j}^G(t)$ is defined as:

$$C_{i,j}^G(t) = B \times \log_2(1 + \gamma_{i,j}^G), \tag{3}$$

where B is the bandwidth assigned to each user and each cluster. As the bandwidth allocation is not a critical aspect for NOMA (it is challenging rather for OMA, see [18], [42]), the channel bandwidth as well as the noise power are assumed to be equal for all clusters.

Now, let us define the model for the transmission power of the FlyBS. The total transmission power of the FlyBS at the time t_k for the user clustering function G is expressed as:

$$P_{TX}(X, Y, H, t_k, G) = \sum_{j=1}^{N_{cl}} \sum_{i=1}^{N_{cu,j}} p_{i,j}^{G,TX}(t_k), \tag{4}$$

where $p_{i,j}^{G,TX}(t_k)$ is the transmission power of the FlyBS to the $u_{i,j}^G$. We assume line-of-sight (LoS) communication, since obstacles appear rather exceptionally between the FlyBS at a relatively high altitude and the vehicles on a sub-urban/rural road, hence, the LoS link is dominant. We evaluate LoS probability in our scenario later in Section IV to validate this assumption. According to the Friis' transmission equation, $p_{i,j}^{G,TX}(t_k)$ is determined as:

$$p_{i,j}^{G,TX}(t_k) = \frac{(4\pi f)^\alpha}{D_{i,j}^{G,TX} D_{i,j}^{G,R} c^\alpha} p_{i,j}^{G,R}(t_k) {d_{i,j}^G}^\alpha(t_k), \\ (1 \le j \le N_{cl}, 1 \le i \le N_{cu,j}), \tag{5}$$

where α denotes the path-loss exponent, $D_{i,j}^{G,TX}$ is the gain of the FlyBS's antenna, $D_{i,j}^{G,R}$ is the gain of the user's antenna, $d_{i,j}^G(t_k)$ represents the distance between the FlyBS and the user $u_{i,j}^G$, f is the communication frequency, and $c = 3 \times 10^8$ m/s is the speed of light. The coefficient $\frac{(4\pi f)^\alpha}{D_{i,j}^{G,TX} D_{i,j}^{G,R} c^\alpha}$ is substituted by Q in the rest of the paper for clarity of the discussions.

Using (5), the total transmission power of the FlyBS is rewritten as:

$$P_{TX}(X, Y, H, t_k, G) = \sum_{j=1}^{N_{cl}} \sum_{i=1}^{N_{cu,j}} Q p_{i,j}^{G,R}(t_k) \times {d_{i,j}^G}^\alpha(t_k), \tag{6}$$

Furthermore, for the propulsion power, we refer to the model provided in [43] for rotary-wing FlyBSs. In particular, let $V_{FlyBS}(t_k)$ denote the FlyBS's speed at t_k. Then, the propulsion power consumption is expressed as a function of $V_{FlyBS}(t_k)$ as:

$$P_{pr}(t_k) = L_0\big(1 + \frac{3V_{FlyBS}^2(t_k)}{U_{\text{tip}}^2}\big) + \frac{\eta_0 \rho s_r A V_{FlyBS}^3(t_k)}{2} + \\ L_i\Big(\sqrt{1 + \frac{V_{FlyBS}^4(t_k)}{4v_{0,h}^4}} - \frac{V_{FlyBS}^2(t_k)}{2v_{0,h}^2}\Big)^{\frac{1}{2}}, \tag{7}$$

where L_0 and L_i are the blade profile and induced powers in hovering status, respectively, U_{tip} is the tip speed of the rotor blade, $v_{0,h}$ is the mean rotor induced velocity during hovering, η_0 is the fuselage drag ratio, ρ is the air density, s_r is the rotor solidity, and A is the rotor disc area. Interested readers can find more details about the model in [43].

B. Problem Formulation

Our goal is to find the position of the FlyBS jointly with the clustering of the users for NOMA and allocation of the transmission power within NOMA clusters to enhance the duration of the communication coverage (denoted by $T_{coverage}$). The communication coverage is defined as the maximum time step t_k at which i) the FlyBS's battery is yet not fully depleted, and ii) the required transmission power at every time step $t_s \le t_k$ remains below the maximum transmission power limit P_{TX}^{max}. The coverage duration depends on the transmission and propulsion power and, hence, on the FlyBS's position, the NOMA user clustering, and the transmission power allocation to the users in the NOMA clusters. Thus, to maximize $T_{coverage}$, we formulate the joint problem of the user clustering, the transmission power allocation, and the FlyBS's positioning while guaranteeing a minimum capacity for the users during the whole $T_{coverage}$ as follows:

$$\big[G_{opt}, [X_{opt}(t_k), Y_{opt}(t_k)], p_{i,j,opt}^{G_{opt},TX}\big] = \\ \underset{\left[G,[X(t_k),Y(t_k)],p_{i,j}^{G,TX}\right]}{\text{argmax}} \; T_{coverage}, \forall j \in \langle 1, N_{cl} \rangle, \forall i \in \langle 1, N_{cu,j} \rangle, \forall k, \\ s.t. \quad C_{i,j}^G(t_k) \ge C_{min}, \forall j \in \langle 1, N_{cl} \rangle, \forall i \in \langle 1, N_{cu,j} \rangle, \forall k, \quad (a) \\ P_{TX}(X, Y, H, t_k, G) \le P_{TX}^{max}, \forall k, \quad (b) \tag{8} \\ \sum_{t_k \le T_{coverage}} (P_{TX}(X, Y, H, t_k, G) + P_{pr}(t_k))(t_k - t_{k-1}) \le E_b. \quad (c) \\ \|\boldsymbol{V}_{FlyBS}(t_k)\| \le V_{FlyBS}^{max}, \quad \forall k, \quad (d) \\ \|\boldsymbol{a}_{FlyBS}(t_k)\| \le a_{FlyBS}^{max}, \quad \forall k. \quad (e)$$

where C_{min} is the minimum instantaneous capacity required by the users, $\|.\|$ denotes the norm of a vector, E_b is the initial available energy in the FlyBS's battery, V_{FlyBS}^{max} and a_{FlyBS}^{max} are the FlyBS's maximum speed and acceleration, respectively, and $\boldsymbol{V}_{FlyBS}(t_k) = \big(V_{FlyBS}^x(t_k), V_{FlyBS}^y(t_k)\big)$ and $\boldsymbol{a}_{FlyBS}(t_k) = \big(a_{FlyBS}^x(t_k), a_{FlyBS}^y(t_k)\big)$ are the FlyBS's velocity and acceleration vectors at the time t_k, respectively. The velocity and acceleration vectors are defined, respectively, as:

$$\boldsymbol{V}_{FlyBS}(t_k) = \frac{\big(X(t_k), Y(t_k)\big) - \big(X(t_{k-1}), Y(t_{k-1})\big)}{(t_k - t_{k-1})},$$
$$\boldsymbol{a}_{FlyBS}(t_k) = \frac{\boldsymbol{V}(t_k) - \boldsymbol{V}(t_{k-1})}{(t_k - t_{k-1})}. \quad (9)$$

The constraint (a) in (8) guarantees that every user receives at least the minimum required capacity C_{min} all the time. In line with [18], [24], [33], the minimum capacity is assumed to be the same for all the users. Such assumption corresponds to the case when the minimum required capacity is provided to all users for their essential and critical services, e.g., to a navigation information for the vehicles or to provide/collect control information related to driving. The constraint (b) ensures that the transmission power does not exceed the maximum transmission power limit. Furthermore, the constraint (c) guarantees that the FlyBS's total power consumption does not exceed the maximum capacity of the FlyBS's battery. Furthermore, the constraints (d) and (e) limit the FlyBS's movement in terms of the incurred speed and acceleration, respectively. We propose to extend $T_{coverage}$ via an efficient positioning of the FlyBS considering the transmission power and propulsion power consumption. However, despite the fact that the propulsion power is significantly larger than the transmission power in general, targeting the optimization of the propulsion power at every time step is not an efficient solution, as such approach is not deterministic. In particular, for the propulsion power to be optimal at every time step, it would be sufficient to determine only the FlyBS's speed corresponding to the minimum propulsion power. From the propulsion-power-minimization standpoint, any positioning of the FlyBS that incurs the minimum propulsion power can be regarded as the optimum position of the FlyBS. In such sense, there are potentially infinite candidate positions. However, since the location of the moving users in the next time step(s) is unknown in general, it would not be possible to tell which of the obtained candidate positions would yield the longest coverage duration. In fact, any of those candidate options can be the solution, because the minimum propulsion power is yielded by a movement to any of the candidate positions. Thus, a random selection of the FlyBS's position out of many candidates should be done at every time step.

In contrast, the minimization of the transmission power at every time step with the constrained propulsion power consumption is an efficient strategy. The rationality of this strategy is justified by stressing the fact that the suboptimal transmission power incurs even a larger transmission power (comparing to the transmission power minimization approach) and, thus, the transmission power reaches the maximum limit P_{TX}^{max} faster. Consequently, to extend the duration of the coverage duration in NOMA, the transmission power to users should be allocated so that the total transmission power remains below the maximum limit of P_{TX}^{max}. Such a solution can be provided based a minimization of the transmission power from the early time steps to avoid an increase in the distance between the FlyBS and the optimum position over time. If the distance between the FlyBS and the optimum position would become too large, reaching the optimum position at later time steps might not be possible due to the practical limitations on the FlyBS's speed and acceleration. In contrast, the positioning of the FlyBS to minimize the transmission power at every time step from the beginning keeps the FlyBS constantly close to the position minimizing the transmission power for NOMA, because the FlyBS's optimum positions from one time step to the next time step are typically close to each other.

Hence, we reformulate the problem of $T_{coverage}$ maximization in (8) to the problem of transmission power minimization with a constraint on the propulsion power consumption included so as to address the FlyBS's battery constraint (i.e., constraint (c) in (8)) as follows:

$$\begin{aligned}
&\big[G_{opt}, [X_{opt}(t_k), Y_{opt}(t_k)], p_{i,j,opt}^{G_{opt},TX}\big] = \\
&\underset{\left[G,[X(t_k),Y(t_k)],p_{i,j}^{G,TX}\right]}{\text{argmin}} \quad P_{TX}, \forall j \in \langle 1, N_{cl}\rangle, \forall i \in \langle 1, N_{cu,j}\rangle, \forall k, \\
&s.t. \quad C_{i,j}^{G}(t_k) \geq C_{min}, \forall j \in \langle 1, N_{cl}\rangle, \forall i \in \langle 1, N_{cu,j}\rangle, \forall k, \quad (a) \\
&\qquad P_{TX}(X, Y, H, t_k, G) \leq P_{TX}^{max}, \forall k, \quad (b) \\
&\qquad P_{pr}(t_k) \leq P_{pr,th}(t_k), \quad \forall k, \quad (c) \\
&\qquad \|\boldsymbol{V}_{FlyBS}(t_k)\| \leq V_{FlyBS}^{max}, \quad \forall k, \quad (d) \\
&\qquad \|\boldsymbol{a}_{FlyBS}(t_k)\| \leq a_{FlyBS}^{max}, \quad \forall k, \quad (e)
\end{aligned} \quad (10)$$

where $P_{pr,th}(t_k)$ in the constraint (c) is the upper bound for the propulsion power consumption. The parameter $P_{pr,th}$ establishes a trade-off between the transmission and propulsion power consumption, so that choosing a lower value of $P_{pr,th}$ leads to a reduction in the propulsion power (hence, to a slower depletion of the FlyBS's battery) while it causes an increase in the transmission power, because the FlyBS would have a limited range of speeds during the flight to reach the position minimizing the transmission power. Furthermore, in an extreme case with $P_{pr,th}$ set to the value corresponding to the minimum propulsion power, the problem (10) corresponds to the case when both the propulsion and transmission powers are minimized. In the subsection III.C, we elaborate a setting of $P_{pr,th}$ to tackle the constraint on the capacity of the FlyBS's battery (i.e., constraint (c) in (8)).

III. Proposed optimal clustering of users for NOMA and positioning of FlyBS

In this section, we present a novel solution to the problem defined in (10) by finding the optimal clustering function G_{opt} as well as the optimal FlyBS's positions over time.

Solving the problem of user clustering for NOMA jointly with the FlyBS's positioning in (10) is challenging, as the constraints (c), (d), and (e) define a non-convex region for the FlyBS's position. Furthermore, the set of the clustering options is potentially of a very large size (exponential with the number of users and the NOMA cluster sizes). In addition, the discrete nature of the set of the clustering options for NOMA makes the optimization problem intractable. To deal with these

challenges, we first target the positioning of the FlyBS for arbitrary clustering function G. We solve the problem of positioning by first relaxing the constraints (c), (d), and (e) in (10) (as explained in subsection III.A), and then deriving the solution to the unrelaxed problem (as presented in subsection III.B). Next, we discuss the setting of the parameter $P_{pr,th}$ for the proposed positioning of the FlyBS in subsection III.C. Last, in subsection III.D we discuss how to find the optimal clustering in (10) via a derivation of necessary conditions for the clustering to be optimal. Such necessary conditions help to reduce significantly the size of the set of the clustering options. Now, to solve the problem of the FlyBS's positioning for the clustering function G we lift the constraints (c), (d), and (e), and solve the relaxed problem in terms of the clustering function G. Then, the derived solution is adjusted to fulfill all constraints.

A. Transmission power minimization and FlyBS positioning

In this subsection we focus on the transmission power optimization and the FlyBS's positioning for any NOMA user clustering G, and we derive the FlyBS's position and the transmission power as functions of the clustering. The relaxed problem of the FlyBS's positioning is defined as:

$$\begin{aligned}\left[[X_{opt}(G,t_k),Y_{opt}(G,t_k)],p^{G,TX}_{i,j,opt}\right] = \\ \underset{\left[[X(G,t_k),Y(G,t_k)],p^{G,TX}_{i,j}\right]}{\operatorname{argmin}} P_{TX}, \\ \forall j \in \langle 1, N_{cl}\rangle, \forall i \in \langle 1, N_{cu,j}\rangle, \forall k, \\ s.t. \quad C^G_{i,j}(t_k) \geq C_{min}, \forall j \in \langle 1, N_{cl}\rangle, \forall i \in \langle 1, N^{max}_{cu}\rangle, \forall k.\end{aligned} \tag{11}$$

In the following, we solve (11) via a determination of the FlyBS's positioning and the user's power allocation for the NOMA user clustering G. To this end, from the constraint in (11) and using (3), it is inferred that $\gamma_{min} \leq \gamma^G_{i,j}$, where $\gamma_{min} = (2^{C_{min}/B} - 1)$ is a positive constant. To find the conditions to reach the minimum transmission power we rewrite $\gamma_{min} \leq \gamma^G_{i,j}$ using (2) and (5) as follows

$$\begin{aligned}\gamma_{min}(\sigma^2 + \frac{\sum_{l=1}^{i-1} p^{G,TX}_{l,j}(t_k)}{Q{d^G_{i,j}}^{\alpha}(t_k)}) \leq \frac{p^{G,TX}_{i,j}(t_k)}{Q{d^G_{i,j}}^{\alpha}(t_k)}, \\ (j \in \langle 1, N_{cl}\rangle, i \in \langle 1, N_{cu,j}\rangle).\end{aligned} \tag{12}$$

After several simple math operations, (12) is transformed to:

$$\begin{aligned}\gamma_{min}\sum_{l=1}^{i-1} p^{G,TX}_{l,j}(t_k) + \gamma_{min}\sigma^2 Q{d^G_{i,j}}^{\alpha}(t_k) \leq p^{G,TX}_{i,j}(t_k), \\ (j \in \langle 1, N_{cl}\rangle, i \in \langle 1, N_{cu,j}\rangle).\end{aligned} \tag{13}$$

Therefore, by writing down (13) for every $j \in \langle 1, N_{cl}\rangle$ and $i \in \langle 1, N_{cu,j}\rangle$, we get:

$$\begin{aligned}\sum_{j=1}^{N_{cl}}\sum_{i=1}^{N_{cu,j}} p^{G,TX}_{i,j}(t_k) \geq \\ \gamma_{min}Q\sigma^2\sum_{j=1}^{N_{cl}}\sum_{i=1}^{N_{cu,j}}\left((1+\gamma_{min})^{N_{cu,j}-i}\right){d^G_{i,j}}^{\alpha}(t_k).\end{aligned} \tag{14}$$

The minimum in (14) is achieved when the equality in (13) holds for $1 \leq j \leq N_{cl}$ and $1 \leq i \leq N_{cu,j}$. Hence, we derive $P_{TX}(X, Y, H, t_k, G)$ as:

$$\begin{aligned}P_{TX}(X, Y, H, t_k, G) = \\ \gamma_{min}Q\sigma^2\sum_{j=1}^{N_{cl}}\sum_{i=1}^{N_{cu,j}}\left((1+\gamma_{min})^{N_{cu,j}-i}\right){d^G_{i,j}}^{\alpha}(t_k)\end{aligned} \tag{15}$$

To find the FlyBS's optimum position (X^G_{opt} and Y^G_{opt}) and to minimize the transmission power in (15), we exploit Downhill Simplex Algorithm (also known as Nelder-Mead Algorithm). The solution is based on a direct search in two-dimensions and a function comparison using simplex, which is a polytope of $m+1$ vertices among m dimensions. The simplex is updated based on the values obtained from expansion, contraction, and shrinkage operations on the vertex at which the function reaches the largest value, and the centroid of the remaining vertices. Now, we explain the details of the Nelder-Mead Algorithm in our problem (see Algorithm 1). The simplex finds the optimal position of the FlyBS at every time step t_k. For our setup, there is a 2-dimensional point in simplex, with the first and second dimensions corresponding to $X(t_k)$ and $Y(t_k)$, respectively. The values for the three vertices of the simplex (denoted as S_1, S_2, S_3) are determined as follows. First, an initial value for S_3 is guessed (in other

Algorithm 1 Find optimal position of the FlyBS for arbitrary clustering G

$\lambda(A)$: standard deviation of elements in set A, λ_0: standard deviation threshold for termination
$f(S_i)$: Transmission power at t_k evaluated at S_i (i.e., $P_{TX}(S_{i,1}, S_{i,2}, H, t_k, G)$).
Sort and rearrange the points as $f(S_1) \leq f(S_2) \leq f(S_3)$.

while $\lambda(f(S_1), f(S_2), f(S_3))) > \lambda_0$ **do**
  compute $S_0 = \text{centroid}\{S_1, S_2\}$
  if $f(S_1) \leq f(S_r) \leq f(S_2)$ **then** $S_3 \leftarrow S_r$
  else compute $S_e = S_0 + \beta(S_r - S_0)$
  end if
  if $f(S_e) \leq f(S_r)$ **then** $S_3 \leftarrow S_e$, and go to step 13
  else $S_3 \leftarrow S_r$, and go to step 13
  end if
  compute $S_c = S_0 + \nu(S_3 - S_0)$.
  if $f(S_c) \leq f(S_3)$ **then** $S_3 \leftarrow S_c$, and go to step 13
  else compute $S_i = S_1 + \delta(S_i - S_1)$ for $1 \leq i \leq 3$, and go to step 13
  end if
  Sort points so that $f(S_1) \leq f(S_2) \leq f(S_3)$.
end while
From (15) calculate transmission power at S_3

Output: $S_3 = (X^G_{opt}(t_k), Y^G_{opt}(t_k)) = \text{argmin}_{\{X(t_k),Y(t_k)\}} P_{TX}$, and $P^{min}_{TX}(G, t_k), \forall k$

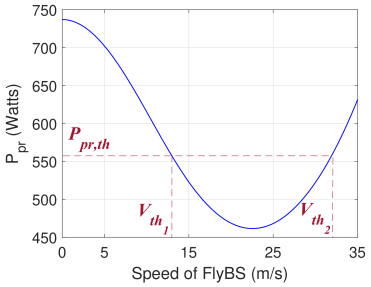

Fig. 2: FlyBS's propulsion power consumption vs. speed. Threshold $P_{pr,th}$ limits the propulsion power consumption and specifies the allowed flight speed range of $[V_{th_1}, V_{th_2}]$.

words, an initial position of the FlyBS at t_k is guessed). We initialize S_3 by the FlyBS's position at the previous time step t_{k-1}. Then, the values for S_1 and S_2 are found by changing the value at one dimension of S_3. In particular, S_3 is initiated with $S_3 = \big(X(t_{k-1}), Y(t_{k-1})\big)$ and, then, S_1 and S_2 are derived as:

$$S_i = \begin{cases} S_3 + \kappa_i S_{3,i} e_i & S_{3,i} \neq 0, \\ S_3 + \epsilon_i e_i & \text{otherwise}, \end{cases} \tag{16}$$

for $1 \leq i \leq 2$, where $S_{3,r}$ denotes the r-th element of S_3, and e_i is the 2-dimensional unit vector with zero elements at all dimensions except the i-th dimension. Furthermore, ϵ_i and κ_i are real coefficients that adjust the convergence of the algorithm. Therefore, the initial simplex includes three different instances of the FlyBS's positions. The algorithm keeps updating the values of the vertices based on expansion, contraction, and shrinkage operations (demonstrated in the lines 4, 9, and 11 in Algorithm 1, respectively) until the standard deviation of the corresponding values of $P_{TX}(X, Y, H, t_k)$ at the simplex's vertices fall below a given threshold.

B. FlyBS's positioning with constrained propulsion power, speed, and acceleration

In the previous subsection, the solution to the FlyBS's position $(X^G_{opt}(t_k), Y^G_{opt}(t_k))$ is derived (in Algorithm 1) to minimize the transmission power for the relaxed optimization problem (11). However, the calculated optimal position $(X^G_{opt}(t_k), Y^G_{opt}(t_k))$ might not be reached at some time steps due to the constraints on the FlyBS's propulsion power, speed, and acceleration, i.e., $P_{pr,th}$, V^{max}_{FlyBS}, a^{max}_{FlyBS}, respectively, in (10). Thus, in this subsection, we address the problem of FlyBS's positioning considering the constraints for the propulsion power, acceleration, and speed. In case the required speed or acceleration to move the FlyBS to the optimal position $(X^G_{opt}(t_k), Y^G_{opt}(t_k))$ (derived from Algorithm 1) exceeds the corresponding limits on the speed or the acceleration (i.e., V^{max}_{FlyBS} and a^{max}_{FlyBS}, respectively), or causes the propulsion power larger than $P_{pr,th}$, the FlyBS moves only to the point that is the closest to the optimal position and, at the same time, can be reached with the speed and the acceleration within their allowed ranges. To derive the point to which the FlyBS should move, let $\big(X^G_{cto}(t_k), Y^G_{cto}(t_k)\big)$ denote the closest point to the optimal position $\big(X^G_{opt}(t_k), Y^G_{opt}(t_k)\big)$ such that the movement from the FlyBS's position at t_{k-1} to $\big(X^G_{cto}(t_k), Y^G_{cto}(t_k)\big)$ does not incur the propulsion power larger than the threshold $P_{pr,th}$ and also the speed and the acceleration are not larger than V^{max}_{FlyBS} and a^{max}_{FlyBS}, respectively. Hence, the problem of FlyBS's positioning is formulated as follows:

$$\begin{aligned} &[\boldsymbol{V}_{FlyBS}(t_k), \boldsymbol{a}_{FlyBS}(t_k), (X^G_{cto}(t_k), Y^G_{cto}(t_k))] = \\ &\underset{\boldsymbol{V}_{FlyBS}(t_k), \boldsymbol{a}_{FlyBS}(t_k)}{\text{argmin}} \; ||(X(t_k), Y(t_k) - (X^G_{opt}(t_k), Y^G_{opt}(t_k))|| \\ &s.t. \quad P_{pr}(t_k) \leq P_{pr,th}(t_k), \quad \forall k \quad (a) \\ &||\boldsymbol{V}_{FlyBS}(t_k)|| \leq V^{max}_{FlyBS}, \quad \forall k \quad (b) \\ &||\boldsymbol{a}_{FlyBS}(t_k)|| \leq a^{max}_{FlyBS}. \forall k \quad (c) \end{aligned} \tag{17}$$

Fig. 2 shows an example of $P_{pr,th}$ and the corresponding range of the FlyBS's speeds $[V_{th_1}, V_{th_2}]$ for which $P_{pr} \leq P_{pr,th}$ for the propulsion power model in (7). The FlyBS's speed should not exceed the allowed range of $[V_{th_1}, \min\{V_{th_2}, V^{max}_{FlyBS}\}]$. Hence, the optimization problem (17) is rewritten by merging the constraints (a) and (b) as a modified constraint on the speed as follows:

$$\begin{aligned} &\big[\boldsymbol{V}_{FlyBS}(t_k), \boldsymbol{a}_{FlyBS}(t_k), \big(X^G_{cto}(t_k), Y^G_{cto}(t_k)\big)\big] = \\ &\underset{\boldsymbol{V}_{FlyBS}(t_k), \boldsymbol{a}_{FlyBS}(t_k)}{\text{argmin}} \; \big\|\big(X(t_k), Y(t_k)\big) - \big(X^G_{opt}(t_k), Y^G_{opt}(t_k)\big)\big\| \\ &s.t. \quad V_{th_1} \leq \|\boldsymbol{V}_{FlyBS}(t_k)\| \leq \min\{V^{max}_{FlyBS}, V_{th_2}\}, \quad (a) \\ &\|\boldsymbol{a}_{FlyBS}(t_k)\| \leq a^{max}_{FlyBS}. \quad (b) \end{aligned} \tag{18}$$

To solve (18), we assume a constant acceleration over very small time steps t_k of the FlyBS's movement. Hence, $\big(X(t_k), Y(t_k)\big)$ is calculated using the motion equation for constant acceleration:

$$\begin{aligned} X(t_k) &= \frac{1}{2}\big(a^x_{FlyBS}(t_k)\big) \times (t_k - t_{k-1})^2 + \\ &\big(V^x_{FlyBS}(t_{k-1})\big) \times (t_k - t_{k-1}) + X(t_{k-1}), \\ Y(t_k) &= \frac{1}{2}\big(a^y_{FlyBS}(t_k)\big) \times (t_k - t_{k-1})^2 + \\ &\big(V^y_{FlyBS}(t_{k-1})\big) \times (t_k - t_{k-1}) + Y(t_{k-1}). \end{aligned} \tag{19}$$

Before presenting the solution to (18), we further elaborate the constraints in (18). Using (19), the constraint (a) in (18) is rewritten as:

$$\begin{aligned} &V_{th_1} \leq \\ &\Big(\big(a^x_{FlyBS}(t_k) + \frac{V^x_{FlyBS}(t_{k-1})}{(t_k - t_{k-1})}\big)^2 + \big(a^y_{FlyBS}(t_k) + \frac{V^y_{FlyBS}(t_{k-1})}{(t_k - t_{k-1})}\big)^2\Big)^{\frac{1}{2}} \\ &\leq \min\{V^{max}_{FlyBS}, V_{th_2}\}. \end{aligned} \tag{20}$$

Furthermore, using the identity $\|\boldsymbol{a}_{FlyBS}(t_k)\| = \big({a^x_{FlyBS}}^2(t_k) + {a^y_{FlyBS}}^2(t_k)\big)^{\frac{1}{2}}$, the constraint (b) in (18) is rewritten in terms of a^x_{FlyBS} and a^y_{FlyBS} as:

$$\big({a^x_{FlyBS}}^2(t_k) + {a^y_{FlyBS}}^2(t_k)\big)^{\frac{1}{2}} \leq a^{max}_{FlyBS}. \tag{21}$$

According to the inequalities in (20), $(a^x_{FlyBS}, a^y_{FlyBS})$ lies inside a ring centered at $\big(-\frac{V^x_{FlyBS}(t_{k-1})}{(t_k-t_{k-1})}, -\frac{V^y_{FlyBS}(t_{k-1})}{(t_k-t_{k-1})}\big)$ with inner and outer radii corresponding to the minimum and maximum limits of $\frac{V_{th_1}}{(t_k-t_{k-1})}$ and $\frac{\min\{V^{max}_{FlyBS}, V_{th_2}\}}{(t_k-t_{k-1})}$, respectively. Fig. 3 shows the region defined by (20) in the $a^x_{FlyBS}-a^y_{FlyBS}$ plane (blue ring). Furthermore, the constraint in (21) defines the inner part of the circle centered at $(0,0)$ with a radius of the FlyBS's acceleration limit a^{max}_{FlyBS} (green circle in Fig. 3). Thus, by incorporating the two constraints in (20) and (21), the problem in (18) is understood as the minimization of $\|\big(X(t_k), Y(t_k)\big) - \big(X^G_{opt}(t_k), Y^G_{opt}(t_k)\big)\|$ over the region enclosed by four curves AB, BC, CD, and DA as shown in Fig. 3.

To proceed with the solution, we use (19) to express the objective function in (18) in terms of $a^x_{FlyBS}(t_k)$ and $a^y_{FlyBS}(t_k)$ as follows:

$$\|\big(X(t_k), Y(t_k)\big) - \big(X^G_{opt}(t_k), Y^G_{opt}(t_k)\big)\| = m\Big(\big(a^x_{FlyBS}(t_k)-\rho_0\big)^2 + \big(a^y_{FlyBS}(t_k)-\sigma_0\big)^2\Big)^{\frac{1}{2}}, \quad (22)$$

$$m = \frac{(t_k - t_{k-1})^2}{2},$$

$$\rho_0 = \frac{\big(V^x_{FlyBS}(t_{k-1})\big)\times(t_k-t_{k-1}) + X(t_{k-1}) - X_{opt}(t_k)}{m},$$

$$\sigma_0 = \frac{\big(V^y_{FlyBS}(t_{k-1})\big)\times(t_k-t_{k-1}) + Y(t_{k-1}) - Y_{opt}(t_k)}{m}.$$

According to (22), the minimum value of $\|\big(X(t_k), Y(t_k)\big) - \big(X^G_{opt}(t_k), Y^G_{opt}(t_k)\big)\|$ is achieved by the closest point $(a^x_{FlyBS}(t_k), a^y_{FlyBS}(t_k))$ to (ρ_0, σ_0). Therefore, the solution to (18) is derived by finding the closest point in the region enclosed by $ABCD$ to (ρ_0, σ_0). To this end, we first find the point on each of the curves AB, BC, CD, and DA that is the closest to (ρ_0, σ_0). Since all the curves AB, BC, CD, and DA are on circles, the closest point to (ρ_0, σ_0) for each curve can be found by finding the intersection of that curve and the line connecting (ρ_0, σ_0) to the center of the circle that the curve lies on. In case that the intersection point lies beyond the curve's endpoints, one of the endpoints yields the minimum distance to (ρ_0, σ_0). The objective function in (22) is evaluated at all four closest candidate points to find the optimal $\big(a^x_{FlyBS}(t_k), a^y_{FlyBS}(t_k)\big)$. Then, we calculate $\big(X(t_k), Y(t_k)\big)$ from (19), which is the optimal solution to (18) (i.e., $\big(X^G_{cto}(t_k), Y^G_{cto}(t_k)\big)$).

C. Determination of $P_{pr,th}$

In this subsection we discuss selection of proper values for the propulsion power limit $P_{pr,th}$ at every time step. Although the proposed solution to the FlyBS's positioning in subsection III.B is valid for any value of $P_{pr,th}$, a fixed $P_{pr,th}$ in (10) may not be very efficient in extending the coverage duration, as the impact of the transmission and propulsion power consumption changes over time due the actual values

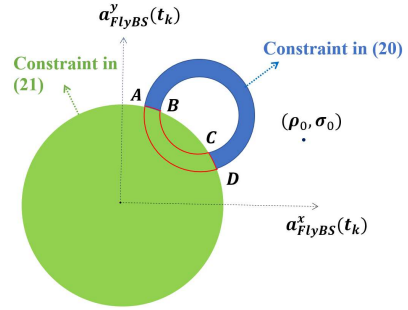

Fig. 3: Regions in $a^x_{FlyBS} - a^y_{FlyBS}$ plane corresponding to the constraints (20) and (21)

of the transmission power and the remaining energy of the FlyBS's battery. Hence, we introduce a varying $P_{pr,th}$ over time. At the beginning, because of a large amount of the remaining energy in the battery, we set $P_{pr,th}$ to the FlyBS's propulsion power consumed at the FlyBS's maximum speed. Then, at every time step t_k ($k > 1$), we estimate the shortest time that it takes for the transmission power to reach the maximum limit of P^{max}_{TX}. More specifically, the estimated time to reach P^{max}_{TX} is denoted by T^{max}_{TX} and calculated as $T^{max}_{TX} = \frac{P^{max}_{TX} - P_{TX}(t_k)}{R^{max}_{TX}(t_k)}$, where $R^{max}_{TX}(t_k)$ is the maximum slope of the increase that can occur between t_k and t_{k+1}. Note that, an accurate evaluation of $R^{max}_{TX}(t_k)$ is not possible in general, as $R^{max}_{TX}(t_k)$ depends on the future location of the users at t_{k+1}. Nevertheless, the values for the slope of the increase in the FlyBS's transmission power in the previous time steps is still a sufficient indicator to estimate $R^{max}_{TX}(t_k)$. Thus, we choose $R^{max}_{TX}(t_k)$ to be the maximum rate of the increase in the transmission power that has actually occurred between two consecutive time steps during the past Δ_t time steps:

$$R^{max}_{TX}(t_k) = \max_s \frac{(P_{TX}(t_s) - P_{TX}(t_{s-1}))}{(t_s - t_{s-1})}, \quad k - \Delta_t + 1 \le s \le k. \quad (23)$$

Choosing lower values for Δ_t results in a less accurate estimation of R^{max}_{TX}, but also an adoption of too high values for Δ_t may result in an inaccurate estimation of R^{max}_{TX}. This is because, the transmission power may have an unusual increase due to a (unusual) movement of the users at some time step t_p and, hence, such an unusual increase in the transmission power should not affect the evaluation of R^{max}_{TX} at every time step t_k with $p < k$. Next, we use the calculated T^{max}_{TX} at t_k to determine $P_{pr,th}$ at t_k. Since the transmission power is estimated to reach the maximum limit of P^{max}_{TX} in the time T^{max}_{TX}, the time when the battery depletes completely should not occur within the next T^{max}_{TX} seconds. Thus, we choose to fulfill the following condition:

$$\frac{E_b(t_0) - E_b(t_k)}{P_{pr,th}(t_k) + P_{TX}(t_k)} \ge T^{max}_{TX}, \quad (24)$$

or equivalently, $P_{pr,th}(t_k) \leq \frac{E_b(t_0)-E_b(t_k)}{T_{TX}^{max}} - P_{TX}(t_k)$. Hence, we set the value of $P_{pr,th}(t_k)$ to $\frac{E_b(t_0)-E_b(t_k)}{T_{TX}^{max}} - P_{TX}(t_k)$ to tackle the constraint on the FlyBS's battery (i.e., constraint (c) in (8)).

D. Clustering of users for NOMA

In the previous subsection, $X_{cto}^G(t_k)$ and $Y_{cto}^G(t_k)$ are derived as functions of the selected clustering G. Hence, evaluating the transmission power $P_{TX}^{min}(G, t_k)$ at the optimal position is enough to find the optimum clustering G_{opt} to solve the optimization problem in (10).

The naive approach to find the optimum clustering is to evaluate $P_{TX}(X_{cto}^G, Y_{cto}^G, t_k)$ for every possible clustering (i.e., to perform an exhaustive search) and, then, to select the clustering with the smallest corresponding $P_{TX}(X_{cto}^G, Y_{cto}^G, t_k)$. However, the number of all possible clustering options can be very large (there are $\prod_{i=1}^{N_{cl}} \binom{N_u - \sum_{j=0}^{i-1} N_{cu,j}}{N_{cu,i}}$ different clustering options for every set of the cluster sizes $\{N_{cu,1}, ..., N_{cu,cl}\}$). Hence, the exhaustive search is not a practical solution for real word applications. In order to address this issue, we reduce the search space size of the problem by characterizing the optimal clustering function. To this end, we first derive the optimal clustering function G_{opt} via Theorem 1 that provides a necessary condition for G_{opt}.

Theorem 1. *Suppose that before clustering of the users, the x-coordinates of the users are sorted as $X_{sorted} = \{x_{l_1}, \ldots, x_{l_{N_u}}\}$, such that $x_{l_1} < ... < x_{l_{N_u}}$. Also, let N_{cu}^{max} and N_k denote the size of the largest cluster and the number of clusters with a size of k, respectively. Then, for the clustering function that minimizes $P_{TX}(X_{cto}^G, Y_{cto}^G, t_k)$ for a given N_{cu}^{max}, the first users in each cluster with a size of N_{cu}^{max} should be $N_{N_{cu}^{max}}$ consecutive users in the sorted sequence X_{sorted}. Similarly, the set including the $(N_{cu,j} - i + 1)$-th user of the j-th cluster ($1 \leq i \leq N_{cu}^{max}$, $j \in \langle 1, N_{cl} \rangle$) should be $\sum_{s=1}^{N_{cu}^{max}-i+1} N_{i+s-1}$ consecutive users in the sorted sequence X_{sorted} after eliminating the selected $(N_{cu,j} - r + 1)$-th users of the j-th cluster ($1 \leq r \leq N_{cu}^{max} - i$).*

Proof. See Appendix A.

In addition to Theorem 1, we also define the following proposition that helps us to further reduce the complexity of the user clustering.

Proposition 1. *All permutations of the users $u_{i,j}^G$ with the same value for $(N_{cu,j} - i)$ along all clusters result in different groupings with the same corresponding $P_{TX}(X, Y, H, t_k, G)$.*

Proof. Suppose that for the grouping function G_1, the users $u_{i,j}^{G_1}$ and $u_{i',j'}^{G_1}$ satisfy $N_{cu,j} - i = N_{cu,j'} - i'$. Also, suppose that the grouping function G_2 is derived by exchanging $u_{i,j}^{G_1}$ and $u_{i',j'}^{G_1}$ between the clusters j and j' (i.e., $u_{i',j'}^{G_2} = u_{i,j}^{G_1}$). Since the FlyBS's distance to the users does not change by modifying the grouping (i.e., $d_{i',j'}^{G_2} = d_{i,j}^{G_1}$), from (15), it is concluded that $P_{TX}(X, Y, H, t_k, G_1) = P_{TX}(X, Y, H, t_k, G_2)$. □

Theorem 1 and Proposition 1 together allow to choose the optimal clustering function. In particular, we collect all different clustering options that meet the necessary conditions in Theorem 1, while Proposition 1 enables to avoid collecting the clustering options that lead to the same transmission power. We first find all possible solutions to $\sum_{r=1}^{N_{cl}} N_{cu,r} = N_u$, where $1 \leq N_{cu,r} \leq N_{cu}^{max}$ as follows. We start with checking the necessary conditions for the equation $\sum_{r=1}^{N_{cl}} N_{cu,r} = N_u$ to obtain the solutions satisfying $1 \leq N_{cu,r} \leq N_{cu}^{max}$. By evaluating $\sum_{r=1}^{N_{cl}} N_{cu,r}$ at the upper and lower bounds in $1 \leq N_{cu,r} \leq N_{cu}^{max}$, we get the necessary conditions $N_{cl} \times N_{cu}^{max} \geq N_u$ and $N_{cl} \leq N_u$, respectively. Next, we consider all possible values 1, …, N_{cu}^{max} for $N_{cu,1}$ and, for each of those values, we rewrite our main equation as $\sum_{r=2}^{N_{cl}} N_{cu,r} = N_u - N_{cu,1}$. For the updated equation (with $N_{cl} - 1$ variables) we check again the necessary conditions for an existence of solution and eliminate those equations that do not fulfill the conditions. Then we consider all N_{cu}^{max} possible values 1, …, N_{cu}^{max} for $N_{cu,2}$ and update the equation similarly as in the previous step. We repeat the same process and collect all solutions for $\{N_{cu,1}, \ldots, N_{cu,cl}\}$ until the necessary conditions are not held anymore. Then, for every set of the solutions (i.e., sizes of the clusters), we find and collect all clustering candidate options derived from Theorem 1. More specifically, we sort the x-coordinates of the users as $x_{l_1} < ... < x_{l_{N_u}}$, and choose $N_{N_{cu}^{max}}$ consecutive elements from the sorted sequence. Therefore, instead of considering all $\binom{N_u}{N_{N_{cu}^{max}}}$ possible subsets, we only have $(N_u - N_{N_{cu}^{max}} + 1)$ options. According to Proposition 1, for each selected sequence, all permutations result in the same corresponding transmission power. Thus, we only keep one of many permutations for each sequence. According to Theorem 1 a similar process to the previous step is considered, i.e., the i-th users of all clusters with a size of N_{cu}^{max} are chosen together with the $(i-1)$-th users of the clusters with a size of $N_{cu}^{max} - 1$ together with the $(i-2)$-th users of the clusters with a size of $N_{cu}^{max} - 2$ and so on. This procedure is continued until all users are assigned to clusters. We repeat the same process for all different sizes of clusters, and we collect all the clustering candidates. Then, the transmission power corresponding to every clustering is derived via Algorithm 1. Then, the clustering that yields the minimum transmission power is chosen and applied for NOMA. For every set of the clusters size $\{N_{cu,1}, ..., N_{cu,cl}\}$, the search space size in the proposed clustering is $\prod_{i=1}^{N_{cu}^{max}} (N_u - \sum_{j=0}^{i-1} N_{N_{cu}^{max}-j} + 1)$. The total complexity of the proposed solution is then calculated by summing the complexity over all derived sets of the clusters size $\{N_{cu,1}, ..., N_{cu,cl}\}$. For the exhaustive search, there are $\prod_{i=1}^{N_{cl}} \binom{N_u - \sum_{j=1}^{i-1} N_{cu,j}}{N_{cu,i}}$ different clustering options for every set of the cluster size $\{N_{cu,1}, ..., N_{cu,cl}\}$. Thus, the number of options for the exhaustive search becomes extremely large for realistic values of N_u. For example, for $N_{cu}^{max} = 2$ and $N_{cl} = 7$, the search space for the exhaustive search is about

17.2 million options, whereas the proposed solution leads to only 8 options to be checked. This illustrates significant lowering of the complexity by the proposed solution compared to the exhaustive search.

E. Discussion of optimality of the proposed solution

There is no general way to find the optimal solution to the non-convex problem in (10). Hence, we choose the exhaustive search to show the optimality of the proposed solution. Note that, since there are continuous-valued variables in (10), even performing the exhaustive search cannot achieve the exact optimum. Nevertheless, using the exhaustive search allows us to evaluate the maximum possible gap between the derived transmission power from the proposed solution and the optimal transmission power. We do this evaluation via a combination of a discretized exhaustive search and an analysis of the error caused by the discretization. For the discretized exhaustive search, at every time step, we check all possible user clustering options of the users for NOMA, and we find the minimum corresponding transmission power for each clustering option by finding the optimal values of the acceleration and the velocity of the FlyBS. In particular, at every time step t_k, we consider all possible vectors of the FlyBS's acceleration $\boldsymbol{a}_{FlyBS}(t_k) = (a^x_{FlyBS}(t_k), a^y_{FlyBS}(t_k))$ that fulfill the constraint (e) in (10). For the discretized interval of $[-a^{max}_{FlyBS}, a^{max}_{FlyBS}]$ we consider the values starting with $-a^{max}_{FlyBS}$ and increasing with a step size of ξ. Then, for each selected value of, e.g., φ for $a^x_{FlyBS}(t_k)$ from the discretized interval, the value of $a^y_{FlyBS}(t_k)$ should be within the range of $[-\sqrt{{a^{max}_{FlyBS}}^2 - \varphi^2}, \sqrt{{a^{max}_{FlyBS}}^2 - \varphi^2}]$ to meet the constraint (e) in (10). A similar discretization for the interval $[-\sqrt{{a^{max}_{FlyBS}}^2 - \varphi^2}, \sqrt{{a^{max}_{FlyBS}}^2 - \varphi^2}]$ with a step size of ξ is done to find all possible numerical combinations for the acceleration vector. Then, for each possible acceleration vector, we calculate the vector of velocity from (9). For those velocity vectors fulfilling the constraints (c) and (d) in (10), we calculate the FlyBS's position from (19). Next, at the calculated position of the FlyBS, the corresponding transmission power is derived. We repeat this procedure for values of the acceleration vector and for every clustering option. In the following Lemma 2, we define the upper bound for the discretization error for every tested pair $(a^x_{FlyBS}(t_k), a^y_{FlyBS}(t_k)) = (\varphi, \tau)$ over the discretized sets.

Lemma 2. *The maximum error due to discretization of the interval for the exhaustive search for the acceleration values for $a^x_{FlyBS} \in (\varphi, \varphi + \xi)$ and $a^y_{FlyBS} \in (\tau, \tau + \xi)$ is:*

$$|\zeta| \leq \xi^2 |M_{xx}| + 2\xi^2 |M_{xy}| + \xi^2 |M_{yy}| = \xi^2 (|M_{xx}| + 2|M_{xy}| + |M_{yy}|), \tag{25}$$

where M_{xx}, M_{xy}, and M_{yy} are the supremum of $\frac{\partial^2 P_{TX}}{\partial {a^x_{FlyBS}}^2}$, $\frac{\partial^2 P_{TX}}{\partial a^x_{FlyBS} \partial a^y_{FlyBS}}$, and $\frac{\partial^2 P_{TX}}{\partial {a^y_{FlyBS}}^2}$, respectively, over the interval of $a^x_{FlyBS} \in [\varphi, \varphi + \xi]$ and $a^y_{FlyBS} \in [\tau, \tau + \xi]$.

Proof. See appendix B.

Using the error's upper bound in (25), we evaluate the smallest potential value for the transmission power that can occur for $a^x_{FlyBS} \in (\varphi, \varphi + \xi)$ and $a^y_{FlyBS} \in (\tau, \tau + \xi)$. By collecting the calculated lower bound for the transmission power for every candidate clustering option, we find the lowest bound for the transmission power among all clustering options. The lower bound is evaluated for the transmission power in the our scenario in Section IV to confirm that the proposed solution is very close to the optimum.

F. Feasibility of FlyBS positioning and user NOMA clustering and extension to multiple FlyBSs

No solution to the problem defined in (8) exists if the required transmission power to guarantee C_{min} to all users exceeds the maximum transmission power limit of P^{max}_{TX}. Thus, a necessary and sufficient condition for an existence of a solution to (8) is derived using (15) as:

$$Q\sigma^2 (2^{\frac{C_{min}}{B}} - 1) \sum_{j=1}^{N_{cl}} \sum_{i=1}^{N_{cu,j}} \left(2^{\frac{C_{min}}{B} \times (N_{cu,j} - i)}\right) {d^G_{i,j}}^{\alpha}(t_k) \leq P^{max}_{TX} \tag{26}$$

Once the condition in (26) is fulfilled there definitely exists a solution to (8). If the condition (26) (and hence the constraints (a) and (b) in (8)) are not fulfilled for a given setting of the communication-related parameters, the only approach to make the problem in (8) feasible is to increase the number of FlyBSs. The multiple FlyBSs allow to split the load degenerated by the users to avoid a violation of the constraint (a) on C_{min}.

With respect to the single-FlyBS scenario, an association of the users to the FlyBSs and management of interference among the FlyBSs should be handled. For the user association, a straightforward way is to associate the users based on the commonly used approaches, e.g., the received signal strength [50] or K-means [49]. Of course, the proposed positioning of the FlyBSs and NOMA user clustering is optimal only for the given association. Furthermore, in the multi-FlyBS scenario, other FlyBSs cause interference to NOMA clusters within other FlyBSs. The interference level depends on the users' location with respect to other FlyBSs. Hence, the FlyBS's positioning and the user clustering should be extended by taking the impact of interference from other FlyBSs into account. The user association makes the problem of the FlyBS's positioning and user's clustering NP-hard in general. Solving such problem optimally is itself a challenging and complex task, thus, we leave it for future research.

IV. Simulations and Results

In this section, we provide details of models and simulation settings adopted for evaluation of the proposed solution for NOMA user clustering, power allocation, and FlyBS's positioning. Then, we introduce competitive state-of-the-art algorithms, and we thoroughly analyze the performance of the proposal and demonstrate the advantages of the proposal over the existing solutions.

A. Simulation scenario and models

We consider a scenario where the FlyBS serves users represented by vehicles and/or users in vehicles during a busy traffic or a traffic jam on a road or a highway. In such situation, the FlyBS is a suitable solution to improve the performance of an overloaded network (see, e.g., [39], [40]). The FlyBS is represented by a common rotary-wing UAV. Such UAV can fly typically with a maximum speed of about 25–30 m/s [44]. Thus, the rotary-wing UAV is suitable for our scenario, as the vehicles in the busy traffic or in the traffic jam usually move with speeds within the limits of the common UAV. Following [43], the FlyBS's altitude is fixed at $H = 100$ m.

The users move on a 3-lane highway in the positive direction of the x-axis. The users are distributed uniformly among all three lanes. Within one lane, we set a two-second rule, that is, the minimum safe distance between two vehicles is equal to the distance moved by the vehicles within two seconds. This rule is adopted and suggested for a driving in the real world to roughly maintain a safe distance between the vehicles, while also taking the speed of vehicles into account to specify the minimum distance between the vehicles over time. Furthermore, the speeds are selected uniformly over the intervals {14-16} m/s, {14-17} m/s, and {15-19} m/s for the first, second, and third lanes, respectively. The range of vehicles' speeds is selected considering the maximum flying speed of the FlyBS, as the FlyBS should be able to fly with the served vehicles with a certain speed margin to adjust a relative position with respect to the vehicles. Note that the FlyBS knows the location of users only with a measurement error $e^x_{i,j}$ and $e^x_{i,j}$ uniformly distributed over $[-10, 10]$ m at every time step.

To validate the assumption on the LoS communication, we evaluate the probability of LoS in our scenario as follows. We first solve the problem of the FlyBS's positioning with the assumption of LoS transmission to all the users. Then, we calculate the LoS occurrence (defined by 60% of the first Fresnel zone to be clear of obstacles) in the modeled suburban environment. In line with [47], we assume that the average height, width, and length of the buildings are set to 15 m and the density of the buildings is 13% of the total area. The height of the users' receiving antenna is set to 1.5 m. According to our simulations, the average probability of LoS is 99.6%, 99.1%, and 98.4% in the scenarios with 30, 60, and 90 users, respectively.

The simulations are commonly performed for $C_{min} = 15$ Mbps by each user, however, we also analyze the impact of C_{min} on the performance. Each simulation is of 1200 seconds duration with the user clustering and the transmission power calculated every 0.1 seconds. The results are averaged out over 100 simulation drops. The system parameters are summarized in Table I.

Our proposed solution is investigated for two cases: i) *Communication coverage-maximizing clustering and FlyBS's positioning* (CMCP) for NOMA, as elaborated in Section III and with setting of $V_{th,1} = 12$ m/s, $V_{th,2} = 33$ m/s (see (10)), and ii) *Propulsion power minimization (PPM)*, which is a specific case of the proposed solution with the setting minimizing the propulsion power consumption, i.e., with $V_{th,1} = V_{th,2} = 22.7$ m/s and $P_{pr,th} = 461.6$ W. Both options are compared with the following related state-of-the-art schemes:

TABLE I: Parameter Configurations

System Parameter	Numerical value
Number of users, N_u	{30,60,90}
FlyBS's antenna gain, $D^{j,TX}_{i,G}$	7 dBi [45]
User's antenna gain, $D^{j,R}_{i,G}$	0 dBi [45]
Noise power spectral density, N_i	–174 dBm/Hz
RF frequency, f	2.6 GHz
System bandwidth	100 MHz
Altitude of FlyBS, H	100 meters
User's required capacity, C_{min}	{10,12,15,18,20} Mbps

i) *Sum rate maximization (SRM)* algorithm, introduced in [18], that provides a joint NOMA pairing and FlyBS's positioning for sum rate maximization. Note that the SRM algorithm does not include the constraints on the speed and acceleration in (10). Thus, for a fair comparison, we adjust the FlyBS's speed and acceleration to the closest value within the allowed range in case that the required speed or acceleration exceed their limits.

ii) *enhanced SRM (ESRM)* algorithm that adopts the pairing scheme proposed in [18], but the positioning of FlyBS is enhanced by our proposed optimal positioning in order to reduce the transmission power, as the solution proposed in [18] targets to maximize the sum rate,

iii) *NOMA for static base station (SBS)*, developed in [46], that maximizes the sum capacity for static base station and, hence, does not provide any solution to the FlyBS's positioning,

iv) *enhanced SBS (ESBS)*, that exploits the clustering scheme adopted in [46], and is enhanced with our proposed optimal positioning of the FlyBS to avoid limitations implied by the static base station assumed in [30].

B. Simulation results

In this subsection, we present and discuss simulation results. First, we focus on an evolution of the FlyBS's transmission power consumption over time to demonstrate the advantage of our proposal over the existing solutions in terms of efficiency in transmission power management and consequent enhancement of the NOMA communication coverage. We also compare the performance of the proposed scheme with existing solutions in terms of complexity, average transmission power, maximum potential common capacity, and average propulsion power for various numbers of users (N_u), and minimum required capacities by each user (C_{min}). Furthermore, we evaluate the performance of the proposed solution for different maximum cluster sizes N^{max}_{cu}.

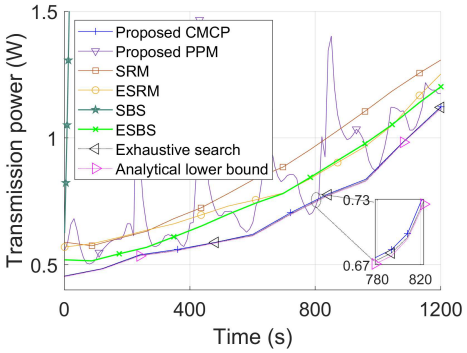

Fig. 4: Transmission power vs. operation time for $N_u = 90$ and $C_{min} = 15$ Mbps. Only part of the values for SBS are shown, as the transmission power is in the order of hundreds of watts.

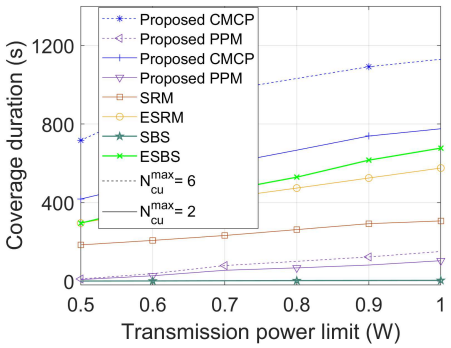

Fig. 5: Duration of communication coverage vs. transmission power limit for different methods and $N_u = 90$ and $C_{min} = 15$ Mbps.

Fig. 4 illustrates an evolution of the transmission power of the FlyBS over time for $C_{min} = 15$ Mbps and for $N_u = 90$. In this figure, we assume NOMA user pairing ($N_{cu}^{max} = 2$, $N_{cl} = 45$) for all existing solutions as these do not allow $N_{cu}^{max} > 2$. In general, the transmission power consumption is increasing over time for all solutions. This is due to a general increase in the relative distance between the first and the last vehicles in the scenario over time, caused by diverse velocities of the vehicles on different lanes, leading to a gradual expansion of the area demarcated by the users. Fig. 4 further shows that the transmission powers corresponding to SRM, ESRM, SBS, and ESBS grow notably faster than for our proposed solution. This faster growth of the transmission power in the existing solutions is due to the sub-optimality of the user clustering in SRM, ESRM, SBS, and ESBS. Furthermore, it is observed that PPM leads to frequent peaks in the transmission power. These peaks are due to the fact that the FlyBS's speed is set to minimize the propulsion power and consequent limitation of the FlyBS's ability in reaching a suitable position at desired time step.

According to Fig. 4, after 1200 s the proposed positioning of the FlyBS applied to SRM (towards ESRM) reduces the transmission power by 6% comparing to the original positioning proposed for the existing SRM. Another notable reduction of up to 5% and 10% compared with the transmission power in ESRM and ESBS, respectively, is achieved by our proposed solution considering a joint positioning of the FlyBS, optimal allocation of transmission power, and optimal user pairing. In total, the proposed solution reduces the transmission power with respect to the original state-of-the-art solutions SRM and SBS by 15% and 99.95%, respectively. In addition, Fig. 4 shows the transmission power over time for the exhaustive search over the discretized intervals and also the lower bound calculated analytically according to (25). The gap between the transmission power achieved by the proposed CMCP and the exhaustive search is typically lower than 0.15%, and always below 1%. Furthermore, the gap between the results from CMCP and the analytical lower bound is typically lower than 0.2% and always below 1.5%. This small difference demonstrates that the performance of the (suboptimal) proposed solution is very close to the optimal solution.

Next, the coverage duration ($T_{coverage}$ as defined in subsection II.B) achieved by the proposed and competitive schemes is depicted in Fig. 5. The figure shows that the proposed scheme significantly enhances the duration of communication coverage with C_{min} guaranteed to all users. If the transmission power of the FlyBS is limited to 1 Watt (i.e., $P_{TX}^{max} = 1$ W), the FlyBS guarantees C_{min} to all users only for 104 s, 5 s, 677 s, 306 s, and 575 s, for PPM, SBS, ESBS, SRM, and ESRM, respectively. As an impact of the proposed FlyBS's positioning, the duration of NOMA communication coverage in ESRM and ESBS is 42% and 7620% higher than in SRM and SBS, respectively. For pairing ($N_{cu}^{max} = 2$), the proposed combined optimal clustering and optimal FlyBS's positioning further enhances the coverage duration by 35% and 14% comparing to ESRM and ESBS, respectively. Moreover, Fig. 5 also shows an impact of the cluster size, as proposed for CMCP and PPM. The proposed extension of the cluster size to $N_{cu}^{max} = 6$ further prolongs the communication coverage duration of the proposed CMCP by 648%, 96% and 67% with respect to PPM, ESRM and ESBS, respectively. This superior performance is a result of the joint optimization of clustering, power allocation, and positioning of the FlyBS. Note that the coverage duration for PPM is significantly lower than for CMCP, ESRM, and ESBS due to the peaks in the transmission power during the operation (as observed in Fig. 4). Also, the transmission power reached by SBS rises very quickly and it becomes in the order of hundreds of watts after few tens of seconds, since the relative distance between the base station and the users increases notably due to immobility of the static base station. Hence, the results for the SBS are not included in further plots and we illustrate only the results for ESBS which enhances the SBS with our proposed FlyBS's positioning.

We also discuss the impact of the cluster size on the transmission power for the proposed CMCP and PPM in Fig. 6. According to Fig. 6, the average transmission power decreases by increasing the maximum number of users grouped in the cluster (i.e., N_{cu}^{max}). The decrease is getting

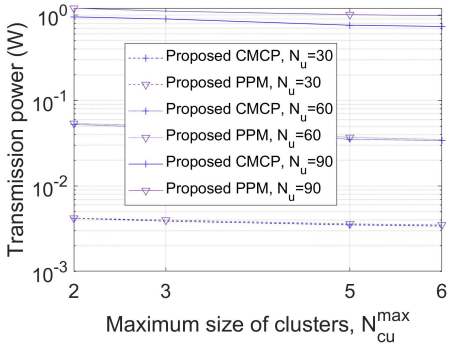

Fig. 6: Average transmission power vs. N_{cu}^{max} for $N_u = 30, 60, 90$, and $C_{min} = 15$ Mbps, for CMCP and PPM.

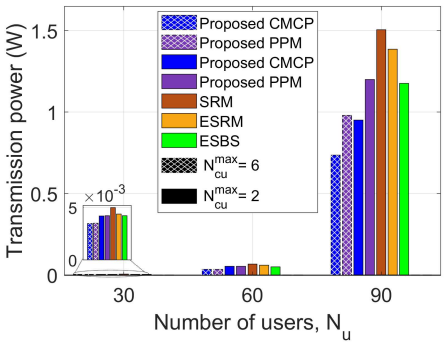

Fig. 7: Average transmission power vs. number of users for different schemes and $C_{min} = 15$ Mbps.

less significant, and the average transmission power saturates with larger N_{cu}^{max} so that the difference between $N_{cu}^{max} = 5$ and $N_{cu}^{max} = 6$ becomes marginal. This saturation is caused by a stronger interference among users in the same cluster if the cluster is of a larger size. Furthermore, the proposed CMCP reduces the transmission power with respect to the PPM by 3%, 6%, and 34% for $N_u = 30$, $N_u = 60$, and $N_u = 90$, respectively.

Next, we investigate the impact of the number of users on the FlyBS's transmission power in Fig. 7. The average transmission power increases with the number of users N_u, as a larger N_u results in a less bandwidth available for each cluster of users. Consequently, a higher transmission power is required to satisfy the required C_{min} for every user. Our proposed solution reaches the lowest transmission power disregarding the number of served users. The highest transmission power is required by the state-of-the-art schemes SRM and SBS. The transmission power is notably reduced by 8% and 99.9% (for $N_u = 90$) by applying our proposed positioning of the FlyBS on the top of the original SRM and SBS towards ESRM and ESBS, respectively. Further significant improvement of 31% and 19% with respect to ESRM and ESBS, respectively, is achieved by our proposal considering joint positioning of the FlyBS, optimal allocation of transmission power, and optimal user clustering (with $N_{cu}^{max} = 2$). Thus, the proposed solution reduces the transmission power with respect to the original state-of-the-art solutions SRM and SBS by 37% and 99.96%, respectively. In addition, by an extension of the cluster size to $N_{cu}^{max} = 6$, the proposed CMCP reduces the transmission power with respect to CMCP with $N_{cu}^{max} = 2$ by 23%. Thus, in total, the proposed CMCP with $N_{cu}^{max} = 6$ reduces the transmission power with respect to SRM and SBS by 47% and 99.97%, respectively.

We show also the FlyBS's propulsion power consumption in Fig. 8. The propulsion power for PPM is lower than all other schemes due to the setting of the propulsion power threshold ($P_{pr,th}$) to the minimum propulsion power. The figure shows that, for $N_u = 30$ and $N_u = 60$, the propulsion power required by the schemes where the proposed positioning is applied (i.e., CMCP, PPM, ESRM, and ESBS) is close to each other (the

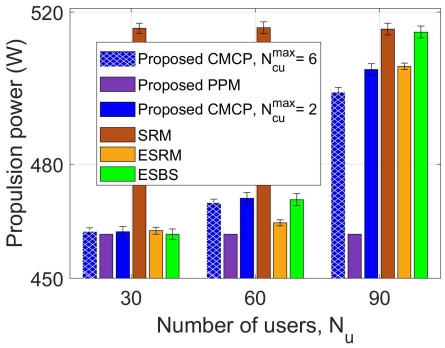

Fig. 8: Average propulsion power consumed by FlyBS vs. number of users for different schemes and $C_{min} = 15$ Mbps.

difference among those schemes is less than 2.5% with the confidence interval of 95%). This is due to the fact that the transmission power is so low for $N_u = 30$ and $N_u = 60$ that the proposed positioning of the FlyBS enhances the coverage duration via the propulsion power reduction (by reducing $P_{pr,th}$) rather than via the transmission power reduction. As a result of such strategy, the propulsion power consumption for CMCP, ESRM, and ESBS becomes similar to PPM.

Next, we investigate the impact of the minimum required capacity C_{min} on the transmission power in Fig. 9. The transmission power for all approaches increases with C_{min} as expected according to (15). Nevertheless, the sub-optimality of the user clustering in the existing state-of-the-art solutions results in a significantly higher rise in the transmission power comparing to our proposed scheme. According to Fig. 9, the proposed CMCP (with $N_{cu}^{max} = 2$) brings up to 47%, 50%, 45%, 100%, and 31% reduction in the transmission power consumption comparing to PPM, SRM, ESRM, SBS, and ESBS, respectively. Furthermore, by the extension of CMCP to the cluster size of $N_{cu}^{max} = 6$, the transmission power is reduced by another 41% with respect to CMCP with $N_{cu}^{max} = 2$. Moreover, the transmission power for PPM is also enhanced by 37% via the extension of $N_{cu}^{max} = 2$ to $N_{cu}^{max} = 6$. Overall, the proposed CMCP (with $N_{cu}^{max} = 6$) brings up to 38%, 70%, 67%, 100%, and 59% reduction in the

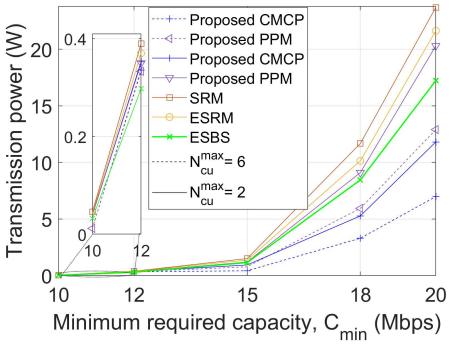

Fig. 9: Average transmission power vs. C_{min} for different algorithms and $N_u = 90$.

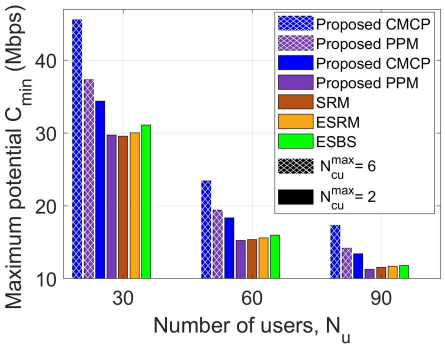

Fig. 10: Maximum potential C_{min} with a fixed transmission power consumption of $P_{fixed}^{G,TX} = 1$ W.

TABLE II: Complexity of the transmission power optimization represented as the number of math operations required to obtain results for user pairing ($N_{cu}^{max} = 2$).

Approach	$N_u = 30$	$N_u = 60$	$N_u = 90$
Proposed CMCP	16	31	46
ESRM	30	60	90
Exhaustive search	2×10^{20}	3.1×10^{49}	1.2×10^{82}

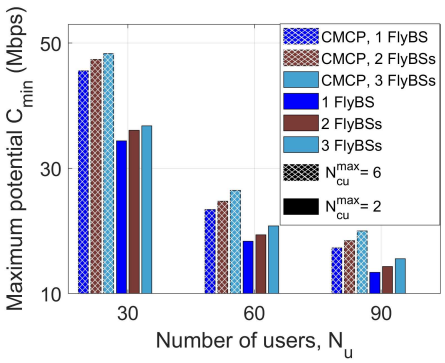

Fig. 11: Maximum potential C_{min} for the proposed CMCP for N_u =30, 60, 90 for 1, 2, and 3 FlyBSs.

transmission power consumption comparing to PPM, SRM, ESRM, SBS, and ESBS, respectively. It is also noted that, the proposed solution presents realistic values for the transmission power in Fig. 9 ([44], [48]).

We also determine the maximum potential C_{min} for the given transmission power $P_{fixed}^{G,TX} = 1$ W in Fig. 10. For $N_{cu}^{max} = 2$, the proposed CMCP increases the maximum potential C_{min} by up to 19%, 13%, 14%, and 16% compared to PPM (with $N_{cu}^{max} = 2$), ESBS, ESRM, and SRM, respectively. Considering also the proposed extension of the NOMA cluster size to $N_{cu}^{max} = 6$, the proposed CMCP improves the maximum potential C_{min} by 53%, 46%, 48%, and 50% compared with PPM (with $N_{cu}^{max} = 6$), ESBS, ESRM, and SRM, respectively.

We further show the maximum potential C_{min} of the proposed CMCP for the scenario with multiple FlyBSs in Fig. 11. We consider the users association based on K-means [49] and orthogonal resources allocated to the FlyBSs. The available bandwidth $N_u \times B$ is split between the FlyBSs proportionally to the number of associated users to each FlyBS. We observe that the maximum potential C_{min} increases with the number of FlyBSs, since the number of associated users to each FlyBS decreases and, at the same time, also the average distance between the FlyBSs and the users decreases. The maximum potential C_{min} reached by single FlyBS is enhanced by 7% and 16% for 2 and 3 FlyBSs, respectively, for both for $N_{cu}^{max} = 2$ as well as $N_{cu}^{max} = 6$. Such an increase in the maximum potential C_{min} confirms that an infeasible guarantee of C_{min} for single FlyBS in (8) can become feasible for a higher number of adopted FlyBSs.

Last, we also compare the complexity of the proposed and state-of-the-art solutions for user pairing in Table II. For each value of N_u the comparison between different algorithms is done under the same number of clusters. The complexity is defined as the number of calculations (math operations) performed by each solution. The complexity of the proposed CMCP can be calculated as explained in Subsection III.D, and the computational complexity of ESRM is linear with respect to N_u. The results are shown for $N_{cu}^{max} = 2$, since ESRM is designed for $N_{cu}^{max} = 2$, and its extension to $N_{cu}^{max} > 2$ is not straightforward. Note that we do not include the complexity of SRM, SBS, or ESBS, as the complexity of these are not easy to calculate. The reason is that the SRM solution is based on bisection search [18], and its complexity is even higher than for ESRM. In SBS and ESBS, the power allocation and clustering are derived using convex optimization [30] for which the complexity cannot be easily determined. Table II confirms that the proposed scheme reduces the complexity significantly with respect to the exhaustive search (1.26×10^{19} times, 10^{48} times, and 2.7×10^{80} times for $N_u = 30$, $N_u = 60$, and $N_u = 90$, respectively), and it is even lower than the complexity of ESRM.

V. Conclusions

In this paper, we have studied the problem of joint optimization of user clustering, transmission power allocation, and FlyBS's positioning in future mobile networks based on

NOMA. We formulate the transmission power optimization problem in terms of the clustering of users for NOMA purposes, and the positioning of the FlyBS over time as the users move. Then, we provide a solution to find the optimum clustering of users, and the FlyBS's positions that yield the minimum transmission power while guaranteeing a minimum required capacity for all users. This allows a significant increase in the NOMA communication coverage duration for the FlyBS. We show that the proposed solution extends the FlyBS's coverage duration by tens of percent.

In the future work, the scenario with multiple FlyBS should be studied. This scenario implies another dimension of the problem related to the user association to individual FlyBSs as well as a management of interference from the FlyBSs [49], [50]. Furthermore, the problem of optimal bandwidth allocation should be considered.

APPENDIX A
PROOF TO THEOREM 1

Proof. We prove Theorem 1 using mathematical contradiction as follow: Let $N_{cl,i}$ denote the number of clusters of a size i. Also, let $cl_{j_1},...,cl_{j_{N_{cl,N_{cu}^{max}}}}$ be the clusters of a size N_{cu}^{max}. Suppose that $\{x_{1,cl_{j_1}}^{G_{opt}}, x_{1,cl_{j_2}}^{G_{opt}}, \dots, x_{1,cl_{j_{N_{cl,N_{cu}^{max}}}}}^{G_{opt}}\} = \{x_{i_1},...,x_{i_{N_{cl,N_{cu}^{max}}}}\}$ with $x_{i_1} < ... < x_{i_{N_{cl,N_{cu}^{max}}}}$. Then, by contradiction, we assume that the users in $\{x_{i_1},...,x_{i_{N_{cl,N_{cu}^{max}}}}\}$ are not consecutive in X_{sorted}, and there exists x_j such that $x_{i_1} < x_j < x_{i_{N_{cl,N_{cu}^{max}}}}$ and $x_j \notin \{x_{i_1},...,x_{i_{N_{cl,N_{cu}^{max}}}}\}$. Also, we assume that, for G_{opt}, x_j is the s-th user in some cluster ($s > 1$). Let G_1 denote the clustering function that is obtained by swapping x_{i_1} and x_j in G_{opt}. Similarly, G_2 denotes the clustering obtained by swapping $x_{i_{N_{cl,N_{cu}^{max}}}}$ and x_j in G_{opt}. From the optimality of G_{opt} it is inferred that:

$$\begin{aligned} &P_{TX}(X,Y,H,t_k,G_{opt})|_{(X_{cto}^{G_{opt}},Y_{cto}^{G_{opt}})} - \\ &P_{TX}(X,Y,H,t_k,G_1)|_{(X_{cto}^{G_{opt}},Y_{cto}^{G_{opt}})} < 0, \\ &P_{TX}(X,Y,H,t_k,G_{opt})|_{(X_{cto}^{G_{opt}},Y_{cto}^{G_{opt}})} - \\ &P_{TX}(X,Y,H,t_k,G_2)|_{(X_{cto}^{G_{opt}},Y_{cto}^{G_{opt}})} < 0. \end{aligned} \tag{27}$$

Now, we rewrite the left-hand side terms in (27) by means of the system parameters as follow:

$$\begin{aligned} &P_{TX}(X,Y,H,t_k,G_{opt})|_{(X_{cto}^{G_{opt}},Y_{cto}^{G_{opt}})} - \\ &P_{TX}(X,Y,H,t_k,G_1)|_{(X_{cto}^{G_{opt}},Y_{cto}^{G_{opt}})} = \\ &\gamma_{min}Q\sigma^2\big((1+\gamma_{min})^{N_{cu}^{max}-1} - (1+\gamma_{min})^{N_{cu}^{max}-s}\big)({d_{i_1}}^{\alpha} - {d_j}^{\alpha}), \\ &P_{TX}(X,Y,H,t_k,G_{opt})|_{(X_{cto}^{G_{opt}},Y_{cto}^{G_{opt}})} - \\ &P_{TX}(X,Y,H,t_k,G_2)|_{(X_{cto}^{G_{opt}},Y_{cto}^{G_{opt}})} = \\ &\gamma_{min}Q\sigma^2\big((1+\gamma_{min})^{N_{cu}^{max}-1} - (1+\gamma_{min})^{N_{cu}^{max}-s}\big)(d_{i_{N_{cl,N_{cu}^{max}}}}^{\alpha} - {d_j}^{\alpha}) \end{aligned} \tag{28}$$

From the first inequality in (27) and the first equality in (28) it is included that $(d_{i_1} - d_j) < 0$. Similarly, from the second inequality in (27) and the second equality in (28) it is concluded that $(d_{i_{N_{cl,N_{cu}^{max}}}} - d_j) < 0$. However, the inequalities $(d_{i_1} - d_j) < 0$ and $(d_{i_{N_{cl,N_{cu}^{max}}}} - d_j) < 0$ cannot hold at the same time given the assumption that $x_{i_1} < x_j < x_{i_{N_{cl,N_{cu}^{max}}}}$ due to following reasons. First, in a movement on a road in the direction of the x-axis, the range of x-coordinates of the users is much larger than the range of y-coordinates. Thus, from $(d_{i_1} - d_j) < 0$ it is concluded that $X_{cto} < \frac{(x_{i_1}+x_j)}{2}$. Similarly, from $(d_{i_{N_{cl}}} - d_j) < 0$ it is concluded that $X_{cto} > \frac{(x_{i_{N_{cl,N_{cu}^{max}}}}+x_j)}{2}$. By incorporating the two derived inequalities $X_{cto} < \frac{(x_{i_1}+x_j)}{2}$ and $X_{cto} > \frac{(x_{i_{N_{cl,N_{cu}^{max}}}}+x_j)}{2}$ we get $x_{i_1} > x_{i_{N_{cl,N_{cu}^{max}}}}$, which contradicts the assumption of $x_{i_1} < x_{i_{N_{cl,N_{cu}^{max}}}}$. Hence, the initial assumption that the users in $\{x_{1,cl_{j_1}}^{G_{opt}}, x_{1,cl_{j_2}}^{G_{opt}}, \dots, x_{1,cl_{j_{N_{cl,N_{cu}^{max}}}}}^{G_{opt}}\}$ are not consecutive is incorrect. Therefore, $\{x_{i_1},...,x_{i_{N_{cl,N_{cu}^{max}}}}\}$ consists of the consecutive users in X_{sorted}. By a similar procedure as above, we verify that the second users of the clusters of a size N_{cu}^{max} and the first users of the clusters of a size $N_{cu}^{max}-1$ should be consecutive values in X_{sorted} after eliminating $\{x_{1,cl_{j_1}}^{G_{opt}}, x_{1,cl_{j_2}}^{G_{opt}}, \dots, x_{1,cl_{j_{N_{cl,N_{cu}^{max}}}}}^{G_{opt}}\}$, and so on so forth for the next users of all clusters. This completes the proof to Theorem 1. □

APPENDIX B
PROOF OF LEMMA 2

Proof. To determine the discretization error in the exhaustive search we use the first-derivative Taylor approximation with respect to a_{FlyBS}^x and a_{FlyBS}^y. Then, the approximation error (denoted by ζ) is expressed in terms of the second derivatives, i.e.,

$$\begin{aligned} \zeta = (a_{FlyBS}^x - \varphi)^2 \frac{\partial^2 P_{TX}}{\partial {a_{FlyBS}^x}^2}|_{(X(\varphi^+),Y(\tau^+))} + \\ (a_{FlyBS}^y - \tau)^2 \frac{\partial^2 P_{TX}}{\partial {a_{FlyBS}^y}^2}|_{(X(\varphi^+),Y(\tau^+))} + \\ 2(a_{FlyBS}^x - \varphi)(a_{FlyBS}^y - \tau)\frac{\partial^2 P_{TX}}{\partial a_{FlyBS}^x \partial a_{FlyBS}^y}|_{(X(\varphi^+),Y(\tau^+))} \end{aligned} \tag{29}$$

where φ^+ and τ^+ are (unknown) values satisfying $\varphi^+ \in [\varphi, \varphi+\xi]$ and $\tau^+ \in [\tau, \tau+\xi]$. Using the triangle inequality, and by the fact that $0 \le a_{FlyBS}^x - \varphi \le \xi$ and $0 \le a_{FlyBS}^y - \tau \le \xi$ for $a_{FlyBS}^x \in [\varphi, \varphi+\xi]$ and $a_{FlyBS}^y \in [\tau, \tau+\xi]$, the error is upper bounded by:

$$\begin{aligned} |\zeta| \le \xi^2|M_{xx}| + 2\xi^2|M_{xy}| + \xi^2|M_{yy}| = \\ \xi^2(|M_{xx}| + 2|M_{xy}| + |M_{yy}|), \end{aligned} \tag{30}$$

□

REFERENCES

[1] B. Li, Z. Fei and Y. Zhang, "UAV Communications for 5G and Beyond: Recent Advances and Future Trends," *IEEE Internet Things J.*, vol. 6, no. 2, 2019.

[2] A. Chriki, H. Touati, H. Snoussi and F. Kamoun, "UAV-GCS Centralized Data-Oriented Communication Architecture for Crowd Surveillance Applications," *IWCMC*, 2019.

[3] A. Puri, "A survey of unmanned aerial vehicles (UAV) for traffic surveillance," January 2005.

[4] J. Lyu, et al., "Placement Optimization of UAV-Mounted Mobile Base Stations," *IEEE Commun. Lett.*, vol. 21, no. 3, 2017.

[5] X. Cheng, et al., "Architecture Design of Communication and Backhaul for UAVs in Power Emergency Communication," *IEEE ICCCBDA* 2019.

[6] X. Li, et al., "A Near-Optimal UAV-Aided Radio Coverage Strategy for Dense Urban Areas," *IEEE Trans. Veh. Technol.*, vol. 68, no. 9, pp. 9098-9109, Sept. 2019.

[7] E. Kalantari, H. Yanikomeroglu, and A. Yongacoglu, "On the number and 3D placement of drone base stations in wireless cellular networks," *IEEE VTC2016-Fall*.

[8] M. Samir, et al., "UAV Trajectory Planning for Data Collection from Time-Constrained IoT Devices," *IEEE Trans. Wireless Commun.*, vol. 19, no. 1, pp. 34-46, Jan. 2020.

[9] L. Wang, "Multiple access mmwave design for UAV-aided 5g communications," *IEEE Wireless Communications*, 2019.

[10] Y. Ji, et al., "Multi-cell Edge Coverage Enhancement Using Mobile UAV-Relay," *IEEE Internet Things Journal*, 2020.

[11] H. Shakhatreh, et al., "Efficient 3D placement of a UAV using particle swarm optimization," *ICICS*, 2017.

[12] X. Liu, J. Miao and P. Wang, "Throughput Optimization of Blocked Data Transmission: A Mobile-Relay-UAV-Assisted Approach," *IEEE ICCC*, 2019.

[13] Z. Wang, L. Duan and R. Zhang, "Adaptive Deployment for UAV-Aided Communication Networks," in *IEEE Trans. Wireless Commun.*, vol. 18, no. 9, Sept. 2019.

[14] M. Nikooroo and Z. Becvar, "Joint Positioning of UAV and Power Control for Flying Base Stations in Mobile Networks," *IEEE WiMOB*, 2019.

[15] M. Nikooroo, Z. Becvar, "Optimizing Transmission and Propulsion Powers for Flying Base Stations," *IEEE WCNC*, 2020.

[16] O. Maraqa, et al., "A survey of rate-optimal power domain noma with enabling technologies of future wireless networks," *IEEE Communications Surveys & Tutorials*, Feb. 2020.

[17] L. Dai, et al., "Non-orthogonal multiple access for 5G: solutions, challenges, opportunities, and future research trends," *IEEE Communications Magazine*, vol. 53, no. 9, pp. 74-81, September 2015.

[18] M. Nguyen and L. Le, "NOMA User Pairing and UAV Placement in UAV-Based Wireless Networks," *IEEE ICC*, 2019.

[19] Z. Ding, et al., "On the Performance of Non-Orthogonal Multiple Access in 5G Systems with Randomly Deployed Users," *IEEE Signal Process. Lett.*, vol. 21, no. 12, Dec. 2014.

[20] K. Chi, Z. Chen, K. Zheng, Y. Zhu and J. Liu, "Energy Provision Minimization in Wireless Powered Communication Networks With Network Throughput Demand: TDMA or NOMA?," *IEEE Trans. Commun.*, vol. 67, no. 9, Sept. 2019.

[21] B. Kim, et al., "Partial Non-Orthogonal Multiple Access (P-NOMA) with Respect to User Fairness," *IEEE VTC2019-Fall*.

[22] S. Timotheou, I. Krikidis, "Fairness for Non-Orthogonal Multiple Access in 5G Systems," *IEEE Signal Process. Lett.*, vol. 22, no. 10, 2015.

[23] M. F. Sohail, C. Y. Leow and S. Won, "Non-Orthogonal Multiple Access for Unmanned Aerial Vehicle Assisted Communication," in *IEEE Access*, vol. 6, pp. 22716-22727, 2018.

[24] J. Kang and I. Kim, "Optimal User grouping for Downlink NOMA," in *IEEE Wireless Commun. Lett.*, vol. 7, no. 5, 2018.

[25] Z. Chen, K. Chi, K. Zheng, Y. Li and X. Liu, "Common Throughput Maximization in Wireless Powered Communication Networks With Non-Orthogonal Multiple Access," *IEEE Trans. Veh. Technol.*, vol. 69, no. 7, July 2020.

[26] Z. Shi, W. Gao, S. Zhang, J. Liu and N. Kato, "Machine Learning-Enabled Cooperative Spectrum Sensing for Non-Orthogonal Multiple Access," *IEEE Trans. Commun.*, vol. 19, no. 9, pp. 5692-5702, Sept. 2020.

[27] W. Peng, W. Gao and J. Liu, "AI-Enabled Massive Devices Multiple Access for Smart City," *IEEE Internet Things Journal*, vol. 6, no. 5, Oct. 2019.

[28] Z. Shi, W. Gao, S. Zhang, J. Liu and N. Kato, "AI-Enhanced Cooperative Spectrum Sensing for Non-Orthogonal Multiple Access," *IEEE Wireless Communications*, vol. 27, no. 2, April 2020.

[29] M. F. Sohail and C. Y. Leow, "Maximized fairness for NOMA based drone communication system," IEEE MICC, 2017.

[30] L. Lei, D. Yuan and P. Värbrand, "On Power Minimization for Non-orthogonal Multiple Access (NOMA)," in *IEEE Commun. Lett.*, vol. 20, no. 12, pp. 2458-2461, Dec. 2016.

[31] A. Nasir, et al., "UAV-Enabled Communication Using NOMA," *IEEE Trans. Commun.*, vol. 67, no. 7, 2019.

[32] P. Sharma, D. Kim, "UAV-Enabled Downlink Wireless System with Non-Orthogonal Multiple Access," *GC Wkshps*, 2017.

[33] J. Baek, S. I. Han and Y. Han, "Optimal Resource Allocation for Non-Orthogonal Transmission in UAV Relay Systems," *IEEE Wireless Commun. Lett.*, vol. 7, no. 3, pp. 356-359, June 2018.

[34] N. Zhao, et al., "Joint Trajectory and Precoding Optimization for UAV-Assisted NOMA Networks," *IEEE Trans. Commun.*, vol. 67, no. 5, pp. 3723-3735, May 2019.

[35] X. Liu, et al., "Placement and Power Allocation for NOMA-UAV Networks," *IEEE Wireless Commun. Lett.*, June 2019.

[36] W. Wang, et al., "Joint Precoding Optimization for Secure SWIPT in UAV-Aided NOMA Networks," *IEEE Trans. Commun.*, vol. 68, no. 8, pp. 5028-5040, Aug. 2020

[37] Xiaowei Pang, et al, "Energy-Efficient Design for mmWave-Enabled NOMA-UAV Networks", *SCI Journal*, 2021.

[38] M. Nikooroo and Z. Becvar, "Optimization of Transmission Power for NOMA in Networks with Flying Base Stations," *IEEE VTC2020-Fall*, 2020.

[39] P. Yang, et al., "Proactive Drone-Cell Deployment: Overload Relief for a Cellular Network Under Flash Crowd Traffic," *IEEE Trans. Intell. Transp. Syst.*, vol. 18, no. 10, pp. 2877-2892, Oct. 2017.

[40] Z. Becvar, et al., "Performance of Mobile Networks with UAVs: Can Flying Base Stations Substitute Ultra-Dense Small Cells?," *European Wireless*, 2017.

[41] K. Senel, H. V. Cheng, E. Björnson and E. G. Larsson, "What Role can NOMA Play in Massive MIMO?," *IEEE J. Sel. Topics Signal Process.*, vol. 13, no. 3, pp. 597-611, 2019.

[42] S. Ahmed, M. Z. Chowdhury and Y. M. Jang, "Energy-Efficient UAV-to-User Scheduling to Maximize Throughput in Wireless Networks," *IEEE Access*, vol. 8, pp. 21215-21225, 2020.

[43] Y. Zeng, J. Xu, and R. Zhang, "Energy Minimization for Wireless Communication With Rotary-Wing UAV," in *IEEE Trans. Wireless Commun.*, Vol. 18, No. 4, April 2019.

[44] A. Fotouhi, et al., "Survey on UAV Cellular Communications: Practical Aspects, Standardization Advancements, Regulation, and Security Challenges," *IEEE Commun. Surveys Tuts.*, vol. 21, no. 4, 2019.

[45] M. Bekhti, et al., "Path planning of unmanned aerial vehicles with terrestrial wireless network tracking," *IEEE WD*, 2016.

[46] L. You and D. Yuan, "A Note on Decoding Order in User Grouping and Power Optimization for Multi-Cell NOMA With Load Coupling," *IEEE Trans. Wireless Commun.*, vol. 20, no. 1, pp. 495-505, Jan. 2021.

[47] J. Turkka and M. Renfors, "Path loss measurements for a non-line-of-sight mobile-to-mobile environment," *International Conference on ITS Telecommunications*, 2008.

[48] "Examples of technical characteristics for unmanned aircraft control and non-payload communications links," *ITU-R,* 2011.

[49] R. Duan, J. Wang, C. Jiang, H. Yao, Y. Ren and Y. Qian, "Resource Allocation for Multi-UAV Aided IoT NOMA Uplink Transmission Systems," *IEEE Internet Things J.*, vol. 6, no. 4, Aug. 2019.

[50] S. Zhang, J. Liu and W. Sun, "Stochastic Geometric Analysis of Multiple Unmanned Aerial Vehicle-Assisted Communications Over Internet of Things," *IEEE Internet Things J.*, vol. 6, no. 3, pp. 5446-5460, June 2019.

3.3 Maximization of minimum user capacity for NOMA

In this section, we investigate the problem of minimum user's capacity maximization via FlyBS's positioning, NOMA user clustering, and transmission power allocation. It is noted that the minimum user's capacity is also regarded as a critical metric as it indicates the fairness of the FlyBS's provided coverage among the users. We propose a geometrical approach with low complexity to cluster the users. Furthermore, we show the relation between a minimization of the transmission power and a maximization of the minimum capacity of the users. The following work presents the reference paper [J4] in that regard.

Maximization of Minimum User Capacity in UAV-Enabled Mobile Networks with NOMA

Mohammadsaleh Nikooroo, *Member, IEEE,* Zdenek Becvar, *Senior Member, IEEE*

***Abstract*—In this letter, we maximize the minimum downlink capacity of moving users in the mobile networks based on non-orthogonal multiple access (NOMA) with flying base stations (FlyBSs) considering practical constraints on the speed, altitude, and transmitting power of the FlyBSs. We propose a geometrical approach allowing us to reflect the users' movement and to derive optimal user clustering for NOMA, positions of the FlyBS, and the transmission power allocation to the users in one cluster served in NOMA at the same time-frequency resources. The proposed solution increases the minimum capacity of all users by 20%-59% comparing to state-of-the-art solutions.**

***Index Terms*—Flying base station, Non-orthogonal multiple access, Minimum capacity, Mobile users, Mobile networks, 6G.**

I. Introduction

In the recent years, unmanned aerial vehicles (UAVs) acting as flying base stations (FlyBSs) have received remarkable interest thanks to their intrinsic characteristics, such as adaptability to environment or potential to improve performance in mobile networks. The advantages offered by the FlyBSs, of course, rely on an efficient radio resource management and FlyBS's positioning. These aspects become even more challenging for non-orthogonal multiple access (NOMA), as the users should be clustered together and the users in each cluster are served at the same radio resources.

Superiority of NOMA over the conventional orthogonal-multiple-access (OMA) is shown in [1]. In [2], an energy-efficient NOMA communication of the FlyBS is further investigated. However, the problem of the FlyBS's positioning is addressed in neither [1] nor [2], as a static FlyBS is assumed. The FlyBS's positioning is targeted, e.g., in [3] and [4] jointly with the transmission power allocation to maximize the sum capacity and to minimize the transmission power, respectively. However, the problem of the NOMA user clustering is not addressed in these papers and only one NOMA cluster is considered. The assumption of single cluster is practical for only scenario with few users due to a high complexity of successive interference cancellation (SIC) decoding commonly adopted to cancel interference within the NOMA cluster [5].

Furthermore, in [6], the authors minimize an energy consumption of the IoT devices in scenarios with the FlyBS collecting data from these devices in NOMA networks. To this end, the FlyBS's trajectory and resource allocation are optimized. Nevertheless, the trajectory is designed for the users being static during the FlyBS's entire mission and an extension towards mobile users is not straightforward.

The mobile users are considered in [7], where joint NOMA user clustering and FlyBS's positioning is investigated to prolong the coverage duration of the users served by the FlyBS. The solution in [7], however, targets 1D scenario, where all users move in the same direction along x-axis (e.g., vehicles on a road). Hence, the clustering in [7] is done based on only the x-coordinate of the users. Then, a heuristic solution for a joint user clustering and FlyBS's positioning to increase the minimum downlink sum capacity is proposed in [8]. The NOMA clusters size is, however, limited to only two users. Furthermore, the solution in [8] does not guarantee any minimum capacity to individual users, hence, some users may end up with zero capacity. The problem of NOMA clustering in the scenario with potentially moving users targeting to minimize the transmission power and to maximize the sum capacity is addressed in [10] and [11], respectively. However, the FlyBS's positioning is considered in neither [10] nor [11], as only a static base station is assumed in both.

Even if the problem of maximization of the minimum capacity for users reflects fairness among users and is heavily addressed in common mobile networks, it is not yet investigated for the NOMA-based networks with FlyBSs serving mobile users. Hence, we maximize the minimum capacity via a joint FlyBS's positioning, transmission power allocation, and NOMA users clustering in the scenario with the moving users. In addition, we consider a generalized model for NOMA, where the cluster sizes can be different and the cluster size of one is allowed, i.e., some users can potentially be served in OMA. We derive a closed-form expression for the transmission power in terms of the FlyBS's position and the NOMA clustering. We also derive necessary conditions for the users' capacities so that the minimum capacity of all users can be maximized. Then, we maximize the minimum capacity via the FlyBS's positioning and the transmission power allocation to the users and we find the optimal user clustering.

II. System model and problem formulation

In this section, we explain the system model and then formulate the problem of user clustering, power allocation, and FlyBS's positioning.

We consider one FlyBS serving N_u mobile users $U = \{u_1, u_2, \ldots, u_{N_u}\}$ as depicted in Fig. 1. In our NOMA model, the users are assigned into different clusters such that the users in each cluster share the same channel at the same time,

Mohammadsaleh Nikooroo and Zdenek Becvar are with Department of Telecommunication Engineering, Faculty of Electrical Engineering, Czech Technical University in Prague, Czech Republic, e-mail: (nikoomoh@fel.cvut.cz, and zdenek.becvar@fel.cvut.cz).

This work has been supported by Grant No. LTT20004 funded by Ministry of Education, Youth and Sports.

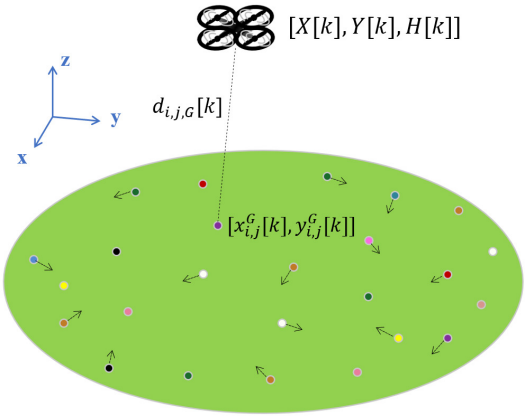

Fig. 1: System model with multiple mobile users deployed within coverage area of the FlyBS. The circles with the same color represent the users in the same NOMA cluster.

however different clusters are served at different (orthogonal) channels. Let $\mathbb{G}$ denote the space of all possible functions that group the users into N_{cl} clusters with $N_{cu,j}$ users in the j-th cluster. We assume that $N_{cu,j} \in [1, N_{cu}^{max}]$, where N_{cu}^{max} is the maximum potential size of each cluster and it is practically related to an incurred complexity in the SIC decoder. Each function $G \in \mathbb{G}$ is defined as a bijective mapping G: $[1, N_u] \rightarrow [1, N_{cl}] \times [1, N_{cu}^{max}]$. Furthermore, let $u^G_{1,j}, u^G_{2,j}, \ldots, u^G_{N_{cu,j},j}$ denote the users assigned by the function G to cluster j. Let $\boldsymbol{l_M}[k] = \big[X[k], Y[k], H[k]\big]^T$ and $\boldsymbol{l^G_{i,j}}[k] = \big[x^G_{i,j}[k], y^G_{i,j}[k]\big]^T$ denote the locations of the FlyBS and $u^G_{i,j}$, respectively, at the time step k . In SIC, suppose that the user $u^G_{i,j}$ ($i \in [1, N_{cu,j}-1]$) cancels the interfering signals from the users $u^G_{i',j}$ ($\forall i' \in [i+1, N_{cu,j}]$) to extract its own signal (note that the adopted decoding order would not affect optimality since finding the index of users in clusters is subject to optimization instead). Consequently, the achievable SINR $\gamma^G_{i,j}$ for $u^G_{i,j}$ is:

$$\gamma^G_{i,j}[k] = \frac{p^{G,R}_{i,j}[k]}{\sigma^2 + \sum_{l=1}^{i-1} p^{G,R}_{i,l,j}[k]}, \quad (1 \le i \le N_{cu,j}), \quad (1)$$

where σ^2 is the noise power, $p^{G,R}_{i,j}$ is the received power by $u^G_{i,j}$, and $p^{G,R}_{i,l,j}$ represents the interference at $u^G_{i,j}$ caused by the signals transmitted to another user $u^G_{l,j}$ in the same cluster j.

The channel capacity $C^G_{i,j}$ of the user $u^G_{i,j}$ is calculated as $C^G_{i,j}[k] = B\log_2(1+\gamma^G_{i,j}[k])$, where B is the bandwidth assigned to each NOMA cluster.

Next, we formulate the FlyBS's total transmission power as $P_{TX}(\boldsymbol{l}, k, G) = \sum_{j=1}^{N_{cl}} \sum_{i=1}^{N_{cu}} p^{G,T}_{i,j}$, where $p^{G,T}_{i,j}$ is the transmission power of the FlyBS to the i-th user $u^G_{i,j}$ in the j-cluster calculated by the Friis' transmission equation as:

$$p^{G,T}_{i,j} = \frac{\zeta}{(\frac{\lambda}{\lambda+1}\bar{\epsilon} + \frac{1}{\lambda+1}\tilde{\epsilon})} p^{G,R}_{i,j} d^{\alpha}_{i,j,G}[k] = Q p^{G,R}_{i,j} d^{\alpha}_{i,j,G}[k], \quad (2)$$

where $p^{G,R}_{i,j}$ is the received signal power by the user $u^G_{i,j}$, $d_{i,j,G}$ denotes the distance between the FlyBS and the user $u^G_{i,j}$, ζ is a parameter depending on communication frequency and gain of antennas. Furthermore, λ is the Rician fading factor, $\bar{\epsilon}$ is the line-of-sight (LoS) component satisfying $|\bar{\epsilon}| = 1$, and $\tilde{\epsilon}$ denotes the non-line-of-sight (NLoS) component satisfying $\tilde{\epsilon} \sim CN(0,1)$, and α is the pathloss exponent.

Using (2), the total transmission power P_{TX} is rewritten as: $P_{TX}(\boldsymbol{l_M}, k, G) = \sum_{j=1}^{N_{cl}} \sum_{i=1}^{N_{cu,j}} Q p^{G,R}_{i,j} {d_{i,j,G}}^{\alpha}[k]$.

Our goal is to find the position of the FlyBS jointly with the transmission power allocation to the users and the NOMA clustering of the users to maximize the minimum capacity $\eta[k]$ at every time step k. We formulate this problem as:

$$\max_{\left[G, p^{G,T}_{i,j}, \boldsymbol{l_M}\right]} \eta[k], \quad (3)$$

$$s.t. \quad C^G_{i,j}[k] \ge \eta[k], \quad (3a)$$

$$P_{TX}(\boldsymbol{l_M}, k, G) \le P^{max}_{TX}, \forall k, \quad (3b)$$

$$H_{min} \le H[k] \le H_{max}\ , \quad (3c)$$

$$\big|\big|\boldsymbol{l_M}[k] - \boldsymbol{l_M}[k-1]\big|\big| \le V_{max}\delta_k, \quad (3d)$$

where δ_k in (3d) is the duration between time steps $k-1$ and k. The constraint (3b) guarantees that the FlyBS's transmission power is within the maximum transmission power limit P^{max}_{TX}, and the constraints (3c) and (3d) limit the FlyBS's altitude to $[H_{min}, H_{max}]$ and the FlyBS's speed to V_{max}.

III. Proposed FlyBS Positioning, Transmission Power Allocation, and User Clustering

In this section, we first transform of the problem to more convenient transmission power minimization. Then, we describe the proposed users clustering and FlyBS positioning.

A. Maximization of minimum capacity via minimization of transmission power

The user's capacity and so the minimum capacity (objective) in (3) are not convex or concave. Furthermore, the discrete function G makes the problem (3) non-tractable. To tackle these challenges, we propose a solution based on a conversion of the objective in (3). To this end, we first elaborate the characteristics of the optimal solution to (3) (denoted by η^*) and its relevance to the transmission power via Proposition 1.

Proposition 1. *In the optimal solution to (3), $C^G_{i,j} = \eta^*, \forall i, j$.*

Proof. We first show that P_{TX} is an increasing function of $C^G_{i,j}$. To this end, from (1) and (2), we observe that $p^{G,T}_{1,j} = Q\sigma^2\gamma^G_{1,j}[k]d^{\alpha}_{1,j,G}[k]$. Thus, $p^{G,T}_{1,j}$ increases with $\gamma^G_{1,j}[k]$. Furthermore, from (1) and (2), $p^{G,T}_{i,j}$ is rewritten as:

$$p^{G,T}_{i,j} = \sigma^2\gamma^G_{i,j}[k]d^{\alpha}_{i,j,G}[k] + \gamma^G_{i,j}[k]\sum_{l=1}^{N_{cu,j}-1} p^{G,T}_{l,j}. \quad (4)$$

From the recursive formula in (4), we observe that $p^{G,T}_{i,j}$ also increases with $\gamma^G_{i,j}$ and, consequently, with $C^G_{i,j}$ (since $\gamma^G_{i,j}[k] = 2^{\frac{C^G_{i,j}[k]}{B}-1}$). Now, by contradiction, suppose that the capacity received by some user $u^G_{i',j'}$ would be greater than η^* in the optimal solution to (3). In such case, decreasing $C^G_{i',j'}$

as long as it still remains larger than or equal to η^* would not decrease the minimum capacity η^* while it decreases the transmission power. This means that, given the maximum transmission power limit P_{TX}^{max}, we can always first reduce the capacity of the users to η^* (to reduce the transmission power) and, then, we can increase the capacity of all users together by increasing the power to all users (exploiting the reduced transmission power) until the transmission power reaches the P_{TX}^{max}. This proves the Proposition 1. □

It is deduced from the proof of the Proposition 1 that, once the optimal G and $\boldsymbol{l_M}$ are derived, the optimal power allocation $p_{i,j}^{G,T}$ in (3) is determined from (4) and by setting the FlyBS's total transmission power to P_{TX}^{max}. Furthermore, Proposition 1 indicates the connection between the maximization of η^* and the minimization of P_{TX} as elaborated and demonstrated in the following Corollaries.

Corollary 1. *Using the expression for $p_{i,j}^{G,T}$ in (4) and by the fact that the capacity of all users is η^* and $\gamma^*[k] = 2^{\frac{\eta^*[k]}{B}-1}$, the total transmission power is calculated as:*

$$P_{TX}(\boldsymbol{l_M}, k, G) = \gamma^* Q \sigma^2 \sum_{j=1}^{N_{cl}} \sum_{i=1}^{N_{cu,j}} (1+\gamma^*)^{N_{cu,j}-i} d_{i,j,G}^{\alpha}, \quad (5)$$

Corollary 2. *Following the Proposition 1 and given that the transmission power increases with the capacity η^* and vice versa, the solution to the user clustering and FlyBS's positioning in (3) can be alternatively derived via solving the following problem of transmission power minimization:*

$$\min_{[G,\boldsymbol{l_M}]} P_{TX}[k], \forall k, \quad (6)$$

$$s.t. \quad \text{(3c), (3d)},$$

$$C_{i,j}^{G}[k] = \eta_{arb}, i \in [1, N_{cu,j}],\ j \in [1, N_{cl}], \quad (6a)$$

where η_{arb} is an arbitrary user capacity. The constraint (6a) *ensures that every user receives the capacity of exactly η_{arb}.*

Note that the value of η_{arb} does not affect the optimal G or $\boldsymbol{l_M}$ in (6) (see Proposition 1), but it is selected such that the constraint (3b) would not be violated (so that there would exist a feasible solution). The power minimization problem in (6) is more convenient for FlyBS's positioning and user clustering, because the maximization of minimum capacity requires the knowledge of which user receiving the smallest (minimum) capacity among all users. However, such knowledge is hard to obtain without determining the user clustering. On the other hand, the objective in (3) and the constraints (3c) and (3d) are convex with respect to $\boldsymbol{l_M}$. Hence, for a fixed clustering function G, the optimal FlyBS's position is efficiently derived using CVX. Note that (6a) is translated into $\gamma[k] = 2^{\frac{\eta_{arb}[k]}{B}-1}$, which is used to write the transmission power as in (5).

B. Determination of user clustering and FlyBS positioning

Although the optimal position for each clustering can be derived (as explained in the previous subsection), finding the optimal clustering by an exhaustive search is not always feasible, because, even if all the clusters would be of the same size, there are $\frac{N_u!}{N_{cl}!}$ different clustering options, which could be extremely large even for small N_u.Hence, to tackle the user clustering, we derive all *promising* clustering options to reduce complexity and we select the one maximizing the performance. First, let's define a necessary condition for the optimal clustering. To do this, we introduce the following terminology. Let Λ denote a set of points in the xy-plane. The subset $T \subset \Lambda$ is said to form an "exclusively convex polygon" if the convex hull determined by T does not enclose any point from $\Lambda - T$. Furthermore, let Ψ denote the set of points in the xy-plane corresponding to the users' locations. Now, we define the necessary condition via Theorem 1.

Theorem 1. *Denoted by $\Theta_{e,q}$ the set of e-th users in clusters of size q, for the optimal clustering G_{opt} minimizing P_{TX}, $\Theta_{1,N_{cu}^{max}}$ forms an exclusively convex polygon in Ψ. Moreover, $\Theta_{2,N_{cu}^{max}} \cup \Theta_{1,N_{cu}^{max}-1}$ is an exclusively convex polygon in $\Psi - \Theta_{1,N_{cu}^{max}}$. Similarly, $\Theta_{1,N_{cu}^{max}-i} \cup ... \cup \Theta_{i,N_{cu}^{max}-1}$ is an exclusively convex polygon in the set of unselected users, i.e., $\Psi - \cup_{r=1}^{i} \cup_{j=0}^{r-1} \Theta_{r,N_{cu}^{max}-j}$ for $(1 \leq i \leq N_{cu}^{max} - 1)$.*

Proof. Let $N_{cl,i}$ denote the number of clusters of size i and $cl_{j_1}, ..., cl_{j_{N_{cl,N_{cu}^{max}}}}$ be the clusters of size N_{cu}^{max}. Suppose that $\Theta_{1,N_{cu}^{max}} = \{u_{1,cl_{j_1}}^{G_{opt}}, u_{1,cl_{j_2}}^{G_{opt}}, ..., u_{1,cl_{j_{N_{cl,N_{cu}^{max}}}}}^{G_{opt}}\} = \{u_{i_1}, ..., u_{i_{N_{cl,N_{cu}^{max}}}}\}$. By contradiction, we assume there exists user u_j such that u_j belongs to the convex hull for $\{u_{i_1}, ..., u_{i_{N_{cl,N_{cu}^{max}}}}\}$, but $u_j \notin \{u_{i_1}, ..., u_{i_{N_{cl,N_{cu}^{max}}}}\}$. Furthermore, suppose that the convex polygon's vertices are $\{u_{v_1}, ..., u_{v_q}\}$. For G_{opt}, we assume that u_j is the user at the s-th position in some cluster. Let G_l denote the clustering function obtained by swapping u_{v_l} from the polygon and u_j in G_{opt} for $l \in [1, q]$. From the optimality of G_{opt}, it is inferred that $(P_{TX}(G_{opt}) - P_{TX}(G_l)) < 0$. Now, we rewrite $(P_{TX}(G_{opt}) - P_{TX}(G_l))$ at (X_{opt}, Y_{opt}) by means of the system parameters as:

$$\gamma^{arb} Q \sigma^2 (d_{i_l}^{\alpha} - d_j^{\alpha})((1+\gamma^{arb})^{N_{cu}^{max}-1} - (1+\gamma^{arb})^{N_{cu}^{max}-s}) \quad (7)$$

From the inequality $P_{TX}(G_{opt}) - P_{TX}(G_l) < 0$ and from (7), it is concluded that $d_{i_l} - d_j < 0$ for $l \in [1, q]$. Since the points in $\{u_{v_1}, ..., u_{v_q}\}$ create the convex polygon, the set of inequalities $d_{i_l} - d_j > 0$ also demarcates the convex polygon Γ_i. Now, for any $w \in [1, q]$, let's consider the edge from Γ_i corresponding to $d_{i_w} = d_j$. Since Γ_i is convex, all the vertices in Γ_i lie in the halfplane defined by $d_{i_w} > d_j$. This implies that the intersection of the inequalities $d_{i_l} - d_j < 0$ $(\forall l \in [1, q])$ is an empty set. This contradicts the initial assumption that the points corresponding to the users in $\Theta_{1,N_{cu}^{max}}$ do not create the exclusively convex polygon. By a similar procedure, the second users of the clusters of size N_{cu}^{max} and the first users of the clusters of size $N_{cu}^{max}-1$ should also create an exclusively convex polygon in the set remained from Ψ, and so on so forth for the next users of all clusters. This completes the proof. □

In order to apply Theorem 1, we now find all subsets of the users forming an exclusively convex polygon. We develop our algorithm based on a method provided in [9], where general

convex polygons (CPs) are found based on a target vertex size. The solution in [9] cannot be immediately used in our case, as we need to find CPs with a certain total number of points belonging either to the vertices or to the interior of the CP. Hence, we extend the general solution in [9] to enable a selection of the exclusively convex polygons of an arbitrary size m from the set Ψ, see Algorithm 1. The set of points Ψ represents the locations of the users in the xy-plane. Following [9], the principle of finding such CPs is to first set the lowermost point in the polygon (line 2 in Algorithm 1) and, then, create sequences of vertices by collecting all next candidate points (users) to be included in the sequence (lines 3 and 5). The addition of the points to the sequence should not violate the convexity presumption of the polygon (line 5). After adding new vertex to our sequence of vertices (line 9), we check the number of enclosed points by the CP of the sequence (lines 7 and 12). Then, sequences containing more points than m are excluded from the vertex search.

Following the proposed search for polygons in Algorithm 1, we now find the optimal clustering using Theorem 1. Note that, in Theorem 1, the size of the clusters is prespecified. Hence, we should first find all possible sets of the cluster sizes $\{N_{cu,1}, \ldots, N_{cu,cl}\}$ with a maximum cluster size of N_{cu}^{max}. Then, for each derived set $\{N_{cu,1}, \ldots, N_{cu,cl}\}$, we apply Theorem 1 as follows. To determine the first users in the NOMA clusters with a size of N_{cu}^{max}, we execute Algorithm 1 for $m = N_{cl,N_{cu}^{max}}$ and collect all candidate sets of users. Next, for each obtained candidate set, we determine the second users in the clusters with a size of N_{cu}^{max} as well as the first users in the clusters with a size of $N_{cu}^{max} - 1$. To this end, we apply Algorithm 1 for $m = N_{cl,N_{cu}^{max}} + N_{cl,N_{cu}^{max}-1}$ over the set of the remaining users and so on and so forth until every user is assigned to one cluster.

Algorithm 2 summarizes the whole proposed solution to (3). First, the optimum position of the FlyBS is determined (line 1) using CVX for each clustering derived by Algorithm 1. Next, the clustering and corresponding position yielding the smallest transmission power are selected (lines 2-3) and the transmission power is allocated (line 4) via (4).

The computational complexity of the proposed solution is determined by the number of clustering candidate options and by the calculation of the transmission power and the FlyBS's position from the simulations. By caluclating the order of complexity with respect to the system parameters, the total computational complexity is $O({N_{cl}}^{0.83N_{cu}^{max}} {N_u}^{1.81N_{cu}^{max}})$. Despite the exponential complexity with respect to N_{cu}^{max}, complexity is still low and allows a fast enough processing for practical applications, as N_{cu}^{max} is relatively low in real-world applications due to an implementation complexity of SIC for large N_{cu}^{max}.

IV. Simulations and results

In this section, we provide details of models and setting adopted for the performance evaluation and we demonstrate the advantages of the proposal over state-of-the-art schemes.

Algorithm 1 Find all exclusively convex polygons of size m

$U_q \subset \Psi$: halfspace of points with y-coordinate larger than that of q
$H_{q,w}$: halfspace to the left of the directed line qw
$S = \Psi$: initial set for the lowermost point when counting polygons
$\Omega_s \leftarrow []$: Matrix to store sequences of vertices on top of s
$CP(\Phi)$: convex polygon (CP) obtained from the vertices Φ

1: **while** $S \neq \emptyset$ **do**
2: $s \leftarrow$ point with smallest y-coordinate in S, $\Omega_s \leftarrow [\Omega_s, s]$
3: **for** every point $q \in U_s$ **do** add q to every row in Ω_s
4: delete rows in Ω_s whose size of CP is larger than m
5: **for** every $w \in U_s \cap H_{s,q}$ **do** add w to every row in Ω_s
6: **for** $j = 1$, $j \leq$ rows(Ω_s), $j++$ **do**
7: delete row j if $|CP(\Omega_s(j,:))| > m$
8: **end for**
9: $q \leftarrow w$
10: **end for**
11: **end for**
12: delete rows in Ω_s whose size of CP is not equal to m
13: $S \leftarrow S - \{s\}$
14: **end while**

Output: Ω_s, $s \in \Psi$: vertex sequences of convex polygons of size m

A. Simulation scenario and models

We consider a scenario with 60–240 active users in an outdoor event (sports, festivals, etc.) within 500 m×500 m area. The users are assumed to leave the area through four exit paths in the $\pm$ directions of the x and y axes with $N_u/4$ users on each path. We consider three crowds on each path with $N_u/12$ users in each crowd with the speed of users in the first, second, and third crowds uniformly distributed over intervals of [0.6, 1.4] m/s, [1, 2] m/s, and [1.5, 2.5] m/s, respectively.

Following [8] we assume $\alpha = 2$. Omni-directional antennas with gains of 7 dBi and 0 dBi for the FlyBS and the users are considered, respectively. The radio frequency of 2.6 GHz and the bandwidth of 100 MHz are selected. Note that the bandwidth is equal for all clusters. Spectral density of noise is set to -174 dBm/Hz. The allowed range for the FlyBS's altitude is H_{min} =150 m and H_{min} =350 m. The maximum transmission power P_{TX}^{max} is set to 1 W. Each simulation lasts for 1200 seconds with the problem (3) solved every second. The results are averaged out over 100 simulation drops.

We compare our proposal with following state-of-the-art works: i) maximization of the minimum sum capacity among all clusters via FlyBS's positioning and NOMA pairing [8] (labeled as *max-min-C*), ii) transmission power minimization via NOMA clustering for static base stations (SBSs) [10] (*min-Tx*), iii) sum capacity maximization via NOMA clustering for the SBS [11] (*max-C*), iv) enhanced version of [10] with our proposed FlyBS positioning (*E-min-Tx*), and v) enhanced

Algorithm 2 Optimal user clustering and FlyBS positioning

1: derive optimal $\boldsymbol{l}_M[k]$ via CVX for each clustering from Alg. 1
2: calculate P_{TX} for each clustering according to (5)
3: optimal $G \leftarrow \text{argmin}_G\, P_{TX}$
4: calculate $p_{i,j}^{G,T}$ from (4)

Output: optimal $\left[G, p_{i,j}^{G,T}, \boldsymbol{l}_M\right]$

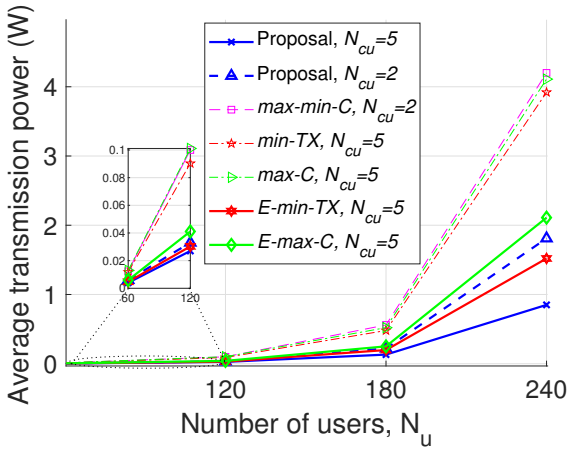

Fig. 2: Transmission power required for N_u users, $C^*_{arb} =$ 4 Mbps.

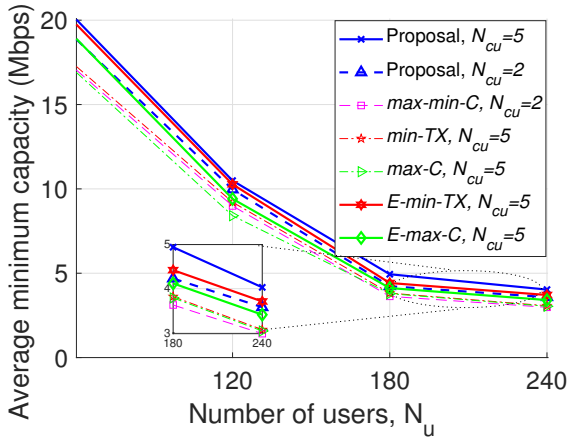

Fig. 3: Average minimum capacity achieved by all N_u users.

version of [11] with our proposed positioning (*E-max-C*).

B. Simulation results

In this subsection, we present and discuss simulation results. Fig. 2 demonstrates the transmission power increases with the number of users, because less bandwidth is available for each user and a larger transmission power is required (see (4)). All benchmarks require notably larger transmission power compared to our proposed solution. As *max-min-C* supports only $N_{cu}^{max} = 2$, we compare it with the proposed solution for $N_{cu}^{max} = 2$ and the proposal reduces the transmission power by 67%. By an extension of the cluster size to $N_{cu}^{max} = 5$, the transmission power required by our proposal is further reduced by 54% compared to the proposal with $N_{cu}^{max} = 2$. This is because for a larger cluster size, fewer clusters are created and more bandwidth can be allocated to each cluster resulting in a lower transmission power. Overall, the proposed solution (with $N_{cu}^{max} = 5$) reduces the transmission power by 78% and 80% with respect to *min-Tx*, *max-C*, respectively. The extension of *min-Tx* and *max-C* with our proposed FlyBS positioning towards *E-min-TX* and *E-max-C* demonstrates that our positioning reduces the transmission power of the original *min-TX* and *max-C* by 67% and 59%, respectively.

Fig. 3 shows that the average minimum capacity η^* decreases with the number of users, because the more users are served by the FlyBS, the narrower channel is allocated to each user, as the whole available bandwidth is split among clusters. The proposed solution improves the average η^* compared to *max-min-C* by up to 20% (for $N_{cu}^{max} = 2$). In addition, the average η^* is enhanced by 17% for our proposal if N_{cu}^{max} is increased to 5. In total, compared to *max-min-C*, *min-Tx*, *max-C*, *E-min-Tx*, *E-max-C* the proposed solution (for $N_{cu}^{max} = 5$) increases the average η^* by 35%, 44%, 59%, 11%, and 20%, respectively.

V. Conclusions

In this letter, we have provided a geometrical approach to derive NOMA clustering, transmission power allocation to the users, and the FlyBS's positioning maximizing the minimum capacity among all users. We have shown that the proposed solution enhances the minimum capacity by tens of percent with respect to state-of-the-art work. In the future, the scenario with multiple FlyBSs shall be studied.

References

[1] T. Hou, et al, "UAV-to-Everything (U2X) Networks Relying on NOMA: A Stochastic Geometry Model," *IEEE Trans. Veh. Technol.*,July 2020.

[2] H. Zhang, et al, "Energy Efficiency Optimization for NOMA UAV Network With Imperfect CSI," *IEEE J. Sel. Areas Commun.*, 2020.

[3] R. Zhang, et al, "Joint Location and Transmit Power Optimization for NOMA-UAV Networks via Updating Decoding Order," *IEEE Wireless Commun. Lett.*, vol. 10, no. 1, 2021.

[4] D. Hu, et al, "Joint Position, Decoding Order, and Power Allocation Optimization in UAV-Based NOMA Downlink Communications," *IEEE Syst. J.*, vol. 14, no. 2, June 2020.

[5] L. Lei, et al, "On Power Minimization for Non-orthogonal Multiple Access (NOMA)," *IEEE Commun. Lett.*, vol. 20, no. 12, Dec. 2016.

[6] J. Zhao, et al, "NOMA-Aided UAV Data Collection System: Trajectory Optimization and Communication Design," *IEEE Access*, vol. 8, 2020.

[7] M.Nikooroo and Z.Becvar, "Optimal Positioning of Flying Base Stations and Transmission Power Allocation in NOMA Networks", *IEEE Trans. Wireless Commun.,* 2021.

[8] M. Nguyen and L. Le, "NOMA User Pairing and UAV Placement in UAV-Based Wireless Networks," *ICC*, 2019.

[9] J. Mitchell, et al., "Counting convex polygons in planar point sets," *Information Processing Letters*, Vol. 56, No. 1, 1995.

[10] F. Guo, et al, "QoS-aware User Grouping Strategy for Downlink Multi-Cell NOMA Systems," *IEEE Trans. Wireless Commun.*, Early Access.

[11] S. P. Kumaresan, et al, "Efficient User Clustering Using a Low-Complexity Artificial Neural Network (ANN) for 5G NOMA Systems," *IEEE Access*, vol. 8, 2020.

3.4 Minimization of FlyBSs propulsion power with guarantee of sum capacity

Next, we focus on the major difference between airship-based FlyBSs and static BSs, that is, the energy consumption due to FlyBSs' mobility. To this end, we investigate the extent of FlyBSs remaining idle like a static BS, as well as FlyBSs considering a relocation to enhance the system's performance. Such movements come at a cost of propulsion energy consumption. Hence, to study such trade-off between performance and energy consumption, we target to minimize the propulsion energy consumption of the FlyBSs. Such task is done on the condition that a minimum "expected" sum capacity in the network is guaranteed all the time. To this end, an analytical solution to the FlyBSs' positioning is proposed.

In the following, we present the studied problem along with the results (representing the references [C4] and [J1]).

Reducing Energy Consumed by Repositioning of Flying Base Stations Serving Mobile Users

Zdenek Becvar, Pavel Mach, Mohammadsaleh Nikooroo
Department of Telecommunication Engineering, Faculty of Electrical Engineering
Czech Technical University in Prague
Technicka 2, 166 27 Prague, Czech Republic
{zdenek.becvar, machp2, nikoomoh}@fel.cvut.cz

***Abstract*—Unmanned Aerial Vehicles (UAVs), acting as flying base stations (FlyBSs), are seen as a promising solution for future mobile networks, as the FlyBSs can serve space and time varying heterogeneous traffic in areas where deployment of conventional static base stations is uneconomical or infeasible. However, an energy consumption of the FlyBSs is a critical issue. In this paper, we target a scenario where the FlyBSs serve slowly moving users, e.g., visitors of an outdoor music festival or a performance. In such scenario, rotary-wing FlyBSs are not efficient due to a high energy consumption while not moving (given by an effect of a "helicopter" dynamics). Hence, we consider small airships or balloons. We develop a closed-form solution that determines new positions of the FlyBSs so that the energy consumption for a movement of the FlyBSs is reduced significantly (by 45-94% depending on the number of deployed FlyBSs) while sum capacity of the users is decreased only marginally (less than 1% for before-mentioned energy savings). Moreover, the proposed solution does not require any prediction of users' movement, thus, it is not affected by the prediction error or uncertainty of the users' behavior.**

***Index Terms*—Energy consumption, mobile users, flying base station, UAV, 6G**

I. Introduction

In future mobile networks, Unmanned Aerial Vehicles (UAVs) acting as flying base stations (FlyBSs) are expected to help with serving a diverse and space-time varying requirements of users and machines, or during emergency situations [1]–[3]. The concept of FlyBSs, however, imposes many challenges (listed, e.g., in [2], [4]), such as a determination of optimal positions of the FlyBSs, optimization of trajectories of FlyBs, or mobility and radio resource management, to name a few.

Another critical challenge is related to an energy consumption of the FlyBSs. The FlyBSs are supposed to be powered by energy sources of a limited capacity used not only for communication with the users and the network, but also for flying. Consequently, an operational time of the FlyBSs is reduced if the energy would not be used in an efficient way. The energy or power consumption of the FlyBSs is considered, e.g., in [5]–[9]. In [5], [6], the authors minimize transmission power under the constraint of guaranteeing data rate for all user equipment (UE). In [7], the energy consumption for communication is constrained by keeping at least the same size of coverage area and the lower consumption is achieved via movement of the FlyBSs providing connectivity to the devices at certain positions (stopping points). An energy efficient collection of data from sensors [10] by means of the FlyBSs is addressed in [8], [9]. In [8], the scheduling of the FlyBSs for data collection and forwarding of the data to conventional static base stations (SBSs) is proposed. In [9], the minimization of a transmission power for communication of sensors in a hierarchical manner (via cluster heads) with the FlyBSs is based on a scheduling of communication of individual cluster heads and the FlyBSs. In [11], [12], the objective is to minimize the energy consumed for both communication and movement of the FlyBSs in the scenario where the FlyBSs flight over a set of static ground nodes and exchange data with each of them sequentially. To this end, the authors design an algorithm that plans trajectories among the ground nodes and communication/hovering time in order to minimize the overall energy consumed by the FlyBS. All these works targeting energy efficiency take into account only static UEs with known coordinates, which are not changing over time. Such scenario corresponds, for example, to a collection of data from static IoT/machine-type devices, but the solution cannot be applied to a dynamic environment with moving UEs due to complexity of the solution and the fact that the solutions rely on the knowledge of future UEs' positions.

Mobile UEs are considered, e.g., in [13]–[16]. In [13], however, only single FlyBS is considered and an extension towards multi-FlyBS scenario is not straightforward. Then, in [14], the authors solve the positioning jointly with association of the UEs via k-means algorithm. In [15], the authors optimize jointly the network capacity and energy consumption of the UEs. In [16], the authors focus on the coverage maximization and interference mitigation. Nevertheless, none of these papers consider the energy consumption of the FlyBSs.

This work was supported by the Czech Science Foundation (GACR) under Grant P102-18-27023S.

The energy consumption in the scenario with the mobile UEs is addressed in our prior works [15], [17]. Specifically, in [15], we consider the energy efficiency only at the UE side. Then, in [17], we jointly optimize a transmission power of the FlyBSs and the power spent for movement of the FlyBSs while communication capacity is not impaired. To this end, a closed-form solution for transmission power setting and determination of the FlyBS coordinates is proposed in [17]. Such solution is easy to implement, but it is designed and suitable only for a single FlyBS. Also, the closed-form solution tracks the UEs strictly and, thus, it can lead to a high energy consumption for repositioning of the FlyBS if few UEs move rapidly despite the fact that the sum capacity of all UEs would change only negligibly.

In this paper, we focus on a saving of the energy spent for movement of FlyBSs while guaranteeing close-to-optimum sum capacity of the users in the scenario where the FlyBSs provide continuous communication service to the mobile (*moving*) users, such as pedestrians. In related works, where the authors also target the energy minimization, see e.g., [11], [12], the addressed problem is an analogy to the one with a traveling salesman problem as the positions of the UEs are known and, more important, do not change over time. In our case, we assume mobile UEs, thus, there is no knowledge of future positions of these UEs. As a result, any advanced planning of the FlyBS trajectory is not easy and the FlyBSs should adjust their positions only based on the actual positions of the UEs. Of course, such problem could be solved via prediction of the users' movement. Nevertheless, the prediction of the users' movement is a complex problem with a significant uncertainty in terms of the prediction accuracy.

To this end, we propose a new concept of the FlyBS movement optimization that eliminates redundant movement of the FlyBSs while circumventing the need for an accurate prediction or estimation of the future users' movement. Under a realistic assumption of the known actual positions of the UEs (as in many existing works, see, e.g., [11], [18]), we analytically determine suitable future positions of the FlyBSs so that the users' sum capacity remains close to an achievable maximum while the energy spent for the flying of the FlyBSs is significantly reduced and, thus, an operational time of the FlyBSs is extended. Unlike many other papers, we consider moving users, for example, pedestrians. In [11], the authors develop a power consumption model for rotary-wing UAVs. The model indicates that the power consumption is relatively high for static or slowly moving rotary-wing UAVs. This is a result of helicopter dynamics, see e.g., [19]. Thus, in the scenarios with pedestrians (e.g., visitors of an outdoor event, music festival) considered in our paper, the optimal position of the FlyBSs will not change significantly and the change will be similar or even lower than the movement speed of the users. Hence, we consider FlyBSs represented by, e.g., small balloons or airships, for which the slow movement or even temporary hovering at the same position is not a drawback from energy consumption point of view [1], [20]. Via simulations, we show that the proposed approach can reduce the energy spent for the FlyBS movement by tens of percent while the impact on the sum capacity is negligible. We show that the energy saving can be controlled by an adjustment of the minor acceptable degradation in the sum capacity.

The rest of the paper is organized as follows. The next section outlines the system model considered in this paper. Then, in Section III, we propose a solution that analytically derives new positions of the FlyBSs so that the energy consumed for flying is reduced and we illustrate the principle of the proposed idea on an example. In Section, IV, simulation scenario and models are outlined and performance of the proposed solution is analyzed and discussed. Last, Section V concludes the paper and outlines potential future works.

II. System Model and problem formulation

In this section, we define our system model and we formulate the problem that will be solved later in the paper.

A. System Model

Let's assume N UEs distributed within an area covered by M FlyBSs. The positions of the UEs are defined as $\boldsymbol{U} = \{\boldsymbol{u_1}, \boldsymbol{u_2}, \ldots, \boldsymbol{u_N}\}$, where $\boldsymbol{u_n} = [x_n, y_n, z_n] \in \mathbb{R}^3$ for $\forall n \in \langle 1, N \rangle$. Similarly, the FlyBSs are located at the positions $\boldsymbol{V} = \{\boldsymbol{v_1}, \boldsymbol{v_2}, \ldots, \boldsymbol{v_M}\}$, where $\boldsymbol{v_m} = [x_m, y_m, z_m] \in \mathbb{R}^3$ for $\forall m \in \langle 1, M \rangle$. Note that both UEs and FlyBSs are moving over time and the coordinates of each FlyBSs are updated depending on the UEs movement. Initial positions of all FlyBSs and an association of the UEs to the FlyBSs are solved via k-means clustering algorithm [14].

The theoretical optimum position of the m-th FlyBSs from the sum capacity point of view is represented by the center of gravity of the UE's positions [13], i.e., $X_{opt,m} = \frac{1}{n_m} \sum_{\forall n \in N_m} \alpha_n x_n$ and $Y_{opt,m} = \frac{1}{n_m} \sum_{\forall n \in N_m} \alpha_n y_n$ where n_m is the number of the UEs associated to the m-th FlyBS, $\alpha_n \in \langle 0, 1 \rangle$ is the relative throughput requirement of the UE_n and N_m is the set of UEs associated to the m-th FlyBS. Note that the FlyBSs are supposed to operate in an outdoor area, thus, we can assume that the positions of the UEs are known as in related works (see, e.g., in [11], [18]). As the UEs move, the k-means clustering algorithm is continuously repeated to determine jointly the association of the UEs to the FlyBSs and the optimal positions of the FlyBSs as in [14]. Note that we consider 3D positions of all entities, however, the movement takes place in 2D space and the altitudes of the FlyBSs and the UEs are set to the constant values of 150 m [1], [21] and 1.5 m, respectively, for the sake of clarity of the analytical derivation of the solution. An extension towards 3D space is straightforward and analogical to the derivation of the solution for 2D.

The downlink communication capacity of the n-th UE connected to the m-th FlyBS is defined as:

$$C_{n,m} = B_{n,m} \times \log_2 (1 + \gamma_{n,m}) \tag{1}$$

where $B_{n,m}$ stands for the channel bandwidth between the n-th UE and the m-th FlyBS (bandwidth is the same for all

UEs connected to the same FlyBSs), and $\gamma_{n,m}$ represents the SINR between the n-th UE and the m-th FlyBS defined as:

$$\gamma_{n,m} = \frac{P_m^T h_{n,m}}{\sigma^2 + \sum_{i=1,\ i\neq m}^{M} P_i^T h_{n,i}} \tag{2}$$

where P_m^T is the transmission power of the m-th FlyBS that serves the n-th UE, P_i^T stands for the transmission power of the i-th FlyBS that interferes to the communication of the n-the UE, $h_{n,m}$ is the the channel gain between the n-th UE and its serving m-th FlyBS, $h_{n,i}$ represents the channel gain between the n-th UE and the i-th interfering FlyBS, and σ is the noise.

All FlyBSs use the same band, thus, interference is present at the UEs attached to different FlyBSs. The overall bandwidth $B_m = N_m B_{n,m}$ is the same for all FlyBSs and each FlyBS assigns orthogonal channels of the same bandwidth to its underlaying UEs.

Note that the communication between the FlyBSs and the network (e.g., communication with the existing static BSs) and its specific implementation or potential limitation does not change our proposed solution. Thus, like in many related works, we assume a high capacity connection of the FlyBSs to the network via, for example, optical wireless links [22], [23].

For the scenario with pedestrians considered in our paper, the rotary-wing FlyBSs are not convenient due to their relatively high power consumption in static or slowly moving mode (this is a result of an effect in helicopter dynamics, see, e.g., [19] or the power consumption model developed in [11]). Thus, we focus on the FlyBSs represented, e.g., by balloons or airships, for which the power consumption is proportional to the distance traveled between two points and the power consumption is negligible if these FlyBSs are not moving as the gravity if compensated by a static buoyancy [24]. We assume that the FlyBS follows the shortest distance between a current location $v_k(t) = [X_{cur},\ Y_{cur}]$ and a new determined location $v_k(t+1) = [X_{new},\ Y_{new}]$, i.e., the FlyBS moves for the distance $D_{mov} = \sqrt{(X_{cur} - X_{new})^2 + (Y_{cur} - Y_{new})^2}$. Then, the flying energy is defined as $E_F = D_{mov} \times e_{mov}$ where e_{mov} represents the instantaneous unit energy spent for the movement per unit of distance (e.g., per meter). The hovering energy for balloons, airships, or similar UAVs is considered to be negligible.

B. Problem formulation

Our objective is to reduce the energy spent by all FlyBSs for flying while the sum capacity of the moving UEs is still close to the sum capacity that would be achieved if the FlyBSs would be in their optimum positions from the capacity point of view. Note that our proposed solution is independent of the way how the optimum position is determined. Hence, the problem of the optimum position determination is out of scope of this paper and we adopt the approach based on the center of gravity and k-means (see previous subsection) for our investigation.

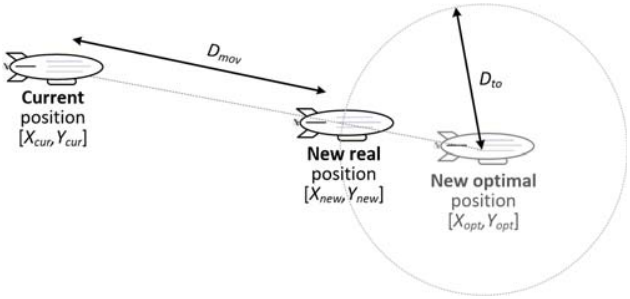

Figure 1. Illustration of the core idea of the proposed solution for elimination of redundant movement.

The optimization problem is then defined as:

$$\begin{aligned} &\underset{\boldsymbol{V}\in\boldsymbol{R}^{2M}}{\text{argmin}} && \sum_{\forall M} E_F \\ &\text{s.t.} && \sum_{i=1}^{N}\sum_{j=1}^{M} C_{i,j} \geq C_{opt} \times \epsilon \end{aligned} \tag{3}$$

where C_{opt} is the capacity achieved by the UEs if the FlyBSs are deployed in the positions X_{opt} and Y_{opt} that lead to the maximum capacity, and $\epsilon \in \langle 0, 1\rangle$ is the constant indicating acceptable degradation of the capacity. Note that the optimum position depends on the actual position of the moving UEs and is derived via k-means according to [14] as explained in previous subsection.

III. Positioning of FlyBSs reducing energy spent for movement

In this section, we propose an approach to derive the new positions of the FlyBSs with respect to the UEs movement. The basic idea behind the solution introduced in this section is that, not every movement of the UEs requires repositioning of the FlyBSs to the position that gives maximum sum capacity (denoted as the new optimal position), because a potential degradation of the UEs capacity could be anyway negligible. Instead, we suggest that the FlyBS does not follow exactly the optimum position [X_{opt},Y_{opt}], but stays in a certain distance D_{to} from the optimum. Thus, instead of the FlyBS traveling to the optimum position, it moves only to the new real position [X_{new}, Y_{new}], which is between the optimum and current positions as illustrated in Fig. 1. This way, we are able to notably decrease the energy consumption of the FlyBSs and prolonging their operation time.

The new real position of the FlyBS is determined knowing the current FlyBS position [X_{cur},Y_{cur}], the new optimal position of the FlyBS [X_{opt},Y_{opt}] (derived from the actual positions of UEs as they move), and the distance D_{to} to this new optimal position. The new optimal position is determined from the actual positions of the UEs associated to the given FlyBSs. The assumption on the knowledge of the UEs position is reasonable as the FlyBSs are assumed to serve outdoor UEs where relatively accurate positioning of the UEs is possible; this assumption is commonly considered in most of the related

works as explained in Section II. As we show via simulations, common positioning errors of the satellite navigation systems in an order of a meter [25] does not impact on the performance notably. The new real position is represented by an intersection of the straight line between the current and new optimal positions with the circle positioned so that its center corresponds to the new optimal position of the FlyBS and radius D_{to}.

Lemma 1. *The new coordinates [X_{new}, Y_{new}] of the FlyBS are determined in a closed-form as:*

$$X_{new} = X_{opt} \mp \frac{\sqrt{(2X_{opt}(1+S^2))^2 - 4(1+S^2)(X_{opt}^2)(1+S^2) - D_{to}^2)}}{2(1+S^2)} \quad (4)$$
$$Y_{new} = Y_{opt} + (X_{new} - X_{opt})S$$

where S represents the slope of the line and it is defined as $S = (Y_{cur} - Y_{opt})/(X_{cur} - Y_{opt})$.

Proof. From Fig. 1, we can see that the movement from the current to the new optimal position follows the straight line that interconnects the current coordinates [X_{cur},Y_{cur}] to the optimal ones [X_{opt},Y_{opt}]. Also the new position [X_{new},Y_{new}] lies on that line. By using equation of the line, we can write: $Y_{new} = Y_{opt} + (X_{new} - X_{opt})S$. Now, we need to determine the intersection of the line with the circle with the center at [X_{opt},Y_{opt}] and with the radius D_{to}. As the new real position of the FlyBS lies on the circle, we can define the circle as: $D_{to}^2 = (X_{new} - X_{opt})^2 + (Y_{new} - Y_{opt})^2$. Then, inserting $Y_{new} = Y_{opt} + (X_{new} - X_{opt})S$ to the equation of the circle and after several few mathematical operations, we get:

$$X_{new}^2(1+S^2) - X_{new}2X_{opt}(1+S^2) + X_{opt}^2(1+S^2) - D_{to}^2 = 0 \quad (5)$$

Solving this quadratic equation, we get:

$$X_{new} = X_{opt} \pm \frac{\sqrt{(2X_{opt}(1+S^2))^2 - 4(1+S^2)(X_{opt}^2)(1+S^2) - D_{to}^2)}}{2(1+S^2)} \quad (6)$$

Then, by insertion of X_{new} to the equation of the line, we get Y_{new} coordinate as $Y_{new} = Y_{opt} + (X_{new} - X_{opt})S$. ■

Note that the Lemma and proof are defined for the case when $X_{cur} \neq X_{opt}$. In case $X_{cur} = X_{opt}$ (i.e., horizontal line), $X_{new} = X_{cur} = X_{opt}$ and $Y_{new} = Y_{opt} \pm D_{to}$. We can simplify the determination of both coordinates analogically for the vertical line (i.e., if $Y_{cur} = Y_{opt}$).

Obviously, the solution to quadratic equation gives two sets of new coordinates [X_{new1},Y_{new1}] and [X_{new2}, Y_{new2}]. As the new coordinates [X_{new},Y_{new}], the set that leads to a less movement is selected, i.e., the set that leads to a smaller distance $\sqrt{(X_{cur} - X_{new*})^2 + (Y_{cur} - Y_{new*})^2}$ where X_{new*} (Y_{new*}) stands for the x (y) coordinate corresponding to X_{new1} and X_{new2} (Y_{new1} and Y_{new2}).

The above described approach leads to a "smoothening" of the FlyBSs' movement. In other words, the FlyBSs do not copy the movement of the UEs accurately, but naturally avoids a redundant and not beneficial movement whenever possible as illustrated in Fig. 2.

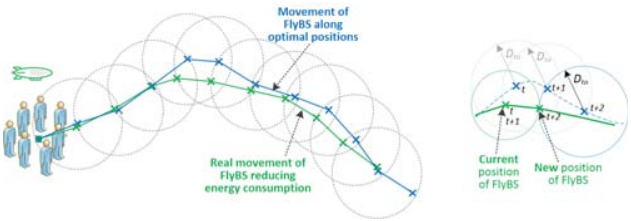

Figure 2. Example of FlyBS movement considering proposed concept (green color) with respect to optimum positions (blue color). Right figure shows zoom of the middle part of left figure to indicate how and when the movement takes place. Each cross determines decision instance, i.e., at these positions new position of FlyBS is determined.

IV. Performance evaluation

In this section, first, simulation scenario, models, and metrics are outlined and summarized. Then, we provide discussion of simulation results.

A. Simulation scenario, models, and metrics

We assume an area with a size of 1000 x 1000 m. Within this area, 1000 UEs are dropped as the FlyBSs are supposed to serve heavily loaded scenarios with a high UE density. A half of the UEs (i.e., 500 UEs) is dropped randomly into the area and their movement corresponds to random walk mobility model with a speed of 1 m/s. The second half of the UEs is randomly distributed into $N_{cr} = 6$ "crowds" and follows a crowd mobility model inspired by [26]. Movement of each crowd is defined by coordinates of its center $W = \{w_1, w_2, \ldots, w_{N_{cr}}\}$, where $w_{N_{cr}} \in R^2$ for $\forall n_{cr} \in \langle 1, N_{cr} \rangle$ and by a cluster radius $R_{cluster} = 20$ m, which is the same for all clusters. Then the UEs of the second half are randomly assigned to one of these clusters and dropped within the corresponding radius. Each UE in the cluster follows the global movement direction of the center of the cluster, which is moving with a speed of 1 m/s. On the top of it, each UE within the cluster can also change its direction by $\pm 15^\circ$ and speed by $\pm$ 0.4 m/s with respect to the cluster center. Thus, all UEs in the cluster move with a speed from range of 0.6 to 1.4 m/s. Note that the UEs of the second group (i.e., crowd) cannot leave the cluster radius. The UEs are served by one to five FlyBSs. The optimal FlyBS positioning and the association of the UEs to the FlyBSs are done jointly by k-means algorithm according to [14] as indicated in the system model.

To determine the channel quality among the UEs and the FlyBSs, we follow free space path loss model. We assume carrier frequency of 2.6 GHz, bandwidth of 20 MHz, and transmission power of the FlyBSs is set to a common value of 15 dBm. Noise with a density of -174 dBm/Hz is also considered and interference perceived by the UEs from neighboring FlyBSs is determined as a sum of all interfering signals.

The simulations are of a 1800 seconds duration and the simulations are repeated 500 times with different UEs deployment and movement in each simulation run to suppress an impact

Table I
SIMULATION PARAMETERS

Parameter	Value
Simulation area	1000 m x 1000 m
Carrier frequency	2.6 GHz
Bandwidth	20 MHz
Number of UEs	1000
Number of FlyBSs	1, 3, 5
Tx power of FlyBSs	15 dBm
Height of FlyBSs	150 m [1] [21]
Height of UEs	1.5m
Noise power spectral density	-174 dBm/Hz

of randomness. Key simulation parameters and settings are summarized in Table I.

The proposed solution is compared with performance of the optimum positioning providing maximum capacity (as proposed, e.g., in [13], [14]). We define two performance metrics:

- *Relative energy consumption* of FlyBSs – determined as an average energy consumption of individual FlyBSs for movement over whole simulations related to the consumption of the energy by FlyBSs moving in the optimum positions (determined by k-means according to [14]).
- *Relative sum capacity* of the UEs – defined as a total capacity of all UEs averaged over whole simulation time related to the capacity achieved by the FlyBSs in the optimum positions (determined by k-means according to [14]).

Note that we present both performance metrics as relative values (from 0 to 1) with respect to performance in the optimum positions of the FlyBSs. The relative metrics eliminate an impact of specific energy consumption model. Thus, in all figures, the optimum positioning from the capacity point of view reaches relative capacity and energy consumption of 1.

B. Simulation results and discussion

First, we investigate the relative energy consumed by the FlyBSs for flying in Fig. 3. Note that the optimum positioning according to [14] is independent of D_{to} (the FlyBSs are always in the optimum positions). Thus, the energy consumption is always maximum and relative energy consumption of the optimum positioning is always equal to 1.

The energy consumption of the FlyBSs for the proposed solution reduces with increasing distance from the FlyBS to the optimum position (depicted on x-axes). This is a result of the fact that the FlyBSs do not follow exactly the optimum position, but avoid redundant movements, which cost additional energy while having only negligible impact on the sum capacity. The energy consumption goes down rapidly even for lower values of D_{to} (more than 35% and 45% energy saved for D_{to} equals to 10 m and 20 m, respectively, for all numbers of FlyBSs). Then, the energy consumption starts decreasing more slowly with D_{to}. Such behavior results from the fact that for a larger D_{to}, any notable redundant movement of the FlyBSs is already avoided, so there is less space for additional savings.

Fig. 3 also shows that if only one FlyBS is deployed, the energy saving is a bit slower for very low values of D_{to} comparing to 3 or 5 FlyBSs. For example, for D_{to} = 2 m, the saving is 13%, 22% and 20% for 1, 3, and 5 FlyBSs, respectively; however, for D_{to} = 50 m, the saving is 83%, 66% and 63% for 1, 3, and 5 FlyBSs, respectively. The reason for such behavior is the fact that for one FlyBS, the distribution of the UEs in whole area is rather homogeneous despite the crowds. Thus, in fact, the FlyBS stays close to the center of the area and its movement is limited (usually up to tens of centimeters per second) due to almost homogeneous deployment of the UEs. Contrary, for more FlyBSs, the whole area is split into several smaller sub-areas, each served by individual FlyBSs, and the distribution of the UEs within these sub-areas is less homogeneous due to a presence of the

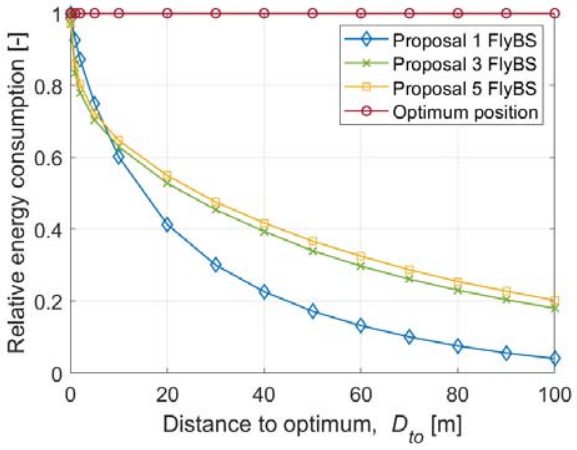

Figure 3. Relative energy consumption of FlyBSs for movement (flying) with respect distance of FlyBSs from their optimum position (determined by k-means [14]).

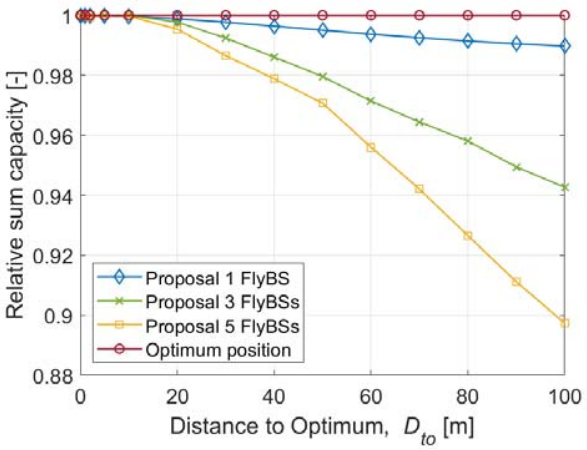

Figure 4. Relative sum capacity of UEs with respect to distance of FlyBSs from of their optimum position (determined by k-means [14]).

crowds of UEs (see description of mobility model in previous subsection). Also, for more FlyBSs, the energy consumption is not decreasing so quickly for larger values of D_{to} due to a need for re-association of the UEs and each re-association can lead to relatively large movement, especially if the FlyBSs stay far from the optimum position.

In previous figure, a significant saving in the energy spent for movement of the FlyBSs is shown for the proposed solution. Now, let's investigate an impact on the sum capacity of the UEs in Fig. 4. Again, the optimum positioning according to [14] is independent of D_{to} and reaches maximum possible sum capacity, thus the relative sum capacity of this algorithm is equal to 1. The sum capacity achieved by the proposed solution slightly decreases as the distance to the optimum position increases. Such trend is expectable, because if the FlyBSs are not in the optimum locations, the sum capacity of the UEs is degraded due to a lower quality of the communication channels for most of the UEs. The more FlyBSs are deployed, the more significant relative decrease in the sum capacity is experienced by the UEs. This trend (more FlyBSs leading to more significant degradation in the sum capacity) is, again, a result of the lower homogeneity of the UEs distribution if the area served by one FlyBS becomes smaller. Then, a relatively small variation of the positions of UEs not followed by update of the FlyBS position can lead to a negative impact on the channel quality, interference, and consequently on the sum capacity. However, an important observation from Fig. 4 is that the relative degradation of the sum capacity with D_{to} is negligible with respect to a decrease in the energy consumption (presented in Fig. 3). For example, for D_{to} = 5 m, the sum capacity is degraded only by less than 0.01% for 1, 3, as well as 5 FlyBSs. Such drop in the sum capacity is absolutely negligible, however, the energy consumption for the same D_{to} is reduced notably by 25%, 30%, and 28% (for 1, 3, and 5 FlyBSs, respectively). Even for a very large D_{to} (e.g. 50 m), the sum capacity is degraded only by 0.5%, 2.0%, and 2.9% for 1, 3, and 5 FlyBS, while 83%, 66%, and 63% of the energy spent by FlyBSs is saved. Thus, the energy saving is many times (ten to hundred times) higher than the decrease in the sum capacity.

Taking into account the parameter ϵ expressing an acceptable degradation of the sum capacity (see (3)), we can determine the acceptable D_{to} from Fig. 4 for the given ϵ. For example, if we set $\epsilon = 0.01$, i.e., the degradation of the sum capacity is up to 1%, in Fig. 4, we see that such condition is still fulfilled by D_{to} = 90, 30, and 20 m for 1, 3, and 5 FlyBSs respectively. Then, from Fig. 3, the energy saving is estimated for these values of D_{to} as 94%, 55%, and 45% for 1, 3, and 5 FlyBSs, respectively.

In Fig. 5, we illustrate a behavior of the proposed solution on a sample situation with one FlyBS for 700 simulation steps (i.e., 700 seconds). The figure shows the optimal positions (X and Y coordinates) of the FlyBS over time (red color) and positions of the FlyBS if the proposed solution is applied with four different values of D_{to}. As D_{to} increases, the FlyBS can save energy by avoiding redundant movement.

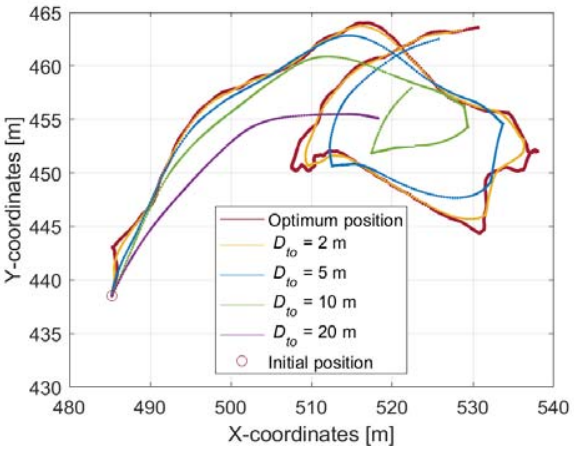

Figure 5. Illustrative example of an impact of D_{to} on movement (coordinates) of one FlyBS over time, red color represents optimum positions (maximum sum capacity) determined by k-means, other colors correspond to the FlyBS positions over time for proposed solution with different D_{to}.

V. Conclusions

In this paper, we have proposed a closed-form solution that reduces the energy consumption for movement of the FlyBSs, represented by small airships or balloons, serving the mobile users. The proposed solution saves the energy by avoiding redundant movement of the FlyBSs in case the movement of the users is not significant. The energy saving is at the cost of a marginal reduction in the users' sum capacity. For example, if the capacity degradation is limited to up to 1%, still the energy saving is 94%, 55%, and 45% if 1, 3, and 5 FlyBSs are deployed. An important aspect is that the proposed solution does not require any type of prediction of future users' movement.

In the future, the proposed solution can be enhanced towards consideration of the joint optimization of movement and transmission powers of the FlyBSs.

References

[1] S. Chandrasekharan, et al, "Designing and Implementing Future Aerial Communication Networks," IEEE Communications Magazine, 2016.

[2] L. Gupta, R. Jain, and G. Vaszkun, "Survey of Important Issues in UAV Communication Networks," IEEE Communications Surveys & Tutorials, Vol. 18, No. 2, Secondquarter 2016.

[3] A. Fotouhi, et al, Survey on UAV Cellular Communications: Practical Aspects, Standardization Advancements, Regulation, and Security Challenges, IEEE Communications Surveys Tutorials, Early Access, March 2019.

[4] M. Mozaffari, W. Saad, M. Bennis, Y. Nam, and M. Debbah, "A tutorial on FlyBSs for wireless networks: Applications, challenges, and open problems", IEEE Communications Surveys & Tutorials, 2019.

[5] M. Mozaffari, W. Saad, M. Bennis, and M. Debbah, "Optimal transport theory for power-efficient deployment of unmanned aerial vehicles," IEEE ICC, 2016.

[6] Y. Zeng and R. Zhang, "Energy-Efficient UAV Communication With Trajectory Optimization," IEEE Transactions on Wireless Communications, Vol. 16, No. 6, 2017.

[7] M. Mozaffari, W. Saad, M. Bennis, and M. Debbah, "Unmanned Aerial Vehicle with Underlaid Device-to-Device Communications: Performance and Tradeoffs," IEEE Transactions on Wireless Communications, Vol. 15, No. 6, 2016.

[8] K. Li, W. Ni, X. Wang, R. P. Liu, S. S. Kanhere, and S. Jha, "Energy Efficient Cooperative Relaying for Unmanned Aerial Vehicles," IEEE Transactions on Mobile Computing, Vol. 15, No. 6, June 2016.

[9] A. Abdulla, Z. M. Fadlullah, H. Nishiyama, N. Kato, F. Ono, and R. Miura, "Toward Fair Maximization of Energy Efficiency in Multiple UAS-Aided Networks: A Game-Theoretic Methodology," IEEE Transactions on Wireless Communications, Vol. 14, No. 1, 2015.

[10] I. Chatzigiannakis, A. Kinalis, S. Nikoletseas, J. Rolim, "Fast and energy efficient sensor data collection by multiple mobile sinks," ACM international workshop on Mobility management and wireless access (MobiWac 2007), October 2007.

[11] Y. Zeng, J. Xu, R. Zhang, "Energy Minimization for Wireless Communication with Rotary-Wing FlyBS", IEEE Transactions on Wireless Communications, Vol. 18, No. 4, April 2019.

[12] W. Wu, Y. Zeng, and R. Zhang, "Joint Trajectory and Communication Design for Multi-UAV Enabled Wireless Networks," IEEE Transactions on Wireless Communications, Vol. 17, No. 3, March 2018.

[13] Z. Becvar, M. Vondra, P. Mach, J. Plachy, D. Gesbert, "Performance of Mobile Networks with UAVs: Can Flying Base Stations Substitute Ultra-Dense Small Cells?", European Wireless, 2017.

[14] B. Galkin, J. Kibilda, and L. A. DaSilva, "Deployment of UAV-mounted access points according to spatial user locations in two-tier cellular networks," Wireless Days, 2016.

[15] Z. Becvar, P. Mach, J. Plachy, M.F.P. de Tuleda, "Positioning of Flying Base Stations to Optimize Throughput and Energy Consumption of Mobile Devices", IEEE VTC-Spring 2019, 2019.

[16] H. Huang, A. Savkin, "A Method for Optimized Deployment of Unmanned Aerial Vehicles for Maximum Coverage and Minimum Interference in Cellular Networks," IEEE Transactions on Industrial Informatics, Vol. 15, Issue 5, May 2019.

[17] M. Nikooroo, Z. Becvar, "Joint Positioning of UAV and Power Control for Flying Base Stations in Mobile Networks", IEEE WiMOB 2019.

[18] R. I. Bor-Yaliniz, A. El-Keyi, and H. Yanikomeroglu, "Efficient 3-D placement of an aerial base station in next generation cellular networks," IEEE ICC 2016.

[19] J. G. Leishman, "Principles of Helicopter Aerodynamics," Cambridge University Press, Cambridge, 2006.

[20] K. Gomez, et al. "Aerial Base Stations with Opportunistic Links for Next Generation Emergency Communications," IEEE Communications Magazine 2016.

[21] B. Van der Bergh, A. Chiumento, and S. Pollin, "LTE in the Sky: Trading Off Propagation Benefits with Interference Costs for Aerial Nodes," IEEE Communications Magazine, 2016.

[22] A. Harris, J. J. Sluss, H. H. Refai, and P. G. LoPresti, "Alignment and tracking of a free-space optical communications link to a UAV," Digital Avionics Systems Conference, 2005.

[23] Stefan Roth, Ali Kariminezhad, and Aydin Sezgin, "Base-Stations Up in the Air: Multi-UAV Trajectory Control for Min-Rate Maximization in Uplink C-RAN," IEEE ICC 2019.

[24] W. Zhua, Y. XuJ. Li, and L. Zhang, "Performance analysis of rotatable energy system of high-altitude airships in real wind field," Aerospace Science and Technology, 2020.

[25] A. El Abbous, N. Samama, "A Modeling of GPS Error Distributions," European Navigation Conference (ENC), 2017.

[26] S. Patil, et al, "Modeling and Simulation of Mobility of Crowds," International Conference on Analytical and Stochastic Modeling Techniques and Applications, 2013.

On Energy Consumption of Airship-based Flying Base Stations Serving Mobile Users

Zdenek Becvar, *Senior member, IEEE,* Mohammadsaleh Nikooroo, *Student member, IEEE,* Pavel Mach *Member, IEEE*

***Abstract*—Flying base stations (FlyBSs) can serve space-time varying heterogeneous traffic in the areas, where a deployment of conventional static base stations is uneconomical or unfeasible. We focus on energy consumption of the FlyBSs serving moving users. For such scenario, rotary-wing FlyBSs are not efficient due to a high energy consumption while hovering at a fixed location. Hence, we consider airship-based FlyBSs. For these, we derive an analytical relation between the sum capacity of the users and the energy spent for flying. We show theoretical bounds of potential energy saving with respect to a relative sum capacity guarantee to the users for single FlyBS. Then, we generalize the problem towards multiple FlyBSs and we propose an algorithm minimizing the energy consumption of the FlyBSs serving moving users under a constraint on the minimum relative sum capacity guarantee. The proposed algorithm reduces the energy consumed by the airship-based FlyBSs for flying by dozens of percent at a cost of only a marginal and controlled degradation in the sum capacity. For example, if the degradation in the sum capacity up to 1% is allowed, 55.4%, 67.5%, and 90.7% of the energy is saved if five, three, and one FlyBSs are deployed, respectively.**

***Index Terms*—Energy consumption, sum capacity, trade-off, mobile users, flying base station, unmanned aerial vehicles, 6G**

I. Introduction

Unmanned Aerial Vehicles (UAVs) are applied to many use-cases encompassing space-air-ground-sea applications [1], such as an area monitoring, where ad-hoc communication among the UAVs should be ensured [2] [3]. Besides, the UAVs acting as flying base stations (FlyBSs) are expected to help serving diverse and space-time varying requirements of users during peak traffic periods or emergency situations [4]–[8], or to offload computation from the users [9]. However, as indicated in [5] or [10], the concept of FlyBSs imposes challenges, such as a determination of the FlyBSs' positions, optimization of the FlyBSs' trajectories, or mobility and radio resource management. Another critical challenge is related to energy consumption of the FlyBSs, which are supposed to be powered by energy sources of limited capacity, such as batteries. Moreover, the energy is spent not only for communication with the users, but also for flying. Consequently, an operational time of the FlyBSs is shortened if the energy is not used efficiently.

Zdenek Becvar, Mohammadsaleh Nikooroo, and Pavel Mach are with the Department of Telecommunication Engineering, Faculty of Electrical Engineering, Czech Technical University in Prague, Czech Republic. Emails: zdenek.becvar, nikoomoh, machp2@fel.cvut.cz .

This work was supported by the Czech Science Foundation (GACR) under Grant P102-18-27023S and by the Ministry of Education, Youth and Sports under Grant LTT20004.

Manuscript received April 19, 2021; revised August 16, 2021.

The energy (or power) consumption of the FlyBSs is considered, e.g., in [11]–[28]. In [11], the FlyBS's transmission power allocation to user equipments (UEs) is investigated to maximize energy efficiency. Then, the transmission power is optimized jointly with association of the UEs to the FlyBSs and ground base stations in [12]. However, as the UEs are static, also the FlyBS's position does not change in both [11] [12]. In [13], the authors optimize 3D trajectory of the FlyBSs together with resource and power allocation in an urban environment to maximize the minimum throughput of the UEs. Then, in [14], the throughput of the UEs is maximized via successive convex optimization of the FlyBSs' 3D positions and the transmission power. The UEs' throughput is maximized also in [15] via interference mitigation in three-tier space-air-ground heterogeneous networks with optimized altitude of the FlyBSs' hovering and uplink transmission power control. In [16]–[18], the authors minimize the transmission power while guaranteeing data rate and/or communication quality for all UEs. In [19], energy consumption for communication is constrained by keeping at least the same size of a coverage area and a lower energy consumption is achieved via a movement of the FlyBSs providing connectivity to the UEs at certain positions (stopping points). An energy efficient collection of data from static sensors by the FlyBSs is addressed in [20] [21]. In [20], scheduling of the FlyBSs collecting and forwarding data to the conventional static base stations (SBSs) is proposed. In [21], minimization of the transmission power for communication of sensors in a hierarchical way via cluster heads (CHs) is achieved by a smart scheduling of the communication of individual CHs and the FlyBSs.

A relaying via the FlyBSs acting in an energy-efficient transparent mode is investigated in [22], where the static UEs are associated to the FlyBSs and the FlyBSs are positioned by deep neural networks in order to maximize throughput. Nevertheless, the energy consumption for communication and flying is not considered. In [23] [24], the objective is to minimize the energy consumed for both communication and movement of the FlyBSs in the scenario, where the FlyBSs fly over a set of static UEs and exchange data with the UEs sequentially. To this end, the authors design an algorithm that plans trajectories among the UEs and allocate time for communication and hovering in order to minimize the overall energy consumed by the FlyBSs. A communication of the static UEs via multiple FlyBSs is addressed also in [25], where the authors minimize the traveling time of these FlyBSs while collecting data from the UEs.

Scheduling of the UEs' communication and transmission

power and bandwidth allocation together with a design of the FlyBS's trajectory in order to serve sequentially the static UEs is consider in [26]. Then, a design of a circular trajectory for the FlyBS serving multiple static UEs is proposed in [27]. The authors derive an energy efficient trajectory so that the UEs in a defined area are served with a certain quality of the communication channel. In [28], the authors consider the energy consumption in joint FlyBSs' trajectory determination, transmission power setting, and scheduling of the UEs to maximize the sum throughput.

All papers [11]–[28] targeting the power/energy aspects of the FlyBSs, however, take only static UEs with apriori known coordinates into account. Such scenario corresponds, for example, to a collection of data from static IoT/machine-type devices (e.g., smart-meters) in a way that the FlyBS serves a group of the UEs/devices and, then, continues to serve another group (a "sequential communication" of the FlyBS with the UEs). Such solution is, however, applicable only when the UEs do not require any real-time services and do not care if the communication resources are available at the very moment or in few seconds or even minutes. In contrast, we focus on the problem, when the UEs require continuous services with a low latency and cannot wait seconds or minutes till the connectivity is provided. Moreover, the problem addressed in related papers [11]–[21], [23]–[28] relies on the apriori knowledge of the future UEs' positions to plan the trajectory of FlyBS among the static UEs in a sequential way. Hence, the targeted problem in these papers is an analogy to the traveling salesman problem. Unfortunately, the solutions developed in these papers cannot be easily extended to an environment with moving UEs with positions not known in advance and changing over time.

The mobile UEs are considered, e.g., in [29]–[32]. In [29], the authors analyze performance of the mobile network with single FlyBS serving the mobile UEs. Multiple FlyBSs are assumed in [30], where the authors solve the positioning of the FlyBSs jointly with an association of the UEs via k-means algorithm. In [31], the authors optimize the network capacity and the energy consumption of the UEs. In [32], the coverage maximization and interference mitigation are addressed. Nevertheless, none of [29]–[32] consider the energy consumed by the FlyBSs.

The mobile UEs and the energy consumption of the FlyBSs are considered in [33], where the authors optimize the FlyBSs' trajectories and the UEs' association for a multi-antenna transmission. However, the proposed gradient-ascent-based solution requires to select future positions of the FlyBSs upon a knowledge of an impact of the selected actions on the performance. In practice, testing various trajectories over moving UEs is not possible, since the UEs' positions change for each iteration. Furthermore, a physical wired connection among the FlyBSs, assumed in [33] to allow a coordination and the energy sharing among FlyBSs, limits practical applications.

The energy consumption of the single FlyBS in the scenario with mobile UEs is tackled in [34] [35], where the transmission power of single FlyBS and its energy spent for flying are jointly optimized. A closed-form solution for the transmission power setting and determination of the FlyBS's coordinates is derived. Even though such solution is easy to implement, it is designed only for single FlyBS and cannot be easily extended to multiple FlyBSs. Also, the closed-form solution tracks the UEs strictly and, thus, leads to an unnecessary energy consumption.

The works considering mobile UEs [29]–[35] assume rotary-wing FlyBSs. However, the power consumption is relatively high for static or slowly moving rotary-wing FlyBSs, as shown e.g. in [23]. This is a result of helicopter dynamics, see e.g., [36]. Thus, in the scenarios with pedestrians (e.g., visitors of an outdoor event, sports, or city festival) considered in our paper, the rotary-wing FlyBSs would operate in a high energy consumption regime. Hence, we focus on the airship-based FlyBSs represented by, e.g., small balloons or airships, for which a slow movement or even temporary hovering at the same position is not a drawback from the energy consumption point of view [4] [37] [28].

Our objective is to reduce the energy spent for the airship-based FlyBSs' movement while guaranteeing a close-to-optimum sum capacity of the UEs. Unlike [11]–[21], [23]–[28], where the static UEs with apriori known positions are served sequentially, we focus on the scenario with the airship-based FlyBSs providing continuous communication services to the slowly moving UEs (e.g., pedestrians) in rural or sub-urban areas, where a temporary event, such as sport match, music/city festival, or concert, takes place. In such scenario, constructing common infrastructure of mobile networks with dense SBSs might not be economical, since the area is usually lightly crowded and high communication requirements arise only from time to time (e.g., once per week) due to the above-mentioned temporary event. We also focus on the energy consumption, which is neglected in most of the works targeting mobile UEs, see, e.g., [29]–[32]. Besides, the works, where either mobile UEs or energy is taken into account, e.g., [29]–[35], assume the rotary-wing FlyBSs, but these are not efficient for slow moving UEs due to a high energy consumption and the solution tailored for the rotary-wing FlyBSs cannot be applied due to completely different principle of flying and, consequently, different energy consumption models. We propose a new concept of the FlyBSs' 3D movement optimization to eliminate redundant movements of the FlyBSs so that a notable energy saving is reached at a cost of only a marginal degradation in the sum capacity of UEs. Despite assuming mobile (moving) UEs, our solution does not require any knowledge of the future UEs' positions as in the related works targeting the static UEs [11]–[28]. The contribution and novelty presented in this paper are summarized as follows:

- We derive a closed-form relation between the energy consumed by the airship-based FlyBSs for flying and the sum capacity achievable by the served mobile UEs.
- We derive theoretical bounds and trade-offs between the energy consumed by single FlyBS for flying and the sum capacity of the mobile UEs. Further, we show a relation of both the energy consumption and the sum capacity to the positioning of single FlyBS to demonstrate that a slightly sub-optimal movement of the FlyBS in terms of the sum capacity results in a substantial reduction in the the energy consumption for flying.

- We extend the scenario to multiple FlyBSs and we formulate the problem of the flying energy minimization under the sum capacity constraint considering also practical constraints on flying. To solve this problem, we derive a relation between the energy consumption and the sum capacity for multiple FlyBSs serving mobile UEs and we propose an algorithm determining 3D positions of the FlyBSs so that the sum capacity of the moving UEs remains close to a theoretical maximum while the energy spent for flying is significantly reduced.
- We show that the proposed approach reduces the energy spent by the FlyBSs for flying by dozens of percent while the impact on the sum capacity is negligible for a wide range of numbers of the UEs and the FlyBSs. This interesting finding proves the fact that a "perfect positioning" of the airship-based FlyBSs is not necessary in practice, as it is energy demanding while the gain in sum capacity with respect to sub-optimal approaches is insignificant. This allows to relax requirements on the FlyBSs' positioning and provides new degree of freedom for future optimizations in the networks with FlyBSs.

Note that the paper is an extension of our prior work presented in [38], where we show that the energy consumption of the FlyBSs can be reduced by restricting the FlyBSs' 2D movement while a cost represented by a degradation in the sum capacity is marginal.

The rest of the paper is organized as follows. The next section outlines the system model considered in this paper and formulates the problem of energy consumption minimization. Then, in Section III, we provide an overview of general framework for the energy consumption minimization and we analyze trade-offs between the energy consumption and sum capacity for single FlyBS to illustrate theoretical bounds of the energy saving with respect to the sum capacity. Then, in Section IV, we extend the analysis to multiple FlyBSs and we propose a novel algorithm for the positioning of FlyBSs minimizing the energy consumed for flying. In Section V, simulation scenario and models are outlined and performance of the proposed algorithm is analyzed. Last, Section VI concludes the paper and outlines potential future works.

II. System Model and Problem Formulation

In this section, we first define the system model and, then, we formulate the targeted problem. Note that we summarize key parameters and notations used in the paper in Table I.

A. System Model

Let's assume N moving UEs distributed within an area covered by M FlyBSs. Current positions of the UEs at the time t are defined as $\boldsymbol{U}(t) = \{\boldsymbol{u_1}(t), \boldsymbol{u_2}(t), \ldots, \boldsymbol{u_N}(t)\}$, where $\boldsymbol{u_n} = [x_{u,n}(t), y_{u,n}(t), z_{u,n}(t)] \in \mathbb{R}^3$ for $\forall n \in \langle 1, N \rangle$. Similarly, the FlyBSs are located at 3D positions $\boldsymbol{V}(t) = \{\boldsymbol{v_1}(t), \boldsymbol{v_2}(t), \ldots, \boldsymbol{v_M}(t)\}$, where $\boldsymbol{v_m} = [x_{f,m}(t), y_{f,m}(t), z_{f,m}(t)] \in \mathbb{R}^3$ for $\forall m \in \langle 1, M \rangle$. Both the UEs and the FlyBSs move over time and the coordinates of each FlyBS are updated depending on the movement of the UEs. Note that the analysis and solution provided in this paper are independent of the UEs' movement, as we derive the new positions of the FlyBSs in a closed form based only on the actual UEs' positions (i.e., reactive approach). Hence, no mobility model is defined for the purposes of the analysis and we specify mobility models for simulations later in Section V-A.

Table I
Key parameters and notations used in the paper

Param.	Meaning
M, N	Number of FlyBSs and UEs, resp.
$\boldsymbol{u_n}(t)$	3D coordinates of UE n at time t
$\boldsymbol{v_m}(t)$	3D coordinates of FlyBS m at time t
$C_{n,m}$	Capacity of UE n to FlyBS m
C_{opt}	Maximum sum capacity of all UEs
$B_{n,m}$	Bandwidth of UE n served by FlyBS m
$a_{n,m}$	Association of UE n to FlyBS m
$\gamma_{n,m}$	SINR between UE n and FlyBS m
$p^R_{n,m}$	Received power at UE n from FlyBS m
σ^2	Noise plus background interference
$G^{T/R}_m$	Gain of Tx and Rx antennas
$d_{n,m}$	Distance between UE n and FlyBS m
$\alpha_{n,m}$	Path-loss exp. between UE n and FlyBS m
P^T_m	Transmission power of FlyBS m
$\varsigma_{n,m}$	Channel fading between UE n and FlyBS m
$E_{F,m}$	Energy spent by FlyBS m to fly from $v_m(t)$ to $v_m(t+1)$
e_m	Energy for the movement of FlyBS m per unit distance
E_s	Energy saving wrt path maximizing sum capacity
D_o	Distance of FlyBS to optimum position (reaching C_{opt})
d_m	Distance FlyBS m moves between time t and $t+1$
ϵ	Maximum allowed degradation in sum capacity
ν, ω_n	Substitutions defined in Proposition 2
A, r_m	Substitutions defined in Theorem 3
θ	Angle between two segments of FlyBS path
$d_{m,req}$	Movement distance of FlyBS m to meet required capacity
d_{max}	Max. distance FlyBS can move between time t and $t+1$
ΔC	Increase in sum capacity due to FlyBS movement
ΔC_{step}	Capacity change within a sub-step of FlyBS movement
ΔC_{target}	Increase in sum capacity to fulfill capacity constraint
$h_{min/max}$	Minimum and maximum allowed altitude of FlyBS

Initial positions of all FlyBSs and association of the UEs to the FlyBSs are solved via commonly used k-means clustering algorithm, such as in [30]. As the UEs move, the k-means algorithm is continuously repeated to associate the UEs to the FlyBSs. Note that the principle of our algorithm introduced later in this paper is independent of the the UEs' association and arbitrary approach for the UEs' association, such as the one based on machine learning proposed in [22], can be adopted without changing our analysis or the proposed algorithm. We adopt k-means as an example, because k-means converges fast (in order of microseconds) due to its polynomial complexity while it provides a good performance for the UEs' association [30].

The downlink communication capacity of the n-th UE from the m-th FlyBS is defined as:

$$C_{n,m} = B_{n,m} \log_2 (1 + \gamma_{n,m}) \tag{1}$$

where $B_{n,m}$ stands for the channel bandwidth between the n-th UE and the m-th FlyBS (as our proposed solution does not depend on the selected bandwidth allocation, we assume the equal bandwidth allocation among the UEs connected to the same FlyBSs), and $\gamma_{n,m}$ represents the SINR between the n-th UE and the m-th FlyBS considering also interference from other FlyBSs, as we assume the scenario with all FlyBSs

occupying the same band. Thus, $\gamma_{n,m}$ is defined as:

$$\gamma_{n,m} = \frac{p^R_{n,m}}{\sigma^2 + \sum_{i=1,\ i\neq m}^{M} p^R_{n,i}} \tag{2}$$

where $p^R_{n,m}$ and $p^R_{n,i}$ are the received powers at the n-th UE from the serving m-th FlyBS and the i-th interfering FlyBS, respectively, and σ^2 represents the sum of the noise and the background interference (e.g., from neighboring cells).

The received power $p^R_{n,m}$ is proportional to the distance $d_{n,m}$ between the n-th UE and the m-th FlyBS and is generally defined as:

$$p^R_{n,m} = \frac{P^T_m G^T_m G^R_n c^{\alpha_{n,m}} \varsigma_{n,m}}{(4\pi f)^{\alpha_{n,m}} d^{\alpha_{n,m}}_{n,m}} = \frac{Q_{n,m}}{d^{\alpha_{n,m}}_{n,m}} \tag{3}$$

where P^T_m is the transmission power of the m-th FlyBS, G^T_m and G^R_n are the gains of the FlyBS's and UE's antennas, respectively, f is the communication frequency, $c = 3 \times 10^8$ m/s is the speed of light, $\alpha_{n,m}$ represents the path loss exponent (of any positive value suitable for both line-of-sight, LoS, and non-line-of-sight, NLoS, communications) for the channel between the n-th UE and the m-the FlyBS, and $\varsigma_{n,m}$ represents the channel fading between the m-th FlyBS and the n-th user. We substitute $\frac{P^T_m G^T_m G^R_n c^{\alpha_{n,m}}}{(4\pi f)^{\alpha_{n,m}}}$ with $Q_{n,m}$ for an ease of representation in the rest of the paper. Note that aspects related to channel estimation are left out, since this problem is addressed in many other works (e.g., [39] [40]) and key concept remains similar as for the SBSs, since we focus on slow moving pedestrians with a low speed. Consequently, also the FlyBSs move with low speed far below speeds supported by 5G. Thus, we can neglect an impact of outdated CSI.

Note that the communication between the FlyBSs and the network (i.e., with the SBSs) and its specific implementation or potential limitation does not change principle of our proposed solution. Thus, like in many related works, we assume a high capacity backhaul connection of the FlyBSs to the network via, for example, optical wireless links [41] [42].

For the scenario with pedestrians, considered in this paper, the rotary-wing FlyBSs are not convenient due to their relatively high power consumption in a static or slowly moving mode. This high consumption is a result of the helicopter dynamics' effect (see, e.g., [23] [36]). Thus, we focus on the airship-based FlyBSs. The power consumption of the airships is proportional to the distance traveled between two points and the power consumption of the airships is negligible if the airship are not moving, since the gravity is compensated by a static buoyancy [43]. We assume the FlyBS follows the shortest path between the current location $v_m(t) = [x(t), y(t), z(t)]$ and a new determined location $v_m(t+1) = [x(t+1), y(t+1), z(t+1)]$, i.e., the m-th FlyBS moves for the distance $d_m = \sqrt{(x(t) - x(t+1))^2 + (y(t) - y(t+1))^2 + (z(t) - z(t+1))^2}$.

Having in mind the power consumption of the airship is negligible when the airship hovers at the same position the energy spent by the m-the FlyBS to fly from $v_m(t)$ to $v_m(t+1)$ is defined as $E_{F,m} = d_m e_m$, where e_m represents the instantaneous unit energy spent for the movement of the m-th FlyBS per unit of distance (e.g., per meter). The overall energy consumption of the FlyBSs includes also transmission power spent for communication (data as well as signaling, channel estimation, flight control, etc.), and consumption of the circuitry. However, the overall transmission power is typically between 10 and 30 dBm (0.01–1 W) [18] [44] [45] and is significantly (few orders of magnitude) lower than the power required for flying [23] [35] [46] [47] [43]. Hence, we neglect the energy spent for communication. Besides, also the circuitry power is typically constant and cannot be influenced in frame of our targeted problem. Thus, we leave out the circuitry consumption to avoid veiling the gains directly related to our proposal.

B. Problem formulation

We focus on saving of the energy spent by the FlyBSs for flying while keeping the sum capacity of the moving UEs still close to the maximum achievable sum capacity. Thus, we minimize the energy consumption and the problem addressed in this paper is defined as:

$$\begin{aligned} \hat{\boldsymbol{V}}(\boldsymbol{t}) = \underset{\boldsymbol{V}\in\boldsymbol{R}^{3M}}{\text{argmin}} \quad & \sum_{m=1}^{M} E_{F,m} \\ \text{s.t.} \quad & (a)\ \sum_{n=1}^{N}\sum_{m=1}^{M} a_{n,m} C_{n,m} \geq C_{opt} \times (1-\epsilon), \\ & (b)\ d_m \leq d_{max}, \\ & (c)\ h_{min} \leq z_{f,m} \leq h_{max}, \end{aligned} \tag{4}$$

where $a_{n,m} = 1$ if the n-th UE is associated to the m-th FlyBS, otherwise $a_{n,m} = 0$, C_{opt} is the sum capacity achieved by the UEs if the FlyBSs are deployed at the positions that lead to the maximum sum capacity, and $\epsilon \in \langle 0, 1\rangle$ is the constant indicating the maximum allowed degradation in the sum capacity (no degradation is allowed for $\epsilon = 0$; and note that ϵ is typically set to a fixed value according to users' required communication quality), d_{max} is the maximum distance the FlyBS can move per time step (reflecting movement speed limit), and h_{min} and h_{max} are the minimum and maximum allowed altitudes of the FlyBS, respectively.

For clarity of explanations and derivations, but without lost of generality, we leave out $a_{n,m}$ in the rest of the paper and we set $C_{n,m} = 0$ if the n-th UE is not connected to the m-th FlyBS.

III. Analysis and Bounds for Energy Saving and Sum Capacity of Single FlyBS

In this section, we first outline a general framework and a core idea behind the energy consumption minimization (i.e., saving the energy) for the airship-based FlyBSs. Then, we analytically derive a relation and trade-offs between a potential saving in the energy consumed for flying and a decrease in the sum capacity. The analysis is done for single FlyBS, as it allows to illustrate theoretical bounds for the energy saving and the sum capacity in an easy-to-follow way without interaction among FlyBSs (interference and mutual impact on positions). Note that an extension towards multiple FlyBSs follows in Section IV.

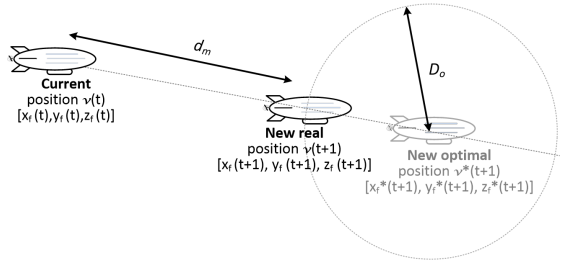

Figure 1. Illustration of a core idea of the proposed solution for elimination of redundant movement. Note that if the FlyBS is within the distance D_o from the new optimal position, no movement is necessary.

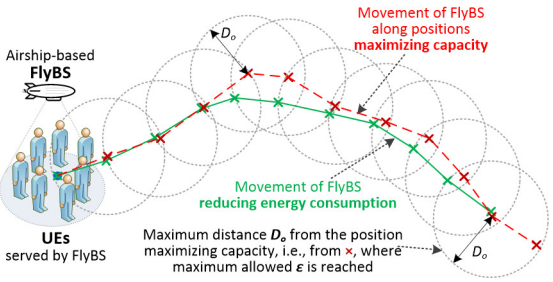

Figure 2. Example of FlyBS movement considering proposed concept (green solid line) with respect to positions yielding maximum sum capacity (red dashed line). Each cross "×" identifies a point where new position of FlyBS is determined and circles represent distance D_o from the optimum FlyBS's position maximizing capacity within which the allowed sum capacity degradation ϵ is not exceeded.

A. Framework for FlyBS positioning to save energy for flying

Existing algorithms focusing on the scenario with the mobile UEs typically navigate the FlyBS(s) to follow the position maximizing the capacity. Hence, in the related existing works, the FlyBS moves frequently to increase the capacity offered to the UEs. In our scenario with the slow-moving pedestrian UEs served by the airship-based FlyBS, which is efficient for such scenario, the frequent changes of the FlyBS' position notably drain their battery while achieving only a marginal improvement in the sum capacity. Consequently, the sum capacity maximization leads inevitably to "redundant" movements of the FlyBS. However, due to logarithmic dependence of the capacity on the distance (which is related to the channel quality), some of the FlyBS's movements introduce only a marginal improvement in the sum capacity while a notable additional energy is consumed by the FlyBS for flying. The work presented in this paper is based on a presumption that not every movement of the UEs should necessarily lead to a repositioning of the FlyBSs to the position yielding the maximum sum capacity (denoted as the new optimal position). To this end, we suggest to avoid the "redundant" movements so that the FlyBS does not follow exactly the optimum position (i.e., position yielding the maximum capacity) $\boldsymbol{v}^*(t+1) = [x_f^*(t+1),\ y_f^*(t+1),\ z_f^*(t+1)]$. Thus, instead of traveling to the optimum position, the FlyBS moves only to a new position $\boldsymbol{v}(t+1) = [x_f(t+1),\ y_f(t+1),\ z_f(t+1)]$, which is between the optimum and current positions to avoid the redundant movement, as illustrated in Fig. 1.

The new real position of the FlyBS is determined knowing the current FlyBS position $\boldsymbol{v}(t) = [x_f(t),\ y_f(t),\ z_f(t)]$, the new optimal position of the FlyBS $\boldsymbol{v}^*(t+1) = [x_f^*(t+1),\ y_f^*(t+1),\ z_f^*(t+1)]$, and the distance D_o to this new optimal position. Finding of the optimum positions of the FlyBS is a linear programming problem, hence, we derive the optimum position numerically by the Nelder-Mead simplex search (see details in [48]). Such approach is, however of a high complexity making it impractical for real networks. Therefore, we also investigate the performance for the positions of the FlyBS derived by a commonly adopted low-complexity (polynomial) and fast converging, but sub-optimal (in terms of the sum capacity) approach via k-means (see, e.g., [30]) and via state-of-the-art successive convex optimization outlined in [14]. Note that our proposed solution is independent of the approach for the optimum positions' determination. Hence, we consider these three approaches for our investigation to show performance for i) complex, but well-performing, ii) low-complexity, but slightly worse performing, as well as iii) state-of-the-art approaches.

The new real position of the FlyBS is represented by an intersection of the straight line between the current and new optimal positions and the sphere defined by the radius $D_o(t+1)$ whose center corresponds to the optimal position of the FlyBS. The new 3D coordinates of the FlyBS are defined in following lemma.

Lemma 1. *The new position of the FlyBS is determined in a closed-form as:*

$$\boldsymbol{v}(t+1) = \boldsymbol{v}(t) + \frac{(\boldsymbol{v}^*(t+1) - \boldsymbol{v}(t))}{||\boldsymbol{v}^*(t+1) - \boldsymbol{v}(t)||} \times \max\{0, (||\boldsymbol{v}^*(t+1) - \boldsymbol{v}(t)|| - D_o(t+1))\} \tag{5}$$

Proof. In case that $||\boldsymbol{v}^*(t+1) - \boldsymbol{v}(t)|| \leq D_o(t+1)$, the FlyBS would not move, as the constraint (4a) is already fulfilled. Furthermore, in case that $||\boldsymbol{v}^*(t+1) - \boldsymbol{v}(t)|| > D_o(t+1)$, the movement of the FlyBS starts from $\boldsymbol{v}(t)$ and continues towards $\boldsymbol{v}^*(t+1)$. The movement distance is $d_m = ||\boldsymbol{v}^*(t+1) - \boldsymbol{v}(t)|| - D_o(t+1)$ according to Fig. 1. Hence, the displacement vector of the FlyBS is $\frac{(\boldsymbol{v}^*(t+1) - \boldsymbol{v}(t))}{||\boldsymbol{v}^*(t+1) - \boldsymbol{v}(t)||} d_m$, where $\frac{(\boldsymbol{v}^*(t+1) - \boldsymbol{v}(t))}{||\boldsymbol{v}^*(t+1) - \boldsymbol{v}(t)||}$ is the unit vector for the movement towards $\boldsymbol{v}^*(t+1)$. This concludes the proof. ■

The above described approach leads to a natural "smoothening" of the FlyBS's movement. In other words, the FlyBS do not copy the movement of UEs accurately, but naturally avoids a redundant and non-beneficial movement as illustrated in Fig. 2.

B. Analysis of energy consumption and sum capacity trade-offs for single FlyBS

In the case of single FlyBS, no interference among the FlyBSs applies, thus, the downlink communication capacity of the n-th UE is defined as:

$$C_n = B_n \times \log_2 \left(1 + \frac{p_n^R}{\sigma^2}\right) \tag{6}$$

Note that we omit index of the FlyBS in this subsection for clarity of presentation, as only one FlyBS is considered.

For clarity of derivations, we remove also the constraints on the FlyBS flight (4b) and (4c) in this subsection. Then, the problem formulated in (4) is simplified to:

$$\begin{aligned} \boldsymbol{V^*(t)} = \underset{\boldsymbol{V}\in\boldsymbol{R}^{3M}}{\operatorname{argmin}} \quad & E_F \\ \text{s.t.} \quad & \sum_{n=1}^{N} C_n \geq C_{opt} \times (1-\epsilon) \end{aligned} \tag{7}$$

To solve this problem analytically, we first modify the constraint in (7) and we define relation between the allowed degradation in the sum capacity ϵ and the distance D_o, which the FlyBS keeps from the optimum position as indicated in Proposition 2.

Proposition 2. *The constraint $\sum_{n=1}^{N} C_n \geq C_{opt} \times (1-\epsilon)$ in (7) can be replaced with the following constraint*

$$d\left[\boldsymbol{v}(t), \boldsymbol{v}^*(t)\right] < D_o(t) \tag{8}$$

where $d\left[\boldsymbol{v}(t), \boldsymbol{v}^*(t)\right]$ represents the distance between the points $\boldsymbol{v}(t)$ and $\boldsymbol{v}^*(t)$ representing the current and the optimal positions of the FlyBS at the time t .

The constraint (8) indicates that the new 3D position of the FlyBS lies in the sphere with the center at $\boldsymbol{v}^*(t)$ and with the radius:

$$D_o(t) = \left(\frac{\nu - C_{opt} \times (1-\epsilon)}{\sum_{n=1}^{N} \omega_n} \right)^{\frac{1}{2}} \tag{9}$$

where ν and ω_n are substitutions of the system parameters (including, among others, 3D coordinates of the FlyBS) defined in Appendix A to simplify the formulation.

Proof. Please see Appendix A. ■

To quantify efficiency of the positioning in terms of the energy consumption, we define the energy saving metric E_s representing the amount of energy saved by the optimized positioning with respect to the positioning maximizing the sum capacity. To evaluate the energy saving E_s, let's first expand the general high-level illustration of the principle presented in Fig. 1 into multiple consecutive steps of the FlyBS's movement as shown in Fig. 3. The FlyBS's movement can be decomposed into movements corresponding to short time steps (from t to $t+1$, from $t+1$ to $t+2$, etc.). Each segment of the movement is described by its length and by its angle θ with respect to the previous segment. Note that this angle is used for the purpose of analysis and can be of any value (i.e., $\theta \in [0, 2\pi]$). The figure depicts two possible paths of the FlyBS, each with two segments. The first path (red dashed line) corresponds to the FlyBS movement achieving the maximum sum capacity while the second path (green solid line) represents a shorter path resulting in the saving in energy consumed for flying.

Considering the airship-based FlyBS, as explained in Section II, a potential energy saving is proportional to the ratio of the energy consumption over the energy efficient (green solid) path and the energy consumption over the path maximizing the sum capacity (red dashed). Hence, the relative saved energy E_s for the movement of single FlyBS is expressed by (10).

The E_s expresses the achievable energy saving in relation to the loss in sum capacity (with respect to the theoretical maximum achievable capacity) for single FlyBS. The energy saving E_s is proportional to D_o that is, in turn, proportional to ϵ (i.e., allowed degradation in the sum capacity with respect to C_{opt}, see (9)). Thus, with increasing ϵ, D_o increases as well and, consequently, more energy is saved (see (10)). Note that $E_s = 1$ corresponds to 100% of saved energy while $E_s = 0$ represents no saving at all. A visualization and a quantification of the trade-off between the energy savings and the sum capacity according to (10) are provided in Section V focused on performance evaluation.

IV. Energy Efficient Positioning of Multiple FlyBSs

In this section, we extend the single FlyBS scenario to multiple FlyBSs. First, we derive energy consumption of the FlyBS with respect to required changes in the sum capacity considering mutual impact (interference and positioning) of the FlyBSs. Then, we propose algorithm minimizing the energy consumed by the FlyBSs for flying under the constraints on sum capacity and flying in (4). Last, we discuss complexity and potential limitations of the algorithm.

A. Energy consumption and sum capacity for multiple FlyBSs

An extension towards multiple FlyBSs assumes to consider a mutual interference among the FlyBSs. Thus, the channel capacity of the n-th UE associated to the m-th FlyBS ($C_{m,n}$) is defined in line with (1) and (2). For analysis of the energy consumption and sum capacity trade-offs in this section, we first approximate the sum capacity of multiple FlyBSs in the following theorem.

Theorem 3. *The sum capacity of N UEs served by M FlyBSs is approximated as:*

$$\sum_{m=1}^{M}\sum_{n=1}^{N} C_{n,m} \approx A - \sum_{m=1}^{M} r_m d^2\left[\boldsymbol{v_m}(t), \boldsymbol{v_m^*}(t)\right] \tag{11}$$

and the constraint (4a) can be reformulated to:

$$\sum_{m=1}^{M} r_m d^2\left[\boldsymbol{v_m}(t), \boldsymbol{v_m^*}(t)\right] \leq A - C_{opt} \times (1-\epsilon) \tag{12}$$

$$E_s = 1 - \frac{d[\boldsymbol{v}(t),\boldsymbol{v}(t+1)]+d[\boldsymbol{v}(t+1),\boldsymbol{v}(t+2)]}{d[\boldsymbol{v}(t),\boldsymbol{v}^*(t+1)]+d[\boldsymbol{v}^*(t+1),\boldsymbol{v}^*(t+2)]} = 1 - \frac{d[\boldsymbol{v}(t),\boldsymbol{v}^*(t+1)]+d[\boldsymbol{v}(t+1),\boldsymbol{v}^*(t+2)]-D_o(t+1)-D_o(t+2)}{d[\boldsymbol{v}(t),\boldsymbol{v}^*(t+1)]+d[\boldsymbol{v}^*(t+1),\boldsymbol{v}^*(t+2)]} =$$
$$1 - \frac{d\left[\boldsymbol{v}(t),\boldsymbol{v}^*(t+1)\right]-\left(D_o(t+1)+D_o(t+2)\right)+\sqrt{D_o^2(t+1)+d^2[\boldsymbol{v}^*(t+1),\boldsymbol{v}^*(t+2)]-2D_o(t+1)d[\boldsymbol{v}^*(t+1),\boldsymbol{v}^*(t+2)]cos(\theta(t+1))}}{d\left[\boldsymbol{v}(t),\boldsymbol{v}^*(t+1)\right]+d\left[\boldsymbol{v}^*(t+1),\boldsymbol{v}^*(t+2)\right]} \tag{10}$$

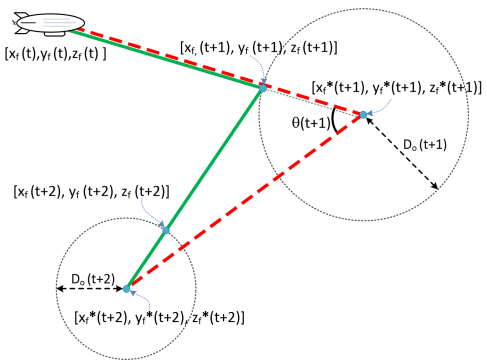

Figure 3. Illustrative example of single FlyBS movement over several (two) positions; the dashed red line is the "state-of-the-art" movement maximizing the sum capacity while the solid green line is the movement reducing the energy consumed for flying.

where A and r_m are substitutions defined in Appendix B to simplify the formulation.

Proof. Please see Appendix B. ■

To derive also the energy consumed for flying of individual FlyBSs, we first determine the required movement ($d_{m,req}$) of the m-th FlyBS ($1 \leq m \leq M$) leading to the increase in the sum capacity ΔC, which is required to fulfill the constraint (4a). Thus, ΔC is the difference between the sum capacity offered by all FlyBSs at the time $t-1$ and at the time t, i.e.,:

$$\Delta C = \sum_{m=1}^{M}\sum_{n=1}^{N} C_{n,m}(t) - \sum_{m=1}^{M}\sum_{n=1}^{N} C_{n,m}(t-1) \tag{13}$$

Now, exploiting the reformulated constraint from Theorem 3, we define ΔC as a function of the m-th FlyBS's movement for the distance $d_{m,req}$ required to fulfill the constraint, i.e.,:

$$\begin{aligned}\Delta C = \sum_{m=1}^{M}\sum_{n=1}^{N} C_{n,m}(t+1) - \sum_{m=1}^{M}\sum_{n=1}^{N} C_{n,m}(t) = \\ (A - \sum_{m=1}^{M} r_m(d\left[\boldsymbol{v_m}(t), \boldsymbol{v_m^*}(t)\right] + d_{m,req})^2) - \\ (A - \sum_{m=1}^{M} r_m d^2\left[\boldsymbol{v_m}(t), \boldsymbol{v_m^*}(t)\right]) = \\ -r_m\left(d_{m,req}^2(t+1) + 2d\left[\boldsymbol{v_m}(t), \boldsymbol{v_m^*}(t)\right] d_{m,req}(t+1)\right)\end{aligned} \tag{14}$$

We can rewrite (14) to:

$$(d_{m,req}(t+1) + d\left[\boldsymbol{v_m}(t), \boldsymbol{v_m^*}(t)\right])^2 = d^2\left[\boldsymbol{v_m}(t), \boldsymbol{v_m^*}(t)\right] - \frac{\Delta C}{r_m} \tag{15}$$

From (15), the value of $d_{m,req}(t+1)$ is simply expressed as:

$$d_{m,req}(t+1) = -d\left[\boldsymbol{v_m}(t), \boldsymbol{v_m^*}(t)\right] \pm \sqrt{d^2\left[\boldsymbol{v_m}(t), \boldsymbol{v_m^*}(t)\right] - \frac{\Delta C}{r_m}} \tag{16}$$

Between two values resulting from (16), we choose the one with a smaller absolute value, as the smaller movement incurs lower energy consumption:

Algorithm 1 Determination of new positions for FlyBSs minimizing energy consumption

1: $\mathcal{M} \leftarrow \{1, ..., M\}$, $[x_{f,m}(t+1), y_{f,m}(t+1), z_{f,m}(t+1)] \leftarrow [x_{f,m}(t), y_{f,m}(t), z_{f,m}(t)]$, $d_{m,tot} = 0\ \forall m \in \mathcal{M}$
2: $\Delta C_{target} \leftarrow C_{opt} \times (1-\epsilon) - \sum_{n=1}^{N}\sum_{m=1}^{M} C_{n,m}$
3: **while** $\Delta C_{target} > 0$ **do**
4: Calculate $[E_{F,1}, ..., E_{F,M}]$ from (18)
5: $m_0 \leftarrow \text{argmax}_{m\in\mathcal{M}}(\frac{\Delta C_{step}}{E_{F,m}})$
6: Calculate $d_{m_0,req}(t+1)$ from (17) with setting $\Delta C = \Delta C_{step}$
7: **if** $d_{m_0,req}(t+1) > d_{max}$ **then** $d_{m_0,req}(t+1) \leftarrow d_{max}$ and calculate ΔC from (14) **end if**
8: Calculate new posit. $[x_{f,m_0}(t+1), y_{f,m_0}(t+1), z_{f,m_0}(t+1)]$ of m_0-th FlyBS via (1)
9: **if** $z_{f,m_0}(t+1) > h_{max}$ **or** $z_{f,m_0}(t+1) < h_{min}$ **then**
10: $d_{m_0,req}(t+1) \leftarrow \left|\left|\frac{h_{max(min)} - z_{f,m_0}(t)}{z_{f,m_0}(t+1) - z_{f,m_0}(t)} \times \frac{(\boldsymbol{v^*_{m_0}}(t+1) - \boldsymbol{v_{m_0}}(t))}{||\boldsymbol{v^*_{m_0}}(t+1) - \boldsymbol{v_{m_0}}(t)||}\right|\right|$ and calculate ΔC (14) and $\boldsymbol{v_{m_0}}$ (1)
11: **end if**
12: **if** $d_{m_0,tot}(t+1) + d_{m_0,req}(t+1) > d_{max}$ **then**
13: $d_{m_0,req}(t+1) \leftarrow d_{max} - d_{m_0,tot}(t+1)$, calculate ΔC from (14) and $\boldsymbol{v_{m_0}}$ from (1), and $\mathcal{M} \leftarrow \mathcal{M} - \{m_0\}$
14: **else** $d_{m_0,tot}(t+1) \leftarrow d_{m_0,tot}(t+1) + d_{m_0,req}(t+1)$ **end if**
15: $\Delta C_{target} = \Delta C_{target} - \Delta C$
16: **end while**

$$|d_{m,req}(t+1)| = \min\left\{\left|-d\left[\boldsymbol{v_m}(t), \boldsymbol{v_m^*}(t)\right] - \sqrt{d^2\left[\boldsymbol{v_m}(t), \boldsymbol{v_m^*}(t)\right] - \frac{\Delta C}{r_m}}\right|, \left|-d\left[\boldsymbol{v_m}(t), \boldsymbol{v_m^*}(t)\right] + \sqrt{d^2\left[\boldsymbol{v_m}(t), \boldsymbol{v_m^*}(t)\right] - \frac{\Delta C}{r_m}}\right|\right\} \tag{17}$$

Then, the energy consumption for flying of the m-th FlyBS leading to ΔC is:

$$E_{F,m}(t+1) = e_m d_{m,req}(t+1) \tag{18}$$

B. Energy efficient positioning of multiple airship-based FlyBSs

Exploiting the relation between the sum capacity and the energy consumption derived in the previous subsection, we propose an algorithm that determines the positions of arbitrary number of FlyBSs so that the energy spent for flying is minimized while the sum capacity still satisfies the constraint (4a). We distinguish two cases according to the constraint:

1) If the *capacity constraint (4a)* ***is satisfied***, the FlyBSs should not move to avoid redundant consumption of the energy for flying.
2) If the *capacity constraint (4a)* ***is not satisfied***, a movement of at least one of the FlyBSs is required to satisfy the users requirements on communication capacity.

As the first case does not require any movement, we now focus on the second case. The FlyBSs move with small steps as summarized in Algorithm 1. At the beginning (line 2 in Algorithm 1), the required increase in the sum capacity to fulfill the constraint ΔC_{target} reflecting the users' requirements is determined. The ΔC_{target} is split into small sub-steps $\Delta C_{step} \in (0; \Delta C_{target}\rangle$. In each sub-step, the energy consumption for the required increase in sum capacity is calculated from (18) for each FlyBS (line 4). The FlyBS, whose movement yields the highest gain in the sum capacity at the cost of the smallest energy consumption is selected,

i.e., in each sub-step, we select the FlyBS m_0 maximizing $\frac{\Delta C_{step}}{E_{F,m}}$ (see line 5). As $C_{step} > 0$, ΔC_{target} decrements over sub-steps and the algorithm converges. Note that selection of a larger ΔC_{step} leads to a lower number of sub-steps with a longer FlyBS's movement in each sub-step (thus, keeps low computation complexity), but the longer movement of the FlyBS in each sub-step results to a sub-optimal new position of the FlyBS. The sub-optimality results from the fact that the selected FlyBS m_0 keeps moving even if its $\frac{\Delta C_{step}}{E_{F,m0}}$ is no longer maximal among all FlyBSs. Our experiments show that setting of ΔC_{step} to few kbps guarantees close-to-optimum performance and still keeps a low number of sub-steps. Hence, we set ΔC_{step} to 10 kbps in this paper.

Now, using (17), we determine the distance $d_{m_0,req}(t+1)$ for which the selected FlyBS m_0 should move to reach ΔC_{step} (line 6). If the resulting $d_{m_0,req}(t+1)$ exceeds d_{max} and violates constraint (4b), the FlyBS moves only for d_{max} and ΔC is updated via (14) (line 7). Then, new position of the selected FlyBS m_0 is determined via (1) (line 8). If the new position would lead to a movement below minimum or above maximum allowed altitudes (constraint (4c)), the coordinates $\boldsymbol{v_{m_0}}$ of the FlyBS are adjusted and ΔC is also updated (lines 9–11). After this, we also verify if the total movement of single FlyBS over all sub-steps towards ΔC_{target} still fulfills the constraint (4b) (lines 12–14) and ΔC is updated together with the FlyBS's coordinates $\boldsymbol{v_{m_0}}$ if the constraint is violated (line 13). Since the violation of (4b) indicates that the FlyBS m_0 cannot further move in the next sub-steps, m_0 is excluded from the set of all FlyBS considered for movement in next iterations (line 13). Finally, ΔC_{target} is decreased by ΔC_{step} (line 15). The process of the FlyBS selection and movement (lines 4–15) is repeated until the constraint (4a) is not fulfilled, i.e., as long as $\Delta C_{target} > 0$. Algorithm 1 is repeated again if the capacity constraint in (4a) becomes not fulfilled in the future, e.g., due to the UEs' movement.

C. Complexity and potential limitations

To determine the computation complexity of Algorithm 1, first, let us remind the proposed solution consists of two steps: i) an approximation of the sum capacity, and ii) a positioning of the FlyBSs based on the approximated sum capacity (Algorithm 1). The complexity of the approximation in the step i) is $O(M)$ for each UE, where M is the number of FlyBSs. Thus, the complexity of the step i) is $O(MN)$, where N is the number of UEs and this complexity is linear with respect to both the number of UEs and the number of FlyBSs. Then, the complexity of the step ii) is $O(1/\Delta C_{step})$. Hence, the total complexity of the proposed solution is $O(MN/\Delta C_{step})$, which makes the algorithm fast and easy to implement in practical systems.

Our algorithm is designed for the airship-based FlyBSs and would not work well for the rotary-wing FlyBSs, since the rotary-wing FlyBSs exhibit completely different energy consumption behavior. However, this limitation is implied by our targeted scenario, where the rotary-wing FlyBSs are not efficient, see Section I. Furthermore, the FlyBSs should cooperate together. Still, solutions considered commonly in the related works assuming a control of the FlyBSs centrally from the network via SBSs can be adopted in a way that the algorithm is processed by the network and decisions are, then, delivered to individual FlyBSs. Hence, no extra signaling or information exchange is required with respect to the related works.

V. Performance evaluation

In this section, first, simulation scenario, models, and metrics are outlined. Then, we illustrate bounds of theoretical energy saving related to the sum capacity of the UEs for single FlyBS. Last, we investigate the energy saving in the scenario with multiple FlyBSs and we demonstrate an efficiency of the proposed algorithm comparing to the optimum as well as state-of-the-art solutions for the FlyBS positioning.

A. Simulation scenario, models, and metrics

We assume the area of 1000 $\times$ 1000 m as in [12]. Within this area, 40 or 1000 UEs [12] [33] [35] are dropped as the FlyBSs are supposed to serve heavily loaded scenarios with a high UEs' density. To mimic a realistic scenario, we model the UEs' mobility as a mixture of random way-point and cluster-based mobility models. To this end, a half of the UEs (i.e., 500 UEs) are dropped randomly within the simulation area and move according to the commonly used random walk mobility model with a speed of 1 m/s. The second half of the UEs (another 500 UEs) are randomly distributed into $N_{cr} = 6$ "crowds" and these UEs follow the crowd mobility model inspired by [49]. The movement of each crowd is defined by coordinates of the crowd's center $W = \{w_1, w_2, \ldots, w_{N_{cr}}\}$, where $w_{Ncr} \in R^2$ for $\forall n_{cr} \in \langle 1, N_{cr} \rangle$. Each cluster is of 20 m radius. Then, the 500 UEs belonging to the second half are randomly assigned to one of these clusters and dropped within the corresponding radius. Each UE in the cluster follows the global movement vector of the cluster, which moves with a speed of 1 m/s. On the top of the cluster movement, each UE within the cluster can also change its movement by $\pm 15^\circ$ and speed by ± 0.4 m/s with respect to the cluster center (i.e., the clustered UEs move with the uniformly distributed speed of $0.6 - 1.4$ m/s). Note that the UEs cannot leave the cluster radius.

We deploy up to five FlyBSs to serve the UEs [12] [33] [35]. The FlyBSs' traveled distance per second is limited to $d_{max} = 25$ m and the altitude to $h_{min} = 30$ m and $h_{max} = 350$ m. The channel between UE and FlyBS is determined via mixed LoS/NLoS path loss model with 10% probability of NLoS and 90% of LoS, as we focus on an outdoor scenario with the UEs in an open area. LoS and NLoS channels are modeled via the free space path loss with $\alpha_{n,m} = 2$ and $\alpha_{n,m} = 3$ in (3), respectively. We assume carrier frequency of 2.6 GHz [35], bandwidth of 20 MHz [50], and transmission power of the FlyBSs of 15 dBm [33] [44]. Noise and background interference from the neighboring SBSs with a density of -174 dBm/Hz [12] [35] and -130 dBm/Hz, respectively, are also considered to reflect our scenario, where a common infrastructure of mobile networks is not exactly in the served area like in the case of, for

Table II
SIMULATION PARAMETERS

Parameter	Value
Carrier frequency	2.6 GHz [35]
Bandwidth	20 MHz [50]
Number of UEs	40 and 1000 [12], [33], [35]
Number of FlyBSs	1, 3, 5 [12], [33], [35]
Tx power of FlyBSs	15 dBm [33], [44]
Height of UEs	1.5m [50]
FlyBS altitude limits h_{min} and h_{max}	30 m and 350 m
FlyBS flight constraint d_{max}	25 m
Noise power spectral density	–174 dBm/Hz [12], [35]
Background interference	–130 dBm/Hz

example, music festival in rural area. Note that the interference among the FlyBSs is derived as a sum of all interfering signals and it is added up to the noise and background interference from the neighboring SBSs.

The simulations are of 1800 seconds duration and the simulations are repeated 500 times with different UEs' deployments and movements in each simulation run to suppress an impact of randomness. Key simulation parameters and settings are summarized in Table II.

The proposed solution is compared with following approaches:

- *Numerical positioning*, which determines the positions of the FlyBSs to maximize the sum capacity numerically via Nelder-Mead simplex.
- *Positioning based on k-means*, introduced in [30], represents the common approach adopted for positioning in recent works, as it is of polynomial complexity only (thus converges fast).
- *Positioning via successive convex optimization*, representing state-of-the-art work determining the FlyBSs' positions to maximize the minimum capacity, as proposed in [14].

Note that up to our best knowledge, there is no paper targeting the minimization of the energy consumption for flying of the airship-based FlyBSs serving mobile UEs and comparison with the works for static UEs is not possible due to the nature of such works.

To evaluate a performance of the proposed algorithm, we define two performance metrics:

- *Energy saving* E_s – determined as relative average amount of the energy consumed by the proposal with respect to the average energy consumed by the algorithms determining the FlyBSs (sub-)optimal positions numerically, by k-means, and via successive convex optimization, during the whole simulation.
- *Sum capacity degradation* – relative difference between the sum capacity achieved by the the proposed algorithm and by the FlyBSs in the (sub-)optimum positions. Note that the sum capacity approximation in Theorem 3 does not apply in the simulations.

Note that we present both performance metrics as relative values (from 0 to 1) with respect to performance in the (sub-)optimum positions of the FlyBSs, since the relative metrics eliminate an impact of a specific setting of the energy consumption model.

B. Theoretical bounds of energy saving for single FlyBS

For easy interpretation of the trade-offs in energy saving and sum capacity, let us first illustrate a relation between the distance of the FlyBS from the optimum position D_o and the allowed degradation in sum capacity ϵ for typical FlyBS's altitudes [4] [51] in Fig. 4.

Fig. 4 indicates that D_o first rises quickly with increasing ϵ and, then, starts slowly saturating. This is implied by the logarithmic relation between the capacity and path loss with respect to the distance. We illustrate the results for various altitudes of the FlyBS to indicate that there is almost linear dependence between the FlyBS's altitude and D_o. Thus, the higher the FlyBS is, the higher the distance from the optimum position is acceptable in order to fulfill the maximum allowed degradation in the sum capacity. In general, relatively large values of D_o (in order of ones to few dozens of meters) still lead to only a negligible decrease in the sum capacity. For example, to guarantee the sum capacity degradation below 1% (i.e., $\epsilon = 0.01$), the FlyBS can stay about up to 1.1 m, 2.3 m, 5.5 m, 12 m, 18.5 m, and 37 m from the optimum position for the FlyBS at altitudes of 10 m, 20 m, 50 m, 100 m, 150 m, and 300 m, respectively. This finding itself can be interpreted so that the sub-optimal FlyBS's positions in order of few meters lead to only a negligible degradation in the sum capacity. Such outcome significantly relaxes requirements on finding the optimum positions of the FlyBSs.

Now, let's investigate the trade-off between energy saving and sum capacity degradation according to (10). In Fig. 5, we illustrate three examples of common practical cases representing the UEs moving along: *i)* straight street ($\theta = \pi$) with length of L meters, *ii)* right-angled streets (i.e., under the angle $\theta = \pi/2$), each street with length of $L/2$, and *iii)* streets with length of $L/2$ under the angle of $\theta = \pi/4$.

We analyze the energy saving of single FlyBS depending on the street length L, its direction (defined by the angle θ), and D_o in Fig. 6. We show the energy saving for the allowed sum capacity degradation of 0.5% ($\epsilon = 0.005$) and 4% ($\epsilon = 0.04$) corresponding to D_o of 12 m and 39 m, respectively, for the FlyBS's altitude of 150 m. Note that D_o is derived from ϵ via (9), as visualized in Fig 4. The results in Fig. 6 indicate that the longer the street is (i.e., the higher value of L), the less energy can be saved. This is justified by the fact that the longer the movement in the same direction is, the proportionally lower part of the movement can provide some energy saving. Let us illustrate this on an example of rather extreme case with a long direct street ($\theta = \pi$) and all UEs moving along the street in the same direction. For such street, the optimum position yielding the maximum sum capacity "moves" along with the UEs in the same direction. Thus, any energy saving is possible only at the beginning of the street until the optimum position is not farther than D_o from the initial position of the FlyBS. Once the optimum position becomes farther than D_o, the constraint (4a) would not hold unless the FlyBS moves as well. However, as the UEs keep moving in the same direction, the FlyBS

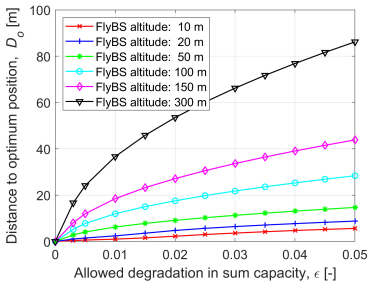

Figure 4. Relation between distance to optimum D_o with respect to allowed degradation in sum capacity of UEs ϵ.

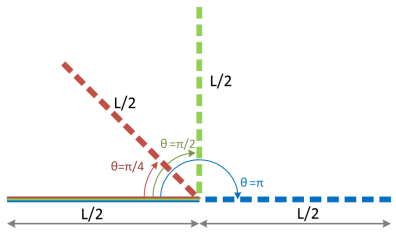

Figure 5. Examples of UEs' movement along: *i)* straight street ($\theta = \pi$), *ii)* right-angled streets ($\theta = \pi/2$), and *iii)* streets under angle of $\theta = \pi/4$.

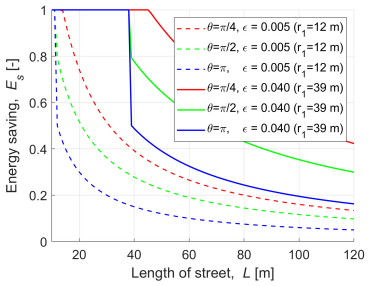

Figure 6. Relative amount of saved energy of FlyBS for flying; $E_s = 0$ represents no saving, $E_s = 1$ corresponds to 100% of energy being saved.

should also keep moving in the same direction. Thus, when the optimum becomes at the distance D_o from the FlyBS position for the first time, the FlyBS is forced to move all the time and no saving is possible to fulfill the constraint (4a). Thus, with prolongation of the street (higher L), the $D_o(t)$ becomes relatively smaller with respect to L and the energy saving is also reduced.

Furthermore, Fig. 6 demonstrates that more notable energy saving is observed if the angle between two streets θ is more acute. The reason is that the more acute angle enables to eliminate more significant part of the movement. In other words, the FlyBS moves less, as the UEs remain within D_o for a longer time. We also observe that a significant (dozens of percent) saving in the energy consumed for flying is possible despite a very low (few percent or less) degradation in the sum capacity is allowed. This very positive trade-off theoretically allows to save a significant amount of the energy for flying at a cost of only a marginal degradation in the sum capacity.

The analysis and results in Fig. 6 indicate that the energy saving is more likely for "more random" movement of the UEs rather than for a uniform direct movement of all UEs in the same direction. Such finding is, however, positive as the UEs are supposed to move at least a bit randomly in most of real-world situations.

C. Energy saving for multiple FlyBSs

Now, let's focus on the energy saving and the sum capacity in the scenario with multiple FlyBSs. For this investigation, we assume a general area without streets (e.g., a square in a city, a concert, a sport event, or an emergency situation in an open area), where some of the UEs move randomly and some follow a crowd movement model as explained in Section V-A.

Fig. 7 and Fig. 8 show the energy saving and corresponding sum capacity degradation ϵ (reflecting the users' requirements, see (4)), respectively, of the proposed algorithm with respect to the FlyBSs' positioning derived by three approaches outlined in Section V-A, i.e., *numerically via simplex* (left subplots), by *k-means* (middle subplots), and by state-of-the-art 3D positioning maximizing the minimum capacity via *successive convex optimization* (right subplots). The figures show results for lightly loaded network represented by 40 UEs (blue lines) and heavily loaded network with 1000 UEs (black lines) to demonstrate a scalability of our proposal. For the lower number of UEs, the gain with respect to the state-of-the-art works is a bit smaller (up to several to dozens percent decrease if the number of UEs drops 25-times, i.e., from 1000 to 40). This behavior is expectable, as the lower number of UEs imposes less pressure on communication and, hence, even less efficient solutions do not suffer much from sub-optimal decisions. A notable energy saving is observed with respect to all three competitive algorithms disregarding the number of FlyBSs, however, more significant energy saving is reached for a lower number of FlyBSs. The higher saving for less FlyBSs is due to a lower level of mutual interference among the FlyBSs and, at the same time, due to the fact that the more FlyBSs are deployed, the smaller area is served by each FlyBS and its movement is limited to this smaller area. Note that the decrease in energy savings with the number of FlyBSs is very small (just few percent when the number of FlyBSs is increased from three to five) and the savings are still significant (far above 60%) even for five FlyBSs. Hence, the solution is applicable even for large-scale scenarios.

In all three subplots in Fig. 7, the amount of saved energy increases with relaxation of the constraint on the sum capacity (i.e., with increasing ϵ). The energy saving first raises promptly when $\epsilon > 0$, since even a small allowed degradation in the capacity enables notable energy savings. With further increase in ϵ, the savings get saturated, since the saving reaches its maximum given by the users movement pattern. The energy for flying is saved significantly even if the allowed decrease in the sum capacity is very low (i.e., for very low ϵ). For example, for the allowed degradation in the sum capacity of 1% ($\epsilon = 0.01$), 55.4%, 67.5%, and 90.7% of the energy is saved compared to the numerical derivation of the optimum position (left subplot) if five, three, and one FlyBSs are deployed, respectively. The numerical derivation of the optimum position is not practical due to a high complexity. Thus, we show also the performance of the proposed scheme with respect to a more practical state-of-the-art solution determining the position of the FlyBSs based on low-complexity k-means (middle subplot in Fig. 7) and based on successive convex optimization (right subplot in Fig. 7). With respect to the k-means-based determination of the positions, the proposal achieves even more significant energy saving and 77.2%, 88.2%, and 98.8% of the energy is

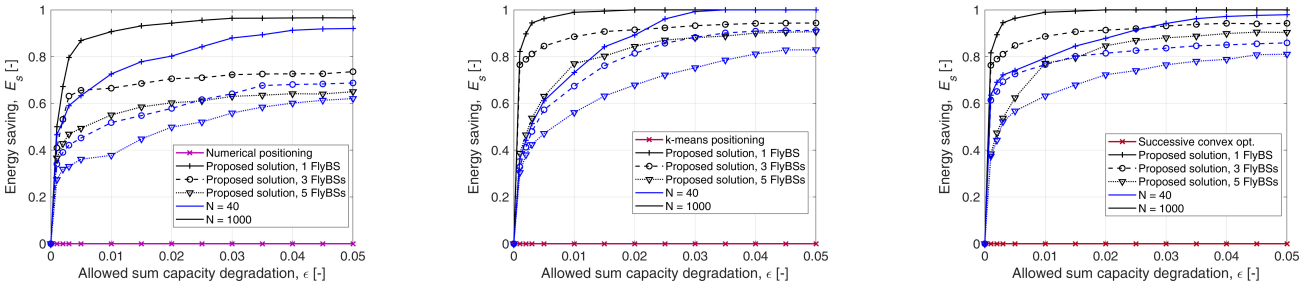

Figure 7. Relative energy saving of proposed FlyBSs' positioning with respect to energy consumed by positioning: maximizing sum capacity derived *numerically* (left), based on *k-means* (middle), and *based on successive convex optimization* (right).

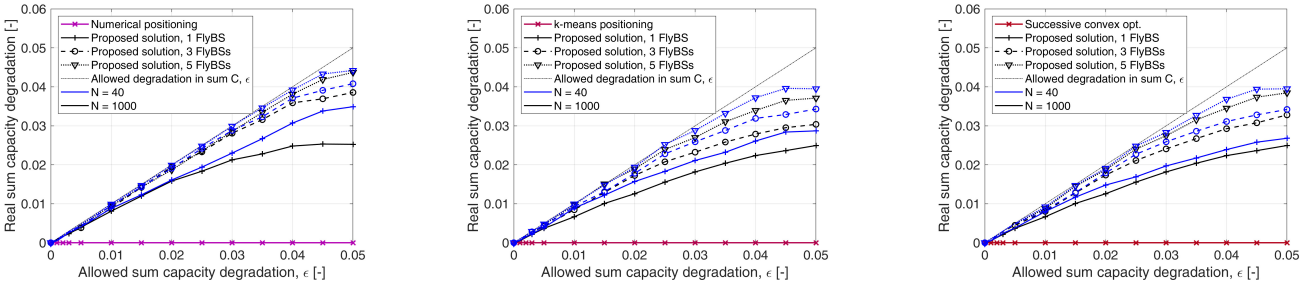

Figure 8. Sum capacity degradation due to proposed energy-efficient positioning with respect to maximum sum capacity determined: *numerically* (left), by *k-means* (middle), and *based on successive convex optimization* (right).

saved for five, three, and one FlyBSs, respectively, if only 1% degradation in the sum capacity is allowed (i.e., $\epsilon = 0.01$). Similar energy saving of 77.1%, 88.6%, and 98.9% for five, three, and one FlyBSs, respectively, if $\epsilon = 0.01$ is reached by the proposal also with respect to the positioning based on successive convex optimization. The reason for higher savings reached by the proposal compared to the k-means and the successive convex optimization than the savings compared to the numerical solution is the fact that both the k-means and the successive convex optimization provide a sub-optimal sum capacity (lower than for the numerical solution) and, thus, enable our proposed algorithm to avoid the redundant movement even more notably.

Note that ϵ defines the maximum *"allowed"* degradation in the sum capacity, however, even a lower degradation can be actually experienced by the UEs. Thus, in Fig. 8, we illustrate the real sum capacity degradation observed in the simulations with respect to the given allowed degradation ϵ. The figure confirms that the real degradation in the sum capacity is safely below the allowed one (dotted straight line in figures) and the capacity constraint (4a) is satisfied.

Comparing the proposal with the positioning maximizing the sum capacity numerically in Fig. 8, left subplot, for 1% real degradation in the sum capacity, ϵ corresponds to 0.0105, 0.0110, and 0.0125 and, consequently, the real energy saving (determined for these values of ϵ in Fig. 7, left subplot) is 55.7%, 67.9%, and 91.9% for five, three, and one FlyBSs, respectively. The real degradation in the sum capacity comparing the proposal and the k-means is presented in Fig. 8 (middle subplot). For the same allowed sum capacity degradation of 1%, the real degradation is only about 0.90%, 0.80%, and 0.59% for five, three, and one FlyBSs, respectively. Thus, considering the real sum capacity degradation of 1% (corresponding to ϵ of 0.011, 0.0125, and 0.0175), the energy saving of 77.9%, 89.4%, and 99.5% is observed for five, three, and one FlyBSs, respectively. Last, Fig. 8 (right subplot) depicts the real degradation in the sum capacity with respect to the successive convex optimization-based positioning. For the allowed sum capacity degradation of 1%, the real degradation corresponds to ϵ of 0.011, 0.0120, and 0.015. Consequently, the real energy saving reaches 77.7%, 89.6%, and 99.4% for five, three, and one FlyBSs, respectively, compared to the successive convex optimization.

These results confirm the efficiency of the proposed algorithm and demonstrate that a significant saving in the energy for flying of the airship-based FlyBSs is achieved at a negligible cost represented by only marginal decrease in the sum capacity of the UEs. The results can be also interpreted in the way that an imprecise positioning of the FlyBSs (in order of dozens of decimeters to few meters) does not lead to any notable reduction in the sum capacity. Such finding gives a new degree of freedom for future optimization of the networks with the FlyBSs.

We investigate also an impact of the UEs' speed on both the energy saving and the sum capacity compared to the positioning of the FlyBSs maximizing the sum capacity numerically via simplex in Fig. 9 for the allowed degradation in sum capacity of 4% (i.e., $\epsilon = 0.04$). The figure demonstrates there is no notable impact (variation is about 2%) on both the energy saving (left subplot) and the sum capacity degradation (right subplot). This is due to the fact that there is no strong direct dependency of the proposed algorithm on the speed of UEs and the algorithm still forces the FlyBS to reach the same distance to optimum D_o (see (9)). Besides, the right subplot

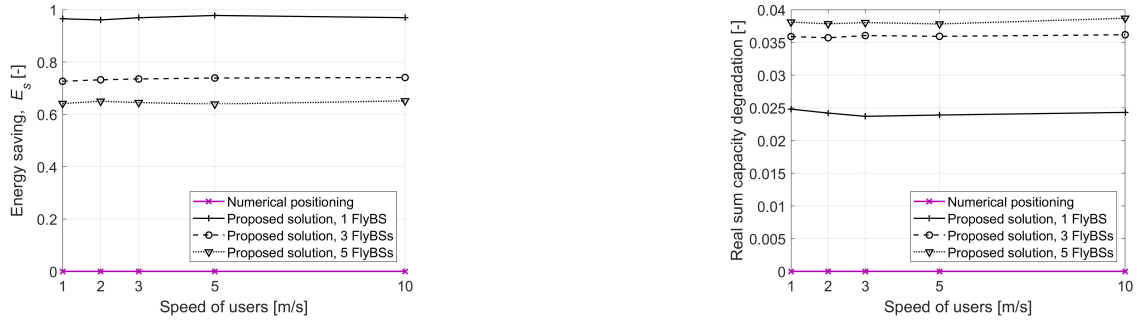

Figure 9. Impact of speed of UEs on energy saving (left subplot) and sum capacity (right subplot) with respect to the numerical positioning for allowed degradation in sum capacity $\epsilon = 0.04$

confirms that the real sum capacity degradation is safely below the allowed 4%.

Furthermore, in Fig. 10, we demonstrate that the fairness in capacity of individual UEs (defined as Jain's fairness index) is similar for our proposal and for state-of-the-art works. Our algorithm even slightly improves the fairness (by few percent) if ϵ increases compared to the state-of-the-art works, since the larger ϵ provides additional flexibility in balancing the capacity among UEs.

To illustrate fast convergence of the proposed algorithm, we plot the average number of iterations over the capacity step ΔC_{step} (see Algorithm 1) in Fig. 11. This figure confirms that the larger the step of the FlyBS movement is (i.e., larger ΔC_{step}), the faster the FlyBSs converge to their final positions. However, already ΔC_{step} of roughly 10 kbps requires only about two iterations. This means that only two FlyBSs move in each step. Such fast convergence does not limit practical applications. Note that all previous figures are plotted for ΔC_{step} of 10 kbps.

In Fig. 12, an example of the FlyBS trajectory in 3D space (left subplot) and projection to 2D (right subplot) is shown for three FlyBSs. We observe that each FlyBS changes 3D position in a certain area depending on the UEs' movement and the FlyBSs' positions are also influenced by interference from neighboring FlyBSs to the UEs. Hence, if one FlyBS initiates some movement towards other FlyBSs motivated by new UE's positions, the other FlyBSs adapt to that movement with a similar movement pattern to keep their served UEs also satisfied. Fig. 12 also indicates optimum position of the FlyBSs derived numerically to illustrate that a notable reduction in the redundant movements of the FlyBSs is achieved by the proposed approach.

VI. Conclusions

In this paper, we have derived and analyzed a relation between the sum capacity and the energy consumed for flying by the airship-based FlyBSs serving the mobile (moving) UEs. We have analytically shown theoretical bounds for the energy saving of the FlyBSs with respect to the sum capacity degradation. Then, we have proposed novel algorithm reducing the energy consumed for flying while still guaranteeing close to optimum sum capacity. If the sum capacity degradation is limited to 1%, the proposed algorithm enables energy saving of 55.4%, 67.5%, and 90.7% if five, three, and one FlyBSs are deployed, respectively, compared to the numerically determined position maximizing the sum capacity. The results indicate that a "perfect positioning" of the airship-based FlyBSs is not necessary and an error in the positioning in order of few meters have only marginal impact on the sum capacity. This finding provides a new degree of freedom for future research and development of algorithms for networks with FlyBSs.

In the future, the presented analysis and the proposed algorithm can be enhanced towards a joint optimization of the energies spent for flying and for communication. Besides, considering battery lifetime and charging aspects in the problem of FlyBSs positioning, e.g., as done for vehicles in [53], is a challenging topic.

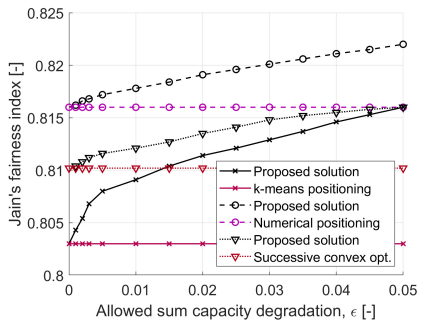

Figure 10. Fairness in capacity experienced by users with respect to allowed sum capacity degradation ϵ for five FlyBSs.

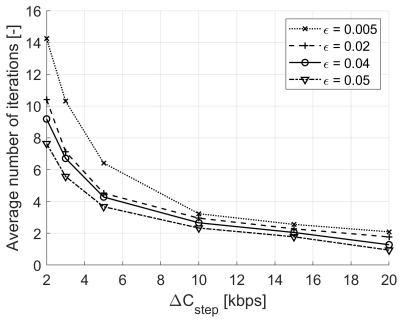

Figure 11. Number of iterations performed in the proposed positioning for different ΔC_{step} and various values of allowed degradation in sum capacity ϵ for five FlyBSs.

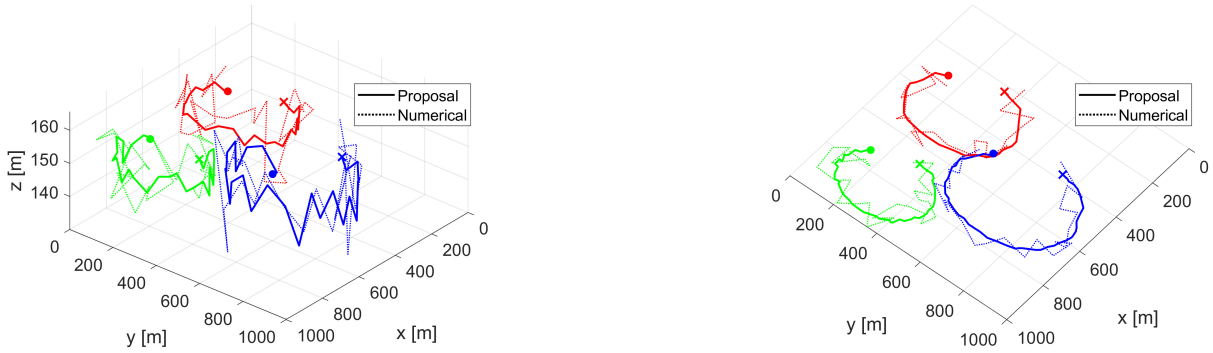

Figure 12. Example of movement of three FlyBSs for the proposed algorithm (solid lines) and positioning derived numerically (dotted lines), "•" and "×" markers indicate starting and finishing positions of the FlyBSs in 3D (left) and 2D projection (right).

APPENDIX A

This appendix provides the proof to Proposition 2. Let us start with the sum capacity definition from system model (Section II), i.e.,:

$$\sum_{n=1}^{N} C_n = \sum_{n=1}^{N} B_n \log_2\left(1+\frac{p_n^R}{\sigma^2}\right) = \sum_{n=1}^{N} B_n \log_2\left(1+\frac{Q_n}{\sigma^2 d_n^{\alpha_n}}\right). \quad (19)$$

Now, we approximate log function with respect to parameter X using linear approximation:

$$\log_2(a+X) \approx \frac{1}{\ln(2)}\big(\ln(a+as\tau) - \frac{s\tau}{1+s\tau} + \frac{X}{a(1+s\tau)}\big), \quad (20)$$

where $s = \lfloor \frac{X}{a\tau} \rfloor$. We also use the polynomial approximation with respect to an arbitrary X:

$$(a+X)^k \approx (a+qa\delta)^k + k(a+qa\delta)^{k-1}(X-qa\delta), \quad (21)$$

where $q = \lfloor \frac{X}{a\delta} \rfloor$. Note that the values of τ and δ in (20) and (21), respectively, are approximation parameters, and choosing a smaller τ and δ results in a smaller error in the linear approximations (up to a certain low value of both, as the UEs' distribution is discrete), but the smaller error is at the cost of a higher computation complexity.

By applying (20) and (21) (with $\frac{Q_n}{\sigma^2 d_n^{\alpha_n}}$ as X), the sum capacity from (19) is rewritten for the optimal FlyBS position $[x_f^*, y_f^*, z_f^*]$ as:

$$\sum_{n=1}^{N} C_n \approx \sum_{n=1}^{N} \frac{B_n}{\ln(2)}\big(\ln(1+s_n\tau) - \frac{s_n\tau}{1+s_n\tau} + \frac{Q_n}{(1+s_n\tau)d_n^{\alpha_n}\sigma^2}\big) = \sum_{n=1}^{N} \frac{B_n}{\ln(2)}\big(\ln(1+s_n\tau) - \frac{s_n\tau}{1+s_n\tau}\big) + \sum_{n=1}^{N} \frac{B_n Q_n}{(1+s_n\tau)\sigma^2\ln(2)}\Big((x_f^*-x_{u,n})^2 + (y_f^*-y_{u,n})^2 + \big((z_f^*-z_{u,n})^2 - \Upsilon^2\big) + \Upsilon^2\Big)^{-\frac{\alpha_n}{2}}, \quad (22)$$

where $\Upsilon \neq 0$ is arbitrary value for the approximation. The expression (22) is then:

$$\sum_{n=1}^{N} C_n \approx \sum_{n=1}^{N} \frac{B_n}{\ln(2)}(\ln(1+s_n\tau) - \frac{s_n\tau}{1+s_n\tau}) + \sum_{n=1}^{N} \frac{B_n Q_n}{(1+s_n\tau)\sigma^2\ln(2)} \times \Big(\mu_n^{-\frac{\alpha_n}{2}} + (\frac{-\alpha_n\mu_n^{-\frac{\alpha_n}{2}-1}}{2})\big((x_f^*-x_{u,n})^2 + (y_f^*-y_{u,n})^2 + \big((z_f^*-z_{u,n})^2 - \Upsilon^2\big) - k_n\delta\Upsilon^2\big)\Big) = \sum_{n=1}^{N} \frac{B_n}{\ln(2)}(\ln(1+s_n\tau) - \frac{s_n\tau}{1+s_n\tau}) + \sum_{n=1}^{N} \frac{B_n Q_n}{(1+s_n\tau)\sigma^2\ln(2)}\Big(\mu_n^{-\frac{\alpha_n}{2}} + \frac{k_n\delta\alpha_n}{2}\mu_n^{-\frac{\alpha_n}{2}-1}\Upsilon^2 - \frac{\alpha_n\mu_n^{-\frac{\alpha_n}{2}-1}}{2}(x_f^{*2} + x_{u,n}^2 - 2x_f^*x_{u,n} + y_f^{*2} + y_{u,n}^2 - 2y_f^*y_{u,n} + z_f^{*2} + z_{u,n}^2 - 2z_f^*z_{u,n} - \Upsilon^2)\Big) = \nu - \big(\sum_{n=1}^{N}\omega_n\big)(d^2[\boldsymbol{v}^*, \boldsymbol{v_o}]), \quad (23)$$

where $\boldsymbol{v_o} = [x_{f,o}, y_{f,o}, z_{f,o}]$, and

$$k_n = \lfloor \frac{\big((x_f^*-x_{u,n})^2 + (y_f^*-y_{u,n})^2 + (z_f^*-z_{u,n})^2 - \Upsilon^2\big)}{\Upsilon^2\delta} \rfloor,$$

$$\mu_n = \Upsilon^2(1+k_n\delta), s_n = \lfloor \frac{Q_n}{\sigma^2 d_i^{\alpha_n}\tau} \rfloor, \omega_n = \frac{B_i Q_i \alpha_n \mu_n^{-\frac{\alpha_n}{2}-1}}{2\sigma^2(1+s_n\tau)\ln(2)},$$

$$[x_{f,o}, y_{f,o}, z_{f,o}] = \Big[\frac{\sum_{n=1}^{N}\omega_n x_{u,n}}{\sum_{n=1}^{N}\omega_n}, \frac{\sum_{n=1}^{N}\omega_n y_{u,n}}{\sum_{n=1}^{N}\omega_n}, \frac{\sum_{n=1}^{N}\omega_n z_{u,n}}{\sum_{n=1}^{N}\omega_n}\Big],$$

$$\nu = \frac{(\sum_{n=1}^{N}\omega_n x_{u,n})^2}{\sum_{n=1}^{N}\omega_n} + \frac{(\sum_{n=1}^{N}\omega_n y_{u,n})^2}{\sum_{n=1}^{N}\omega_n} + \frac{(\sum_{n=1}^{N}\omega_n z_{u,n})^2}{\sum_{n=1}^{N}\omega_n} - \sum_{n=1}^{N}\omega_n x_{u,n}^2 - \sum_{n=1}^{N}\omega_n y_{u,n}^2 - \sum_{i=n}^{N}\omega_n z_{u,n}^2 + \sum_{n=1}^{N}\frac{B_n}{\ln(2)} \times \Big(\ln(1+s_n\tau) - \frac{s_n\tau}{1+s_n\tau}\Big) + \sum_{n=1}^{N}\frac{B_n Q_n}{\sigma^2(1+s_n\tau)\ln(2)} \times \Big(\mu_n^{-\frac{\alpha_n}{2}} + (\frac{k_n\mu_n^{-\frac{\alpha_n}{2}-1}\delta\alpha_n + \alpha_n\mu_n^{-\frac{\alpha_n}{2}-1}}{2})\Upsilon^2\Big). \quad (24)$$

The expression in (23) allows to directly evaluate $\sum_{n=1}^{N} C_n$ at $[x_f, y_f, z_f]$. To this end, using the approximation in (23),

the constraint $\sum_{n=1}^{N} C_n \geq C_{opt} \times (1-\epsilon)$ from (7) is rewritten as:

$$\nu - \Big(\sum_{i=1}^{N} \omega_n\Big)\left((x_f^* - x_{f,o})^2 + (y_f^* - y_{f,o})^2 + (z_f^* - z_{f,o})^2\right) \geq C_{opt} \times (1-\epsilon), \tag{25}$$

$$(x_f^* - x_{f,o})^2 + (y_f^* - y_{f,o})^2 + (z_f^* - z_{f,o})^2 \leq D_o^2(t), \tag{26}$$

where $D_o(t) = \left(\frac{\nu - C_{opt}\times(1-\epsilon)}{\sum_{n=1}^{N}\omega_i}\right)^{\frac{1}{2}}$ as observed from (25), and $x_{f,o}$, $y_{f,o}$, $z_{f,o}$ are, in line with (24), the coordinates of the FlyBS at which $\sum_{n=1}^{N} C_n$ reaches its maximum for $[x_f, y_f, z_f]$. Consequently, $[x_{f,o}, y_{f,o}, z_{f,o}] = [x_f^*, y_f^*, z_f^*]$ and (26) represents the distance $d\left[\boldsymbol{v}(t), \boldsymbol{v}^*(t)\right]$. Thus, (26) can be rewritten as $d\left[\boldsymbol{v}(t), \boldsymbol{v}^*(t)\right] < D_o(t)$. This concludes the proof.

APPENDIX B

To provide proof to Theorem 3, let us first analyze the constraint (a) in the problem defined in (4) for multiple FlyBSs. From (1), (2), and (3), we get:

$$\sum_{m=1}^{M}\sum_{n=1}^{N} a_{n,m}C_{n,m} = \sum_{m=1}^{M}\sum_{n=1}^{N} a_{n,m}B_{n,m} \times \log_2(1+ \frac{p_{n,m}^R}{\sigma^2 + \sum_{j=1,m\neq j}^{M} p_{n,j}^R}) = \sum_{m=1}^{M}\sum_{n=1}^{N} a_{n,m}B_{n,m} \times \Big(\log_2(\sigma^2 + \frac{Q_{n,m}}{d_{n,m}^{\alpha_{n,m}}} + \sum_{j=1,m\neq j}^{M} \frac{Q_{n,j}}{d_{n,j}^{\alpha_{n,m}}}) - \log_2(\sigma^2 + \sum_{j=1,m\neq j}^{M} \frac{Q_{n,j}}{d_{n,j}^{\alpha_{i,j}}})\Big) \tag{27}$$

Next, using the linear approximation as defined in (21), we approximate $\frac{Q_{n,m}}{d_{n,m}^{\alpha_{n,m}}}$ in (27) as:

$$\frac{Q_{n,m}}{d_{n,m}^{\alpha_{n,m}}} = Q_{n,m}\Big((x_{f,m}^* - x_{u,n})^2 + (y_{f,m}^* - y_{u,n})^2 + \big((z_{f,m}^* - z_{u,n})^2 - \Upsilon^2\big) + \Upsilon^2\Big)^{-\frac{\alpha_{n,m}}{2}} \approx Q_{n,m}\Big(\eta_{n,m}^{-\frac{\alpha_{n,m}}{2}} - \frac{\alpha_{n,m}}{2}\eta_{n,m}^{-\frac{\alpha_{n,m}}{2}-1}\Big((x_{f,m}^* - x_{u,n})^2 + (y_{f,m}^* - y_{u,n})^2 + ((z_{f,m}^* - z_{u,n})^2 - \Upsilon^2) - k_{n,m}\tau\Upsilon^2\Big)\Big), \tag{28}$$

$$\eta_{n,m} = \Upsilon^2(1+k_{n,m})\delta, \quad k_{n,m} = \lfloor \frac{\big((x_{f,m}^* - x_{u,n})^2 + (y_{f,m}^* - y_{u,n})^2 + (z_{f,m}^* - z_{u,n})^2 - \Upsilon^2\big)}{\Upsilon^2\delta} \rfloor,$$

A similar approximation is done also for $\frac{Q_{n,m}}{d_{n,m}^{\alpha_{n,m}}}$. Then, the sum capacity in (27) is approximated as:

$$\sum_{m=1}^{M}\sum_{n=1}^{N} a_{n,m}C_{n,m} \approx \sum_{m=1}^{M}\sum_{n=1}^{N} a_{n,m}B_{n,m}\Big(\log_2\Big(\sigma^2 + Q_{n,m}\Big(\Gamma_{n,m}\big((x_{f,m}^* - x_{u,n})^2 + (y_{f,m}^* - y_{u,n})^2 + (z_{f,m}^* - z_{u,n})^2 - \Upsilon^2 - k_{n,m}\delta\Upsilon^2\big)\Big) + \sum_{j=1,m\neq j}^{M} Q_{n,j}\Big(\Gamma_{n,j}((x_{f,j}^* - x_{u,n})^2 + (y_{f,j}^* - y_{u,n})^2 + (z_{f,j}^* - z_{u,n})^2 - \Upsilon^2 - k_{n,j}\delta\Upsilon^2)\Big)\Big) - \log_2\Big(\sigma^2 + \sum_{j=1,m\neq j}^{M} Q_{n,j}\Big(\Gamma_{n,j}\big((x_{f,j}^* - x_{u,n})^2 + (y_{f,j}^* - y_{u,n})^2 + (z_{f,j}^* - z_{u,n})^2 - \Upsilon^2 - k_{n,j}\delta\Upsilon^2\big)\Big)\Big) = \sum_{m=1}^{M}\sum_{n=1}^{N} a_{n,m}B_{n,m} \times \Bigg(\log_2\Big(\psi_{n,m} + \sum_{j=1}^{M}\Big(Q_{n,j}\Gamma_{n,j} \times \big((x_{f,j}^* - x_{u,n})^2 + (y_{f,j}^* - y_{u,n})^2 + (z_{f,j}^* - z_{u,n})^2 - \Upsilon^2\big)\Big)\Big) - \log_2\Big(\phi_{n,m} + \sum_{j=1,m\neq j}^{M}\Big(Q_{n,j}\Gamma_{n,j} \times \big((x_{f,j}^* - x_{u,n})^2 + (y_{f,j}^* - y_{u,n})^2 + (z_{f,j}^* - z_{u,n})^2 - \Upsilon^2\big)\Big)\Big)\Bigg) \tag{29}$$

where $\Gamma_{n,m} = \big(\Upsilon^2(1 + k_{n,m}\delta)\big)^{-\frac{\alpha_{n,m}}{2}} - \frac{\alpha_{n,m}}{2}\big(\Upsilon^2(1 + k_{n,m}\delta)\big)^{-\frac{\alpha_{n,m}}{2}-1}$; $\phi_{n,m} = \sigma^2 - \sum_{j=1,m\neq j}^{M} Q_{n,j}\Gamma_{n,j}k_{n,j}\delta\Upsilon^2$; $\psi_{n,m} = \sigma^2 - Q_{n,m}\Gamma_{n,m}k_{n,m}\delta\Upsilon^2 - \sum_{j=1,m\neq j}^{M} Q_{n,j}\Gamma_{n,j}k_{n,j}\delta\Upsilon^2$.

Using the approximation in (29), we get:

$$\sum_{m=1}^{M}\sum_{n=1}^{N} a_{n,m}C_{n,m} \approx \sum_{m=1}^{M}\sum_{n=1}^{N} a_{n,m}B_{n,m} \times \Bigg(\frac{\sum_{j=1}^{M} Q_{n,j}\Gamma_{n,j}}{\ln(2)\psi_{n,m}(1+\lambda_{n,m}\tau)} \times \big((x_{f,m}^* - x_{u,n})^2 + (y_{f,m} - y_{u,n})^2 + (z_{f,m}^* - z_{u,n})^2 - \Upsilon^2\big) + \ln\big(\psi_{n,m}(1+\lambda_{n,m}\tau)\big) - \frac{\lambda_{n,m}\tau}{1+\lambda_{n,m}\tau} - \frac{\sum_{j=1,m\neq j}^{M} Q_{n,j}\Gamma_{n,j}}{\phi_{n,j}(1+\beta_{n,m}\tau)} \times \big((x_{f,m}^* - x_{u,n})^2 + (y_{f,m}^* - y_{u,n})^2 + (z_{f,m}^* - z_{u,n})^2 - \Upsilon^2\big) + \ln\big(\phi_{n,m}(1+\beta_{n,m}\tau)\big) - \frac{\beta_{n,m}\tau}{1+\beta_{n,m}\tau}\Bigg) \tag{30}$$

where

$$\beta_{n,m} = \lfloor \frac{1}{\tau\phi_{n,j}} \times \sum_{j=1,m\neq j}^{M}\Big(Q_{n,j}\Gamma_{n,j}\big((x_{f,j}^* - x_{u,n})^2 + (y_{f,j}^* - y_{u,n})^2 + (z_{f,j}^* - z_{u,n})^2 - \Upsilon^2\big)\Big) \rfloor, \xi_{n,m} = \Gamma_{n,m} \times \Big((x_{f,m}^* - x_{u,n})^2 + (y_{f,m}^* - y_{u,n})^2 + (z_{f,m}^* - z_{u,m})^2 - \Upsilon^2\Big) + \sum_{j=1,m\neq j}^{M} Q_{n,j}\Gamma_{n,j}\Big((x_{f,j}^* - x_{u,n})^2 + (y_{f,j}^* - y_{u,n})^2 + (z_{f,j}^* - z_{u,n})^2 - \Upsilon^2\Big), \lambda_{n,m} = \lfloor \frac{\xi_{n,m}}{\tau\psi_{n,m}} \rfloor. \tag{31}$$

The sum capacity defined in (30) is further simplified to:

$$\sum_{m=1}^{M}\sum_{n=1}^{N} C_{n,m} \approx A - \sum_{m=1}^{M} r_m\Big((x_{f,m}^* - x_{f,o,m})^2 + (y_{f,m}^* - y_{f,o,m})^2 + (z_{f,m}^* - z_{f,o,m})^2\Big), \tag{32}$$

where the following substitutions are adopted:

$$A = B_{n,m}\Upsilon^2\Big(\frac{-\sum_{m=1}^{M} Q_{n,m}\Gamma_{n,m}}{\ln(2)\psi_{n,m}(1+\lambda_{n,m}\tau)} + \frac{\sum_{m=1,m\neq j}^{M} Q_{n,j}\Gamma_{n,j}}{\phi_{n,m}(1+\beta_{n,m}\tau)}\Big) + \sum_{m=1}^{M}\sum_{n=1}^{N}\left(\frac{B_{n,m}}{\ln(2)}\sum_{m=1}^{M}\left(\ln(\psi_{i,m}(1+\lambda_{i,m}\tau)) - \frac{\lambda_{i,m}\tau}{1+\lambda_{i,m}\tau}\right)\right) - \sum_{m=1}^{M}\sum_{n=1}^{N}\left(\frac{B_{n,m}}{\ln(2)}\sum_{j=1,m\neq j}^{M}\left(\ln\left(\phi_{n,j}(1+\beta_{n,j}\tau)\right) - \frac{\beta_{n,j}\tau}{1+\beta_{n,j}\tau}\right)\right) - \sum_{n=1}^{N}\zeta_{n,m}x_{u,n}^2 - \sum_{n=1}^{N}\zeta_{n,m}y_{u,n}^2 - \sum_{n=1}^{N}\zeta_{n,m}z_{u,n}^2 + \frac{(\sum_{n=1}^{N}\zeta_{n,m}x_{u,n})^2}{\sum_{n=1}^{N}\zeta_{n,m}} + \frac{(\sum_{n=1}^{N}\zeta_{n,m}y_{u,n})^2}{\sum_{n=1}^{N}\zeta_{n,m}} + \frac{(\sum_{n=1}^{N}\zeta_{n,m}z_{u,n})^2}{\sum_{n=1}^{N}\zeta_{n,m}}\Big),$$

$$\zeta_{n,m} = \frac{B_{n,m}}{\ln(2)}\sum_{m=1}^{M}\big(Ml_m - (M-1)s_m\big),$$

$$l_m = \sum_{n=1}^{N}\sum_{m=1}^{M}\frac{Q_{n,m}\Gamma_{n,m}}{\psi_{n,m}(1+\lambda_{n,m}\tau)}, \quad r_m = \sum_{n=1}^{N}\zeta_{n,m},$$

$$s_m = \sum_{n=1}^{N}\sum_{m=1}^{M}\frac{Q_{n,m}\Gamma_{n,m}}{\phi_{n,m}(1+\beta_{n,m}\tau)}, x_{f,o,m} = \frac{\sum_{n=1}^{N}\zeta_{n,m}x_{u,n}}{\sum_{i=n}^{N}\zeta_{n,m}},$$

$$y_{f,o,m} = \frac{\sum_{n=1}^{N}\zeta_{n,m}y_{u,n}}{\sum_{n=1}^{N}\zeta_{n,m}}, z_{f,o,m} = \frac{\sum_{n=1}^{N}\zeta_{n,m}z_{u,n}}{\sum_{n=1}^{N}\zeta_{n,m}}. \quad (33)$$

Since the sum capacity reaches its maximum for $[x_{f,m}, y_{f,m}, z_{f,m}] = [x_{f,o,m}, y_{f,o,m}, z_{f,o,m}]$ it is concluded that $[x^*_{f,m}, y^*_{f,m}, z^*_{f,m}] = [x_{f,o,m}, y_{f,o,m}, z_{f,o,m}]$ according to (32). Then, we use the approximation in (32) to evaluate the sum capacity at $[x_{f,m}, y_{f,m}, z_{f,m}]$ as follow:

$$\sum_{m=1}^{M}\sum_{n=1}^{N}C_{n,m} \approx A - \sum_{m=1}^{M} r_m d^2\left[\boldsymbol{v_m}(t), \boldsymbol{v^*_m}(t)\right] \quad (34)$$

Given the approximation derived in (34), the constraint (4a) is rewritten as:

$$\sum_{m=1}^{M}\sum_{n=1}^{N}C_{n,m} \approx A - \sum_{m=1}^{M} r_m d^2\left[\boldsymbol{v_m}(t), \boldsymbol{v^*_m}(t)\right] \geq C_{opt}\times(1-\epsilon) \quad (35)$$

To conclude the proof, (35) is directly rewritten to the form in Theorem 3:

$$\sum_{m=1}^{M} r_m d^2\left[\boldsymbol{v_m}(t), \boldsymbol{v^*_m}(t)\right] \leq A - C_{opt}\times(1-\epsilon) \quad (36)$$

REFERENCES

[1] H. Guo, J. Li, J. Liu, N. Tian, N. Kato, "A Survey on Space-Air-Ground-Sea Integrated Network Security in 6G," IEEE Communications Surveys & Tutorials, vol. 24, no. 1, 2022.

[2] J. Wang, C. Jiang, Z. Han, Y. Ren; R.G. Maunder, L. Hanzo, "Taking Drones to the Next Level: Cooperative Distributed Unmanned-Aerial-Vehicular Networks for Small and Mini Drones," IEEE Vehicular Technology Magazine, Sept. 2017.

[3] J. Zhang, T. Chen, S. Zhong, J. Wang, W. Zhang, X. Zuo, R. G. Maunder, L. Hanzo, "Aeronautical Ad Hoc Networking for the Internet-Above-the-Clouds," Proceedings of the IEEE, vol. 107, no. 5, May 2019.

[4] S. Chandrasekharan, et al, "Designing and Implementing Future Aerial Communication Networks," IEEE Communications Magazine, 2016.

[5] L. Gupta, R. Jain, and G. Vaszkun, "Survey of Important Issues in UAV Communication Networks," IEEE Communications Surveys & Tutorials, Vol. 18, No. 2, Secondquarter 2016.

[6] A. Fotouhi, et al, "Survey on UAV Cellular Communications: Practical Aspects, Standardization Advancements, Regulation, and Security Challenges," IEEE Communications Surveys Tutorials, Early Access, March 2019.

[7] H. Guo, X. Zhou, J. Liu, Y. Zhang, "Vehicular intelligence in 6G: Networking, communications, and computing," Vehicular Communications, vol. 33, January 2022.

[8] R. I. Bor-Yaliniz, A. El-Keyi, and H. Yanikomeroglu, "Efficient 3-D placement of an aerial base station in next generation cellular networks," IEEE ICC 2016.

[9] Q. Hu, Y. Cai , G. Yu, Z. Qin, M. Zhao, G Ye Li, "Joint offloading and trajectory design for UAV-enabled mobile edge computing systems," IEEE Internet Things J., vol. 6, no. 2, pp. 1879-1892, April 2019.

[10] M. Mozaffari, W. Saad, M. Bennis, Y. Nam, and M. Debbah, "A tutorial on FlyBSs for wireless networks: Applications, challenges, and open problems", IEEE Communications Surveys & Tutorials, 2019.

[11] S. T. Muntaha, S. A. Hassan, H. Jung and M. S. Hossain, "Energy Efficiency and Hover Time Optimization in UAV-Based HetNets," IEEE Transactions on Intelligent Transportation Systems, vol. 22, no. 8, Aug. 2021.

[12] M. Sami, J. N. Daigle, "User Association and Power Control for UAV-Enabled Cellular Networks," IEEE Wireless Communications Letters, vol. 9, no. 3, March 2020.

[13] Q. Hu, Y. Cai, A. Liu, G. Yu, G.Y. Li, "Low-Complexity Joint Resource Allocation and Trajectory Design for UAV-Aided Relay Networks With the Segmented Ray-Tracing Channel Model," IEEE Trans. Wireless Commun., vol. 19, no. 9, 2020.

[14] I. Valiulahi, C. Masouros, "Multi-UAV Deployment for Throughput Maximization in the Presence of Co-Channel Interference," IEEE Internet of Things journal, March 2021.

[15] J. Wang, C. Jiang, Z. Wei, C. Pan, H. Zhang, Y. Ren, "Joint UAV Hovering Altitude and Power Control for Space-Air-Ground IoT Networks", IEEE Internet of Things Journal, Vol. 6, No. 2, April 2019.

[16] M. Mozaffari, W. Saad, M. Bennis, and M. Debbah, "Optimal transport theory for power-efficient deployment of unmanned aerial vehicles," IEEE ICC, 2016.

[17] Y. Zeng and R. Zhang, "Energy-Efficient UAV Communication With Trajectory Optimization," IEEE Transactions on Wireless Communications, Vol. 16, No. 6, 2017.

[18] L. Wang, B. Hu, S. Chen, "Energy Efficient Placement of a Drone Base Station for Minimum Required Transmit Power," IEEE Wireless Communications Letters, vol. 9, no. 12, December 2020.

[19] M. Mozaffari, W. Saad, M. Bennis, and M. Debbah, "Unmanned Aerial Vehicle with Underlaid Device-to-Device Communications: Performance and Tradeoffs," IEEE Transactions on Wireless Communications, Vol. 15, No. 6, 2016.

[20] K. Li, W. Ni, X. Wang, R. P. Liu, S. S. Kanhere, and S. Jha, "Energy Efficient Cooperative Relaying for Unmanned Aerial Vehicles," IEEE Transactions on Mobile Computing, Vol. 15, No. 6, June 2016.

[21] A. Abdulla, Z. M. Fadlullah, H. Nishiyama, N. Kato, F. Ono, and R. Miura, "Toward Fair Maximization of Energy Efficiency in Multiple UAS-Aided Networks: A Game-Theoretic Methodology," IEEE Trans. on Wireless Communications, 2015.

[22] M. Najla, Z. Becvar, P. Mach, D. Gesbert, "Positioning and Association Rules for Transparent Flying Relay Stations," IEEE Wireless Communications Letters, vol. 10, no. 6, pp. 1276-1280, June 2021.

[23] Y. Zeng, J. Xu, R. Zhang, "Energy Minimization for Wireless Communication with Rotary-Wing FlyBS", IEEE Transactions on Wireless Communications, Vol. 18, No. 4, April 2019.

[24] W. Wu, Y. Zeng, and R. Zhang, "Joint Trajectory and Communication Design for Multi-UAV Enabled Wireless Networks," IEEE Transactions on Wireless Communications, Vol. 17, No. 3, March 2018.

[25] J. Lee and V. Friderikos, "Path Optimization for Flying Base Stations in Multi-Cell Networks," IEEE Wireless Communications and Networking Conference (WCNC), 2020.

[26] F. Zeng, Z. Hu, Z. Xiao, H. Jiang, S. Zhou, W. Liu, D. Liu, "Resource Allocation and Trajectory Optimization for QoE Provisioning in Energy-efficient UAV-enabled Wireless Networks," IEEE Transactions on Vehicular Technology, 2020.

[27] C. Qiu Z. Wei, Z. Feng, P. Zhang, "Backhaul-Aware Trajectory Optimization of Fixed-Wing UAV-Mounted Base Station for Continuous Available Wireless Service," IEEE Access, 2020.

[28] S. Ahmed, M. Z. Chowdhury, Y. M. Jang, "Energy-Efficient UAV-to-User Scheduling to Maximize Throughput in Wireless Networks," IEEE Access, vol. 8, 2020.

[29] Z. Becvar, M. Vondra, P. Mach, J. Plachy, D. Gesbert, "Performance of Mobile Networks with UAVs: Can Flying Base Stations Substitute Ultra-Dense Small Cells?", European Wireless, 2017.
[30] B. Galkin, J. Kibilda, and L. A. DaSilva, "Deployment of UAV-mounted access points according to spatial user locations in two-tier cellular networks," Wireless Days, 2016.
[31] Z. Becvar, P. Mach, J. Plachy, M.F.P. de Tuleda, "Positioning of Flying Base Stations to Optimize Throughput and Energy Consumption of Mobile Devices", IEEE VTC-Spring 2019, 2019.
[32] H. Huang, A. Savkin, "A Method for Optimized Deployment of Unmanned Aerial Vehicles for Maximum Coverage and Minimum Interference in Cellular Networks," IEEE Transactions on Industrial Informatics, Vol. 15, Issue 5, May 2019.
[33] Y.S. Wang, Y.W.P. Hong, W.T. Chen," Trajectory Learning, Clustering, and User Association for Dynamically Connectable UAV Base Stations," IEEE Transactions on Green Communications and Networking, 2020.
[34] M. Nikooroo, Z. Becvar, "Optimization of Transmission Power for NOMA in Networks with Flying Base Stations", IEEE Vehicular Technology Conference (IEEE VTC-Fall 2020), 2020.
[35] M. Nikooroo, Z. Becvar, "Optimal Positioning of Flying Base Stations and Transmission Power Allocation in NOMA Networks" IEEE Transactions on Wireless Communications, February 2022.
[36] J. G. Leishman, "Principles of Helicopter Aerodynamics," Cambridge University Press, Cambridge, 2006.
[37] K. Gomez, et al. "Aerial Base Stations with Opportunistic Links for Next Generation Emergency Communications," IEEE Communications Magazine 2016.
[38] Z. Becvar, P. Mach, M. Nikooroo, "Reducing Energy Consumed by Repositioning of Flying Base Stations Serving Mobile Users", IEEE Wireless Communications and Networking Conference (IEEE WCNC 2020), 2020.
[39] D. Fan, F. Gao, B. Ai, G. Wang, Z. Zhong, Y. Deng, A. Nallanathan, "Channel Estimation and Self-Positioning for UAV Swarm," IEEE Transactions on Communications," vol. 67, no. 11, Nov. 2019.
[40] Z. Mai, Y. Chen, H. Zhao, L. Du, C. Hao, "A UAV Air-to-Ground Channel Estimation Algorithm Based on Deep Learning," Wireless Personal Communications, 2022.
[41] A. Harris, J. J. Sluss, H. H. Refai, and P. G. LoPresti, "Alignment and tracking of a free-space optical communications link to a UAV," Digital Avionics Systems Conference, 2005.
[42] S. Roth, A. Kariminezhad, and A. Sezgin, "Base-Stations Up in the Air: Multi-UAV Trajectory Control for Min-Rate Maximization in Uplink C-RAN," IEEE ICC 2019.
[43] W. Zhu, Y. Xu, J. Li, and L. Zhang, "Performance analysis of rotatable energy system of high-altitude airships in real wind field," Aerospace Science and Technology, 2020.
[44] Y. Gao, et al, "Robust Trajectory and Power Control for Cognitive UAV Secrecy Communication," IEEE Access, 2020.
[45] D. Yang, Q. Wu, Y. Zeng and R. Zhang, "Energy Tradeoff in Ground-to-UAV Communication via Trajectory Design," IEEE Transactions on Vehicular Technology, vol. 67, no. 7, pp. 6721-6726, July 2018.
[46] P. Merlet, "Flight Mechanics of an Airship," KTH Stockholm, Sweden, 2020.
[47] Y. Xia, " Design and Realization of Indoor Airships with Two Actuation Units and Energy Performance Analysis," Eindhoven University of Technology, 2018.
[48] J.C. Lagarias, J. A. Reeds, M. H. Wright, P. E. Wright. "Convergence Properties of the Nelder-Mead Simplex Method in Low Dimensions." SIAM Journal of Optimization, Vol. 9, No. 1, 1998.
[49] S. Patil, et al, "Modeling and Simulation of Mobility of Crowds," International Conference on Analytical and Stochastic Modeling Techniques and Applications, 2013.
[50] 3GPP, "Study on channel model for frequencies from 0.5 to 100 GHz,"3GPP document TR 38.901, v16.1.0, 2020.
[51] B. Van der Bergh, A. Chiumento, and S. Pollin, "LTE in the Sky: Trading Off Propagation Benefits with Interference Costs for Aerial Nodes," IEEE Communications Magazine, 2016.
[52] A. El Abbous, N. Samama, "A Modeling of GPS Error Distributions," European Navigation Conference (ENC), 2017.
[53] J. Liu, H. Guo, J. Xiong, N. Kato, J. Zhang, Y. Zhang, "Smart and Resilient EV Charging in SDN-Enhanced Vehicular Edge Computing Networks," IEEE Journal on Selected Areas in Communications, Jan. 2020.

3.5 Energy-efficient maximization of sum capacity

In addition to our provided works on power minimization (transmission, propulsion, total), we also take a different approach and we consider the sum capacity of the network as the objective. For such a goal, the minimum quality of service to each mobile user is also considered at all time. The optimization problem is done via an allocation of the transmission power and a positioning of the FlyBS. As the sum capacity is a non-convex problem, challenges regarding the optimization are introduced and dealt with. In addition to the user's minimum required capacity, a constraint on the FlyBS's propulsion power consumption is also included so that the optimization of the sum capacity would not lead to excessive consumption of energy. An analytical solution based on geometrical interpretation of the constraints is provided, and a low-complexity solution to the optimization problem is proposed. The following work is the reference [C1] that presents our contribution to the described problem.

QoS-Aware Sum Capacity Maximization for Mobile Internet of Things Devices Served by UAVs

Mohammadsaleh Nikooroo[1], Zdenek Becvar[1], Omid Esrafilian[2], David Gesbert[2]
[1] *Faculty of Electrical Engineering Czech Technical University in Prague*, Prague, Czech Republic
[2] *Communication Systems Department, EURECOM*, Sophia Antipolis, France
[1]{nikoomoh,zdenek.becvar}@fel.cvut.cz, [2]{esrafili,gesbert}@eurecom.fr

***Abstract*—The use of unmanned aerial vehicles (UAVs) acting as flying base stations (FlyBSs) is considered as an effective tool to improve performance of the mobile networks. Nevertheless, such potential improvement requires an efficient positioning of the FlyBS. In this paper, we maximize the sum downlink capacity of the mobile Internet of Things devices (IoTD) served by the FlyBSs while a minimum required capacity to every device is guaranteed. To this end, we propose a geometrical approach allowing to derive the 3D positions of the FlyBS over time as the IoTDs move and we determine the transmission power allocation for the IoTDs. The problem is formulated and solved under practical constraints on the FlyBS's transmission and propulsion power consumption as well as on flying speed. The proposed solution is of a low complexity and increases the sum capacity by 15%-46% comparing to state-of-the-art works.**

***Index Terms*—Flying base station, UAV, Transmission power, Propulsion power, Sum capacity, Mobile IoT device, 6G.**

I. Introduction

Deployment of unmanned aerial vehicles (UAVs) acting as flying base stations (FlyBSs) is a promising way to improve performance in 6G mobile networks, since the FlyBSs offer a high mobility and an adaptability to the environment via flexible movement in 3D. Potential benefits offered by the FlyBSs, however, comes along with challenges related to radio resource management and positioning of the FlyBSs [1], [2], [3], [4], [5], [6].

The problem of the FlyBS's positioning is investigated in many recent works. The objectives targeted in those works include a maximization of the downlink sum capacity [7], a maximization of the minimum capacity [8], a maximization of the uplink capacity [9], a maximization of the sum of uplink and downlink capacities [10], [11], a maximization of the minimum average capacity for device-to-device communication [12], a maximization of the minimum capacity in networks of sensors or Internet of Things devices (IoTDs) [13], a minimization of the FlyBS's power consumption [14], a minimization of the number of FlyBSs to guarantee users' QoS requirements [15]. However, the users considered in [7]-[15] are static (i.e., do not change their location over time). This is a required assumption in the solutions provided by those works in [7]-[15], and the FlyBS's entire trajectory is derived before the beginning of mission knowing that the users do not move during the mission. An extension of the solutions in these papers to the scenario with moving users is not straightforward. Furthermore, a guarantee of the minimum capacity to the users is not considered in [7], [10], [11], hence, the solutions cannot be adopted in applications, where the quality of service is concerned.

A solution potentially applicable to the scenarios with moving users is outlined in [16], where the FlyBSs' altitude is optimized to maximize the average system throughput. Then, in [17], the authors optimize the number of FlyBSs and their positions to maximize sum capacity. However, neither [16] nor [17] provide any guarantee of the minimum capacity to the users. In [18], the sum capacity is maximized via a positioning of the FlyBSs using reinforcement learning. Furthermore, the problem of the transmission power allocation is investigated in [19] to maximize the energy efficiency, i.e., the ratio of the sum capacity to the total transmission power consumption. The minimum required capacity in [18] and [19] is assumed to be equal for all users. Besides, the FlyBS's positioning is not addressed in [19] at all and the transmission power allocation is not considered in [18]. Then, the minimum capacity of the users is maximized via the FlyBS's positioning and the transmission power allocation in [20]. Nevertheless, no constraint on the FlyBS's speed is considered.

Surprisingly, there is no work targeting the sum capacity maximization in a practical scenario with *moving sensors/IoTDs* and with the *minimum capacity guaranteed to the individual sensors/IoTDs*. All related works are either focused on the scenario where data is collected from static users with apriori known coordinates or no minimum capacity is guaranteed to the users. We target the scenario with mobile devices and the minimum capacity guarantee and we propose a low-complexity solution based on an alternating optimization of the FlyBS's positioning and the transmission power allocation to the devices. The proposed optimization is done with respect to the feasibility region that is derived via a proposed geometrical approach. With respect to a majority of the related works, we also consider practical aspects and constraints of the FlyBSs including limits on the flying speed, transmission power, and propulsion power.

The rest of this paper is organized as follows. In Section

This work was supported by the project No. LTT 20004 funded by Ministry of Education, Youth and Sports, Czech Republic and by the grant of Czech Technical University in Prague No. SGS20/169/OHK3/3T/13, and partially by the HUAWEI France supported Chair on Future Wireless Networks at EURECOM.

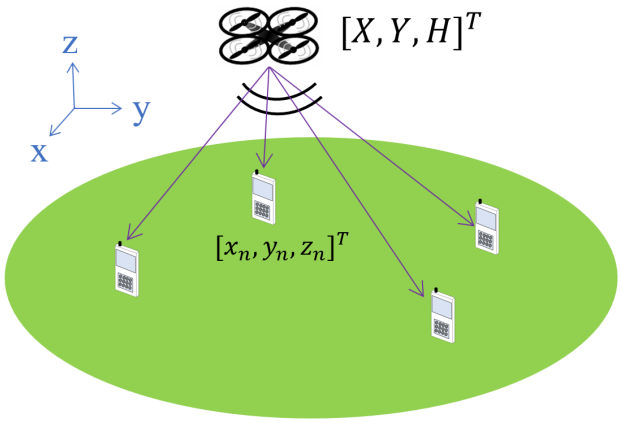

Fig. 1: System model with mobile IoTDs placed within the coverage area of the FlyBS.

II we provide the system model for FlyBS-enabled sensor network and we formulate the problem of sum capacity maximization. Next, we propose a method to check the feasibility of a solution to the FlyBS's positioning and transmission power allocation in Section III. Then, we propose a solution based on an alternating optimization of the transmission power allocation and the FlyBS's positioning in section IV. A geometrical approach is proposed for the FlyBS's positioning. Then, in section V, the adopted simulation scenario and parameters are specified and the performance of our proposed solution is shown and compared with state-of-the art schemes. Last, we conclude the paper and outline the potential future extensions in Section VI.

II. System Model and Problem Formulation

In this section, we first define the system model. Then, we formulate the constrained problem of the sum capacity maximization.

In our system model, one FlyBS serves N sensors/IoTDs $\{u_1, ..., u_N\}$ in an area as shown in Fig. 1. Let $\boldsymbol{l}(t) = \big[X[k], Y[k], H[k]\big]^T$ denote the location of the FlyBS at time step k. We refer to the IoTDs/sensors as nodes in the rest of this paper. Let $\boldsymbol{v_i}[k] = \big[x_i[k],\ y_i[k], z_i[k]\big]^T$ denote the coordinates of node i at time step k. Then, $d_i[k]$ denotes Euclidian distance of node i to the FlyBS at time step k.

We adopt orthogonal downlink channel allocation for all nodes. Thus, the channel capacity of node i is:

$$C_i[k] = B_i \log_2 \left(1 + \frac{p_i^R[k]}{N_i + I}\right), \tag{1}$$

where B_i denotes the bandwidth of the i-th node's channel (note that B_i can differ among nodes), N_i is the noise power at the i-th node's channel, I denotes the background interference from neighboring base stations (both flying and static), and $p_i^R[k]$ is the received power by the i-th node at time step k.

Let $\boldsymbol{p}^T = [p_1^T, ..., p_N^T]$ denote the FlyBS's transmission power allocated to all N nodes. According to the Friis' transmission equation, the received signal's power at node i ($i \in [1, N]$) from the FlyBS is calculated as:

$$p_i^R[k] = Q_i\big(\frac{\gamma}{\gamma+1}\overline{h}_i + \frac{1}{\gamma+1}\tilde{h}_i\big)p_i^T[k]d_i^{-\alpha_i}[k], \tag{2}$$

where the coefficient Q_i is a parameter depending on the communication frequency and gain of antennas. Furthermore, γ is the Rician fading factor, $\overline{h}_i$ is the line-of-sight (LoS) component satisfying $|h_n| = 1$, and $\tilde{h}_i$ denotes the non-line-of-sight (NLoS) component satisfying $\tilde{h}_i \sim CN(0, 1)$, and α_i is the pathloss exponent of the channel for node i.

For the propulsion power consumption, we refer to the model provided in [21] for rotary-wing UAVs. More specifically, the propulsion power is expressed as:

$$P_{pr}[k] = L_0\big(1 + \frac{3V_F^2[k]}{U_{\text{tip}}^2}\big) + \frac{\eta_0 \rho s_r A V_F^3[k]}{2} + L_i\Big(\sqrt{1 + \frac{V_F^4[k]}{4v_{0,h}^4}} - \frac{V_F^2[k]}{2v_{0,h}^2}\Big)^{\frac{1}{2}}, \tag{3}$$

where $V_F[k]$ is the FlyBS's speed at the time step k. Furthermore, L_0 and L_i are the blade profile and induced powers in hovering status, respectively, U_{tip} is the tip speed of the rotor blade, $v_{0,h}$ is the mean rotor induced velocity during hovering, η_0 is the fuselage drag ratio, ρ is the air density, s_r is the rotor solidity, and A is the rotor disc area.

Our goal is to find the position of the FlyBS to maximize the sum capacity at every time step k while the node's minimum required capacity is always guaranteed with practical constraints implied by FlyBSs. Hence, we formulate the problem of the sum capacity maximization as follows:

$$\max_{\boldsymbol{p^T}[k], \boldsymbol{l}[k]} C_{tot}[k], \forall k, \tag{4}$$

$$\text{s.t.} \quad C_i[k] \geq C_i^{min}[k], \quad i \in [1, N], \tag{4a}$$

$$H_{min}[k] \leq H[k] \leq H_{max}[k], \tag{4b}$$

$$||\boldsymbol{l}[k] - \boldsymbol{l}[k-1]|| \leq V_F^{max}\delta_k, \tag{4c}$$

$$P_{pr}[k] \leq P_{pr,th}[k], \tag{4d}$$

$$\sum_{i=1}^{N} p_i^T[k] \leq p_{max}^T, \quad p_i^T[k] \geq 0, \tag{4e}$$

where $C_{tot}[k] = \sum_{i=1}^{N} C_i[k]$ is the sum capacity of the nodes at time step k, $C_i^{min}[k]$ denotes the minimum capacity required by node i at time step k, H_{min} and H_{max} are the minimum and maximum allowed flying altitude of the FlyBS at the time step k, respectively, and are set according to the environment as well as the flying regulations. Furthermore, V_F^{max} is the FlyBS's maximum supported speed, δ_k is the duration between the time steps $k-1$ and k, $||.||$ is the $\mathcal{L}_2$ norm, and p_{max}^T is the FlyBS's maximum transmission power limit. The constraint (4a) ensures that every node always receives the required capacity. Furthermore, (4b) and (4c) restrict the FlyBS's speed to the range of $[0, V_F^{max}]$ and $\big[H_{min}[k], H_{max}[k]\big]$, respectively. In addition, the constraints (4d) and (4e) assure that the FlyBS's propulsion power and total transmission power would not exceed $P_{pr,th}$ and p_{max}^T,

respectively. In practice, the value of $P_{pr,th}$ can be set/adjusted at every time step and according to available remaining energy in the FlyBS's battery to prolong the FlyBS's operation.

Challenging aspects to solve (4) include: i) before the positioning of the FlyBS, a feasibility of the solution to (3) should be verified due the constraints (4a)-(4e), and ii) the objective function C_{tot} and the constraint (4e) are non-convex with respect to $\boldsymbol{l}$.

To tackle the aspect i), we propose a geometrical approach with a low complexity to check the feasibility of any solution to (4). If there is a feasible solution, the proposed approach further determines the feasibility domain used for a derivation of the FlyBS's positions. To tackle the aspect ii), we propose a suboptimal solution using an alternating optimization of the transmission power allocation and the FlyBS's positioning based on a local approximation of the objective function. In particular, we propose an iterative approach based on two steps: 1) an optimization of the transmission power allocation $\boldsymbol{p^T}$ at the given position of the FlyBS and, 2) an update (optimization) of the FlyBS's position for the derived vector $\boldsymbol{p^T}$ from the step 1 via a consideration of the feasibility domain defined by the constraints in (4). We elaborate the derivation of feasibility domain in Section III. Then, we explain our proposed alternating optimization of the transmission power and the FlyBS's positioning in Section IV.

III. Feasibility of a Solution

In this section, we present a geometrical approach to check the feasibility of an arbitrary solution to (4) via a consideration of the constraints in (4). Let us first rewrite the constraint (4a) for an arbitrary setting of the transmission power allocation $\boldsymbol{p^T}$ to individual nodes by means of (1) and (2) as follows:

$$C_i = B_i \log_2 \left(1 + \frac{Q_i p_i^T}{{d_i}^{\alpha_i}(N_i + I)}\right) \geq C_i^{min}, \tag{5}$$

which yields

$$d_i \leq \left(\frac{Q_i p_i^T}{(2^{\frac{C_i^{min}}{B_i}} - 1)(N_i + I)}\right)^{\frac{1}{\alpha_i}} = \rho_i, \quad 1 \leq i \leq N. \tag{6}$$

Each of the N inequalities in (6) demarcates a sphere in 3D space. In particular, for every $i \in [1, N]$, the inequality in (6) implies that the FlyBS lies inside or on the sphere with a center at the location of node i and with a radius of ρ_i.

Next, the constraint (4b) defines the next position of the FlyBS on or between the planes $z = H_{min}[k]$ and $z = H_{max}[k]$. In addition, according to Fig. 2, the constraint (4d) is translated as $V_F \in [V_F^{th,1}, V_F^{th,2}]$. By combining this inequality with (4c) we get

$$||\boldsymbol{l}[k] - \boldsymbol{l}[k-1]|| \leq (\min\{V_{F,max}, V_F^{th,2}\})\delta_k, \tag{7}$$

and

$$||\boldsymbol{l}[k] - \boldsymbol{l}[k-1]|| \geq V_F^{th,1}\delta_k. \tag{8}$$

The equations (7) and (8) define the FlyBS's next possible position as the border or inside of a region enclosed by two spheres centered at $\boldsymbol{l}[k-1]$ (i.e., the FlyBS's position at the previous time step) and with radii of $V_F^{th,1}\delta_k$ and $(\min\{V_{F,max}, V_F^{th,2}\})\delta_k$. Furthermore, to interpret the constraint (4e) in terms of the FlyBS's position, in following Lemma 1, we derive a necessary condition for the FlyBS's next position so that there exists a feasible position of the FlyBS for an arbitrary setting of $\boldsymbol{p^T}$.

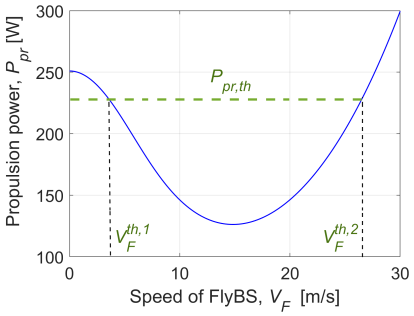

Fig. 2: Propulsion power model vs. speed for rotary-wing FlyBS.

Lemma 1. *For the power allocation vector $\boldsymbol{p^T}$ at time step $k-1$, a necessary condition for a feasibility of any solution to the positioning of the FlyBS at time step k is:*

$$\left|\left|\boldsymbol{l}[k] - \boldsymbol{\theta_0}(\boldsymbol{p^T}, k)\right|\right| \leq \Upsilon(\boldsymbol{p^T}, k), \tag{9}$$

where $\boldsymbol{\theta_0}(\boldsymbol{p^T}, k) = [\frac{\sum_{i=1}^N \iota_i x_i}{\sum_{i=1}^N \iota_i}, \frac{\sum_{i=1}^N \iota_i y_i}{\sum_{i=1}^N \iota_i}, H]$, *and ι_i is a substitution derived in the proof, and* $\Upsilon(\boldsymbol{p^T}, k) = (\frac{p_{max}^T - \chi}{\sum_{i=1}^N \iota_i})^{\frac{1}{2}}$.

proof. Please see Appendix A

Note that, an existence of a feasible solution is contingent upon all the constraints in (4) and not only the condition (9). Thus, we now analyze the feasibility of any solution to (4) by incorporating the constraints derived for the FlyBS's next position. In order to check if these inequalities hold at the same time, we propose the following low-complexity approach. Let cl_i $(i \in [1, +2])$ denote $N+2$ spheres defined by the inequalities (6), (7), and (9). Note that we deal with (7) later in this section. The N spheres represented by (6) have centers at the same position as their corresponding nodes. Furthermore, the sphere indicated by (7) has a center at the FlyBS's position at time step $k-1$.

Then, for each pair of spheres sp_j and sp_k, we consider their intersection. There are three different cases regarding the intersection: i) sp_j and sp_k have no intersection point and lie completely outside each other, ii) sp_j and sp_k have no intersection points and one of these spheres lies inside the other one, iii) sp_j and sp_k intersect on their borders which is in the shape of a circle (assuming that a single point is also a circle with radius of zero). Note that any two spheres from the set of spheres indicated by (4a) do not completely overlap, as each sphere has a distinct center. Furthermore, if any sphere represented by (7) or (9) is identical to another sphere, we simply ignore one of those spheres.

For the case i, we conclude that at least two of the

constraints in (4) do not hold at the same time and, thus, there is no feasible solution to (4). For the case ii, one of the constraints in (4) corresponding to the outer sphere is automatically fulfilled if the other constraint (the one corresponding to the inner sphere) holds. In such case, we ignore the constraint corresponding to the outer sphere and the rest of the constraints are dealt with according to case i or iii. For the case iii, we propose the following low-complexity method to verify the non-emptiness of the intersections of the spheres (in other words, a feasibility of a solution to (4)): given the fact that the intersection of a plane and a sphere is circle (if not empty), we search for the intersection of the spheres only on certain planes. In particular, corresponding to each of the $N+2$ spheres sp_j, consider two horizontal planes $pl_{j,1}$ and $pl_{j,2}$ that are tangent to sp_j (one at the topmost point on sp_j and one at the lower most point). Then, we remove from the set of the derived planes those that do not fulfill the altitude constraint (4b). Hence, at most $2N+4$ horizontal planes are derived. Next, for each of the remaining planes, we find the intersection of the plane and all the spheres. Let $cl_{l,k,1}$ and $cl_{j,k,2}$ be the intersection (circle) of sp_k on $pl_{j,1}$ and on $pl_{j,2}$, respectively. On each plane, we derive and collect the intersection points of each two of such circles. Then, we verify whether there are any points in the set of the collected points that would lie inside or on the border of all the circles on the same plane. In case that there are no such points on any of the planes, there is no feasible solution to (4) as all the constraints in (4) cannot be met at the same time. Otherwise, there would be a solution if the remaining condition (8) is also met for at least one of those eligible candidate points. From the described process, the computational complexity of the proposed feasibility check scales as $(2N+4) \times \binom{N+2}{2} \times (N+2)$, i.e., it is $O(N^4)$.

In the next section, we target the problem of power allocation and the FlyBS's positioning in (4) and we show how the FlyBS's position is determined with respect to the constraint spheres sp_j ($j \in [1, N+2]$) derived in this section.

IV. FlyBS positioning and power allocation

In this section, we outline our proposed FlyBS's positioning and transmission power allocation maximizing the sum capacity under the feasibility condition derived in Section III.

Our proposed solution is based on alternating optimization updating the transmission power $\boldsymbol{p^T}$ and the FlyBS's position $\boldsymbol{l}$ at every time step. First, note that for a given $\boldsymbol{l}$, the problem of the $\boldsymbol{p^T}$ optimization is solved via CVX, as the sum capacity in (4) is concave, and the constraints in (4) are convex with respect to $\boldsymbol{p^T}$. Once $\boldsymbol{p^T}$ is optimized at the given position $\boldsymbol{l}$, we optimize $\boldsymbol{l}$ to maximize the sum capacity while considering the constraints in (4). To this end, we first consider the problem of the sum capacity maximization regardless of the constraints in (4). As the sum capacity is non-convex with respect to the FlyBS's position, we provide a solution based on a local approximation of the sum capacity in the form of a radial function with respect to the FlyBS's position as elaborated in the following Lemma 2.

Lemma 2. *The sum capacity C_{tot} is approximated as a radial function with respect to $\boldsymbol{l}[k]$ as:*

$$C_{tot}[k] \approx W(\boldsymbol{p^T}, k) - \zeta(\boldsymbol{p^T}, k)\big|\big|\boldsymbol{l}[k] - \boldsymbol{S_0}(\boldsymbol{p^T}, k)\big|\big|^2, \quad (10)$$

where the substitutions $W(\boldsymbol{p^T}, k)$, $\zeta(\boldsymbol{p^T}, k)$, and $\boldsymbol{S_0}(\boldsymbol{p^T}, k)$ are constants with respect to $\boldsymbol{l}[k]$ as presented in the proof.

proof. Please see Appendix B

According to (10), the FlyBS achieves the maximum capacity at the location $\boldsymbol{S_0}$. In addition, the sum capacity increases when the FlyBS's distance to $\boldsymbol{S_0}$ decreases. This helps to derive the FlyBS's position for the constrained problem in (4) in following way. The FlyBS's position is updated to $\boldsymbol{S_0}$ (as in (19)) if all constraints in (4) are fulfilled, i.e., if $\boldsymbol{S_0}$ lies inside the feasibility region denoted by $\mathcal{R}_f$. Otherwise, $\boldsymbol{S_0}$ lies outside of $\mathcal{R}_f$ and the optimal position of the FlyBS (optimal with respect to (10)) is, then, the closest point from $\mathcal{R}_f$ to $\boldsymbol{S_0}$. If $\boldsymbol{S_0}$ lies outside of $\mathcal{R}_f$, we refer to the derived spheres representing the constraints in (4) (i.e., sp_j for $j \in [1, N+2]$, see Section III) to find the closest point from $\mathcal{R}_f$ to $\boldsymbol{S_0}$ and we provide a geometrical solution to determine the FlyBS's position as follows (also demonstrated in Algorithm 1). Due to the compactness of $\mathcal{R}_f$, the closest point of $\mathcal{R}_f$ to $\boldsymbol{S_0}$ lies on the boundary of $\mathcal{R}_f$ belonging also to the border of at least one of the $(N+2)$ spheres sp_j. The closest point from any sphere sp_j to $\boldsymbol{S_0}$ is determined by finding the intersection of sp_j and the straight line connecting $\boldsymbol{S_0}$ to the center of sp_j. Hence, we first find the closest point of each sp_j to $\boldsymbol{S_0}$ (corresponding to line 1 in Algorithm 1). Next, we derive all mutual intersections (circles) of each pair of spheres sp_j and sp_k and we find the closest point from each of the intersection circles to $\boldsymbol{S_0}$ (line 2 in Algorithm 1- derivation steps not shown here to avoid cluttering, more details can be found in [24]). Similarly, we find the intersections of each sphere sp_j ($j \in [1, N+2]$) with each of the planes $z = H_{min}$ and $z = H_{max}$ and then we find the closest points on those intersection circles to $\boldsymbol{S_0}$ (lines 3 and 4 in Algorithm 1). After collecting all those closest points to $\boldsymbol{S_0}$, we discard those collected points that do not fulfill all the conditions in (4) (line 5 in Algorithm 1). Last, in the remaining set of candidate points, the point with smallest distance to $\boldsymbol{S_0}$ is the optimal position of the FlyBS (line 6 in Algorithm 1).

Once the FlyBS's position $\boldsymbol{l}$ is updated, the power allocation

Algorithm 1 Determination of the FlyBS positioning

Input: sp_j ($j \in [1, N+2]$), and planes $z = H_{min}$, $z = H_{max}$
$\boldsymbol{\Lambda} = []$: set of closest points to $\boldsymbol{S_0}$ from the border of $\mathcal{R}_f$

1: $\boldsymbol{\Lambda} \leftarrow \boldsymbol{\Lambda} \cup \text{argmin}_{\boldsymbol{A} \in sp_j} ||\boldsymbol{S_0} - \boldsymbol{A}||, \forall j$
2: $\boldsymbol{\Lambda} \leftarrow \boldsymbol{\Lambda} \cup \text{argmin}_{\boldsymbol{D} \in sp_j \cap sp_k} ||\boldsymbol{S_0} - \boldsymbol{D}||, \forall j, k$
3: $\boldsymbol{\Lambda} \leftarrow \boldsymbol{\Lambda} \cup \text{argmin}_{\boldsymbol{B} \in sp_j \cap z = H_{min}} ||\boldsymbol{S_0} - \boldsymbol{B}||, \forall j$
4: $\boldsymbol{\Lambda} \leftarrow \boldsymbol{\Lambda} \cup \text{argmin}_{\boldsymbol{C} \in sp_j \cap z = H_{max}} ||\boldsymbol{S_0} - \boldsymbol{C}||, \forall j$
5: $\boldsymbol{\Lambda} \leftarrow \boldsymbol{\Lambda} - \{\boldsymbol{l} \in \boldsymbol{\Lambda} | \sim (4b) \vee q \notin \cap_{j=1}^{N+2} sp_j, \}$
6: $\boldsymbol{l} \leftarrow \text{argmin}_{\boldsymbol{l} \in \boldsymbol{\Lambda}} ||\boldsymbol{S_0} - \boldsymbol{l}||$

Output: FlyBS's position ($\boldsymbol{l}$)

$\boldsymbol{p^T}$ is again optimized at the new $\boldsymbol{l}$. The updated $\boldsymbol{p^T}$ would change the spheres sp_j ($j \in [1, N+2]$) and also $\boldsymbol{S_0}$. Thus, the alternating optimization of $\boldsymbol{p^T}$ and $\boldsymbol{l}$ continues until the FlyBS's displacement at some iteration falls below a given threshold ϵ or until the maximum number of iterations is reached. The complexity of finding the FlyBS's position at each time step is $O(N^4)$.

V. Simulations and Results

In this section, we present models and simulations adopted for a performance evaluation of the proposed solution, and we show gains of the proposal over state-of-the-art schemes.

A. Simulation scenario and models

We assume an area with a size of 600 x 600 m. Within this area, 60 to 180 nodes are dropped. A half of the nodes move based on a random-walk mobility model with a speed of 1 m/s. The other half of the nodes are randomly distributed into six clusters of crowds. The centers of three of the clusters move at a speed of 1 m/s, where each node in those clusters moves with a uniformly distributed speed of [0.6, 1.4] m/s with respect to the center of each cluster. The centers of the other three clusters move at a speed of 1.6 m/s with the speed of nodes uniformly distributed over [1.2, 2] m/s with respect to the center of cluster.

A total bandwidth of 100 MHz is selected [22]. Spectral density of noise is set to -174 dBm/Hz. The background interference is set to -100 dBm. We set $\alpha_i = 2.4$ for all nodes. The allowed range for altitude of the FlyBS is $[100, 300]$ m, and the maximum transmission power limit P_{TX}^{max} is 1 W [23]. A maximum speed of 25 m/s is assumed for the FlyBS. The maximum allowed propulsion power consumption (according to (4a)) is set to $P_{pr,th} = 250$ W. Each simulation is of 1200 seconds duration. The results are averaged out over 100 simulation drops.

In addition to our proposal, we show the performance of the following state-of-the-art solutions: i) maximization of the minimum capacity of nodes (referred to as *MMC*) via the FlyBS's positioning and the transmission power allocation, published in [20], ii) allocation of the transmission power to maximize an energy efficiency introduced in [19] (referred to as *EEM*), iii) allocation of the transmission power proposed in [19] extended with K-means-based positioning of the FlyBS, as the solution in [19] does not address the positioning; this approach is denoted as the extended *EEM* (*EEEM*).

B. Simulation results

In this subsection, we present and discuss simulation results. Fig. 3 demonstrates the sum capacity versus number of nodes for $C_i^{min} = 1$ Mbps for all nodes. The sum capacity decreases for larger numbers of nodes for all schemes, because the available bandwidth and the total transmission power is split among more nodes. However, our proposed solution enhances the sum capacity compared to state-of-the-art solutions *MMC*, *EEM*, and *EEEM* by up to 26%, 43%, and 22%, respectively.

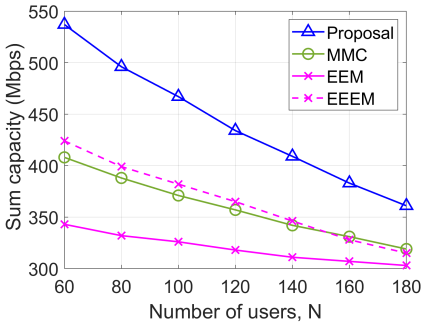

Fig. 3: Sum capacity vs. number of nodes for C_{min} =1 Mbps.

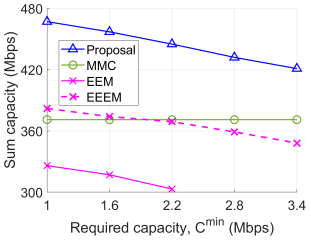

Fig. 4: Sum capacity vs. C_i^{min} for $N = 100$.

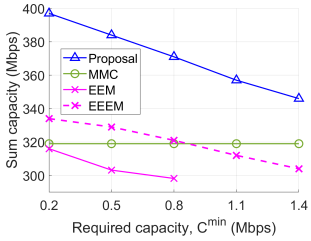

Fig. 5: Sum capacity vs. C_i^{min} for $N = 180$.

Figs. 4 and 5 show an impact of C_{min} on the sum capacity for $N = 100$ and $N = 180$, respectively. The maximum depicted C_i^{min} represents the largest C_i^{min} for which the feasible solution is found. Note that the value of C_i^{min} in *MMC* is not set manually, but it is directly derived by the scheme itself. For $N = 100$ and $N = 180$, the *EEM* does not find a feasible solution for C_i^{min} larger than 2.2 Mbps and 0.8 Mbps, respectively, due to a lack of positioning of the FlyBS. It is observed that the sum capacity decreases by C_i^{min} in the proposed solution, EEM, and EEEM. This is because the increasing C_i^{min} further limits the FlyBS's allowed movement according to (6) and, thus, the FlyBS can explore only a smaller feasibility region to optimize the sum capacity. The proposed solution enhances the sum capacity with respect to *MMC*, *EEM*, and *EEEM* by up to 25%, 46%, and 22%, respectively, for $N = 100$, and by up to 24%, 26%, and 15%, respectively, for $N = 180$.

As our algorithm is iterative, we demonstrate its fast convergence in Figs. 6 and 7 by showing an evolution of the

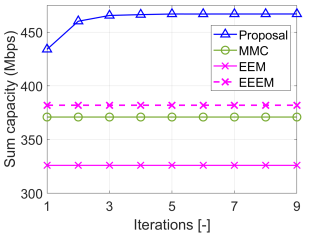

Fig. 6: Convergence of the proposed scheme for $N = 100$.

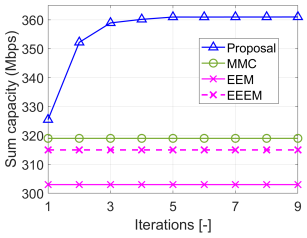

Fig. 7: Convergence of the proposed scheme for $N = 180$.

sum capacity over iterations of the FlyBS's positioning and the transmission power allocation. The state-of-the-art schemes are not iterative, thus, their sum capacity is constant. Still, the proposed solution converges very fast, in about three iterations. Moreover, even the first iteration leads to a notably higher sum capacity comparing to all state-of-the-art solutions. This confirms that iterative approach does not limit feasibility and practical application of the proposed solution.

VI. Conclusions

In this paper, we have provided a geometrical solution maximizing the sum capacity via a positioning of the FlyBS and an allocation of the transmission power to the nodes, while the minimum required capacity to each node is guaranteed. We have shown that the proposed solution enhances the sum capacity by tens of percent compared to state-of-the-art works.

In the future work, a scenario with multiple FlyBSs should be studied along with related aspects, such as a management of interference among FlyBSs and an association of the nodes to the FlyBSs, should be addressed.

Appendix A
Proof to Lemma 1

Proof. Using (5), the constraint (4a) is rewritten as:

$$Q_i^{-1} {d_i}^{\alpha_i}[k](N_i+I)(2^{\frac{C_i^{min}}{B_i}}-1) \leq p_i^T. \quad (11)$$

Then, the necessary condition to fulfill (4e) is that:

$$\sum_{i=1}^{N} Q_i^{-1} {d_i}^{\alpha_i}(N_i+I)(2^{\frac{C_i^{min}}{B_i}}-1) \leq p_{max}^T. \quad (12)$$

To derive an explicit form of (12) in terms of the FlyBS's position, we adopt the following inequality derived from linear Taylor approximation with respect to arbitrary x and for $\eta \geq 1$:

$$(a+x)^\eta \geq (a+\tau e\omega)^\eta + \eta(e+\tau e\omega)^{\eta-1}(x-\tau a\omega), \quad (13)$$

where $\tau = \left\lfloor \frac{x}{a\sigma} \right\rfloor$, and σ is the approximation parameter such that choosing a smaller σ incurs a smaller error. Hence, the approximation error and, thus, the gap to the optimal solution can be set arbitrarily close to zero by adopting a small enough σ. Using (13), for the left-hand side in (12) we write:

$$\sum_{i=1}^{N} Q_i^{-1} {d_i}^{\alpha_i}(N_i+I)(2^{\frac{C_i^{min}}{B_i}}-1) = \sum_{i=1}^{N} Q_i^{-1}(N_i+I)\times$$
$$(2^{\frac{C_i^{min}}{B_i}}-1)\times((X-x_i)^2+(Y-y_i)^2+(H-z_i)^2-H_{min}^2$$
$$+H_{min}^2)^{\frac{\alpha_i}{2}} \geq \sum_{i=1}^{N} Q_i^{-1}(N_i+I)(2^{\frac{C_i^{min}}{B_i}}-1)\times(\mu_i^{\frac{\alpha_i}{2}}-$$
$$\frac{\kappa_i\sigma\alpha_i}{2}\times\mu_i^{\frac{\alpha_i}{2}-1}H_{min}^2+(X^2+x_i^2-2Xx_i+Y^2+y_i^2-$$
$$2Yy_i+H^2+z_i^2-2Hz_i-H_{min}^2)\frac{\alpha_i}{2\mu_i^{-\frac{\alpha_i}{2}+1}}) =$$
$$(\sum_{i=1}^{N}\iota_i)\left|\left|\boldsymbol{l}[k]-\boldsymbol{\theta_0}(\boldsymbol{p^T},k)\right|\right|^2+\chi, \quad (14)$$

where

$$\kappa_i = \left\lfloor \frac{\left|\left|\boldsymbol{l}[k]-\boldsymbol{v_i}\right|\right|^2 - H_{min}^2}{H_{min}^2\sigma} \right\rfloor, \mu_i = H_{min}^2(1+\kappa_i\sigma),$$
$$\iota_i = \frac{1}{2}Q_i^{-1}(N_i+I)(2^{\frac{C_i^{min}}{B_i}}-1)\alpha_i\mu_i^{\frac{\alpha_i}{2}-1}, \quad (15)$$

and

$$\chi = -\sum_{i=1}^{N}\iota_i(x_i^2+y_i^2+z_i^2)+$$
$$\frac{\left(\sum_{i=1}^{N}\iota_i x_i\right)^2+\left(\sum_{i=1}^{N}\iota_i y_i\right)^2+\left(\sum_{i=1}^{N}\iota_i z_i\right)^2}{\sum_{i=1}^{N}\iota_i}+$$
$$\sum_{i=1}^{N} Q_i^{-1}(N_i+I)(2^{\frac{C_i^{min}}{B_i}}-1)(\mu_i^{\frac{\alpha_i}{2}}-\frac{\kappa_i\sigma\alpha_i}{2}\mu_i^{\frac{\alpha_i}{2}-1}H_{min}^2). \quad (16)$$

Then, by incorporating (12) and the right-hand side in (14), Lemma 1 is proved. □

Appendix B
Proof to Lemma 2

Proof. We use the following linear approximation (with respect to Γ) for arbitrary values of Δ and Γ:

$$\log_2(\Delta+\Gamma) \approx \frac{1}{\ln(2)}(\ln(\Delta+\Delta s\xi)+\frac{\Gamma-s\Delta\xi}{\Delta(1+s\xi)}), \quad (17)$$

where $s = \left\lfloor \frac{\Gamma}{\Delta\xi} \right\rfloor$. Note that the approximation error can be set arbitrarily close to zero by choosing small enough ξ.

By taking $\frac{p_i^T}{Q_i {d_i}^{\alpha_i}(N_i+I)}$ as Γ in (17), the sum capacity is rewritten as:

$$C_{tot}[k] = \sum_{i=1}^{N} B_i \log_2\left(1+\frac{Q_i p_i^T}{{d_i}^{\alpha_i}(N_i+I)}\right) \approx$$
$$\sum_{i=1}^{N}\frac{B_i p_i^T((X-x_i)^2+(Y-y_i)^2+(H-z_i)^2-H_{min}^2+H_{min}^2)^{\frac{-\alpha_i}{2}}}{Q_i^{-1}(1+s_i\xi)(N_i+I)\ln(2)}$$
$$+\sum_{i=1}^{N}\frac{B_i}{\ln(2)}(\ln(1+s_i\xi)-\frac{s_i\xi}{1+s_i\xi}) \approx$$
$$\sum_{i=1}^{N}\frac{B_i Q_i p_i^T}{(1+s_i\xi)(N_i+I)\ln(2)}\times(\mu_i^{\frac{\alpha_i}{2}}+\frac{\kappa_i\sigma\alpha_i}{2}\mu_i^{\frac{\alpha_i}{2}-1}H_{min}^2-\frac{\alpha_i\mu_i^{\frac{\alpha_i}{2}-1}}{2}$$
$$\times(X^2+x_i^2-2Xx_i+Y^2+y_i^2-2Yy_i+H^2+z_i^2-2Hz_i-H_{min}^2))$$
$$+\sum_{i=1}^{N}\frac{B_i}{\ln(2)}(\ln(1+s_i\xi)-\frac{s_i\xi}{1+s_i\xi}) = W(\boldsymbol{p^T},k)-(\sum_{i=1}^{N}\varphi_i)\times(($$
$$X-(\frac{\sum_{i=1}^{N}\varphi_i x_i}{\sum_{i=1}^{N}\varphi_i}))^2+(Y-(\frac{\sum_{i=1}^{N}\varphi_i y_i}{\sum_{i=1}^{N}\varphi_i}))^2+(H-(\frac{\sum_{i=1}^{N}\varphi_i z_i}{\sum_{i=1}^{N}\varphi_i}))^2)$$
$$= W(\boldsymbol{p^T},k)-\zeta(\boldsymbol{p^T},k)\left|\left|\boldsymbol{l}[k]-\boldsymbol{S_0}(\boldsymbol{p^T},k)\right|\right|^2, \quad (18)$$

where

$$\boldsymbol{S_0}(\boldsymbol{p^T},k) = [\frac{\sum_{i=1}^{N}\varphi_i x_i}{\sum_{i=1}^{N}\varphi_i}, \frac{\sum_{i=1}^{N}\varphi_i y_i}{\sum_{i=1}^{N}\varphi_i}, \frac{\sum_{i=1}^{N}\varphi_i z_i}{\sum_{i=1}^{N}\varphi_i}], \quad (19)$$

and

$$W(\boldsymbol{p^T}, t_k) = \frac{\left(\sum_{i=1}^{N} \varphi_i x_i\right)^2 + \left(\sum_{i=1}^{N} \varphi_i y_i\right)^2 + \left(\sum_{i=1}^{N} \varphi_i z_i\right)^2}{\sum_{i=1}^{N} \varphi_i}$$
$$- \sum_{i=1}^{N} \varphi_i (x_i^2 + y_i^2 + z_i^2) + \sum_{i=1}^{N} \frac{B_i Q_i p_i^T}{(1+s_i\xi)(N_i+I)\ln(2)} \times$$
$$(\mu_i^{-\frac{\alpha_i}{2}} + \frac{\kappa_i \alpha_i \sigma H_{min}^2 \mu_i^{-1-\frac{\alpha_i}{2}}}{2} + \frac{\alpha_i \mu_i^{\frac{\alpha_i}{2}-1}}{2} H_{min}^2) +$$
$$\sum_{i=1}^{N} \frac{B_i}{\ln(2)} (\ln(1+s_i\xi) - \frac{s_i\xi}{1+s_i\xi}),$$

$$s_i = \left\lfloor \frac{Q_i p_i^T}{\sigma (N_i+I) d_i^{\alpha_i}} \right\rfloor, \quad \varphi_i = \frac{Q_i B_i p_i^T \alpha_i \mu_i^{-1-\frac{\alpha_i}{2}}}{2\,(N_i+I)\,(1+s_i\xi)\ln(2)},$$

$$\zeta(\boldsymbol{p^T}, t_k) = \sum_{i=1}^{N} \varphi_i. \tag{20}$$

This proves Lemma 2. □

REFERENCES

[1] B. Li, et al, "UAV Communications for 5G and Beyond: Recent Advances and Future Trends," *IEEE Internet of Things Journal*, vol. 6, no. 2, April 2019.

[2] P. Mach, et al, "Power Allocation, Channel Reuse, and Positioning of Flying Base Stations With Realistic Backhaul," *IEEE Internet of Things Journal*, vol. 9, no. 3, pp. 1790-1805, 1 Feb.1, 2022.

[3] M. Nikooroo and Z. Becvar, "Optimization of Total Power Consumed by Flying Base Station Serving Mobile Users," *IEEE Trans. Netw. Sci. Eng.*, Early Access, 2022.

[4] M. Mozaffari, et al, "Mobile Internet of Things: Can UAVs Provide an Energy-Efficient Mobile Architecture?," *IEEE GLOBECOM*, 2016.

[5] Y. Spyridis, et al, "Towards 6G IoT: Tracing Mobile Sensor Nodes with Deep Learning Clustering in UAV Networks", *Sensors*, vol. 21, 2021.

[6] O. Esrafilian, R. Gangula and D. Gesbert, "Learning to Communicate in UAV-Aided Wireless Networks: Map-Based Approaches," *IEEE Internet Things J.*, vol. 6, no. 2, 2019.

[7] S. Ahmed, et al, "Energy-Efficient UAV-to-User Scheduling to Maximize Throughput in Wireless Networks," *IEEE Access*, vol. 8, 2020.

[8] J. Ji, et al, "Joint Cache Placement, Flight Trajectory, and Transmission Power Optimization for Multi-UAV Assisted Wireless Networks," *IEEE Transactions on Wireless Communications*, vol. 19, no. 8, 2020.

[9] Z. Wei, et al, "Capacity of Unmanned Aerial Vehicle Assisted Data Collection in Wireless Sensor Networks," *IEEE Access*, vol. 8, 2020.

[10] M. Hua, et al, "3D UAV Trajectory and Communication Design for Simultaneous Uplink and Downlink Transmission," *IEEE Transactions on Communications*, vol. 68, no. 9, 2020.

[11] M. Hua, et al, "Throughput Maximization for Full-Duplex UAV Aided Small Cell Wireless Systems," *IEEE Wireless Communications Letters*, vol. 9, no. 4, 2020.

[12] B. Li, et al, "Full-Duplex UAV Relaying for Multiple User Pairs," *IEEE Internet of Things Journal*, vol. 8, no. 6, 2021.

[13] L. Xie, J. Xu and Y. Zeng, "Common Throughput Maximization for UAV-Enabled Interference Channel With Wireless Powered Communications," *IEEE Transactions on Communications*, vol. 68, no. 5, pp. 3197-3212, May 2020.

[14] Y. K. Tun, et al, "Energy-Efficient Resource Management in UAV-Assisted Mobile Edge Computing," *IEEE Communications Letters*, vol. 25, no. 1, pp. 249-253, Jan. 2021.

[15] L. Shi and S. Xu, "UAV Path Planning With QoS Constraint in Device-to-Device 5G Networks Using Particle Swarm Optimization," *IEEE Access*, vol. 8, pp. 137884-137896, 2020.

[16] M. Ishigami and T. Sugiyama, "A Novel Drone's Height Control Algorithm for Throughput Optimization in Disaster Resilient Network," *IEEE Transactions on Vehicular Technology*, vol. 69, no. 12, 2020.

[17] R. Chen, et al, "Multi-UAV Coverage Scheme for Average Capacity Maximization," *IEEE Communications Letters*, vol. 24, no. 3, 2020.

[18] W. Zhang, et al, "Three-Dimension Trajectory Design for Multi-UAV Wireless Network With Deep Reinforcement Learning," *IEEE Transactions on Vehicular Technology*, vol. 70, no. 1, 2021.

[19] S. T. Muntaha, et al, "Energy Efficiency and Hover Time Optimization in UAV-Based HetNets," *IEEE Transactions on Intelligent Transportation Systems*, vol. 22, no. 8, 2021.

[20] I. Valiulahi and C. Masouros, "Multi-UAV Deployment for Throughput Maximization in the Presence of Co-Channel Interference," in *IEEE Internet of Things Journal*, vol. 8, no. 5, 2020.

[21] Y. Zeng, J. Xu, and R. Zhang, "Energy Minimization for Wireless Communication With Rotary-Wing UAV," in *IEEE Trans. Wireless Commun.*, Vol. 18, No. 4, April 2019.

[22] M. Nikooroo and Z. Becvar, "Optimal Positioning of Flying Base Stations and Transmission Power Allocation in NOMA Networks," *IEEE Trans. Wireless Commun.*, vol. 21, no. 2, pp. 1319-1334, Feb. 2022.

[23] M. Alzenad, et al, "3-D Placement of an Unmanned Aerial Vehicle Base Station (UAV-BS) for Energy-Efficient Maximal Coverage," *IEEE Wireless Communications Letters*, vol. 6, no. 4, pp. 434-437, Aug. 2017.

[24] D. Eberly, "Distance to Circles in 3D ", Geometric Tools, https://www.geometrictools.com/Documentation//DistanceToCircle3.pdf.

3.6 Maximization of sum capacity in multi-hop FlyBS networks with backhaul

Having studied the problem of FlyBS's deployment and resource allocation for FlyBSs operating at the access link, we then take a step forward towards integrating multi-hop communication in FlyBS networks. In particular, a backhaul link is included to establish a connection between the FlyBSs and the ground base station (GBS). Furthermore, some FlyBSs in this architecture act as relays in order to provide connection between the GBS and the other FlyBSs. In such model, the relays could also serve the ground users directly. Constraints on data flow are imposed at the relays to ensure that the capacity of the backhaul links are not less than that of the fronthaul links. We investigate the problem of sum capacity maximization via a positioning of the FlyBSs as well as an association of the users to the BSs (including FlyBSs and the GBS). Due to a discrete nature of user association, and due to a non-convexity of the objective as well as the backhaul constraints, only a suboptimal solution can be provided. To this end, we propose an analytical heuristic solution based on an alternating optimization of the user association and FlyBS's positioning. The following paper (reference [C2]) presents our work for the multi-hop problem as described.

Sum Capacity Maximization in Multi-Hop Mobile Networks with Flying Base Stations

Mohammadsaleh Nikooroo[1], Omid Esrafilian[2], Zdenek Becvar[1], David Gesbert[2]
[1] *Faculty of Electrical Engineering Czech Technical University in Prague*, Prague, Czech Republic
[2] *Communication Systems Department, EURECOM*, Sophia Antipolis, France
[1]{nikoomoh,zdenek.becvar}@fel.cvut.cz, [2]{esrafili,gesbert}@eurecom.fr

***Abstract*—Deployment of multi-hop network of unmanned aerial vehicles (UAVs) acting as flying base stations (FlyBSs) presents a remarkable potential to effectively enhance the performance of wireless networks. Such potential enhancement, however, relies on an efficient positioning of the FlyBSs as well as a management of resources. In this paper, we study the problem of sum capacity maximization in an extended model for mobile networks where multiple FlyBSs are deployed between the ground base station and the users. Due to an inclusion of multiple hops, the existing solutions for two-hop networks cannot be applied due to the incurred backhaul constraints for each hop. To this end, we propose an analytical approach based on an alternating optimization of the FlyBSs' 3D positions as well as the association of the users to the FlyBSs over time. The proposed optimization is provided under practical constraints on the FlyBS's flying speed and altitude as well as the constraints on the achievable capacity at the backhaul link. The proposed solution is of a low complexity and extends the sum capacity by 23%-38% comparing to state-of-the-art solutions.**

***Index Terms*—Flying base station, wireless backhaul, relaying, sum capacity, mobile users, mobile networks, 6G.**

I. Introduction

Unmanned aerial vehicles (UAVs) have attracted an abundance of research interest in wireless communications in the last few years thanks to their high mobility and adaptability to the environment. Deployed as flying base stations (FlyBSs), UAVs can potentially bring a great improvement in applications such as surveillance, emergency situations, or providing user's coverage in areas with unreliable connectivity [1], [2], [3],[4]. Several challenges exist to enable an effective use of FlyBSs, including an efficient cooperation between the FlyBSs' via a management of the resources as well as FlyBSs' positioning. An important case with cooperative FlyBSs is relaying networks where FlyBSs either serve the ground users directly (access link) or relay the data to establish a connection between the users and the ground base station (GBS).

Several recent works target enhancing the performance in networks with relaying FlyBSs. With respect to those works only focusing on the communication at the access link, relaying networks necessitate to consider the backhaul link connecting the users to the GBS. In particular, flow conservation constraints apply at each relay node to ensure a sufficient backhaul capacity for the fronthaul link. The basic model for relaying FlyBS networks is a two-hop architecture where all FlyBSs directly serve users at the access link and also connect directly to the GBS via the backhaul link. A majority of recent works target an enhancement in two-hop relaying networks with a consideration of backhaul.

The problem of resource allocation and FlyBS's positioning is considered in many works targeting various objectives, including optimization of minimum rate for delay-tolerant users [5], energy consumption [6], network profit gained from users [7], sum capacity [8], network latency [9]. The mentioned works [5]-[9] consider a single FlyBS, and an application of those works to multiple-FlyBS scenario is not trivial.

Several works also consider multiple FlyBSs in two-hop relaying networks. In [10] the authors study a joint placement, resource allocation, and user association of FlyBSs to maximize the network's utility. Furthermore, the authors in [11] maximize the sum capacity via FlyBS's positioning, user association, and transmission power allocation. In [12] the minimum rate of the users is maximized via resource allocation and positioning in wireless backhaul networks. Furthermore, the authors in [13] investigate an optimization the FlyBS's position, user association, and resource allocation, to maximize the utility in software-defined cellular networks with wireless backhaul. Due to the introduced flow conservation constraints, an extension of studies/solutions on two-hop FlyBS networks to higher number of hops is often not simple or straightforward. There are quite a limited number of works that consider relaying FlyBSs in networks with more than two hops. In [14] the minimum downlink throughput is maximized by optimizing the FlyBSs' positioning, bandwidth, and power allocation. The provided solution, however, does not address interference management as orthogonal transmissions is assumed. Furthermore, the FlyBSs' altitude is not optimized. Then, in [15] the number of FlyBSs is optimized while ensuring both coverage to all ground users as well as backhaul connectivity to a terrestrial base station. The authors in [16] investigate an interference management scheme based on machine learning and a positioning based on K-means to mitigate interference and FlyBSs' power consumption.

In the view of existing works on relaying FlyBS networks,

This work was supported by the project No. LTT 20004 funded by Ministry of Education, Youth and Sports, Czech Republic and by the grant of Czech Technical University in Prague No. SGS20/169/OHK3/3T/13, and partially by the HUAWEI France supported Chair on Future Wireless Networks at EURECOM.

we are motivated to take one step forward and to address a maximization of sum capacity via a placement of FlyBSs and an association of users in a multi-hop relaying FlyBS architecture where the FlyBSs serving the users at the access link connect to a GBS via another relaying FlyBS. Such an extension from two-hop model would allow a vaster range of user coverage to connect more remote users to the GBS. Unlike the most of related works, in our model, also the GBS and the relay are allowed to serve the users directly. In contrast to most of related works, a reuse of channels from the access link is enabled to establish the backhaul connection. The solution is provided under backhaul constraints.

The main contribution of this paper is explained as follow. We provide a framework based on a multi-hop FlyBS wireless network where the FlyBSs at the access link communicate with a ground base station through a relaying FlyBS. We formulate the network's sum capacity with a consideration of channel resue for the backhaul link. We formulate the problem of sum capacity maximization via an association of the users and a positioning of the FlyBSs at the access link and the relay. In our model, a direct serving of the users by the relaying FlyBS as well as by the GBS is also possible. A heuristic iterative solution is proposed based on an alternating optimization of the FlyBSs' positions at the access link, FlyBS's position at the relay, and then a reassociation of the users to the FlyBSs. An approximation of the sum capacity is proposed to derive a radial function to determine the FlyBSs' optimal directions of movement in the proposed iterative positioning.

The rest of this paper is organized as follows. In Section II we elaborate the system model for multi-hop FlyBS network. Next, the problem of sum capacity maximization is formulated and our proposed solution to the FlyBS's positioning and user association is provided in Section III. Then, in section IV, we specify our adopted simulation scenario and we show the performance of our proposed solution and we compare it with existing works. Last, we conclude the paper and outline the potential extensions for the future work.

II. System Model and Problem Formulation

In this section, we define the system model and provide details about transmission power and channel capacity.

We consider a set of M FlyBSs and a ground base station (GBS) serving N ground users. $M-1$ of those FlyBSs serve at the access link. The backhaul communication between those $M-1$ FlyBSs and the GBS is established via an intermediate relay FlyBS. Fig. 1 illustrates the adopted model. Let $\boldsymbol{L} = \{\boldsymbol{l_1}, \ldots, \boldsymbol{l_M}\}$ be the set of the FlyBS's positions where $\boldsymbol{l_m}[k] = [X_m[k], Y_m[k], H_m[k]]^T$ denote the location of the m-th FlyBS at the time step k $(1 \leq m \leq M)$, where the index $m = M$ indicates the relay. Let $\boldsymbol{l_{M+1}} = [X_{M+1}, Y_{M+1}, H_{M+1}]^T$ denote the GBS's position. Next, let $d_{m_1,m_2}[k]$ denote the Euclidean distance between the m_1-th and m_2-th BSs' receivers (we use the general term BS when referring to both GBS and FlyBSs). Furthermore, let $v_i[k] = [x_n[k], y_n[k], z_n[k]]^T$ denote the coordinates of the n-th ground user at the time step k. Then, $d_{n,m}[k]$ denotes

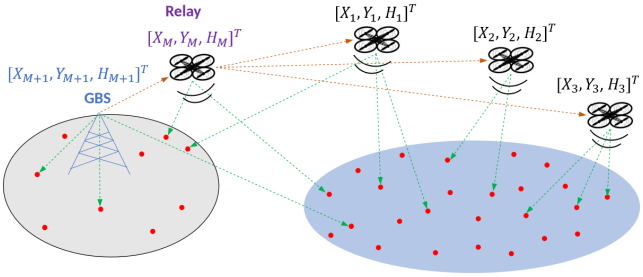

Figure 1: System model with the FlyBSs at the access link, relaying FlyBS, and the GBS serving moving users.

Euclidean distance of the n-th user to the m-th BS. As in many related works, we assume that the current positions of the users are known to the BSs. Also, the FlyBSs can determine their own position [8], [10], [14], [18]. Let $\mathbf{A} = (a_{n,m}) \in \{0,1\}^{N \times (M+1)}$ be the association matrix where $a_{n,m} = 1$ indicates an association of the n-th user to the m-th BS. Note that the users can be directly served by the relay or the GBS as well. Every user cannot be associated to more than one BS. Also, we assume the whole radio band is divided into the set of channels $\mathbf{J} = \{j_1, \ldots, j_C\}$, where channel j_c has a bandwidth of B_c $(1 \leq c \leq C)$. Note that the channels can be of different bandwidth in our model. We adopt orthogonal downlink channel allocation for all users associated to the same BS. Furthermore, let g_n be the index of the channel allocated to the n-th user. Also, we assume I_M and I_{M+1} denote the set of indices of channels allocated to the users served by the relay and by the GBS, respectively. Also, let $I_{M,m}$ be the set of channels' indices used between the relay and the m-th FlyBS at the access link. The relay communicates with users and other FlyBSs using orthogonal channels. Note that, we do not target an optimization of channel allocation due to space limit, and we leave that for future work. Nevertheless, our model works with any channel allocation.

The received power from the m-th FlyBS at the n-th user is denoted as $p^R_{n,m}$ and calculated as:

$$p^R_{n,m} = \Gamma_{n,m}\left(\frac{\gamma}{\gamma+1}\overline{h}_n + \frac{1}{\gamma+1}\tilde{h}_n\right) d_{n,m}^{-\alpha_{n,m}} = Q_{n,m} d_{n,m}^{-\alpha_{n,m}}, \quad (1)$$

where $\Gamma_{n,m}$ is a parameter depending on communication frequency and gain of antennas. Furthermore, γ is the Rician fading factor, $\overline{h}_n$ is the line-of-sight (LoS) component satisfying $|h_n| = 1$, and $\tilde{h}_n$ denotes the non-line-of-sight (NLoS) component satisfying $\tilde{h}_n \sim CN(0,1)$, and $\alpha_{n,m}$ is the pathloss exponent. Note that the coefficient $\Gamma_{n,m}(\frac{\gamma}{\gamma+1}\overline{h}_n + \frac{1}{\gamma+1}\tilde{h}_n) d_{n,m}^{-\alpha_{n,m}}$ is substituted with $Q_{n,m}$ for an ease of presentation in later discussions. Similar relation applies for backhaul link as $p^R_{m_1,m_2,k} = Q_{m_1,m_2,k} d_{m_1,m_2}^{-\alpha_{m_1,m_2}}$ where $p^R_{m_1,m_2,k}$ is the received power at m_1-th BS from m_2-th BS over k-th channel.

The downlink capacity of the n-th user is calculated as

$$C_{n,m} = a_{n,m} B_{g_n} \log_2\left(1 + \frac{p^R_{n,m}}{\sigma^2_{n,m} + \sum_{m' \in \{a_{n,m'}=0\}} p^R_{n,m'}}\right) \quad (2)$$

where $\sigma^2_{n,m}$ is the noise power. Next, the capacity between the relay and the m-th FlyBS is

$$C_{M,m} = \sum_{k \in I_{m,M}} B_k \log_2(1 + \frac{p^R_{m,M,k}}{\sigma^2_{m,M,k} + \sum\limits_{m' \in [1,M+1] \setminus \{M\}} p^R_{m,m',k}}) \tag{3}$$

Also, the link's capacity between the GBS and the relay is

$$C_{M+1,M} = \sum_{k \in [1,K] \setminus I_{M+1}} B_k \log_2(1 + \frac{p^R_{M,M+1,k}}{\sigma^2_{M,M+1,k} + \sum_{m=1}^{M-1} p^R_{M,m,k}}) \tag{4}$$

In the next section we formulate the problem of sum capacity maximization and we elaborate our proposed solution.

III. Problem Formulation and Proposed FlyBS positioning and User Association

In this section, we first introduce the problem of sum capacity maximization. Then, we outline our proposed optimization of user association and FlyBS's positioning.

A. Problem Formulation

The objective is to find a 3D positioning of the FlyBSs as well as an association of users to the BSs (including GBS and relay) to maximize the sum capacity at every time step k while constraints on the FlyBSs' altitude and speed as well as on backhaul are taken into account. Hence, we formulate the problem of the sum capacity maximization as follows:

$$\max_{\boldsymbol{L},\mathbf{A}} \sum_{m=1}^{M} \sum_{n=1}^{N} a_{n,m} C_{n,m}[k], \quad \forall k \tag{5}$$

$$s.t. \quad H_{min,m}[k] \leq H_m[k] \leq H_{max,m}[k], \quad (5a)$$

$$V_{F,m}[k] \leq V^{max}_m, \quad \forall m \in [1,M] \quad (5b)$$

$$\sum_{n=1}^{N} a_{n,m} C_{n,m}[k] \leq C_{M,m}[k], m \in [1, M-1] \quad (5c)$$

$$\sum_{m=1}^{M-1} C_{M,m}[k] \leq C_{M+1,M}[k], \quad (5d)$$

$$a_{n,m}[k] \in \{0,1\}, \sum_{m=1}^{M+1} a_{n,m}[k] \leq 1, \quad (5e)$$

$$\sum_{n=1}^{N} a_{n,m}[k] \leq C, \quad \forall m \in [1, M-1] \quad (5f)$$

$$\sum_{n=1}^{N} a_{n,m}[k] \leq |I_m|, \quad \forall m \in \{M, M+1\}, \quad (5g)$$

where $H_{min,m}$ and $H_{max,m}$ denote the minimum and maximum flying altitude of the m-th FlyBS, respectively, and are determined with respect to the topology of the environment and the flying regulations. Furthermore, V^{max}_m is the m-th FlyBS's maximum supported speed. The constraints (5a) and (5b) always ensures a flight within the allowed range of altitude and speed, respectively. The constraint (5c) guarantees that the backhaul link's capacity between each FlyBS at the access link and the relay is larger than the sum downlink capacity of that FlyBS, and the constraint (5d) implies that the capacity of the GBS-to-relay link is larger than the sum capacity for the links between relay and FlyBSs at the access link. The constraint (5e) indicates that each user is not associated to more than one BS, and the constraints (5f) and (5g) ensure that the number of users associated to each BS cannot exceed the number of channels allocated to each BS.

Challenges regarding the optimization problem in (5) include: 1) the sum capacity function is non-convex with respect to the FlyBSs' positions (i.e., $\boldsymbol{q_m}$, $m \in [1, M]$), 2) the constraints (5c) and (5d) are non-convex with respect to the FlyBSs' positions, and 3) the discrete association function $\mathbf{A}$ in (5) makes the optimization problem non-tractable. To tackle the challenges mentioned above we propose a heuristic solution by the means of approximation and based on converting the objective to a radial function to determine FlyBSs' movement towards an increase in the sum capacity. Then, the proposed solution to (5) is provided based on an alternating optimization of the FlyBSs' positions at the access link, relay's position, and user association. In particular, for a given user association, we propose an iterative approach based on an optimization of positioning of the FlyBSs at the access link under the constraint on their backhaul link and other constraints on their movement. Then, a positioning of the relay is proposed under the constraint on backhaul links between the relay and other BSs. Then, a reassociation of the users to BSs at their updated positions is applied.

B. Approximation of sum capacity as radial function

To proceed with the solution, we first propose and derive an approximation of the objective (sum capacity)that converts the objective to a radial function indicating the direction of movement for all FlyBSs to maximize the sum capacity. To begin with, we rewrite the logarithm term in (2) using (1) as

$$\log_2(1 + \frac{\frac{Q_{n,m}}{\sigma^2_{n,m}} d^{-\alpha_{n,m}}_{n,m}}{1 + \sum_{m' \in \{a_{n,m'}=0\}} \frac{Q_{n,m'}}{\sigma^2_{n,m}} d^{-\alpha_{n,m'}}_{n,m'}}) = \log_2(1 + \frac{Q_{n,m}}{\sigma^2_{n,m}} (d^2_{n,m})^{-\frac{\alpha_{n,m}}{2}} + \sum_{m' \in \{a_{n,m'}=0\}} \frac{Q_{n,m'}}{\sigma^2_{n,m}} (d^2_{n,m'})^{-\frac{\alpha_{n,m'}}{2}}) - \log_2(1 + \sum_{m' \in \{a_{n,m'}=0\}} \frac{Q_{n,m'}}{\sigma^2_{n,m}} (d^2_{n,m'})^{-\frac{\alpha_{n,m'}}{2}}). \tag{6}$$

Then, we use the first-order Taylor approximation $\log_2(1 + X) \approx \frac{X}{\log(2)}$ to expand the logarithm terms on the right-hand side in (6) and we get a linear expression with respect to $(d^2_{n,m})^{-\frac{\alpha_{n,m}}{2}}$. Next, we rewrite the term $(d^2_{n,m})^{-\frac{\alpha_{n,m}}{2}}$ as

$$(\Psi^2 + ((X_m - x_n)^2 + (Y_m - y_n)^2 + (H_m - z_n)^2) - \Psi^2)^{-\frac{\alpha_{n,m}}{2}}, \tag{7}$$

where Ψ is an arbitrary nonzero constant used to expand (7) as follows. The right-hand side in (7) is in the form of $(a + \chi)^k$ where $k = \frac{\alpha_{n,m}}{2}$, $a = \Psi^2$, and $\chi = ((X_m - x_n)^2 + (Y_m - y_n)^2 + (H_m - z_n)^2 - \Psi^2)$. Using the first-order Taylor approximation with respect to χ, (7) is converted to a summation of linear terms with respect to χ. Next, suing the equation $\sum_{n=1}^{N} \beta_n (X_m - x_n)^2 = (\sum_{n=1}^{N} \beta_n)(X_m - \frac{\sum_{n=1}^{N} \beta_n x_n}{\sum_{n=1}^{N} \beta_n})^2 + (\sum_{n=1}^{N} \beta_n x_n^2 - \frac{(\sum_{n=1}^{N} \beta_n x_n)^2}{\sum_{n=1}^{N} \beta_n})$ for any weighted

sum of squares (here shown only for X_m), the sum capacity can be approximated as

$$\sum_{n=1}^{N} C_{n,m}[k] \approx \zeta[k] - \sum_{1\leq m\leq M} \rho_m ||\boldsymbol{l_m}[k] - \boldsymbol{l_{0,m}}[k]||^2. \quad (8)$$

where ζ, ρ_m, and $\boldsymbol{l_{0,m}}$ are constants with respect to $\boldsymbol{l_m}$.

Having the sum capacity as presented in (8), it is seen that for $\rho_m > 0$ ($\rho_m < 0$) a movement of the m-th FlyBS towards (against) $\boldsymbol{l_{0,m}}$ causes an increase in the sum capacity. This fact helps to determine the FlyBS's positions under the constraints (5a)-(5d) as elaborated in the next subsection.

C. Positioning of the FlyBSs at the access link

The approximation in (8) is exploited to reposition the FlyBSs at the access link (repositioning of relay will be addressed separately in the next subsection). First, we relax the GBS-to-relay constraint (5d) and we propose a positioning of the FlyBSs according to the constraints (5a)-(5c). The constraint (5a) limits the position of the m-th FlyBS (q_m) between the planes $z = H_{min,m}[k]$ and $z = H_{max,m}[k]$. Then, the constraint (5b) bounds q_m to the points on or inside of a sphere with a center at $q_m[k-1]$ and with a radius of $V_m^{max}\delta$ where δ is the time distance between two consecutive time steps. Regarding the constraint (5c), there exist terms in $C_{n,m}$ and $C_{M,m}$ (in (2) and (3)) related to the interference from other FlyBSs that complicates a dealing with (5c) as (5c) defines a non-convex region with respect to q_m. To tackle this issue, we use the fact that the FlyBSs' movements are limited at each time step due to the limited speed. We convert (5c) into a convex constraint in following way. First, let $d_{n,m,min}[k]$ and $d_{n,m,max}[k]$ denote the minimum and maximum distances that can occur between the n-th user and the m-th FlyBS at the time step k, respectively. $d_{n,m,min}[k]$ and $d_{n,m,max}[k]$ are calculated using the FlyBSs' speeds as:

$$\begin{aligned} d_{n,m,min} &= ||\boldsymbol{l_m}[k-1] - v_n[k]|| - V_m^{max}\delta, \\ d_{n,m,max} &= ||\boldsymbol{l_m}[k-1] - v_n[k]|| + V_m^{max}\delta. \end{aligned} \quad (9)$$

Hence, the left-hand side in (5c) is upper bounded by

$$\sum_{n=1}^{N} a_{n,m} B_{g_n} \log_2\left(1 + \frac{Q_{n,m} d_{n,m,min}^{-\alpha_{n,m}}}{\sigma_{n,m}^2 + \sum_{m'\in\{a_{n,m'}=0\}} Q_{n,m'} d_{n,m',max}^{-\alpha_{n,m'}}}\right) \quad (10)$$

Next, the lower and upper bounds for $d_{m_1,m_2}[k]$ in (3) are $d_{m_1,m_2,min}[k] = d_{m_1,m_2}[k-1] - (V_{m_1}^{max} + V_{m_2}^{max})\delta$ and $d_{m_1,m_2,max}[k] = d_{m_1,m_2}[k-1] + (V_{m_1}^{max} + V_{m_2}^{max})\delta$, respectively. Thus, the right-hand side in (5c) is lower bounded by

$$\sum_{k\in I_{m,M}} B_k \log_2\left(1 + \frac{Q_{m,M,k} d_{M,m}^{-\alpha_{m,M}}}{\sigma_{m,M,k}^2 + \sum\limits_{m'\in[1,M+1]\setminus\{M\}} Q_{m,m',k} d_{m,m',min}^{-\alpha_{m,m'}}}\right) \quad (11)$$

Hence, we replace (5c) with the constraint (10)≤(11). Based on its derivation, once (10)≤(11) is fulfilled, the constraint (5c) is fulfilled as well. Note that, a derivation of closed-form expression for $d_{M,m}$ from (10)≤(11) is difficult. Nevertheless, the term in (10) is a constant, and the term in (11) is a strictly decreasing function of $d_{M,m}[k]$. Hence, we use bisection method to find an upper bound equivalent to (10)≤(11) as $d_{M,m}[k] \leq D_{M,m}[k]$ for $m \in [1, M-1]$. This inequality defines the border and interior of a sphere with a center at $\boldsymbol{l_m}$ and a radius of $D_{M,m}[k]$. We refer to the combination of (5a), (5b), and (10)≤(11) as the feasibility region, which results from intersections spheres (corresponding to (5b) and to (10)≤(11)) and the region between two planes (as in (5a)).

Having investigated the impact of the constraints (5a)-(5c), we now focus on the approximated objective in (8). According the approximated objective, for $\rho_m > 0$, the m-th FlyBS should move to the closest possible point to $\boldsymbol{l_{0,m}}$ to maximize sum capacity. Similarly, for $\rho_m < 0$, the m-th FlyBS should move as far from $\boldsymbol{l_{0,m}}$ as possible to maximize sum capacity. Therefore, the positioning of the FlyBSs at every time step is based on a minimization of the m-th FlyBS's distance from $\boldsymbol{l_{0,m}}$ if $\rho_m > 0$, or a maximization of the distance from $\boldsymbol{l_{0,m}}$ if $\rho_m < 0$ under the constraints (5a), (5b), and (10)≤(11). Since the feasibility region is continuous if $\boldsymbol{l_{0,m}}$ lays inside of the region, the closest possible point to $\boldsymbol{l_{0,m}}$ is the point $\boldsymbol{l_{0,m}}$ itself and the furthest point to $\boldsymbol{l_{0,m}}$ is on the region's border. If $\boldsymbol{l_{0,m}}$ lays outside of the region, the closest/furthest point of this region to/from $\boldsymbol{l_{0,m}}$ is on the border of the region. This fact enables to find the optimal point by searching on the border of the feasibility region (if $\boldsymbol{l_{0,m}}$ is already not the optimal). Since the feasibility region's border is either sphere, plane, or the intersection of those (which are circles), we thus search for the closest point to $\boldsymbol{l_{0,m}}$ in the described candidate set which consists of spheres and planes and their intersection.

D. Positioning of the relay

Once the FlyBSs' positions at the access link are updated according to the previous subsection III.B, the relay's postioning comes into effect. The relay's movement is done considering (8) and (5d). Note that any movement of the relay would not violate (5c), as all possible movements of the relay are already considered for the derivation of (10)≤(11) in the previous subsection. According to (8) the relay moves towards $\boldsymbol{l_{0,M}}$ if $\rho_M > 0$, or in the direction away from $\boldsymbol{l_{0,M}}$ if $\rho_M > 0$. In addition to the constraints (5a) and (5b), we also consider (5d) to guarantee the requirement on the backhaul capacity. The terms in $C_{M,m}$ and $C_{M+1,M}$ (according to (3) and (4)) include the interference from other BSs that makes the constraint (5d) non-convex with respect to the relay's position. To tackle this issue, in the following, we derive a convex constraint from (5d). By taking a similar approach as in the derivation of (10) and (11), the left-hand side in (5d) is upper bounded by

$$\sum_{m=1}^{M-1} \sum_{k\in I_{m,M}} B_k \log_2\left(1 + \frac{Q_{m,M,k} d_{m,M,min}^{-\alpha_{m,M}}}{\sigma_{m,M,k}^2 + \sum\limits_{m'\in[1,M+1]\setminus\{M\}} Q_{m,m',k} d_{m,m',max}^{-\alpha_{m,m'}}}\right) \quad (12)$$

By a similar approach, the right-hand side of (5d) is lower bounded by

$$\sum_{k\in[1,K]\setminus I_{M+1}} B_k \log_2\left(1+\frac{Q_{M,M+1,k}\, d_{M,M+1}^{-\alpha_{M,M+1}}}{\sigma^2_{M,M+1,k}+\sum_{m=1}^{M-1} Q_{M,m,k}\, d_{M,m,min}^{-\alpha_{m,M}}}\right) \tag{13}$$

Thus, instead of (5d), we consider the constraint (12)$\leq$(13). The term in (12) is a constant, and the term in (13) is strictly decreasing with respect to $d_{M,M+1}$. Hence, there exists $D_{M,M+1}$ such that (12)$\leq$(13) is equivalent to $d_{M,M+1} \leq D_{M,M+1}$, which demarcates the points on and inside a sphere centered at $\boldsymbol{l_0}$ with a radius of $D_{M,M+1}$. The value of $D_{M,M+1}$ is derived using bisection. According to (8) for $\rho_M > 0$ ($\rho_M < 0$) the relay moves to the closest (furthest) point to (from) $\boldsymbol{l_{0,M}}$ fulfilling (5a), (5b), and (12)$\leq$(13). The optimal position is found similarly as in subsection III.B.

E. Association of users to the BSs

After the positioning of the FlyBSs, we update the associated set of users to each BS including the GBS and the relay. It is noted that, the capacity of each user is independent of the association of other users to BSs, as the signal and interference for each user (as in (2)) would be uniquely determined from that user's association. Hence, the problem of user association is solved using linear programming (LP). After updating the association of the users, the next iteration of the FlyBSs' positioning is applied. This iterative method continues until there is no further change in the user association, or until a maximum number of iterations is reached. The proposed iterative solution is applied at every time step.

IV. Simulations and Results

In this section, we present models and simulations adopted for evaluation of our proposed solution, and we demonstrate the advantages of the proposal over state of the art schemes.

A. Simulation scenario and models

We assume two circular areas, one with a radius of 400 m and with the GBS at its center, and another area with a radius of 400 m and with its center 1600 m away from the GBS. 25% of all users are distributed in the first circular area and 75% distributed in the second area. Within each area, half of the users move based on a random-walk mobility model with a speed of 1 m/s. The other half of the users are randomly distributed into six clusters of crowds. The centers of three of the clusters move at a speed of 1 m/s. Each user in those clusters moves with a uniformly distributed speed of [0.6, 1.4] m/s with respect to the cluster's center. Furthermore, the centers of the other three clusters move at a speed of 1.6 m/s with the speed of users uniformly distributed over [1.2, 2] m/s with respect to the center of their corresponding cluster.

A total bandwidth of 100 MHz with C =120 channels of equal bandwidths are assumed. For the GBS and the relay, 20% of the channels are allocated to directly serve the users (i.e., $|I_M| = |I_{M+1}| = 0.2C$), and the rest are allocated for backhaul connection. The backhaul bandwidth is split equally among the FlyBSs at the access link. A maximum transmission power of 37 dBm and 30 dBm is considered for the GBS and the FlyBSs, respectively [17]. The noise power is set to -90 dBm. Pathloss exponents of $\alpha_{n,m}$ =2.8 and α_{m_1,m_2} =2.1 are adopted for BS-to-user and BS-to-BS channels, respectively. An allowed altitude range of $[H_{min,m}, H_{max,m}]$ =[100, 300] m and a maximum speed of 25 m/s are assumed for the FlyBSs. The results are shown for M ={2,3,4,5} FlyBSs. Each simulation has a duration of 1200 seconds. The results are averaged out over 100 simulation drops.

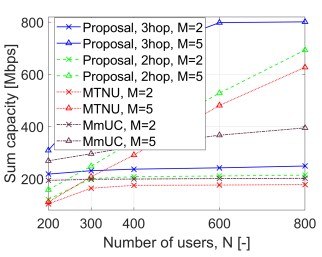

Figure 2: Sum capacity vs. N for different schemes.

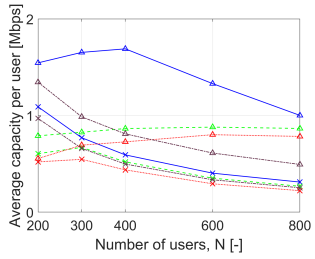

Figure 3: Average user capacity vs. N for different schemes.

We compare our proposal against the performance of the following schemes: *i*) a two-hop version of our proposed solution to FlyBSs' positioning and user association. This model is simply derived from our original proposed model by treating the relay as a ground base station. In such case the positioning of the FlyBSs is done according to subsection III.B., *ii*) state-of-the-art work in [10] where a maximization of total network's utility (referred to as MTNU) is provided in a two-hop relaying FlyBS network via FlyBSs' positioning, user association, and resource allocation. The utility is defined as the sum of logarithm of user's capacities. *iii*) maximization of minimum user's capacity (referred to as MmUC), via FlyBS's positioning and resource allocation published in [14].

B. Simulation results

In this subsection, we present and discuss simulation results. Fig. 2 illustrates the sum capacity achieved by different schemes for different number of users and for M =2,5. According to Fig. 2, the sum capacity increases with the number of users in general for all schemes as there are more (orthogonal) channels used. However, if all available channels are used, the sum capacity would saturate as in such case, not all the users will be served by the FlyBSs and, hence, there is no further increase in the sum capacity of the network. This can be seen in the lines for M =2 in Fig. 2. According to Fig. 2, the proposed solution enhances the sum capacity by 80%, 15%, 14%, 15%, and 17% compared to the two-hop proposal for N = 200, 300, 400, 600, and 800, respectively, and by 109%, 41%, 35%, 38%, and 40% compared to MTNU for N = 200, 300, 400, 600, and 800, respectively, and by 15%, 17%, 19%, 20%, and 23% compared to MmUC for N = 200, 300, 400, 600, and 800, respectively.

Following the comparison in terms of sum capacity, we show the average user capacity in Fig. 3 for different number

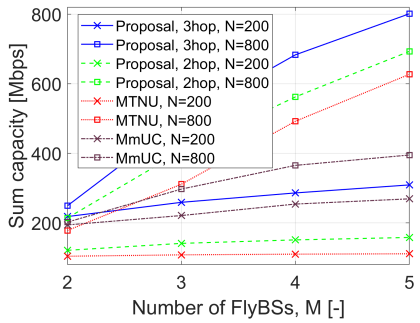

Figure 4: Sum capacity vs. number of FlyBSs for different schemes.

of users and different schemes. According to Fig. 3, the average user capacity increases with N in case that there are unused channels to be allocated to the added users. The two-hop proposal and MTNU with M =2 show a strictly increasing average user capacity for N larger than 200. However, the average user capacity might decrease for larger number of users in case that there are not enough unused channels to accommodate the added users. An example for such trend is presented in Fig.3 for MTNU with M =2 and for the three-hop proposal with M =5 for N larger than 300 and 400, respectively. Note that, the three-hop model has one FlyBS less than the two-hop model at the access link for the same value of M, and so the three-hop model would run out of unused channels at lower values of N compared to two-hop models. Nevertheless, the proposed three-hop solution still outperforms other schemes (with the same M). According to Fig. 3, the proposed three-hop solution increases the average user capacity compared to the two-hop proposal by 80%, 15%, 14%, 15%, and 17% for 200, 300, 400, 600, and 800 users, respectively. Furthermore, compared to MTNU, the proposed three-hop scheme increases the average user capacity by 110%, 41%, 35% 38%, and 40%, respectively. Compared to MmUC, the proposed solution enhances the average user capacity by 13%, 17%, 20% 21%, and 23%, respectively.

Next, Fig. 4 demonstrates the impact of the number of FlyBSs on the sum capacity for different schemes for N = 200 and N = 800. It is observed that, increasing the number of FlyBSs would increase the achieved sum capacity. This is mainly because of two reasons: 1) due to a limited number of channels, more number of users might be served by adding more FlyBSs, 2) even if all the users are already being served by the FlyBSs, adding more FlyBS might lead to a reassociation of some users to a closer FlyBS, resulting in a higher received power at the user despite an incurred interference by the other FlyBSs. According to Fig. 4., for N =200 the proposed solution increases the sum capacity by 80%, 83%, 90%, and 95% compared to two-hop proposal for M= 2,3,4, and 5, respectively, and by 109%, 139%, 160%, and 178% compared to MTNU for M = 2,3,4, and 5, respectively, and by 12%, 17%, 13%, and 15% compared to MmUC for M = 2,3,4, and 5, respectively. Furthermore, for N =800, the proposed solution enhances the sum capacity by 17%, 23%, 21%, and 16% compared to two-hop proposal for M = 2, 3, 4, and 5, respectively, and by 40%, 61%, 39%, and 28% compared to MTNU for M = 2, 3, 4, and 5, respectively, and by 24%, 68%, 87%, and 103% compared to MmUC for M = 2,3,4, and 5, respectively.

V. Conclusions

In this paper, we focus on multi-hop relaying FlyBS networks where there are FlyBSs adopted at both relaying and access links. We maximize the sum capacity with a consideration of backhaul constraints. To this end, we propose an analytical approach based on an alternating optimization of the FlyBSs' positions and an association of users. The proposed solution improves the achieved sum capacity by tens of percent compared to existing solutions. In the future, the problem sum capacity maximization for multiple relays shall be studied.

References

[1] T. Liu, et al, "3D Trajectory and Transmit Power Optimization for UAV-Enabled Multi-Link Relaying Systems," *IEEE Trans. Green Commun. Netw.*, vol. 5, no. 1, 2021.

[2] M. Nikooroo and Z. Becvar, "Optimization of Total Power Consumed by Flying Base Station Serving Mobile Users," *IEEE Trans. Netw. Sci. Eng.*, Early Access, 2022.

[3] G. Li, et al, "Joint User Association and Power Allocation for Hybrid Half-Duplex/Full-Duplex Relaying in Cellular Networks," *IEEE Syst. J.*, vol. 13, no. 2, 2019.

[4] B. Li, et al, "Joint Transmit Power and Trajectory Optimization for Two-Way Multi-Hop UAV Relaying Networks," *IEEE ICC Workshops*, 2020.

[5] Y. Huang, et al, "Bandwidth, Power and Trajectory Optimization for UAV Base Station Networks With Backhaul and User QoS Constraints," *IEEE Access*, vol. 8, 2020.

[6] C. Qiu, et al, "Backhaul-Aware Trajectory Optimization of Fixed-Wing UAV-Mounted Base Station for Continuous Available Wireless Service," *IEEE Access*, vol. 8, 2020.

[7] C. T. Cicek, et al, "Backhaul-Aware Optimization of UAV Base Station Location and Bandwidth Allocation for Profit Maximization," *IEEE Access*, vol. 8, 2020.

[8] Q. Pham, et al, "Joint Placement, Power Control, and Spectrum Allocation for UAV Wireless Backhaul Networks," *IEEE Netw. Lett.*, vol. 3, no. 2, 2021.

[9] Y.Yu, et al, "UAV-Aided Low Latency Multi-Access Edge Computing," *IEEE Trans. Veh. Technol.*, vol. 70, no. 5, 2021.

[10] C. Qiu, et al, "Multiple UAV-Mounted Base Station Placement and User Association With Joint Fronthaul and Backhaul Optimization," *IEEE Trans. Commun.*, vol. 68, no. 9, 2020.

[11] P. Mach, et al, "Power Allocation, Channel Reuse, and Positioning of Flying Base Stations With Realistic Backhaul," *IEEE Internet Things J.*, vol. 9, no. 3, 2022.

[12] N. Iradukunda, et al, "UAV-Enabled Wireless Backhaul Networks Using Non-Orthogonal Multiple Access," *IEEE Access*, vol. 9, 2021.

[13] C. Pan, et al, "Joint 3D UAV Placement and Resource Allocation in Software-Defined Cellular Networks With Wireless Backhaul," *IEEE Access*, vol. 7, 2019.

[14] P. Li and J. Xu, "Placement Optimization for UAV-Enabled Wireless Networks with Multi-Hop Backhaul", *J.Commn.Net*, vol. 3, no. 4, 2018.

[15] J.Sabzehali, et al, "Optimizing Number, Placement, and Backhaul Connectivity of Multi-UAV Networks", arXiv:2111.05457.

[16] L. Wang, et al, "An Integrated Affinity Propagation and Machine Learning Approach for Interference Management in Drone Base Stations," *IEEE Trans. Cogn. Commun. Netw.*, vol. 6, no. 1, 2020.

[17] M. Nikooroo and Z. Becvar, "Optimal Positioning of Flying Base Stations and Transmission Power Allocation in NOMA Networks," *IEEE Trans. Wireless Commun.*, vol. 21, no. 2, 2022.

[18] O. Esrafilian, R. Gangula and D. Gesbert, "Learning to Communicate in UAV-Aided Wireless Networks: Map-Based Approaches," *IEEE Internet Things J.*, vol. 6, no. 2, 2019.

Chapter 4

Conclusion and Future Work

In this Chapter, we first summarize the dissertation and recapitulate main contributions. Then, we further enrich the content of this dissertation by providing suggestions on future steps regarding the expansion of the studied works.

4.1 Summary of dissertation

This dissertation is focused on studying major aspects in mobile networks equipped with UAVs acting as FlyBSs. In the view of impacts on the system's performance made by energy consumption, we attempt to integrate FlyBSs into conventional mobile networks by optimizing the performance from different perspectives while also taking into account the energy consumption. In this regard, several aspects are considered as determining factors of performance in the network, including the FlyBS's positioning, FlyBS's transmission power and propulsion power consumptions, transmission power and resource allocation to the users, association of users to FlyBSs, etc.

In the scope of this dissertation, our main contributions are summarized as follow

- From the perspective of the cost of energy, the problem of total power minimization is targeted in Section 3.1. In this sense, the positioning of the FlyBS only aims to minimize the sum of transmission and propulsion power. Nevertheless, there are constraints regarding the user's required capacity at every time step. Existing solutions could not be applied to scenarios where the user's positions change over time. Hence, we target such scenarios and we provide solutions for a determination of the FlyBS's position for next single/multiple time steps (referred to as SPS/MPS). Other parameters to be optimized include transmission power and bandwidth allocation to each user. For SPS and MPS, we propose analytical closed-form solution and numerical solution based on Simplex, respectively. In order to accommodate

Simplex method, we propose to change the optimization variables in order to automatically fulfill the constraints in the problem, as Simplex works for problems with no constraints on optimization variables only. The solution for MPS is then further enhanced by updating the derived FlyBS's optimal positions over next time steps using a shifting window of a lower size than the MPS's output size. Benchmarked against several schemes with different settings, the proposed solution shows to provide a significant reduction by 16%-91% in the total power.

- In Section 3.2, we study the problem of user coverage maximization in FlyBS networks with NOMA. In scenarios with delay sensitive users where a minimum instantaneous capacity should be guaranteed to the users, prior solutions minimizing the total power or propulsion power cannot always guarantee a favorable user's coverage despite their efficiency in saving the battery's energy. This is due to an inherent negligence to the importance of transmission power in those solutions. Hence, we propose a solution based on a minimization of the transmission power with a consideration of an adjustable constraint to control the propulsion power consumption over time avoiding an unwantedly fast depletion of the FlyBS's battery. Accordingly, we propose to optimize the position of the FlyBS together with the clustering of users for NOMA purposes as well as their order in SIC decoding and transmission power allocation to each user. The proposed NOMA clustering is of a low complexity and it guarantees to yield the minimum transmission power for a given set of clusters' sizes. Unlike the majority of existing works, our solution allows clusters of different sizes, giving the flexibility to reduce the transmission power as much as possible. The proposed solution enhances the coverage duration by up to 67%-270% compared to existing solutions.

- The problem of user clustering for NOMA and FlyBS's positioning is elaborated in Section 3.3 so that the minimum user capacity is minimized. To this end, first, the relation between the problem of transmission power minimization is discussed. Next, the transmission power consumption is optimized via FlyBS's positioning, user's clustering for NOMA, and transmission power allocation to the users. The problem is solved under constrained altitude and speed of the FlyBS. We propose an alternating optimization of the FlyBS's positioning and an optimization of the NOMA clustering together with transmission power allocation and SIC decoding order. In particular, for a preset clustering, the optimization of transmission power is done using CVX. Then, the optimal clustering together with the associated SIC decoding order and transmission power allocation for the users are derived using a proposed novel solution based on a selection of "exclusively convex polygons" on

the plane of points representing the users' positions on the map. With respect to state-of-the-art, the proposed solution significantly enhances the transmission power (by 67%-84%) and, consequently, the minimum user's capacity (by 20%-59%).

- In Section 3.4, The problem of propulsion energy minimization is investigated in networks with airship-based FlyBSs. The total propulsion energy is expressed in terms of the displacements made by the FlyBSs within the unit of time. The goal is to maintain the sum capacity above some given minimum threshold. The novel solution is proposed based on the idea of prioritizing relocation of those FlyBSs that contribute to the sum capacity with the least cost/amount of energy. Existing works focus only on scenarios where the users are represented by static nodes and do not change their solution over time. Hence, we target to study the optimization problem in scenarios with moving users and we propose an iterative converging algorithm with low computational complexity that determines the displacement and the direction of movement for each FlyBS over time to constantly guarantee the network's required sum capacity with the minimum total propulsion power energy. The proposed solution demonstrates a great amount of savings (by 55%-90%) in energy consumption with respect to solutions targeting to maximize the sum capacity.

- In Section 3.5, the problem of sum capacity maximization is studied via an optimization of the FlyBS's placement and transmission power allocation to the users. The problem is solved for constrained transmission power, propulsion power, altitude, and speed of the FlyBS. Furthermore, a minimum capacity is guaranteed to every user at each time step. Existing works either ignore the mentioned practical constraints or do not consider user's quality of service. To this end, and given the fact that the formulated problem is non-convex, we propose a heuristic solution based on an alternating optimization of transmission power allocation and positioning. In such approach, the resulting problem of power allocation is solved using CVX. The feasibility of a solution is also discussed with respect to the constraints in the problem, and a necessary condition is derived. Furthermore, for positioning, a radial approximation of the objective (i.e., sum capacity) so that the movement of the FlyBS is directed with a consideration of i) the point representing the maximum-capacity point regardless of the problem constraints, ii) the non-convex space demarcated by the constraints. The proposed solution is of low complexity and outperforms the state-of-the-art considerably by 15%-46% .

- In Section 3.6, we study the problem of sum capacity maximization in an integrated network of FlyBSs with multi-hop communication and backhaul. The relaying FlyBS establishes a connection between the FlyBSs at the access link and the

GBS. The sum capacity is optimized via a positioning of the FlyBSs and an association of the users to the BSs. The relay and the GBS can also serve the users directly. The formulated problem is solved for constrained FlyBSs' altitude and speed. In addition, the flow conservation constraint at the relay ensures that the backhaul link's capacity is not lower than the fronthaul capacity. Due to non-convexity of the objective (sum capacity) and the discreteness of user association, only a suboptimal solution can be derived. We propose a heuristic solution based on an alternating optimization of the positioning and user association. For positioning, a radial approximation of the sum capacity. The derived approximation function points out to the optimal direction of movement for the FlyBSs. Next, the positioning of the FlyBSs is done sequentially, i.e., firstly for the FlyBSs at the access link and, then, for the relay. Furthermore, as for the non-convex constraint on backhaul link, we propose a novel method to derive a tighter convex constraint such that fulfilling the alternative constraint would automatically fulfill the original constraint. The FlyBSs are relocated using the approximated radial form of the sum capacity and with respect to newly derived setting of the constraints. The proposed solution increases the sum capacity remarkably by 23%-38% compared to state-of-the-art solutions.

4.2 Future research directions

The main goal of this dissertation is to shed light on various understudied aspects of FlyBSs in mobile networks including key challenges raised by FlyBS's power consumption (transmission and propulsion), user's mobility, multiple access and resource allocation, channel reuse, backhaul communication, and user's quality of service. The non-convex nature of many formulated problems in the scope of those challenges may solicit either negligence about practically essential constraints and assumptions or even derivation of inefficient solutions. We believe that this dissertation has addressed a notable span of those challenges. Not only the resolved challenges in this dissertation, as they are, would serve effectively in the favor of 6G networks, also the unresolved issues are now more tangibly understood, and the direction to successfully solve those issues is also somewhat outlined. In the following, we indicate some of the potential research directions in line with this dissertation.

- The problem of FlyBS's positioning could be considered to optimize other metrics in the network, e.g., Jain fairness, number of covered users, and energy efficiency (ratio of sum capacity to the total energy consumption).
- Harvesting the FlyBS's energy can be considered as an aid to enhance duration of

the FlyBS's operation. In this regard, a scheduling of the FlyBS's traveling during the mission adds another layer to the problem that shall be investigated.

- The problem of user scheduling and handover in multiple cells allows for an implementation of the FlyBSs in larger scales. Together with such extension, the aspects of user association to the FlyBSs as well as a management of interference should be investigated.

- An inclusion of FlyBS's communication with satellites allows for an even more extensive connectivity meeting ever-growing demands more readily in the future of wireless communication.

Bibliography

[1] H. Huang and A. V. Savkin, "Deployment of Heterogeneous UAV Base Stations for Optimal Quality of Coverage," in IEEE Internet of Things Journal, vol. 9, no. 17, pp. 16429-16437, 1 Sept.1, 2022, doi: 10.1109/JIOT.2022.3150292.

[2] Z. Wang and J. Zheng, "Performance Modeling and Analysis of Base Station Cooperation for Cellular-Connected UAV Networks," in IEEE Transactions on Vehicular Technology, vol. 71, no. 2, pp. 1807-1819, Feb. 2022, doi: 10.1109/TVT.2021.3123826.

[3] W. Xu et al., "Throughput Maximization of UAV Networks," in IEEE/ACM Transactions on Networking, vol. 30, no. 2, pp. 881-895, April 2022, doi: 10.1109/TNET.2021.3125982.

[4] J. Lee and V. Friderikos, "Interference-aware path planning optimization for multiple UAVs in beyond 5G networks," in Journal of Communications and Networks, vol. 24, no. 2, pp. 125-138, April 2022, doi: 10.23919/JCN.2022.000006.

[5] R. Bajracharya, R. Shrestha, S. Kim and H. Jung, "6G NR-U Based Wireless Infrastructure UAV: Standardization, Opportunities, Challenges and Future Scopes," in IEEE Access, vol. 10, pp. 30536-30555, 2022, doi: 10.1109/ACCESS.2022.3159698.

[6] M. Eskandari, A. V. Savkin and W. Ni, "Consensus-Based Autonomous Navigation of a Team of RIS-Equipped UAVs for LoS Wireless Communication With Mobile Nodes in High-Density Areas," in IEEE Transactions on Automation Science and Engineering, 2022, doi: 10.1109/TASE.2022.3183335.

[7] Q. Chen, H. Zhu, L. Yang, X. Chen, S. Pollin and E. Vinogradov, "Edge Computing Assisted Autonomous Flight for UAV: Synergies between Vision and Communications," in IEEE Communications Magazine, vol. 59, no. 1, pp. 28-33, January 2021, doi: 10.1109/MCOM.001.2000501.

This Bibliography presents the references related to Chapter 1 only. The references for each article in Chapter 3 is included right at the end of that article.

[8] Y. Zeng, J. Xu and R. Zhang, "Energy Minimization for Wireless Communication With Rotary-Wing UAV," in IEEE Transactions on Wireless Communications, vol. 18, no. 4, pp. 2329-2345, April 2019, doi: 10.1109/TWC.2019.2902559.

[9] J. Lee and V. Friderikos, "Interference-aware path planning optimization for multiple UAVs in beyond 5G networks," in Journal of Communications and Networks, vol. 24, no. 2, pp. 125-138, April 2022, doi: 10.23919/JCN.2022.000006.

[10] Z. Yang, W. Xu and M. Shikh-Bahaei, "Energy Efficient UAV Communication With Energy Harvesting," in IEEE Transactions on Vehicular Technology, vol. 69, no. 2, pp. 1913-1927, Feb. 2020, doi: 10.1109/TVT.2019.2961993.

List of Research Projects

Project no. LTT 20004 funded by The Ministry of Education, Youth and Sports.

Project title: "Cooperation with the International Research Centre in Area of Digital Communication Systems".

Project period: 2020-2022.

Project no. SGS20/169/OHK3/3T/13 funded by Czech Tech. Uni. in Prague.

Project period: 2019-2022.

Project no. P102/18/27023S funded by Czech Science Foundation.

Project title: "Communication in Self-optimizing Mobile Networks with Drones".

Project period: 2019-2021.

List of Publications

Publications in line with the dissertation

Journal papers

[J1] Z. Becvar, M. Nikooroo and P. Mach, "On Energy Consumption of Airship-based Flying Base Stations Serving Mobile Users," in *IEEE Transactions on Communications,* 2022, doi: 10.1109/TCOMM.2022.3196654.

[J2] M. Nikooroo and Z. Becvar, "Optimization of Total Power Consumed by Flying Base Station Serving Mobile Users," in *IEEE Transactions on Network Science and Engineering*, vol. 9, no. 4, July-Aug. 2022.

[J3] M. Nikooroo and Z. Becvar, "Optimal Positioning of Flying Base Stations and Transmission Power Allocation in NOMA Networks," in *IEEE Transactions on Wireless Communications*, vol. 21, no. 2, Feb. 2022.

[J4] M. Nikooroo and Z. Becvar, "Maximization of Minimum User Capacity in UAV-Enabled Mobile Networks with NOMA," in *IEEE Networking Letters*, 2022, Early Access, doi: 10.1109/LNET.2022.3197954.

Conference papers

[C1] M. Nikooroo, Z. Becvar, O. Esrafilian, D. Gesbert, "Sum Capacity Maximization in Multi-Hop Mobile Networks with Flying Base Stations", accepted in *IEEE PIMRC Workshops,* 2022.

[C2] M. Nikooroo, O. Esrafilian, Z. Becvar, D. Gesbert, "Sum Capacity Maximization in Multi-Hop Mobile Networks with Flying Base Stations", accepted in *IEEE GLOBECOM,* 2022.

[C3] M. Nikooroo and Z. Becvar, "Optimization of Transmission Power for NOMA in Networks with Flying Base Stations," in *IEEE 92nd Vehicular Technology Conference (VTC2020-Fall),* 2020.

[C4] Z. Becvar, P. Mach and M. Nikooroo, "Reducing Energy Consumed by Repositioning of Flying Base Stations Serving Mobile Users," in *IEEE Wireless Communications and*

Networking Conference (WCNC), 2020.

[C5] M. Nikooroo and Z. Becvar, "Optimizing Transmission and Propulsion Powers for Flying Base Stations," in *IEEE Wireless Communications and Networking Conference (WCNC)*, 2020.

[C6] M. Nikooroo and Z. Becvar, "Joint Positioning of UAV and Power Control for Flying Base Stations in Mobile Networks," in *International Conference on Wireless and Mobile Computing, Networking and Communications (WiMob)*, 2019.

Publications non-related to the dissertation

[C7] M. Kishani, Z. Becvar, M. Nikooroo and H. Asadi, "Reducing Storage and Communication Latencies in Vehicular Edge Cloud," Joint European Conference on Networks and Communications & 6G Summit (EuCNC/6G Summit), 2022.

Citations

[1*] L. Zhou, S. Leng, Q. Wang and Q. Liu, "Integrated Sensing and Communication in UAV Swarms for Cooperative Multiple Targets Tracking," in IEEE Transactions on Mobile Computing, 2022, doi: 10.1109/TMC.2022.3193499.
This paper cites the journal paper [J2]
[2*] Amponis, G.; Lagkas, T.; Zevgara, M.; Katsikas, G.; Xirofotos, T.; Moscholios, I.; Sarigiannidis, P. Drones in B5G/6G Networks as Flying Base Stations. Drones 2022, 6, 39. https://doi.org/10.3390/drones6020039.
This paper cites the journal paper [J3]
[3*] M. Umar Khan, M. Azizi, A. García-Armada and J. J. Escudero-Garzás, "Unsupervised Clustering for 5G Network Planning Assisted by Real Data," in IEEE Access, vol. 10, pp. 39269-39281, 2022, doi: 10.1109/ACCESS.2022.3165799.
This paper cites the journal paper [J3]
[4*] M. Sookhak, A. Mohajerzadeh, "Joint position and trajectory optimization of flying base station in 5G cellular networks, based on users' current and predicted location,", arXiv:2202.03832.
This paper cites the journal paper [J3]
[5*] R. Zhong, X. Liu, Y. Liu and Y. Chen, "Multi-Agent Reinforcement Learning in NOMA-Aided UAV Networks for Cellular Offloading," in IEEE Transactions on Wireless Communications, vol. 21, no. 3, pp. 1498-1512, March 2022, doi: 10.1109/TWC.2021.3104633.
This paper cites the conference paper [C3]
[6*] Amponis, G.; Lagkas, T.; Zevgara, M.; Katsikas, G.; Xirofotos, T.; Moscholios, I.; Sarigiannidis, P. Drones in B5G/6G Networks as Flying Base Stations. Drones 2022, 6, 39. https://doi.org/10.3390/drones6020039.
This paper cites the conference paper [C4]
[7*] Atli, İ.; Ozturk, M.; Valastro, G.C.; Asghar, M.Z. Multi-Objective UAV Positioning Mechanism for Sustainable Wireless Connectivity in Environments with Forbidden Flying Zones. Algorithms 2021, 14, 302. https://doi.org/10.3390/a14110302.
This paper cites the conference paper [C4]
[8*] X. Wen et al., "Improved genetic algorithm based 3-D deployment of UAVs," in Jour-

nal of Communications and Networks, vol. 24, no. 2, pp. 223-231, April 2022, doi: 10.23919/JCN.2022.000014.
This paper cites the conference paper [C6]
[9*] Kim, Jinho, and Kayoung Park. "6G and the Internet of Things: Topic Analysis." Journal of Industrial Integration and Management (2022): 1-19.
This paper cites the conference paper [C6]